DECODING THE SIGNAL: INTERROGATING ELECTROPHILE SIGNALING RESPONSES IN MAMMALIAN CELLS AND *Danio rerio* (ZEBRAFISH)

A Dissertation

Presented to the Faculty of the Graduate School

of Cornell University

In Partial Fulfillment of the Requirements for the Degree of

Doctor of Philosophy

by

Saba Parvez

May 2018

DECODING THE SIGNAL: INTERROGATING ELECTROPHILE SIGNALING RESPONSES IN MAMMALIAN CELLS AND *Danio rerio* (ZEBRAFISH)

Saba Parvez, Ph. D.

Cornell University 2018

Redox homeostasis is crucial for the maintenance of organism fitness and survival. Redox imbalance is a marker of various pathologies including cancer and neurodegenerative diseases. At high levels, reactive electrophilic/oxygen/nitrogen species cause damage to cellular components such as proteins and DNA. More recently, it has come to light that at physiological concentrations the reactive species act as signaling molecules crucial for cellular communication. Given the chemical simplicity of these reactive messengers, it has been a challenge to understand how these reactive small molecules specifically perturb particular proteins—a prerequisite of redox signaling. Traditionally, redox signaling has been studied by swamping a model system (cells/whole organisms) with reactive signals leading to the generation of mixed responses from multiple simultaneous events. Such approaches mimic oxidative stress and are less amenable to the study of redox signaling. Here, I report the development and characterization of the **t**argetable **r**eactive **e**lectrophiles and o**x**idants (T-REX), a unique chemistry-based platform that (1) enables selective modification of redox-sensitive proteins with spatiotemporal precision in complex biological systems, (2) interrogates the consequences of this target-specific redox modification, and (3) allows unbiased screening for novel first-responding sensors capable of sensing reactive redox signals under signal-limited conditions.

As proof-of-concept, I show that T-REX can selectively modify Keap1, an

established electrophile-sensitive protein and an important regulator of the therapeutically-relevant Nrf2/antioxidant response (Nrf2/AR) signaling axis, with the model electrophile 4-hydroxynonenal (HNE). Additionally, my work for the first time shows that low stoichiometry HNE modification of Keap1 is sufficient to trigger AR in biological systems. This work also expands the applicability of T-REX to study redox signaling in zebrafish (Z-REX) and *E. coli*. I report here that selective modification of Keap1 in zebrafish suppresses innate and adaptive immune response. Finally, my collaborative work also shows that T-REX can be used to screen for novel first-responding redox sensors. I show that Akt3, an isoform of the Akt oncogenic kinase, senses electrophilic signals using a unique cysteine residue in the flexible linker region of the enzyme. HNE modification of Akt3 downregulates its kinase activity with functional signaling consequences in cells and zebrafish.

BIOGRAPHICAL SKETCH

Saba Parvez was born and raised in Assam, a beautiful hilly state in Northeast India known for its unique blend of tea. At the age of 12, he was selected by Jawahar Navodaya Vidyalaya for a fully-funded residential education. Having excelled at his secondary education, he was one of the two students in the country to be selected by the Pestalozzi International Village Trust to pursue International Baccalaureate at Hastings College of Arts and Technology in the UK. It was during his time in the UK that he got interested in chemistry. Fortuitously, he was awarded a scholarship to complete his undergraduate degree with a major in Chemistry at Bates College, Maine. It was during undergraduate education that he had a hands-on experience of scientific research through multiple summer research internships and senior thesis research under the guidance of Professor Rachel Austin. More enthused, he pursued a graduate research career. Excited at the prospect of working at the interface of chemistry and biology, he decided to join Professor Yimon Aye's lab at Cornell University. Having joined the lab in the very first year of its establishment, he was at the forefront in driving the lab's research forward. In Professor Aye's lab he primarily worked on developing and validating T-REX, a chemistry-based method to study redox signaling in biological systems. He also collaborated with Professor Robert Weiss' lab in trying to understand the biochemical basis of high level of reactive oxygen species in cells overexpressing the small subunit of ribonucleotide reductase (RNR) enzyme. He was a recipient of the HHMI international predoctoral fellowship during his time at the Aye Lab. After graduation, he plans to start his postdoctoral training in the laboratory of Professor Randall Peterson at the University of Utah, where he will be using zebrafish as a model system to study the molecular details of various disease phenotypes. His career goals are to run an independent research lab in an academic setting.

ACKNOWLEDGMENTS

I would like to express my deepest gratitude to my advisor Professor Yimon Aye for guiding and mentoring me over the years. I am constantly inspired by your hard work and your determination to push the boundaries of science. I am immensely grateful to you for holding me to a high standard and tirelessly motivating me to achieve my highest potential.

I am thankful to my committee members, Professor Rick Cerione and Professor Hening Lin, for their support and for their letters of recommendation.

I would also like to thank Howard Hughes Medical Institute for their financial support granted through predoctoral fellowship.

I am grateful to all my friends who have been a part of this incredible journey. I will forever cherish the friendships I have made in Ithaca, both in the lab and outside. I have learned immensely from the intellectual discussions with the senior postdoctoral members in the lab. The support of my fellow graduate students and undergraduate mentees have made this experience worthwhile. I thank you all from the core of my heart.

I would like to thank my undergraduate research advisor, Professor Rachel Austin for inspiring me to pursue a research career in chemical biology. I am also grateful to Pestalozzi International Village Trust for their support during the formative years of my scientific career. This exciting journey would not have been possible without your help.

I would especially like to thank my family for the love, support, prayers, and constant encouragement during these years. Finally, I would like to thank Shlesma Chhetri, my better half, for being there for me through thick and thin. I could not have done this without you.

TABLE OF CONTENTS

LIST OF FIGURES

LIST OF TABLES

LIST OF ABBREVIATION

RES: Reactive electrophilic species

ROS: Reactive oxygen species

HSAB: Hard/soft acid-base model

HOMO: Highest occupied molecular orbital

LUMO: Lowest unoccupied molecular orbital

LDEs: Lipid-derived electrophiles

HNE: 4-hydroxynonenal

HHE: 4-hydroxyhexenal

ONE: 4-oxononenal

15d-PGJ_2: 15-deoxy-Δ(12,14)-prostaglandin J_2

PGA_2: 8-iso-prostaglandin A_2

OA-NO_2: nitro oleic acid

L-NO_2: nitro linoleic acid

AA-NO_2: nitro arachidonic acid

NF-κB: Nuclear factor kappa-light-chain-enhancer of activated B cells

TPA: 12-O-tetradecanoylphorbol-13-acetate

Keap1: Kelch-like ECH-associated protein 1

Nrf2/NFE2L2: Nuclear factor (erythroid-derived 2)-like 2

PUFA: Polyunsaturated fatty acid

LOX: Lipoxygenase

COX: Cyclooxygenase

GSH: Reduced glutathione

GSSG: Oxidized glutathione

GAPDH: Glyceraldehyde phosphate dehydrogenase

SDS-PAGE: Sodium dodecyl sulfate-polyacrylamide gel electrophoresis

EPR: Electron paramagnetic resonance

LC/GC-MS: Liquid/Gas chromatography coupled mass spectrometry

DNPH: Dinitrophenyl hydrazine

ABPP: Activity-based protein profiling

IA: Iodoacetamide

TEV: Tobacco Etch Virus

T-REX: Targetable reactive electrophiles and oxidants

POI: Protein-of-interest

Ht-PreHNE: Halo targetable photocaged precursor to 4-hydroxynonenal

PMA: Phorbol myristate acetate

E. coli: *Escherichia coli*

HA tag: Human influenza hemagglutinin tag

PCR: polymerase chain reaction

GFP/YFP/CFP: Green/Yellow/Cyan Fluorescent Protein

IF: Immunofluorescence

qRT-PCR: quantitative reverse transcriptase polymerase chain reaction

NQO1: NADPH quinone dehydrogenase 1

HO-1: Heme oxygenase 1

Trx: Thioredoxin

GCLM1: Glutamate-cysteine ligase modifier subunit 1

CMV: Cytomegalovirus

AR(E): Antioxidant response (element)

TMR: Tetramethylrhodamine

FRET: Fluorescence resonance energy transfer

CHAPTER 1

*ELECTROPHILE SIGNALING IN CONTEXT

Once solely considered as markers of oxidative stress, reactive electrophilic species (RES) are now well-appreciated as important cellular signals[1-4]. Biological electrophiles come in a variety of shapes and sizes ranging from short single-carbon formaldehyde to the long-chain 12-nitro-arachidonic acid, and cyclic three-membered epoxides to five-membered α,β-unsaturated carbonyls in prostaglandins[1] (**Figure 1.1**). Considerable effort has been made to understand the chemical principles underlying the reaction between electrophiles and nucleophiles. One of the more widely used models is that of hard/soft acid-base model (HSAB)[5,6]. Hard electrophiles are often positively-charged and are non-polarizable. Soft electrophiles typically have a delocalized charge density, a partial positive charge at the electrophilic center, and are polarizable. According to HSAB, hard electrophiles prefer to react with hard bases and soft electrophiles with soft bases. The basis for this observation is typically ascribed to domination of charge interaction for "hard" and domination of HOMO-LUMO overlap for "soft" interactions[5]. The most signaling-relevant electrophiles are typically 'soft' Michael acceptors that react with 'soft' nucleophiles, principally thiols.

α,β-unsaturated carbonyls (present in micromolar quantities in the basal state in cells [7] but can raise much higher during stress[8]) and nitroalkenes (0.72 nM of nitro-conjugated linoleic acid in human plasma[9], and detected at 10's of nM in heart tissue under stress[10]) are two of the more abundant signaling electrophiles in mammalian cells **(Table 1.1)**. Examples of the former include lipid-derived electrophiles (LDEs) such as the aliphatic LDEs 4-hydroxynonenal (HNE), 4-oxononenal (ONE), and cyclic LDEs

*This chapter is part of a review. "Lost in Translation? Is Redox Signaling the Cell's Pidgin or a Fully-Fledged Creole?" Saba Parvez, Marcus J. C. Long, and Yimon Aye Chemical Reviews, **2017** *Submitted.* Underlined: First-Author

such as 15-deoxy-Δ(12,14)-prostaglandin J_2 (15d-PGJ_2) and 8-iso-prostaglandin A_2 (PGA_2). Nitroalkene-based electrophiles include nitrated-derivatives of fatty acids such as oleic (OA-NO_2), linoleic (L-NO_2), and arachidonic acid (AA-NO_2). These electrophiles modulate numerous processes in human biology—from development[11,12] and aging[13] to cellular homeostasis events such as apoptosis[14], immune response[1,15], and heat shock response[1]. For instance, 15d-PGJ_2 is a potent immune-modulator and downregulates the NF-κB pathway[15]. Nitrofatty acids[16] and HNE[17] inhibit TNFα-induced macrophage activation and 12-O-Tetradecanoylphorbol-13-acetate (TPA)-induced Jurkat T-cell activation, respectively, by regulating NF-κB signaling, as well as activate the Keap1/Nrf2 antioxidant signaling response[18-20].

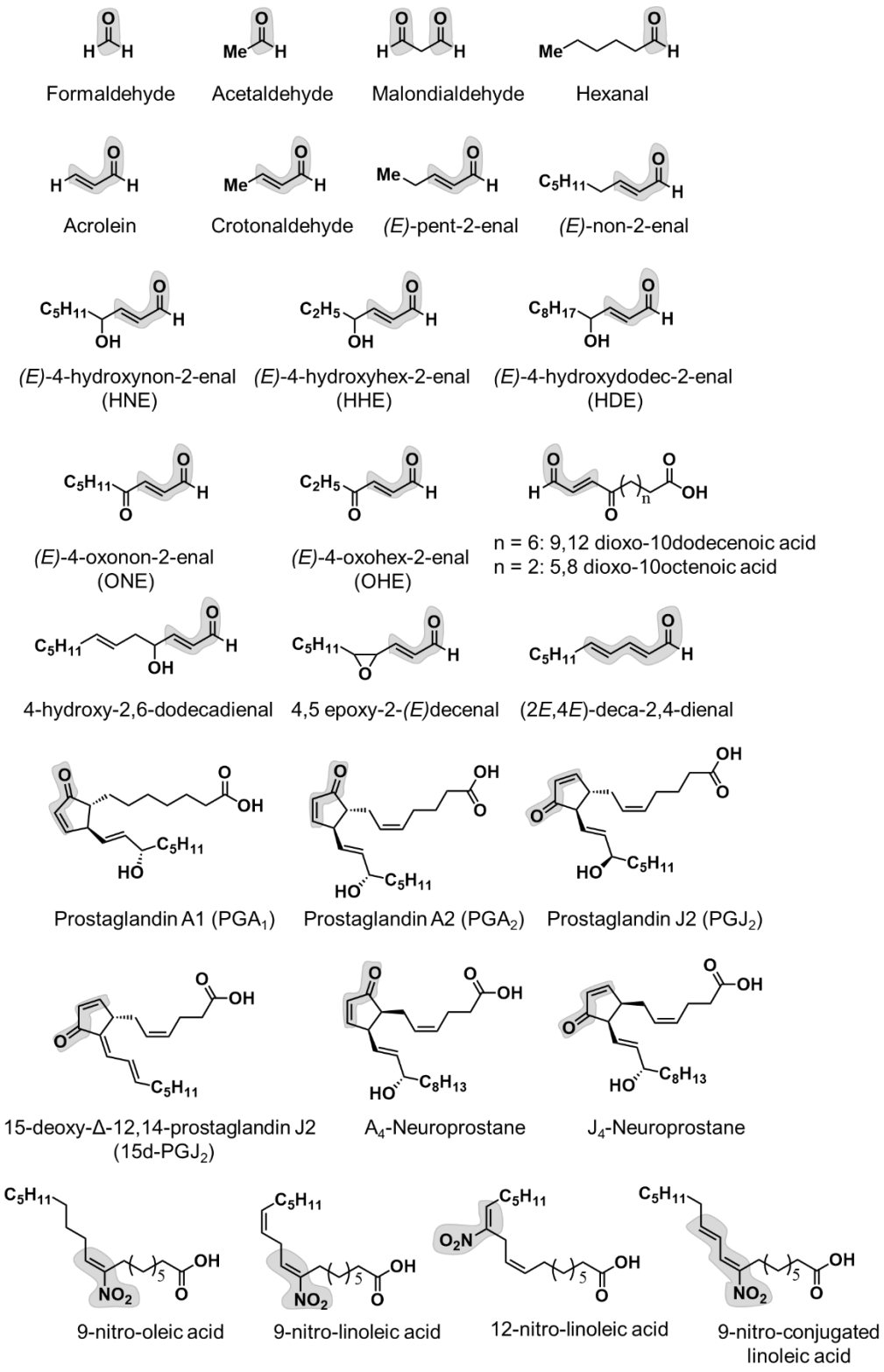

Figure 1.1 A selection of endogenously generated electrophiles in biological systems. The electrophilic component of the molecule is highlighted[1].

Electrophile generation in cells: Enzymatic and Non-enzymatic pathways

LDEs are derived endogenously from both enzymatic and non-enzymatic pathways[1,21]. Polyunsaturated fatty acids (PUFA) are an important source of endogenous LDEs. Peroxidation of PUFAs, either through enzymatic or non-enzymatic pathways, results in the generation of a variety of electrophilic compounds capable of signaling roles[3].

Enzymatic lipid peroxidation pathways

Three classes of enzymes, either working in concert or alone, result in the generation of electrophilic lipid signals. These enzymes consist of the metalloenzymes lipoxygenases (LOX)[21-23], cyclooxygenases (COX)[24-26], and Cytochrome P450[27]. LDEs are primarily generated from two substrates: ω-3 and ω-6 fatty acids. The primary substrate in the ω-6 fatty acid pathway is arachidonic acid (AA). COX and LOX-mediated oxidation of AA generates a wide range of secondary metabolites (only a fraction of which are electrophilic[28,29]) with diverse biological properties including regulating inflammation[30], vasodilation[29,30], platelet aggregation[29,30] etc.

Cyclooxygenases are non-heme-iron-containing proteins that catalyze AA oxidation. Among the two COX isoforms in mammalian cells. COX-1 is expressed in all tissues whereas COX-2 is limited to kidney and brain [31]and only induced in other tissues during inflammation[32]. Both COX-1 and COX-2 generate prostaglandin H2 (PGH_2) from AA-oxidation[29,33] (**Figure 1.2**). PGH_2 is then further oxidized to other prostaglandins mediated by cytochrome-P450 prostaglandin sythetases[29]. Several prostaglandins (15d-PGJ_2, PGA_2 and PGJ_2) contain an α,β-unsaturated carbonyl making

them electrophilic. In the case of 15d-PGJ_2, PGH_2 is first oxidized by the action of prostaglandin D2 (PGD_2) synthetase into an unstable intermediate (PGD_2), which readily dehydrates to yield PGJ_2[34]. PGJ_2 can undergo spontaneous isomerization to generate Δ^{12}-PGJ_2, which in turn dehydrates to yield 15d-PGJ_2 (**Figure 1.2**). In addition to AA, COX-2 also uses omega-3 PUFA as a substrate to generate electrophilic lipid signals. COX-2 in activated macrophages stimulates the production of electrophilic oxo-derivatives from the omega-3 fatty acids docosahexenoic acid (DHA) and eicosapentenoic acid (EPA). The process involves COX-2-catalyzed hydroxylation followed by dehydrogenases-assisted oxidation[35].

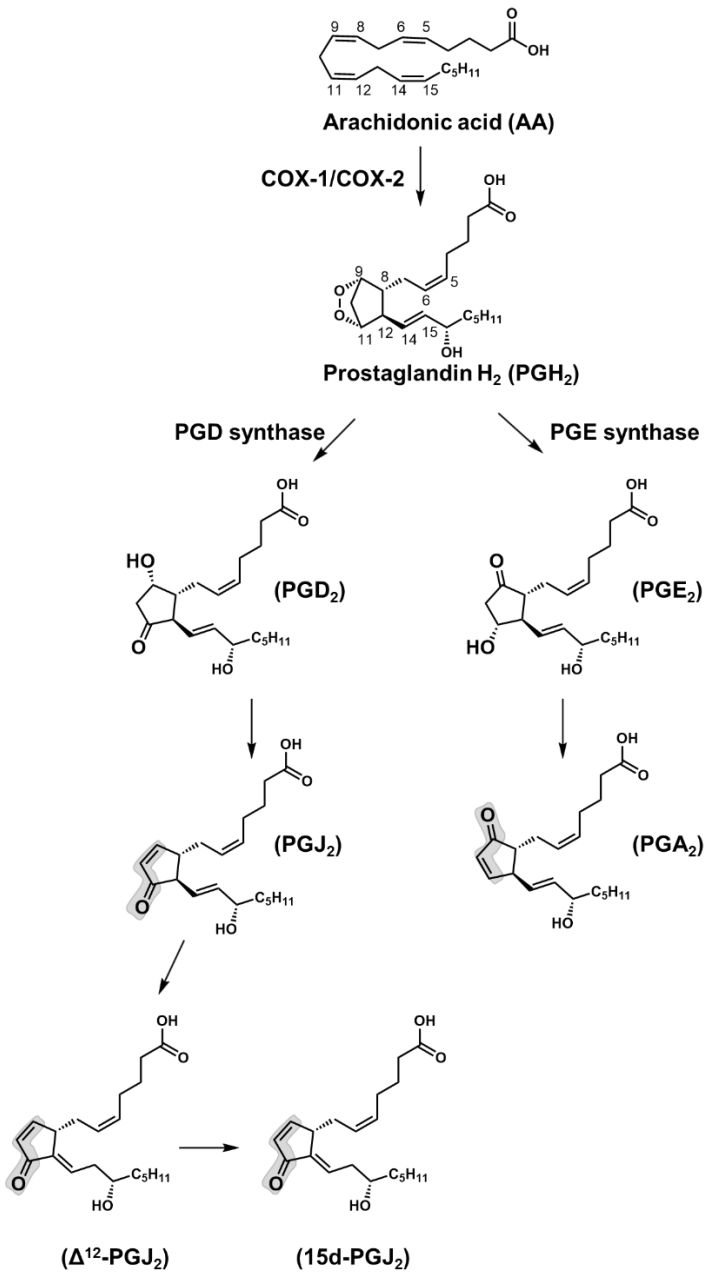

Figure 1.2 Enzymatic generation of lipid-derived electrophiles: COX-1/COX-2-catalyzes the formation of PGH_2 using AA as the substrate. PGH_2 acts as an intermediate for the generation of PGD_2 and PGE_2 by the action of PGD synthase and PGE synthase, respectively. PGH_2 is also an intermediate for the generation of a number of other bioactive non-electrophilic molecules (not shown). PGD2 and PGE2 undergo spontaneous dehydration to yield PGJ_2 and PGA_2, respectively. PGJ_2 can then isomerize to generate Δ^{12}-PGJ_2 and further dehydrate to 15d-PGJ_2[33].

Non-enzymatic lipid peroxidation

Non-enzymatic generation of LDEs is mediated by ROS[1,36]. ROS such as the •OH [37] and the $NO_2^{\bullet}$ radicals[38] are highly reactive and unstable. Once formed, they react rapidly with immediately-accessible biological molecules. One of the key sites of ROS generation is at the plasma membrane and membranes of other organelles. PUFA-rich cell membranes are excellent targets of ROS. Additionally, molecular oxygen concentrates in biological membrane because of its hydrophobicity and serves as an electron donor during lipid peroxidation events. Lipid oxidation is typically triggered by the abstraction of the activated bisallylic hydrogen[39] by a radical oxidant such as $O_2^{\bullet-}$ or •OH (**Figure 1.3**). The resulting doubly-allylic radical can quickly react with molecular oxygen to generate a lipid peroxide radical which can further abstract hydrogen from a neighboring PUFA to form lipid hydroperoxide and a new lipid radical, propagating this radical-chain process[40]. Lipid hydroperoxides generated during the reaction may undergo Hock cleavage (a process of 1,2-carbon migration in a peroxide to form a carbonyl and an alcohol) to generate short chain LDEs such as HNE and HHE, in the case of ω-6 and ω-3 PUFAs, respectively (**Figure 1.3**)[41,42]. HNE, HHE and similar lipid-enal signals are highly reactive and react with nucleophiles by Michael addition. Additionally, the aldehyde functional group can react with lysine to form a Schiff base adducts[43]. Thus, LDEs are bifunctional chemical-signals. Aside from Hock cleavage, the lipid peroxide generated by ROS can cyclize, react further with molecular oxygen, and further rearrange, to form various prostaglandin-like signaling molecules called isoprostanes **(Figure 1.3)**. AA-derived E_2- and D_2-isoprostanes further dehydrate to generate electrophilic A_2- and J_2-isoprostanes.

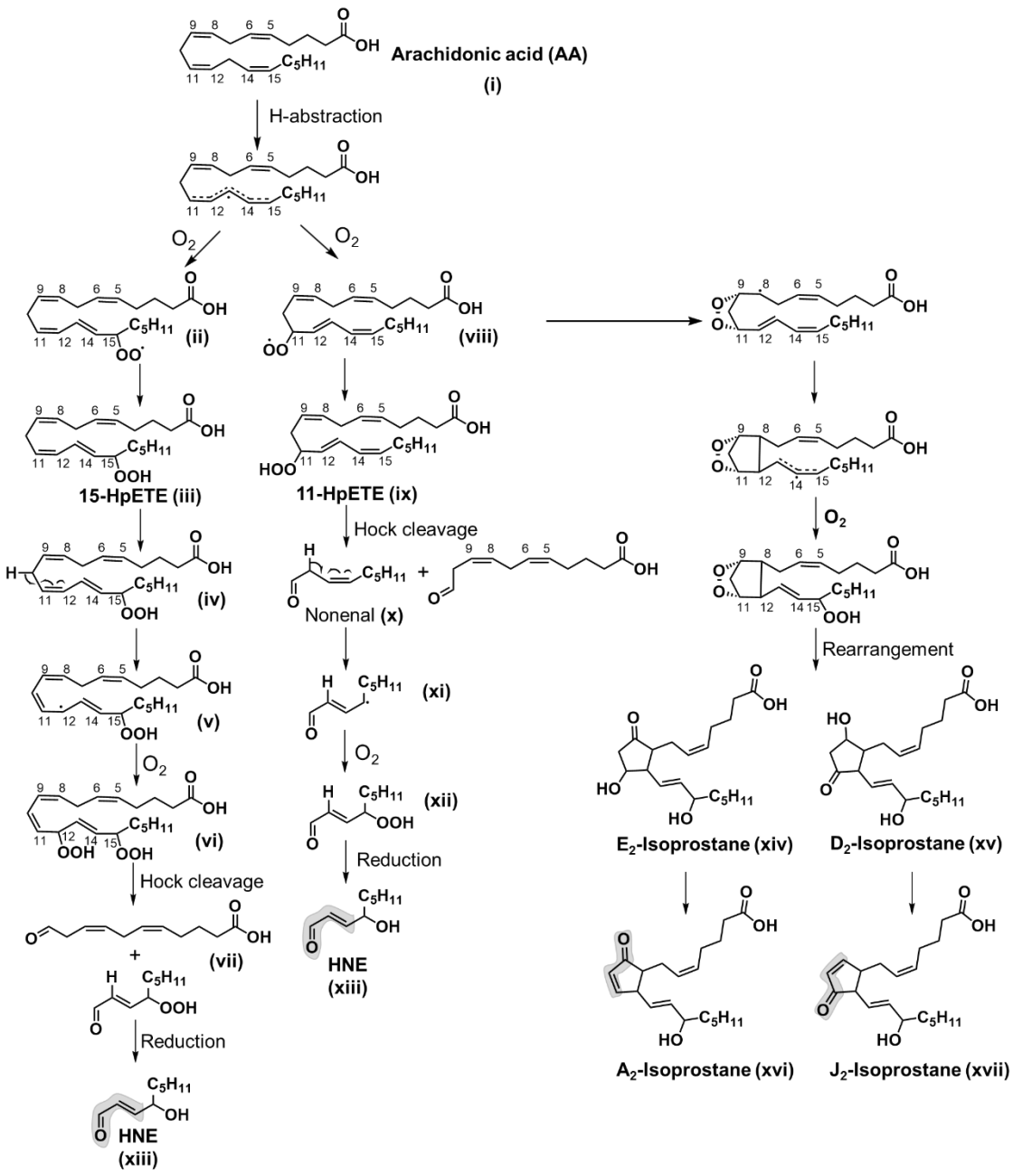

Figure 1.3 Non-enzymatic generation of lipid-derived electrophiles[1,2]: The generation of HNE (xiii) and A_2- (xvi) and J_2-isoprostanes (xvii) from ω-6 fatty acids such as arachidonic acid (AA) (i) is shown here. Reactive radicals such as •OH initiate lipid peroxidation by abstracting a bis-allylic hydrogen from AA (i). Molecular oxygen addition at either C15 or C11 generates the corresponding peroxy radical (ii and viii), which abstracts an H radical (possibly from another AA molecule thus propagating the radical chain reaction) to generate the hydroperoxy intermediates 15-HpETE (iii) and 11-HpETE (ix), respectively. The abstraction of hydrogen at C10 of 15-HpETE forms a radical intermediate which migrates to C12, reacts with another molecule of oxygen,

yielding the dihydroperoxide intermediate (iv). This intermediate then undergoes Hock cleavage to yield HNE as one possible product. 11-HpETE is shown to first undergo a Hock cleavage to generate the nonenal (x), which undergoes oxygenation to yield the hydroperoxide (xii) and its further reduction to generate HNE (xiii). Arachidonic acid peroxidation also generates isoprostanes. The peroxy radical intermediate (viii) at C11 can undergo cyclization, further oxygenation, and rearrangement to yield E2- (xiv) and D2-isoprostanes (xv). Dehydration of the E2- and D2-isoprostanes result in J2 (xvi) and A2-isoprostanes (xvii), respectively. Analogous peroxidation pathway from ω-3 fatty acids such as docosahexenoic acid (DHA) generates HHE.

Nitro-fatty acids generation

Nitric oxide ($NO^{\bullet}$) is mainly enzymatically generated by nitric oxide synthetases[44]. Although $NO^{\bullet}$ radical is unreactive towards protein substrates[45], $NO^{\bullet}$ rapidly reacts with $O_2^{\bullet-}$ to generate ONO_2^- . Peroxynitrites undergo homolytic bond cleavage to form $OH^{\bullet}$ and $NO_2^{\bullet}$[38], both of which are highly reactive and can react with PUFAs at diffusion-controlled limits. $NO_2^{\bullet}$ can abstract bisallylic hydrogen from PUFAs to initiate lipid peroxidation. Additionally, $NO_2^{\bullet}$ reacts with PUFAs to generate nitro fatty acids[46]. The reaction initiates with the addition of a $NO_2^{\bullet}$ radical to the double bond of PUFA forming a resonance-stabilized carbon-centered radical[1] (**Figure 1.4**) . Under low oxygen, another $NO_2^{\bullet}$ reacts with the carbon-centered radical generating a short-lived intermediate that decomposes to form a nitrated fatty acid and nitrous acid (HONO). Presence of excess molecular oxygen favors the generation of lipid hydroperoxide instead. Nitro-fatty acids (NO_2-FA) are important for cellular maintenance and act as ligands to receptors such as PPARγ[47]. Exogenous addition of nitro-oleic acid to mice was shown to protect against myocardial ischemia and reperfusion injury[10]. This was in part mediated through the downregulation of the NF-κB pathway by inactivating the p65 subunit[10].

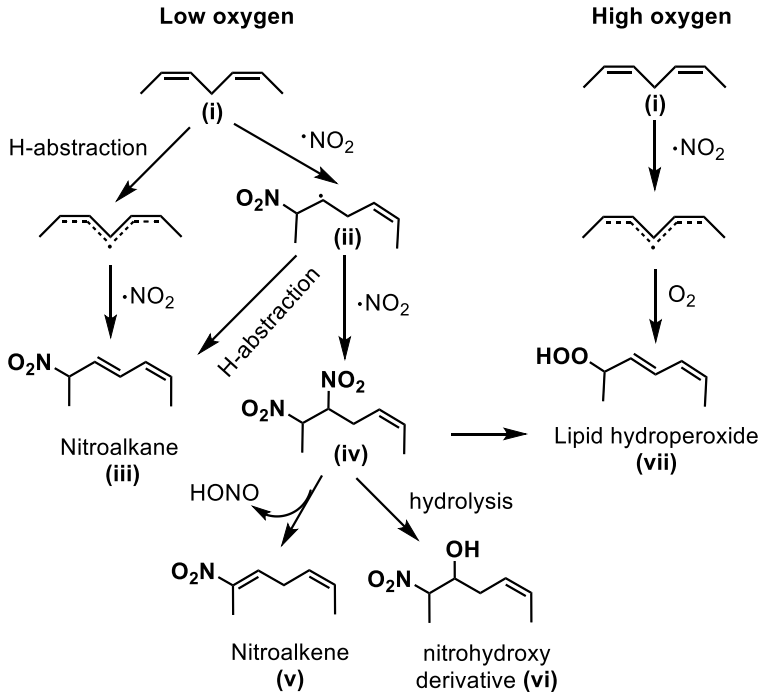

Figure 1.4 Non-enzymatic generation of lipid-derived electrophiles: Generation of nitro fatty acids from unsaturated fatty acids. Under low oxygen condition, NO_2• undergoes radical adduction with unsaturated fatty acids (i) (such as linoleic acid) to generate a nitroalkyl radical intermediate (ii). This intermediate can either abstract a hydrogen to generate nitroalkane (iii) or further react with NO_2• to generate a nitro/nitrite intermediate (iv). Subsequent loss of nitrous acids (HONO) yields a nitroalkene (v) whereas hydrolysis of the intermediate generates a hydroxy-nitro fatty acid (vi). Under high oxygen conditions, a lipid hydroperoxide (vii) is formed instead[10,16,46].

In addition to nitrating lipids, ONO_2^- can also nitrate nucleotides. A recent example of electrophilic nucleotide is 8-nitro-cGMP that is formed by the addition of peroxynitrite to cGMP[48]. 8-nitro-cGMP can guanylate protein thiols[49]. S-guanylation of Keap1 results in loss of its ability to bind Nrf2 and subsequent upregulation of a battery of antioxidant response genes[49,50]. S-guanylation of proteins also releases nitrite NO_2^-, which it itself can act as signaling molecule.

Regulation of RES generation

The basal levels of various RES are maintained at low concentrations **(Table 1.1)** in cells. For example, the concentration of 15d-PGJ_2 in 3T3-L1 preadipocytes is in low picomolar range[51]; and the basal concentration of nitro-conjugated linoleic acid is < 1 nM in human plasma[9]. Oxidative stresses as well as a number of pathological conditions promote RES generation[9]. For instance, myocardial ischemia and reperfusion (I/R) injury significantly upregulate ROS generation. Analysis of myocardial tissue from mice following 30 min of ischemia and 30 min of reperfusion showed a > 15-fold increase in the total levels of nitro-linoleic acid compared to sham-operated mice or mice that underwent only ischaemia[10]. Pathological conditions associated with Alzheimer's and Parkinson's diseases (AD and PD) are also linked to increase in generation/accumulation of RES and RES-conjugated proteins. Brain tissues from patients with mild cognitive impairment and early AD show an increase (~3 fold) in HNE and acrolein levels[52]. Consistent with these results, proteomic analysis of brain tissue reveals significant increase in carbonylated protein in AD and PD patients compared to age-matched controls[53,54]. Under physiological conditions, low levels of RES are maintained by its conjugation to cellular GSH, either spontaneously or catalyzed by glutathione transferases (GSTs). It is proposed that one of the ways RES engender response is by lowering the total GSH pool thus altering the redox balance, which is sensed by proteins[55,56]. While this may be true under high concentrations of RES, accumulating evidence suggests that RES trigger specific response by direct modification of specific proteins[3,11,19,20].

Table 1.1: Estimated cellular concentrations of various lipid-derived electrophiles, their half-lives and second order reaction rate constant with biological molecules

	Cellular concentration	**Half-lives**	**Second-order rate constants with biological molecules $M^{-1}s^{-1}$**
HNE	8 μM[7] 0.3–1 μM[8] 15 μM- 5mM (stressed)[8]	2.5 min in liver cells;[8] < 4 s in rat heart[8]	n-acetyl histidine (0.0021 $M^{-1}s^{-1}$), N-acetyl lysine (0.0013 $M^{-1}s^{-1}$); GSH (1.33 $M^{-1}s^{-1}$), Cysteine (1.21 $M^{-1}s^{-1}$) [57]
Nitro-Fatty acids	0.72 nM (nitro-conjugated linoleic acid) in human plasma[9] ~17 nM of nitro-conjugated linoleic acid in heart tissue under stress)[10] ~9.5 nM of free nitro oleic acid in heart tissue under stress[9] free Nitro oleic acid: ~600 nM in plasma[9]	Nitro linoleic acid ~30 min in phosphate buffer at pH 7.4 at 37 °C[9] Nitro-oleic acid > 2h phosphate buffer at pH 7.4 at 37 °C[9]	GSH with nitro-linoleic acid ~350 $M^{-1}s^{-1}$ at 7.4 at 37 °C[58] GSH with nitro-oleic acid ~180 $M^{-1}s^{-1}$ at 7.4 at 37 °C[58]
Prostaglandins (15d-PGJ_2)	~2 pM of 15d-PGJ_2 in 3T3-LT1 preadipocyte culture medium[51] 1 nM 15d-PGJ_2 intracellular[51]	>48 h in aqueous media at 37 °C for 15d-PGJ_2[51]	GSH with 15d-PGJ_2 ~0.7 $M^{-1}s^{-1}$ at pH 7.4 at 37 °C[58]

External sources of electrophiles

In addition to the endogenous sources, cells are also continually exposed to non-native electrophiles. Exogenous sources include dietary electrophiles[43,59] and environmental pollutants. Isothiocyanates are a family of dietary electrophiles produced by cruciferous vegetables such as broccoli and cabbage. Isothiocyanates like sulforaphane and PEITC are activators of cytoprotective pathways[60] and have anticancer properties[61]. α,β-unsatured carbonyls like curcumin from turmeric[62] and cinnamaldehyde from cinnamon [63]also have protective effects on cells. Cells are also exposed to electrophiles from pollutants[64]. Acrolein is generated by heating oils at high temperature and is also a major constituent of smoke from cigarettes[64] and exhaust fumes[65]. Acrolein is also generated endogenously by the myeloperoxidase-mediated degradation of threonine[66]. While small concentrations may be beneficial, acrolein is a highly-reactive aldehyde that can covalently conjugate with proteins and DNA resulting in electrophilic stress and cell death at higher concentrations[67].

Mechanism of Signal Transduction by electrophiles

In enzyme-catalyzed signaling/metabolic processes, enzyme catalysis results in excellent target- and residue- specificity as well as chemoselectivity (chemical-functional-group selectivity). In enzyme-independent signaling modes, however, it is unclear what factors determine chemoselectivity, and protein target- and residue-selectivity. Two important looming questions in the field of electrophile signaling are: (1) Do the physiochemical properties of the signaling messengers engender target and residue selectivity in electrophile signaling?

And

(2) Are there specific proteins endowed with kinetically "privileged" cysteines that can compete with detoxification processes to gain sufficient occupancy to elicit downstream signaling?

Cysteine Thiols are the primary target of electrophilic modification

Consistent with the importance of the physicochemical properties of the signaling molecules in engendering chemoselectivity, cysteine is the primary target of RES[68-70]. Cysteine is the most nucleophilic residue amongst the canonical amino acids. N-acetyl cysteine and glutathione are around 1000 times more nucleophilic than N-acetyl histidine and N-acetyl lysine (second-order rate constants for addition to HNE 0.0013 and 0.0021 $M^{-1}s^{-1}$, respectively)[57] (**Table 1.1**). Histidine, lysine, and to a lesser extent, arginine, have also been implicated as nucleophilic residues within proteins, although the rate data indicate that a significant rate enhancement or very high concentration will be required to outcompete cysteine (**Figure 1.5**).

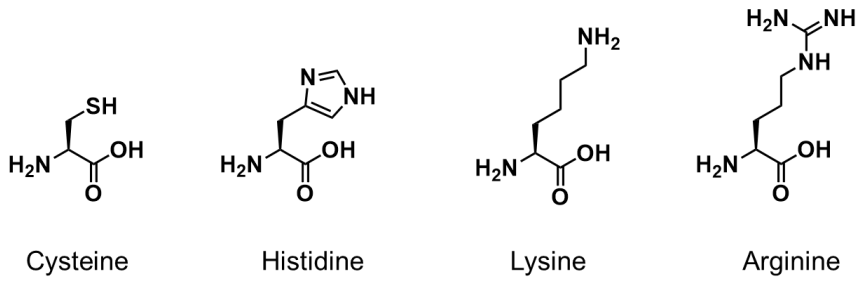

Figure 1.5. Nucleophilic amino acid and amino-acid derived molecules (in order of decreasing nucleophilicity)

Although cysteine is the most nucleophilic amino acid residue, LDE modification on histidine, lysine, and arginine have also been reported upon bolus

treatment of cells or purified proteins. For example, multiple histidine residue modifications on Hsp90 chaperone protein were identified upon treatment of RKO colon cancer cell lines with HNE[71]. Interestingly, the authors identified several histidine residues (and no cysteines) including His450 of Hsp90α and the corresponding His442 of Hsp90β, both residues are critical for binding to client proteins, as targets of HNE modification. A kinetic analysis of histidine residues on Hps90 peptides reaction with HNE revealed very slow reaction kinetics with a first order reaction rate of 30 min^{-1} in cells upon treatment with 250 μM HNE suggesting that these modifications may only be relevant in very high electrophilic stress and may have limited functional importance under signaling conditions. In similar experiments, GAPDH was shown to form adducts to HNE via cysteine, lysine, and histidine[72]. It should, however, be noted that these experiments were conducted with mM concentrations of HNE. Subsequent experiments showed that for GAPDH, adduction at cysteine and histidine were more rapid than lysine[73]. Interestingly, the same paper showed that the active-site cysteine was not modified by HNE, with surface residues being preferred. More reactive HNE analogs, ONE has also been shown to modify nucleophilic sites other than cysteine. One important modification is 4-ONE-ylation of lysine. This modification occurs through amine adduction to the aldehyde function to form a hemiaminal. This function then undergoes E1cb elimination of water to form a stable amide adduct[74]. Intriguingly there is evidence that SIRT2, a histone deacetylase, can remove this modification, at an albeit rather sluggish rate[75].

Reversible and Irreversible RES modification

Many RES modifications are irreversible. Irreversibility can be illustrated by the fact that protein adducts to HNE and similar protein-enone adducts have been resolved by SDS PAGE and detected by mass spectrometry. Nitroolefins, on the other hand, can form reversible adducts to cysteines[1,2,76] (**Figure 1.6**). Interestingly, the apparent second order adduction rate constant for cysteine modification is 355 $M^{-1}s^{-1}$[58], almost 300-fold higher than adduct formation rate of most other endogenous RES. The difference in adduct stabilities between enals and nitroolefins may be due to (1) the difference between the pKa of the protons α-to the carbonyl (30; methyl acetate[77]) and nitro groups (17; nitromethane[78]), and (2) the ability of RES-adducts to undergo further reaction post cysteine conjugation (**Figure 1.7**). Additionally, RES with multiple nucleophile adduction site (such as the Michael acceptor site and the aldehyde in case of cysteine) can form crosslink with two amino acid residues.

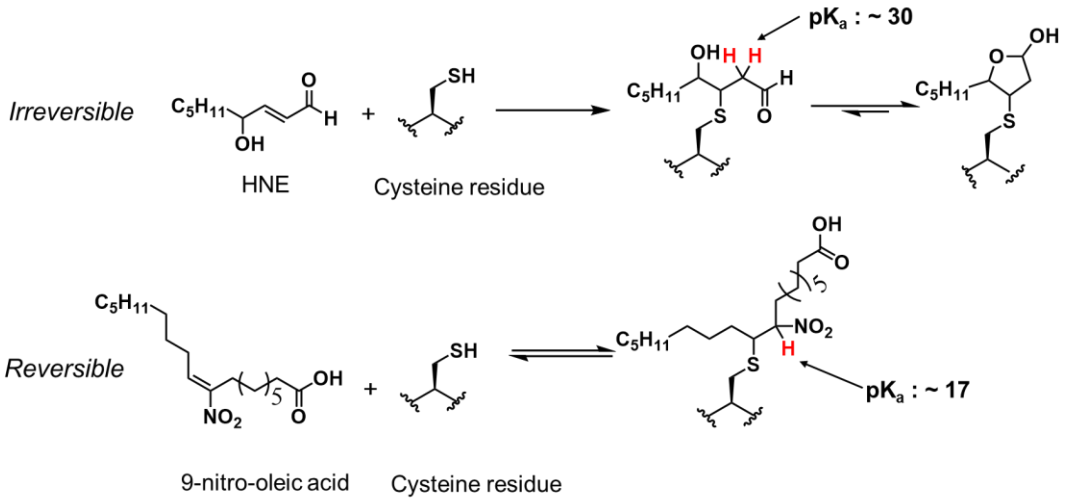

Figure 1.6. Reversible and irreversible RES conjugates: pKa of the hydrogen α to the carbonyl or nitro group affects the reversibility of the thiol conjugates.

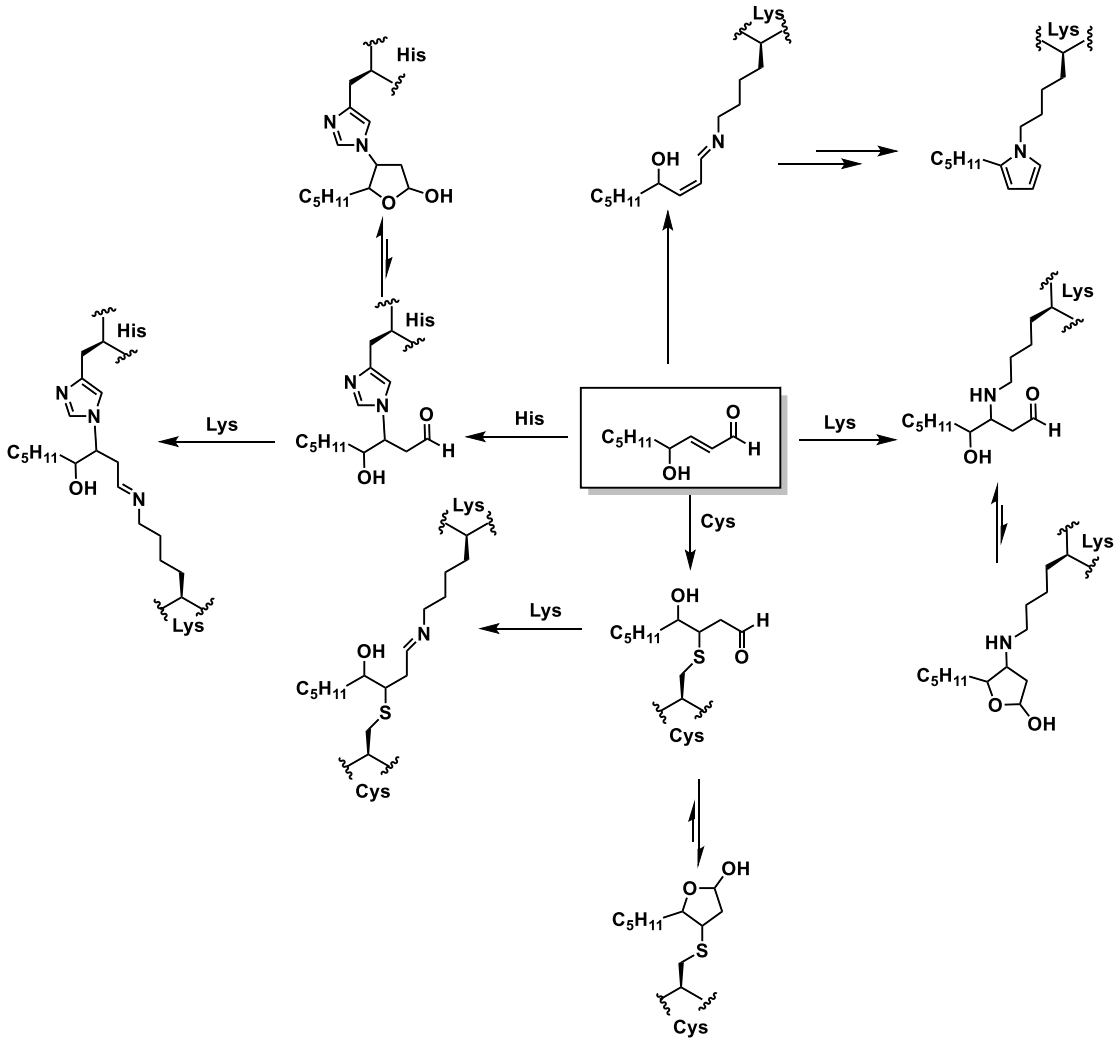

Figure 1.7. Multifunctional RES such as HNE can form multiple different adducts. HNE can form Michael adducts with cysteine, histidine and Lys. It can also form Schiff base with Lysine. Additionally, HNE Michael adducts can also form cross links with another amino acid at the aldehyde electrophilic site.

Current Methods to study electrophile signaling

Detecting RES in biological systems

One of the challenges in studying electrophile signaling is real time detection of RES generation in biological systems. While many small molecule-based[79,80] as well as fluorescent protein-based[81,82] sensors of reactive oxygen species (ROS) have been developed, analogous methods to detect RES have remained limited. This is partly because LDEs classes can contain many different chemical structures but have very similar reactive chemical groups, rendering chemo selectivity a huge issue. These traits are in stark contrast with oxidative redox signals that differ in terms of charge, and type of chemistry (e.g. single vs two electron; nucleophilic addition vs 4+2 cycloaddition/ene) they can undertake. LDEs also react with multiple different amino acids including cysteine, histidine, and lysine generating an increasing diversity of 'chemotypes' that retain RES-like properties. Thus, it is challenging even to design a probe for a specific RES that will not also intercept protein RES adducts.

Detecting lipid-derived radical using electron paramagnetic resonance (EPR)

EPR has been widely used to detect endogenously-generated radical species of relevance in redox signaling[83,84]. The underlying principle of EPR is similar to nuclear magnetic resonance (NMR): an externally-applied magnetic field is used to unpaired electrons (contrasting NMR where nuclei are excited) and energy emitted upon relaxation to the ground state is measured. Thus, molecules with paired electrons (the bulk of biological samples) are not detected by EPR, rendering EPR very sensitive for radical species and high spin metal complex, amongst other paramagnetic biological

complexes. Furthermore, EPR can discriminate between different radical species. This is because each element provides a specific local environment to an electron that affects how energy levels differentiate in a specific magnetic field. Numerically this value is defined by the Lande g-factor (g_e). Additionally, "EPR hyperfine coupling", analogous to *J*-coupling in NMR, resulting from interaction of the magnetic moment of the nuclei of the radical species and that of the unpaired electron provides characteristic spectra for individual radical species. EPR techniques are also highly sensitive and quantitative. Detection of $O_2^{\bullet-}$ by the EPR spin trap method was shown to be 40 times more sensitive than a commonly used spectrophotometric technique involving reduction of ferricytochrome c[85]. Also, the direct quantitation of the amount of redox-active radical present in the sample is facile through the evaluation of EPR signal intensity against appropriate control samples of known concentrations.

A point of consideration is that many of the endogenously-relevant redox signals are highly reactive and short-lived (**Table 1.1**). In fact, the concentration of free radicals can be several to hundreds of folds below the EPR detection limit. Hence EPR techniques for successful detection of these species almost always require a method to trap the radicals using EPR 'silent' probes. The most common of such probes are cyclic nitrones such as 5,5-Dimethyl-1-Pyrroline-N-Oxide (DMPO), 5-Boc-5-methyl-1-Pyrroline-N-Oxide (BMPO), and 5-(Diethoxyphosphoryl)-5-methyl-1-pyrroline-N-oxide (DEPMPO) (**Figure 1.8)**[83,86,87]. To detect a short-lived radical species, an EPR-silent trap is first introduced into the system under study. The trap reacts with the transient redox radical through adduction to the C=N bond. The resultant, relatively stable, dative stabilized radical, N-O$^{\cdot}$, is then detected by EPR (**Figure 1.8, *Inset***).

Therefore, this method is not particularly dynamic, and also quenches the radical, likely inhibiting signaling pathways. Importantly, some spin traps affect signaling pathways, including Erk[88], AR and apoptosis[89].

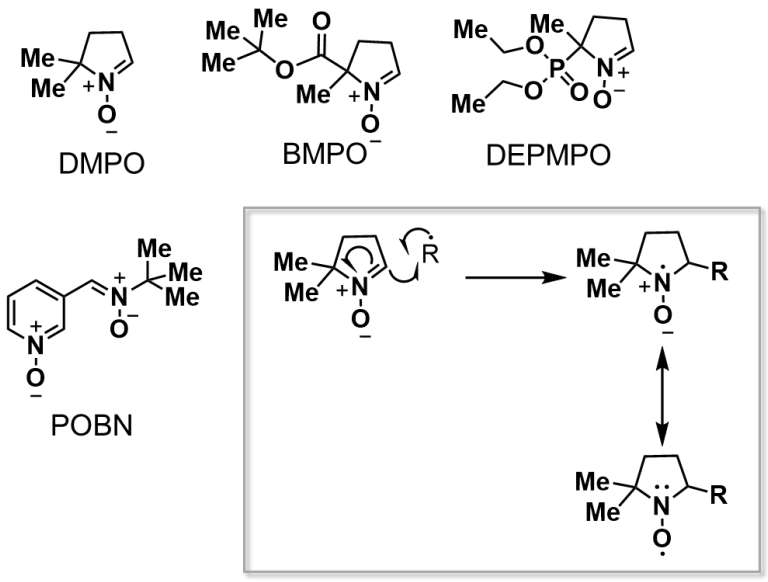

Figure 1.8. A selection of nitrone-based EPR spin traps. *Inset:* Mechanism of a carbon-based lipid radical (R•) adducting with DMPO spin trap to generate a more stable nitroxide radical.

(4-Pyridyl *N*-oxide)-*N*-*tert*-butylnitrone, POBN, another nitrone-based spin trap, and DMPO have been used to study lipid-derived radical generation by oxidation of PUFAs (**Figure 1.8**)[90,91]. POBN has proven especially useful in detection of carbon-based radical such as those generated during lipid peroxidation because of the long half-life of the trapped radical. Carbon-centered radical adducts with POBN have a lifetime of a few hours thus enabling efficient detection[90]. A major disadvantage of using POBN as a spin-trap, however, is that all carbon-based radical adducts with POBN have similar

spectra making discrimination of individual carbon-based radical species from PUFA oxidation impossible. Additionally, POBN adducts resulting from the reaction with oxygen-based radicals, such as lipid peroxy radical intermediates in PUFA oxidation, have very short half-life ($t_{1/2}$ < 10s), thereby limiting their use for detecting oxygen-based radicals[90]. DMPO and EMPO, on the other hand, have proven useful in extending utility to trapping oxygen radicals. The half-life of peroxy and alkoxy adducts of EMPO are on the order of 10 minutes or >1 h, respectively[92].

Spin-trap EPR methods have been used for detecting radical generation in cells[86,93], and have shown promise in multiple *in vivo* studies [94]. Despite their usefulness, EPR-based detection methods have their limitations. Spin-traps can be expensive and have other downsides when used for biological studies such as permeability and cytotoxicity. Moreover, real life biological systems are very complex, so deconvolution of spectra, a common practice in in vitro experiments, is much harder. Additionally, in the case of nitrone-based probes numerous processes can lead to N-O radical products that are EPR active, but are not actually derived through radical attack on the C=N bond[95]. Two principal off pathway processes leading to ESR active products are inverted spin trapping[96] and Forrester-Hepburn reaction[97] (considered to be the most common off pathway mechanism). Finally, EPR-based methods do not allow monitoring radical localization in specific subcellular compartments in whole cells or organisms.

Recently, a clever use of stable nitroxide demonstrated an ability to image carbon-based radical in live cells[98]. The authors used a stable α-substituted nitroxide

conjugated to a fluorophore to generate NBD-Pen, a fluorescent turn-on probe for lipid radical detection. The stable nitroxide acts as a fluorescence quencher of the fluorophore. Adduction of lipid radicals to the nitroxide-radical results in a turning-on of fluorescence. The probe was shown to be selective towards lipid radicals over other biologically-relevant radical species such as $O_2^{\bullet -}$ and $OH^{\bullet}$. The detection limit of the probe was 0.98 nM *in vitro* thus demonstrating excellent sensitivity. The probe was also successful in imaging lipid radical generated in live cells after treatment with diethyl-nitrosamine (DEN), a compound that generates carbon-centered radicals in cells. Furthermore, the authors showed that NBD-Pen could detect lipid radical generation in a rat model of hepatic carcinoma induced by DEN administration. Interestingly, because radical-trapping probe are also radical quenchers, treatment of the probe was shown to alleviate symptoms of oxidative stress, reduce inflammation and apoptosis induced by DEN treatment of live cell and *in vivo*.

Detecting free RES using LC/GC-MS approach

The most general approach to detect free RES in biological samples has been using chromatographic techniques (Liquid chromatography (LC)/Gas Chromatography (GC)) or LC/GC coupled with mass spectrometry[8,9,99,100]. For example, both free and esterified 9/10-nitro-oleic acid (OA-NO_2) has been detected in plasma, red cells extract, and urine of human samples using LC-MS/MS. The free and esterified OA-NO_2 concentration was determined to be ~600 nM and ~300–600 nM, respectively in plasma[9]. HPLC and GC-MS methods has also been used for direct detection of free aldehydes such as HNE in cells extracts and tissue homogenates[100]. Additionally, a more sensitive detection can be achieved by first derivatizing aldehydes with aldehyde-

reactive probes such as, dinitrophenylhydrazine (DNPH) and 1,3-cyclohexanedione and subsequent separation and detection using HPLC. The use of internal standard is required for characterization and quantitation of the sample using HPLC. MS coupled to LC can also be used to detect HNE using mass-to-charge ratio and fragmentation pattern of the derivatized sample[101].

Detecting free RES using novel fluorescent probes

Recently, the Chang Lab has reported the development of multiple probes that selectively detect formaldehyde in cells[102]. Formaldehyde is a metabolite present physiologically at concentrations between 100-400 μM[103,104]. Because of its reactivity, ability to form Schiff bases readily and the ability of those Schiff bases to undergo chemistry readily, chemoselective probes for formaldehyde have been developed. FAP-1 is an example of such sensors[105] (**Figure 1.9**). This molecule can form a Schiff base to formaldehyde and after an aza-Cope rearrangement and hydrolysis give a fluorescent dye (a process leading to an 8-fold increase in fluorescence). Using this probe, exogenous formaldehyde in the 100 μM range was detected. This probe was chemoselective for formaldehyde over various aldehydes (including acetaldehyde and HNE), although it is likely that the probe is selective for formaldehyde over many different aldehydes and ketones as imine formation for acetals and ketones is slower than for formaldehyde, and the cyclohexane-like transition state is severely crowded. Similar formaldehyde selective probes that use 2-Aza-Cope-based detection strategy have also been reported[106-108]. Coupling a promiscuous sensing reaction (e.g. Schiff base formation) to a secondary reaction that only one type of reagent can do efficiently (e.g. 3,3 shift) is a good general mechanism to design a specific probe. A similar strategy

released by the Spiegel lab is their "turn-on" fluorescence sensor of methyl glyoxal[109]. Using a 1,2-diamino functionalized BODIPY probe, allowed fluorescence turn on only by 1,2-dicarbonyl compounds (of which by far the most abundant in cells is methyl glyoxal[110]) (**Figure 1.9**).

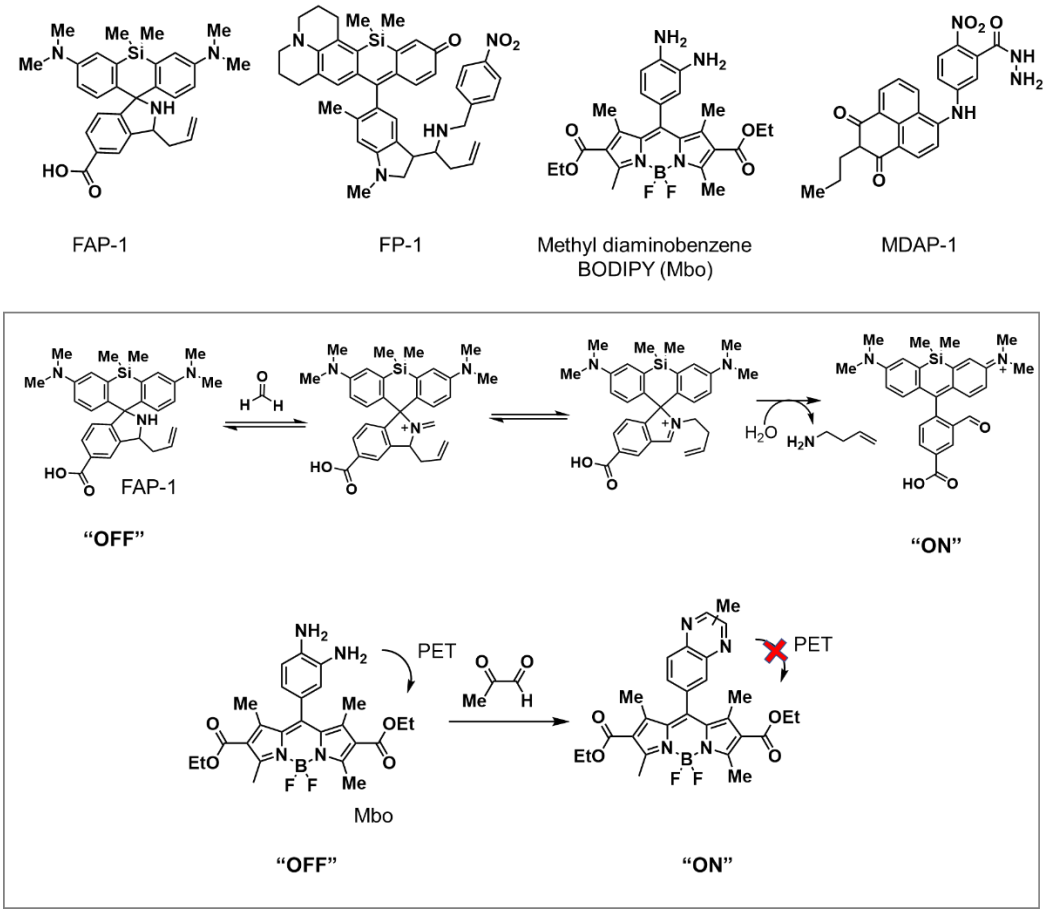

Figure 1.9 Examples of fluorescent probes for the detection of free RES in cells. Inset: *Top:* Mechanism of 2-aza-cope reaction-based fluorescent probes for detecting formaldehyde. *Bottom*: Mechanism of Mbo, a 'turn-on' fluorescent probe for methylglyoxal. Other hydrazine-based probes for detecting malondialdehyde and formaldehyde work on similar principle.

Other detection methods of formaldehyde have used a hydrazine conjugated to a fluorophore [111,102]. In the native state, the free amine on the hydrazine quenches fluorescence of the conjugated fluorophore using photoinduced electron transfer (PET). Upon reaction with the aldehyde, the hydrazine forms a formimine, which blocks PET, thus turning-on fluorescence (**Figure 1.9)**.

Similar methods using hydrazine conjugated fluorophores have also been used to detect other reactive aldehydes. Some probes have been developed wherein a molecule containing a dye and a quencher in tandem is split to a free dye upon exposure of a hydrazide to generic carbonyl-containing compounds[112]. This strategy is quite elegant in its design and can give good signal to noise (again when cells treated with the molecules are exposed to exogenous carbonyl compound). One drawback of this method is that a catalyst is required to drive fragmentation of the self-quenching molecule. Such two-component systems make it particularly difficult to design good controls, and should be avoided. Finally, a similar sensor of malondialdehyde has been reported. In this set up, a pendant hydrazine moiety quenches a dye to which it is attached through PET transfer[113]. When hydrazine reacts with malondialdehyde, PET is reduced, and fluorescence is activated (**Figure 1.9)**.

Indirect method to profile cysteine modification by RES using ABPP

Activity-based protein profiling (ABPP) has emerged as a powerful tool to rank the activities of proteins in a complex proteome. Earlier use of ABPP focused on the use of active-site directed chemical probes to profile cysteine proteases[114] and serine hydrolases[115]. Mass spectrometry platform coupled with ABPP—dubbed tandem

orthogonal proteolysis (TOP)-ABPP—has allowed for simultaneous detection (albeit indirect using proxy probes) of protein targets and the sites modified by chemical probes[116,117]. Using TOP-ABPP it was shown that different classes of electrophiles exhibit distinct labeling profiles in a "soluble mouse proteome" (lysate). Chloroacetamide and α, β-unsaturated ketone probes showed selectivity towards cysteine, whereas phenylsulfonate esters also targeted aspartate, glutamate, tyrosine and histidine residues in addition to cysteines[116]. More importantly, all electrophiles showed reactivity toward functional residues in enzymes despite the large excess of non-functional residues in the proteome, suggesting that functional residues display enhanced nucleophilicity. ABPP using isotope-labeled tags, called isoTOP-ABPP, was recently used to quantitatively profile 'hyper reactive' cysteines in the proteome[117]. isoTOP-ABPP uses a pan-reactive alkylating probe such as iodoacetamide that can covalently modify reactive cysteines in the proteome. Soluble lysate is first treated with different concentrations of the iodoacetamide probe. An alkyne handle on the probe allows for click conjugation with either heavy or light isotope-labeled cleavable tags. Subsequent enrichment of probe-modified reactive cysteines and mass spectrometry allows quantitative comparison of the reactivities of the cysteine residue towards the electrophilic probe. Modification of the ABPP method using a competitive electrophilic probe, called competitive isoTOP-ABPP, has allowed identification of LDE-sensitive sites in the proteomes[70]. In this method, a cell/ soluble proteome is first treated with a competitive electrophilic LDEs. The control set is treated with just the vehicle DMSO (**Figure 1.10)**. Subsequently, both set of cells are lysed independently and the lysate labeled with alkyne-functionalized iodoacetamide. Click using isotope labeled tags and

subsequent MS analysis allows for the quantitation of cysteines that are sensitive to LDE modification. A decrease in ratio of cysteine-containing peptide in the LDE-treated cells compared to untreated samples identifies modified cysteine residues. Competitive isoTOP-ABPP was used to quantitatively profile the reactivities of >1000 proteins to three representative electrophiles HNE, 2-*trans*-hexadecenal (2-HD) and 15d-PGJ_2[70].

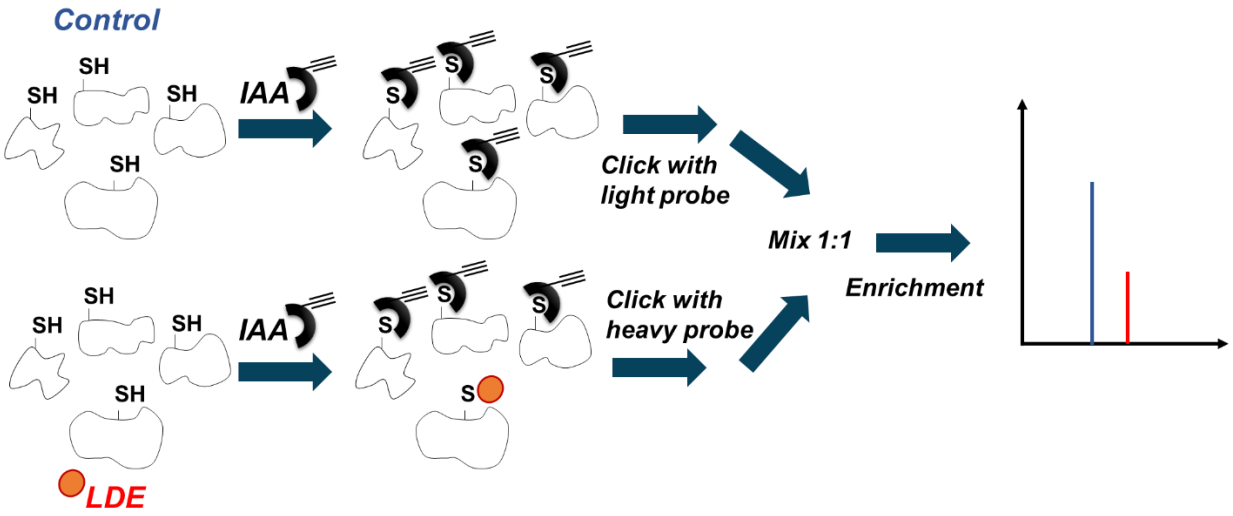

Figure 1.10 Isotope-labeling methods coupled with MS approaches allow quantitative determination of protein modification. In methods such as competitive-isoTOP ABPP, the experimental sample is treated with the desired LDE (red/orange circle) and the control sample is treated with the vehicle. The unreacted cysteines in the protein lysate are then capped with alkylating agents with an alkyne handle (IA alkyne; IAA) which enables click-coupling with isotope labelled and TEV-protease-cleavable-biotin azide. The samples are then mixed 1:1, enriched using streptavidin beads, the bound proteins are eluted using TEV protease, and a MS analysis performed subsequent to trypsin digestion. Proteins labeled with LDE won't react with alkyne-tagged alkylating agents resulting in a loss in signal intensity in MS spectrum.

While indirect approaches to profile RES-sensitive proteome have proven to be invaluable tools, they suffer from several important drawbacks. As this method measures loss of labeling, it is prone to false positives: if modification of a functionally-

coupled residue to a cysteine hinders its ability to label the probe and therefore its detection, it may show up as a positive hit. Independent secondary validation can mitigate such problems, although overall reduces the utility of the method. Additionally, there is no precise information provided on what mechanism leads to loss of the proxy: the profiled residue could possibly be modified in several ways other than by the compound of interest including oxidation, degradation, change in secondary associations and disulfide bond formation. Moreover, ABPP methods require treatment with the probe in lysate because of probe impermeability and/or toxicity[70,117,118]. This strategy is ultimately flawed since different cellular components are at different redox states[119] and the oxidation state of the cysteine residues may be affected giving confounding results. Moreover, uncontrolled bulk exposure of cells and organisms to reactive small-molecule signals may result in global modification of proteins that may not be physiologically relevant. Finally, this method will also likely not be able to identify residues that are endogenously significantly modified (either selectively in one compartment, or globally).

Direct methods to identify protein carbonylation using aldehyde capture

The reaction of hydrazine/hydrazides to aldehydes and ketones is one of the more widely used chemical strategies to capture targets of LDE modification (**Figure 1.11)**[120-122]. Carbonyl groups on LDE-modified protein react with the hydrazine group to form a hydrazone adduct. However, the resulting product contains unstable Schiff base functionality and necessitates reduction with sodium borohydride for downstream analysis. DNPH has been used to capture carbonyl modification on proteins, which can

be detected using anti-DNP antibodies in a method broadly known as OxyBlot[TM123-126]. Moreover, antibodies can be used for enrichment prior to LC-MS identification of protein targets[127]. Recently this method was coupled with 2D SDS-PAGE analysis to identify proteins that are carbonylated upon premature senescence in WI-38 fibroblasts[128]. Hydrazine conjugated with fluorophores[129], biotin[120] or dinitrobenzene have also been developed for determination of protein carbonylation by imaging[129], streptavidin enrichment[130] or western blot[120] respectively. Hydrazide-biotin probe coupled with LC-MS/MS has been used to identify oxidatively-induced protein carbonylation in brains of aged mice[131] and profile targets of various LDEs including HNE[132] , acrolein[133], MDA and ONE [134] (**Figure 1.11A)**. Global analysis of LDE-sensitive proteins upon treatment of human RKO cells with HNE, derivatization of the modified proteins using biotin hydrazide in lysate, and subsequent enrichment coupled with MS identified >1500 HNE-modified targets of which ~400 targets showed increase in HNE adduction upon increasing HNE concentration[132]. In line with the results from isoTOP-ABPP method[117], protein interaction network analysis has indicated several functional cellular networks as the hotspots of HNE modification including those involved in protein folding, degradation, and protein translation[116,117,132]. Surprisingly, only 25% of proteins identified using competitive isoTOP-ABPP were identified using carbonyl capture method. A possible reason could be the use of MDAMB-231 in the former study and RKO cells in the latter. Nonetheless, the small overlap in the HNE-sensitive proteins identified using two different approaches exemplifies the need to exercise caution when choosing the right profiling method for an experiment. A limitation of the DNPH-based method is that the detection of protein modification is not

specific to any particular LDE. Additionally, the reactivity of the hydrazine-based probe should also be taken into consideration. For example, DNPH can also react with sulfenic acid thus complicating the interpretation of results[135]. Finally, DNPH-based derivatizing methods have limited use for detecting modification of proteins by non-carbonyl-based electrophiles.

Profiling electrophile-responsive proteins using specific LDE-analogs

LDE-specific analogs mitigate some of the problems of DNPH-based carbonyl capture (**Figure 1.11B)**. They allow for profiling direct interaction of a specific LDE to proteins in the proteome. Of course, modification of the lipid can drastically change the lipid's properties. However, provided the probe is modified in a position likely to not perturb associations/reactivity too significantly and a good secondary downstream assay is available, this method can be useful. BODIPY conjugated with the electrophilic lipid 15d-PGJ_2 has been used to monitor the subcellular localization of the lipid[136-138]. Additionally, biotin-conjugated 15d-PGJ_2 has enabled enrichment and identification of protein targets of the electrophile in cells and isolated cellular organelles. 15d-PGJ2 was shown to promote calcium-induce swelling of isolated rat liver mitochondria and subsequent cytochrome-C release[139]. This induction was believed to be triggered as a result of covalent modification of various mitochondrial protein targets. Yet another group used a biotinylated probe called PLPBSO, an analog of glycerolphosphotidylcholine, an abundant phospholipid in biological membranes, supplemented to isolated human plasma to identify targets of lipid peroxidation products upon treatment with a free radical initiator[140,141]. Free radical oxidation of PLPBSO

results in oxidative cleavage to generate aldehydes which can modify proteins. LC-MS/MS coupled analysis subsequent to enrichment of protein targets by biotin affinity pulldown revealed apolipoproteinA1 (ApoA1), the principal component of high density lipoprotein, as the most highly lipid derived aldehyde modified protein[141]. Similarly, biotinylated arachidonic acid (AA) has been used to detect targets of various LDEs generated upon co-treatment of cells with oxidants such as hemin[138]. AA generates a number of LDEs upon non-enzymatic lipid peroxidation including HNE, isoketals and isoprostanes all of which are highly reactive and can modify proteins.

However, before using these tagged derivatives one must ensure that introduction of the tag does not significantly alter its physico-chemical and biological properties. It is essential to have appropriate controls to delineate any artifact associated with the tagged probes.

Biorthogonal tags such as alkyne, azido, and cyclooctyne are suitable alternatives to bulky fluorescent and biotin tags (**Figure 1.11B)**. The minor modification minimizes artifacts that can be observed due to even remote functionalization with bulky tags. Proteins modified with alkyne and cyclooctyne functionalized LDEs can be analyzed using in-gel fluorescence or enriched for LC-MS by conjugating with fluorophore or biotin tags using click chemistry and Staudinger ligation, respectively.

Alkyne-functionalized LDEs such as HNE and ONE are now routinely used for MS profiling experiments [68,142-144] (**Figure 1.11C**). One of the earliest examples is the use of HNE-alkyne/azide to profile HNE-sensitive targets in RKO cells[142]. Cells treated with the appropriate probe were lysed and conjugated with biotin-azide/alkyne using

Click chemistry. Subsequent enrichment using streptavidin beads and proteomic analysis identified several heat shock proteins and proteins involved in stress response pathways to be targets of alkyne/Azido-HNE in RKO cell lysate. A recent modification of the method used photo-releasable streptavidin linker to conjugate to HNE alkyne-modified human plasma proteins *in vitro*, thus minimizing elution of non-specific proteins bound to streptavidin beads [144]. Recently, a similar approach was used to profile protein targets of HNE and ONE added to RKO and THP-1 cells[143]. >1000 proteins were identified in each cell type to be sensitive to the electrophiles HNE and ONE. Interestingly, ~ 50% of the protein targets in each cell line were modified by both the electrophiles. Comparison of the protein targets revealed a list of 447 proteins that are susceptible to modification with both electrophiles in both cell types. Not surprisingly, these targets comprised of proteins important in various biological processes including protein translation, DNA replication, protein folding and metabolism[143]. Additionally, treatment with a range of electrophile concentrations and subsequent analyses showed that electrophile protein targets display distinct reactivity profiles in line with results obtained using competitive isoTOP-ABPP profiling methods[70]. However, only ~90 of the 800 targets identified using isoTOP-ABPP were also identified in THP1 cells to be modified with HNE or ONE alkyne at any concentration. The number of overlapping targets was even lower in RKO cells (64 targets) demonstrating that the individual method opted for MS profiling can have significant influence on the protein targets being identified. A recent advancement of the method to capture protein targets of electrophiles using LDE-analogs incorporated isotopically-labeled and photocleavable

azido-biotin reagent to capture and quantitatively assess protein targets of HNE alkyne in cells[68].

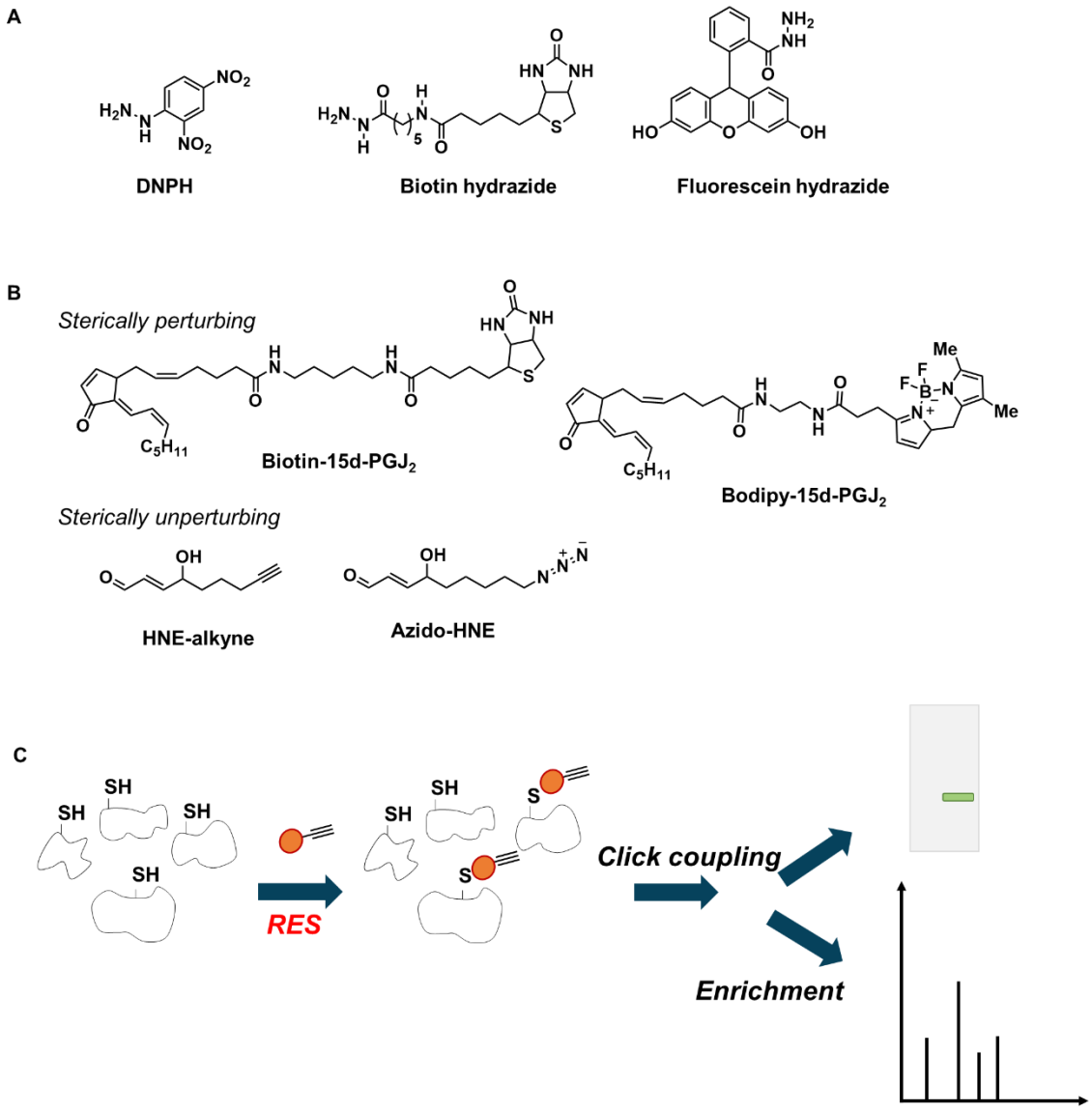

Figure 1.11: (**A**) A selection of nucleophilic probes used for aldehyde capture of proteins-modified with endogenous electrophilic signals. Biotinylated and fluorescently-labeled hydrazide can be used for aldehyde capture for detection by WB/mass spectrometry and in-gel fluorescence, respectively. (**B**) Biotinylated and fluorescently-labeled LDEs can also be used to directly enrich or detect protein targets. Alternatively, alkyne and azide functional groups provide non-intrusive handles to assess protein targets of electrophiles. (**C**) Schematic of direct methods for profiling LDE sensitive cysteines in the proteome. Cells/lysate are treated with an excess of

alkyne-functionalized RES (red diamond). Modified proteins are either observed using in-gel fluorescence after click-coupling with fluorophore-azide or enriched using streptavidin beads post click coupling with biotin azide. Subsequent MS reveals the modified peptides and the site of modification.

Limitation of current methods to study redox signaling

While current proteomics-based methods have proven extremely powerful in identifying LDE-sensitive proteins in the proteome, they suffer from some important drawbacks. Firstly, they all employ a bolus treatment of cells and model organisms with supra-physiological concentrations of reactive electrophiles. As discussed in the preceding sections, electrophilic modifications of protein targets are non-enzyme mediated and covalent in nature. While the relatively higher nucleophilicity of cysteine compared to other nucleophilic amino acid residues provides some degree of chemoselectivity, the covalent modifications on proteins by reactive electrophiles accrue over time as a function of dose of the electrophile treatment as well as the duration of treatment. As discussed above, HNE modifies ~1000 cysteine-active targets in a typical bolus dosing regimen. Thus, while these high-throughput methods have indeed been successful in identifying novel sensors, oftentimes, *important sensors are lost in noise stemming from off-target modifications of highly abundant proteins*.

Another significant challenge is the functional validation of an identified redox sensor. Many conventional signaling pathways function through a gain of function or a dominant loss of function, whereby target-specific and low stoichiometry modifications are sufficient to elicit a functional response. It is likely that redox signaling pathways also act in a similar way. Unfortunately, current *bolus dosing approaches provide no control in terms of target specificity or the stoichiometry of modification on a given*

redox sensing proteins. Bolus dosing methods typically recapitulate complete loss of function and are less amenable to the study of redox signaling

Furthermore, functional validation of a redox-sensing protein is currently undertaken using genetic approaches, such as mutation of a sensing cysteine residue to a corresponding serine/alanine or genetic knockdown of a redox-sensing protein. As we will discuss in the subsequent chapters, some proteins are promiscuous sensors of electrophiles and show functional redundancy in cysteine modification required for signaling responses thereby making mutation of a single sensing residue redundant. Knock-down strategies are useful; however, they disrupt signaling nodes. Additionally, during validation typically cells/organism lacking the sensing protein or expressing the mutant protein are again treated using bolus dosing regimen. As we will discuss in subsequent chapters, signaling pathways are highly complex. A biological outcome is controlled by multiple proteins, many of which can be redox-sensitive, that regulate each other and frequently cross-talk. Bolus dosing methods inevitably modify multiple proteins simultaneously making the functional outcome extremely challenging to interpret.

Considering the problems associated with current approaches, there is a need to develop a transposable method that will (1) Identify proteins that are true sensors of RES under electrophile-limited conditions (2) Selectively modify a single redox-sensitive protein in a spatial- and temporal-controlled manner in an otherwise unperturbed cellular/organismal backdrop (3) Uncover the functional consequence of a target-specific and low occupancy modification in cells and in whole organism.

The subsequent chapters discuss the development and use of such a method.

References

(1) Schopfer, F. J.; Cipollina, C.; Freeman, B. A. Formation and Signaling Actions of Electrophilic Lipids. *Chem. Rev.* **2011,** *111* (10), 5997.

(2) Rudolph, T. K.; Freeman, B. A. Transduction of Redox Signaling by Electrophile-Protein Reactions. *Science Signaling* **2009,** *2* (90), re7.

(3) Long, M. J. C.; Aye, Y. The Die Is Cast: Precision Electrophilic Modifications Contribute to Cellular Decision Making. *Chem. Res. Toxicol.* **2016,** *29* (10), 1575.

(4) Higdon, A.; Diers, A. R.; Oh, J. Y.; Landar, A.; Darley-Usmar, V. M. Cell signalling by reactive lipid species: new concepts and molecular mechanisms. *The Biochemical journal* **2012,** *442* (3), 453.

(5) Schwöbel, J. A. H.; Koleva, Y. K.; Enoch, S. J.; Bajot, F.; Hewitt, M.; Madden, J. C.; Roberts, D. W.; Schultz, T. W.; Cronin, M. T. D. Measurement and Estimation of Electrophilic Reactivity for Predictive Toxicology. *Chem. Rev.* **2011,** *111* (4), 2562.

(6) LoPachin, R. M.; Gavin, T. Reactions of electrophiles with nucleophilic thiolate sites: relevance to pathophysiological mechanisms and remediation. *Free Radic. Res.* **2016,** *50* (2), 195.

(7) Yang, Y.; Sharma, A.; Sharma, R.; Patrick, B.; Singhal, S. S.; Zimniak, P.; Awasthi, S.; Awasthi, Y. C. Cells Preconditioned with Mild, Transient UVA Irradiation Acquire Resistance to Oxidative Stress and UVA-induced Apoptosis: Role Of 4-Hydroxynonenal In Uva-Mediated Signaling For ApoptosiS. *J. Biol. Chem.* **2003,** *278* (42), 41380.

(8) Esterbauer, H.; Schaur, R. J.; Zollner, H. Chemistry and biochemistry of 4-hydroxynonenal, malonaldehyde and related aldehydes. *Free Radic. Biol. Med.* **1991,** *11* (1), 81.

(9) Baker, P. R. S.; Lin, Y.; Schopfer, F. J.; Woodcock, S. R.; Groeger, A. L.; Batthyany, C.; Sweeney, S.; Long, M. H.; Iles, K. E.; Baker, L. M. S.et al. Fatty Acid Transduction of Nitric Oxide Signaling: Multiple Nitrated Unsaturated Fatty Acid Derivatives Exist In Human Blood And Urine And Serve As Endogenous Peroxisome Proliferator-Activated Receptor Ligands. *J. Biol. Chem.* **2005,** *280* (51), 42464.

(10) Rudolph, V.; Rudolph, T. K.; Schopfer, F. J.; Bonacci, G.; Woodcock, S. R.; Cole, M. P.; Baker, P. R. S.; Ramani, R.; Freeman, B. A. Endogenous generation and protective effects of nitro-fatty acids in a murine model of focal cardiac ischaemia and reperfusion. *Cardiovasc. Res.* **2010,** *85* (1), 155.

(11) Long, M. J.; Lin, H.-Y.; Parvez, S.; Zhao, Y.; Poganik, J. R.; Huang, P.; Aye, Y. β-TrCP1 Is a Vacillatory Regulator of Wnt Signaling. *Cell Chemical Biology 24* (8), 944.

(12) Nusse, R. Wnt signaling in disease and in development. *Cell Res.* **2005,** *15* (1), 28.

(13) Gil, L.; Siems, W.; Mazurek, B.; Gross, J.; Schroeder, P.; Voss, P.; Grune, T. Age-associated analysis of oxidative stress parameters in human plasma and erythrocytes. *Free Radic. Res.* **2006,** *40* (5), 495.

(14) Dalleau, S.; Baradat, M.; Gueraud, F.; Huc, L. Cell death and diseases related to oxidative stress:4-hydroxynonenal (HNE) in the balance. *Cell Death Differ.* **2013,** *20* (12), 1615.
(15) Rossi, A.; Kapahi, P.; Natoli, G.; Takahashi, T.; Chen, Y.; Karin, M.; Santoro, M. G. Anti-inflammatory cyclopentenone prostaglandins are direct inhibitors of IκB kinase. *Nature* **2000,** *403*, 103.
(16) Cui, T.; Schopfer, F. J.; Zhang, J.; Chen, K.; Ichikawa, T.; Baker, P. R. S.; Batthyany, C.; Chacko, B. K.; Feng, X.; Patel, R. P.et al. Nitrated Fatty Acids: Endogenous Anti-inflammatory Signaling Mediators. *J. Biol. Chem.* **2006,** *281* (47), 35686.
(17) Ji, C.; Kozak, K. R.; Marnett, L. J. IκB Kinase, a Molecular Target for Inhibition by 4-Hydroxy-2-nonenal. *J. Biol. Chem.* **2001,** *276* (21), 18223.
(18) Villacorta, L.; Zhang, J.; Garcia-Barrio, M. T.; Chen, X.-l.; Freeman, B. A.; Chen, Y. E.; Cui, T. Nitro-linoleic acid inhibits vascular smooth muscle cell proliferation via the Keap1/Nrf2 signaling pathway. *American journal of physiology. Heart and circulatory physiology* **2007,** *293* (1), H770.
(19) Parvez, S.; Fu, Y.; Li, J.; Long, M. J. C.; Lin, H.-Y.; Lee, D. K.; Hu, G. S.; Aye, Y. Substoichiometric Hydroxynonenylation of a Single Protein Recapitulates Whole-Cell-Stimulated Antioxidant Response. *J. Am. Chem. Soc.* **2015,** *137* (1), 10.
(20) Lin, H.-Y.; Haegele, J. A.; Disare, M. T.; Lin, Q.; Aye, Y. A Generalizable Platform for Interrogating Target- and Signal-Specific Consequences of Electrophilic Modifications in Redox-Dependent Cell Signaling. *J. Am. Chem. Soc.* **2015,** *137* (19), 6232.
(21) Cipollina, C. Endogenous Generation and Signaling Actions of Omega-3 Fatty Acid Electrophilic Derivatives. *BioMed Research International* **2015,** *2015*, 13.
(22) Rothe, T.; Gruber, F.; Uderhardt, S.; Ipseiz, N.; Rössner, S.; Oskolkova, O.; Blüml, S.; Leitinger, N.; Bicker, W.; Bochkov, V. N.et al. 12/15-lipoxygenase–mediated enzymatic lipid oxidation regulates DC maturation and function. *The Journal of Clinical Investigation* **2015,** *125* (5), 1944.
(23) Clark, S. R.; Guy, C. J.; Scurr, M. J.; Taylor, P. R.; Kift-Morgan, A. P.; Hammond, V. J.; Thomas, C. P.; Coles, B.; Roberts, G. W.; Eberl, M.et al. Esterified eicosanoids are acutely generated by 5-lipoxygenase in primary human neutrophils and in human and murine infection. *Blood* **2011,** *117* (6), 2033.
(24) Groeger, A. L.; Cipollina, C.; Cole, M. P.; Woodcock, S. R.; Bonacci, G.; Rudolph, T. K.; Rudolph, V.; Freeman, B. A.; Schopfer, F. J. Cyclooxygenase-2 generates anti-inflammatory mediators from omega-3 fatty acids. *Nature Chemical Biology* **2010,** *6*, 433.
(25) Cipollina, C.; Salvatore, S. R.; Muldoon, M. F.; Freeman, B. A.; Schopfer, F. J. Generation and Dietary Modulation of Anti-Inflammatory Electrophilic Omega-3 Fatty Acid Derivatives. *PLoS One* **2014,** *9* (4), e94836.
(26) Hwa Lee, S.; Rangiah, K.; Williams, M. V.; Wehr, A. Y.; DuBois, R. N.; Blair, I. A. Cyclooxygenase-2-Mediated Metabolism of Arachidonic Acid to 15-Oxo-

eicosatetraenoic Acid by Rat Intestinal Epithelial Cells. *Chem. Res. Toxicol.* **2007,** *20* (11), 1665.
(27) Fischer, R.; Konkel, A.; Mehling, H.; Blossey, K.; Gapelyuk, A.; Wessel, N.; von Schacky, C.; Dechend, R.; Muller, D. N.; Rothe, M.et al. Dietary omega-3 fatty acids modulate the eicosanoid profile in man primarily via the CYP-epoxygenase pathway. *J. Lipid Res.* **2014,** *55* (6), 1150.
(28) Dennis, E. A.; Norris, P. C. Eicosanoid Storm in Infection and Inflammation. *Nature reviews. Immunology* **2015,** *15* (8), 511.
(29) Belton, O.; Fitzgerald, D. J. Cyclooxygenase isoforms and atherosclerosis. *Expert Rev. Mol. Med.* **2004,** *5* (9), 1.
(30) Shibata, T.; Kondo, M.; Osawa, T.; Shibata, N.; Kobayashi, M.; Uchida, K. 15-Deoxy-Δ12,14-prostaglandin J2 : a prostaglandin d2 metabolite generated during inflammatory processes. *J. Biol. Chem.* **2002,** *277* (12), 10459.
(31) Hoffmann, C. COX-2 in Brain and Spinal Cord - Implications for Therapeutic Use. *Curr. Med. Chem.* **2000,** *7* (11), 1113.
(32) Jones, D. A.; Carlton, D. P.; McIntyre, T. M.; Zimmerman, G. A.; Prescott, S. M. Molecular cloning of human prostaglandin endoperoxide synthase type II and demonstration of expression in response to cytokines. *J. Biol. Chem.* **1993,** *268* (12), 9049.
(33) Rouzer, C. A.; Marnett, L. J. Endocannabinoid Oxygenation by Cyclooxygenases, Lipoxygenases, and Cytochromes P450: Cross-Talk between the Eicosanoid and Endocannabinoid Signaling Pathways. *Chem. Rev.* **2011,** *111* (10), 5899.
(34) Chen, Y.; Morrow, J. D.; Roberts, L. J. Formation of Reactive Cyclopentenone Compounds in Vivo as Products of the Isoprostane Pathway. *J. Biol. Chem.* **1999,** *274* (16), 10863.
(35) Cipollina, C. Endogenous Generation and Signaling Actions of Omega-3 Fatty Acid Electrophilic Derivatives. *BioMed research international* **2015,** *2015*, 501792.
(36) Ayala, A.; Mu; oz, M. F.; Arg; elles, S. Lipid Peroxidation: Production, Metabolism, and Signaling Mechanisms of Malondialdehyde and 4-Hydroxy-2-Nonenal. *Oxid. Med. Cell. Longev.* **2014,** *2014*, 31.
(37) Halliwell, B. How to characterize an antioxidant: an update. *Biochem. Soc. Symp.* **1995,** *61*, 73.
(38) Radi, R. Peroxynitrite, a Stealthy Biological Oxidant. *The Journal of Biological Chemistry* **2013,** *288* (37), 26464.
(39) Pratt, D. A.; Mills, J. H.; Porter, N. A. Theoretical Calculations of Carbon−Oxygen Bond Dissociation Enthalpies of Peroxyl Radicals Formed in the Autoxidation of Lipids. *J. Am. Chem. Soc.* **2003,** *125* (19), 5801.
(40) Porter, N. A.; Lehman, L. S.; Weber, B. A.; Smith, K. J. Unified mechanism for polyunsaturated fatty acid autoxidation. Competition of peroxy radical hydrogen atom abstraction, .beta.-scission, and cyclization. *J. Am. Chem. Soc.* **1981,** *103* (21), 6447.
(41) Yin, H.; Xu, L.; Porter, N. A. Free Radical Lipid Peroxidation: Mechanisms and Analysis. *Chem. Rev.* **2011,** *111* (10), 5944.

(42) Schneider, C.; Porter, N. A.; Brash, A. R. Routes to 4-Hydroxynonenal: Fundamental Issues in the Mechanisms of Lipid Peroxidation. *The Journal of Biological Chemistry* **2008,** *283* (23), 15539.
(43) Groeger, A. L.; Freeman, B. A. Signaling Actions of Electrophiles: Anti-inflammatory Therapeutic Candidates. *Mol. Interventions* **2010,** *10* (1), 39.
(44) Tennyson, Andrew G.; Lippard, Stephen J. Generation, Translocation, and Action of Nitric Oxide in Living Systems. *Chemistry & Biology 18* (10), 1211.
(45) Paulsen, C. E.; Carroll, K. S. Cysteine-Mediated Redox Signaling: Chemistry, Biology, and Tools for Discovery. *Chem. Rev.* **2013,** *113* (7), 4633.
(46) Freeman, B. A.; Baker, P. R. S.; Schopfer, F. J.; Woodcock, S. R.; Napolitano, A.; d'Ischia, M. Nitro-fatty Acid Formation and Signaling. *The Journal of Biological Chemistry* **2008,** *283* (23), 15515.
(47) Gorczynski, M. J.; Smitherman, P. K.; Akiyama, T. E.; Wood, H. B.; Berger, J. P.; King, S. B.; Morrow, C. S. Activation of peroxisome proliferator-activated receptor γ (PPARγ) by nitroalkene fatty acids: importance of nitration position and degree of unsaturation. *J. Med. Chem.* **2009,** *52* (15), 4631.
(48) Akaike, T.; Nishida, M.; Fujii, S. Regulation of redox signalling by an electrophilic cyclic nucleotide. *The Journal of Biochemistry* **2013,** *153* (2), 131.
(49) Sawa, T.; Zaki, M. H.; Okamoto, T.; Akuta, T.; Tokutomi, Y.; Kim-Mitsuyama, S.; Ihara, H.; Kobayashi, A.; Yamamoto, M.; Fujii, S.et al. Protein S-guanylation by the biological signal 8-nitroguanosine 3′,5′-cyclic monophosphate. *Nat. Chem. Biol.* **2007,** *3*, 727.
(50) Fujii, S.; Sawa, T.; Ihara, H.; Tong, K. I.; Ida, T.; Okamoto, T.; Ahtesham, A. K.; Ishima, Y.; Motohashi, H.; Yamamoto, M.et al. The Critical Role of Nitric Oxide Signaling, via Protein S-Guanylation and Nitrated Cyclic GMP, in the Antioxidant Adaptive Response. *The Journal of Biological Chemistry* **2010,** *285* (31), 23970.
(51) Bell-Parikh, L. C.; Ide, T.; Lawson, J. A.; McNamara, P.; Reilly, M.; FitzGerald, G. A. Biosynthesis of 15-deoxy-Δ(12,14)-PGJ(2) and the ligation of PPARγ. *J. Clin. Invest.* **2003,** *112* (6), 945.
(52) Williams, T. I.; Lynn, B. C.; Markesbery, W. R.; Lovell, M. A. Increased levels of 4-hydroxynonenal and acrolein, neurotoxic markers of lipid peroxidation, in the brain in Mild Cognitive Impairment and early Alzheimer's disease. *Neurobiology of Aging 27* (8), 1094.
(53) Sultana, R.; Perluigi, M.; Newman, S. F.; Pierce, W. M.; Cini, C.; Coccia, R.; Butterfield, D. A. Redox Proteomic Analysis of Carbonylated Brain Proteins in Mild Cognitive Impairment and Early Alzheimer's Disease. *Antioxidants & redox signaling* **2010,** *12* (3), 327.
(54) Verrastro, I.; Pasha, S.; Tveen Jensen, K.; Pitt, A. R.; Spickett, C. M. Mass Spectrometry-Based Methods for Identifying Oxidized Proteins in Disease: Advances and Challenges. *Biomolecules* **2015,** *5* (2), 378.
(55) Ji, Y.; Dai, Z.; Wu, G.; Wu, Z. 4-Hydroxy-2-nonenal induces apoptosis by activating ERK1/2 signaling and depleting intracellular glutathione in intestinal epithelial cells. *Sci. Rep.* **2016,** *6*, 32929.

(56) Lee, H.-R.; Cho, J.-M.; Shin, D.-h.; Yong, C. S.; Choi, H.-G.; Wakabayashi, N.; Kwak, M.-K. Adaptive response to GSH depletion and resistance to l-buthionine-(S,R)-sulfoximine: involvement of Nrf2 activation. *Mol. Cell. Biochem.* **2008,** *318* (1), 23.
(57) Doorn, J. A.; Petersen, D. R. Covalent Modification of Amino Acid Nucleophiles by the Lipid Peroxidation Products 4-Hydroxy-2-nonenal and 4-Oxo-2-nonenal. *Chem. Res. Toxicol.* **2002,** *15* (11), 1445.
(58) Baker, L. M. S.; Baker, P. R. S.; Golin-Bisello, F.; Schopfer, F. J.; Fink, M.; Woodcock, S. R.; Branchaud, B. P.; Radi, R.; Freeman, B. A. Nitro-fatty Acid Reaction with Glutathione and Cysteine: kinetic analysis of thiol alkylation by a michael addition reaction. *The Journal of biological chemistry* **2007,** *282* (42), 31085.
(59) Eggler, A. L.; Savinov, S. N. Chemical and biological mechanisms of phytochemical activation of Nrf2 and importance in disease prevention. *Recent advances in phytochemistry* **2013,** *43*, 121.
(60) Dinkova-Kostova, A. T.; Kostov, R. V. Glucosinolates and isothiocyanates in health and disease. *Trends in Molecular Medicine 18* (6), 337.
(61) Zhang, Y.; Talalay, P. Anticarcinogenic Activities of Organic Isothiocyanates: Chemistry and Mechanisms. *Cancer Res.* **1994,** *54* (7 Supplement), 1976s.
(62) Dinkova-Kostova, A.; Talalay, P. *Relation of structure of curcumin analogs to their potencies as inducers of Phase 2 detoxification enzymes*, 1999.
(63) Huang, T.-C.; Chung, Y.-L.; Wu, M.-L.; Chuang, S.-M. Cinnamaldehyde Enhances Nrf2 Nuclear Translocation to Upregulate Phase II Detoxifying Enzyme Expression in HepG2 Cells. *J. Agric. Food Chem.* **2011,** *59* (9), 5164.
(64) Feng, Z.; Hu, W.; Hu, Y.; Tang, M.-s. Acrolein is a major cigarette-related lung cancer agent: Preferential binding at p53 mutational hotspots and inhibition of DNA repair. *Proc. Natl. Acad. Sci. U. S. A.* **2006,** *103* (42), 15404.
(65) Linnell, R. H.; Scott, W. E. Diesel Exhaust Composition and Odor Studies. *J. Air Pollut. Control Assoc.* **1962,** *12* (11), 510.
(66) Anderson, M. M.; Hazen, S. L.; Hsu, F. F.; Heinecke, J. W. Human neutrophils employ the myeloperoxidase-hydrogen peroxide-chloride system to convert hydroxy-amino acids into glycolaldehyde, 2-hydroxypropanal, and acrolein. A mechanism for the generation of highly reactive alpha-hydroxy and alpha,beta-unsaturated aldehydes by phagocytes at sites of inflammation. *J. Clin. Invest.* **1997,** *99* (3), 424.
(67) Moghe, A.; Ghare, S.; Lamoreau, B.; Mohammad, M.; Barve, S.; McClain, C.; Joshi-Barve, S. Molecular Mechanisms of Acrolein Toxicity: Relevance to Human Disease. *Toxicol. Sci.* **2015,** *143* (2), 242.
(68) Yang, J.; Tallman, K. A.; Porter, N. A.; Liebler, D. C. Quantitative Chemoproteomics for Site-Specific Analysis of Protein Alkylation by 4-Hydroxy-2-Nonenal in Cells. *Anal. Chem.* **2015,** *87* (5), 2535.
(69) Chen, Y.; Cong, Y.; Quan, B.; Lan, T.; Chu, X.; Ye, Z.; Hou, X.; Wang, C. Chemoproteomic profiling of targets of lipid-derived electrophiles by bioorthogonal aminooxy probe. *Redox Biology* **2017,** *12* (Supplement C), 712.

(70) Wang, C.; Weerapana, E.; Blewett, M. M.; Cravatt, B. F. A chemoproteomic platform to quantitatively map targets of lipid-derived electrophiles. *Nat Meth* **2014,** *11* (1), 79.
(71) Connor, R. E.; Marnett, L. J.; Liebler, D. C. Protein-Selective Capture to Analyze Electrophile Adduction of Hsp90 by 4-Hydroxynonenal. *Chemical Research in Toxicology* **2011,** *24* (8), 1275.
(72) Uchida, K.; Stadtman, E. R. Covalent attachment of 4-hydroxynonenal to glyceraldehyde-3-phosphate dehydrogenase. A possible involvement of intra- and intermolecular cross-linking reaction. *J. Biol. Chem.* **1993,** *268* (9), 6388.
(73) Ishii, T.; Tatsuda, E.; Kumazawa, S.; Nakayama, T.; Uchida, K. Molecular Basis of Enzyme Inactivation by an Endogenous Electrophile 4-Hydroxy-2-nonenal: Identification of Modification Sites in Glyceraldehyde-3-phosphate Dehydrogenase. *Biochemistry* **2003,** *42* (12), 3474.
(74) Shibata, T.; Shimozu, Y.; Wakita, C.; Shibata, N.; Kobayashi, M.; Machida, S.; Kato, R.; Itabe, H.; Zhu, X.; Sayre, L. M.et al. Lipid Peroxidation Modification of Protein Generates N(ϵ)-(4-Oxononanoyl)lysine as a Pro-inflammatory Ligand. *The Journal of Biological Chemistry* **2011,** *286* (22), 19943.
(75) Jin, J.; He, B.; Zhang, X.; Lin, H.; Wang, Y. SIRT2 Reverses 4-Oxononanoyl Lysine Modification on Histones. *J. Am. Chem. Soc.* **2016,** *138* (38), 12304.
(76) Batthyany, C.; Schopfer, F. J.; Baker, P. R. S.; Durán, R.; Baker, L. M. S.; Huang, Y.; Cerveñansky, C.; Branchaud, B. P.; Freeman, B. A. Reversible Post-translational Modification of Proteins by Nitrated Fatty Acids in Vivo. *J. Biol. Chem.* **2006,** *281* (29), 20450.
(77) Zhang, X. M.; Bordwell, F. G.; Van Der Puy, M.; Fried, H. E. Equilibrium acidities and homolytic bond dissociation energies of the acidic carbon-hydrogen bonds in N-substituted trimethylammonium and pyridinium cations. *The Journal of Organic Chemistry* **1993,** *58* (11), 3060.
(78) Matthews, W. S.; Bares, J. E.; Bartmess, J. E.; Bordwell, F. G.; Cornforth, F. J.; Drucker, G. E.; Margolin, Z.; McCallum, R. J.; McCollum, G. J.; Vanier, N. R. Equilibrium acidities of carbon acids. VI. Establishment of an absolute scale of acidities in dimethyl sulfoxide solution. *J. Am. Chem. Soc.* **1975,** *97* (24), 7006.
(79) Guo, H.; Aleyasin, H.; Dickinson, B. C.; Haskew-Layton, R. E.; Ratan, R. R. Recent advances in hydrogen peroxide imaging for biological applications. *Cell & Bioscience* **2014,** *4* (1), 64.
(80) Kalyanaraman, B.; Darley-Usmar, V.; Davies, K. J. A.; Dennery, P. A.; Forman, H. J.; Grisham, M. B.; Mann, G. E.; Moore, K.; Roberts, L. J.; Ischiropoulos, H. Measuring reactive oxygen and nitrogen species with fluorescent probes: challenges and limitations. *Free Radic. Biol. Med.* **2012,** *52* (1), 1.
(81) Stöcker, S.; Van Laer, K.; Mijuskovic, A.; Dick, T. P. The Conundrum of Hydrogen Peroxide Signaling and the Emerging Role of Peroxiredoxins as Redox Relay Hubs. *Antioxidants & redox signaling* **2017**, DOI:10.1089/ars.2017.7162 10.1089/ars.2017.7162.

(82) Lukyanov, K. A.; Belousov, V. V. Genetically encoded fluorescent redox sensors. *Bba-Gen Subjects* **2014,** *1840*.
(83) Spasojević, I. Free radicals and antioxidants at a glance using EPR spectroscopy. *Crit. Rev. Clin. Lab. Sci.* **2011,** *48* (3), 114.
(84) Villamena, F. A.; Zweier, J. L. Detection of reactive oxygen and nitrogen species by EPR spin trapping. *Antioxid. Redox Signal.* **2004,** *6* (3), 619.
(85) Roubaud, V.; Sankarapandi, S.; Kuppusamy, P.; Tordo, P.; Zweier, J. L. Quantitative Measurement of Superoxide Generation Using the Spin Trap 5-(Diethoxyphosphoryl)-5-methyl- 1-pyrroline-N-oxide. *Anal. Biochem.* **1997,** *247* (2), 404.
(86) Abbas, K.; Babić, N.; Peyrot, F. Use of spin traps to detect superoxide production in living cells by electron paramagnetic resonance (EPR) spectroscopy. *Methods* **2016,** *109* (Supplement C), 31.
(87) Villamena, F. A.; Zweier, J. L. Detection of Reactive Oxygen and Nitrogen Species by EPR Spin Trapping. *Antioxidants & redox signaling* **2004,** *6* (3), 619.
(88) Kelicen, P.; Cantuti-Castelvetri, I.; Pekiner, C.; Paulson, K. E. The spin trapping agent PBN stimulates H2O2-induced Erk and Src kinase activity in human neuroblastoma cells. *Neuroreport* **2002,** *13* (8), 1057.
(89) Das, A.; Gopalakrishnan, B.; Voss, O. H.; Doseff, A. I.; Villamena, F. A. Inhibition of ROS-induced apoptosis in endothelial cells by nitrone spin traps via induction of phase II enzymes and suppression of mitochondria-dependent pro-apoptotic signaling. *Biochem. Pharmacol.* **2012,** *84* (4), 486.
(90) Venkataraman, S.; Schafer, F. Q.; Buettner, G. R. Detection of Lipid Radicals Using EPR. *Antioxidants & redox signaling* **2004,** *6* (3), 631.
(91) North, J. A.; Spector, A. A.; Buettner, G. R. Detection of lipid radicals by electron paramagnetic resonance spin trapping using intact cells enriched with polyunsaturated fatty acid. *J. Biol. Chem.* **1992,** *267* (9), 5743.
(92) Stolze, K.; Udilova, N.; Nohl, H. In *Biol. Chem.*, 2002; Vol. 383.
(93) Swartz, H. M. Use of nitroxides to measure redox metabolism in cells and tissues. *Journal of the Chemical Society, Faraday Transactions 1: Physical Chemistry in Condensed Phases* **1987,** *83* (1), 191.
(94) Swartz, H. M.; Khan, N.; Buckey, J.; Comi, R.; Gould, L.; Grinberg, O.; Hartford, A.; Hopf, H.; Hou, H.; Hug, E.et al. Clinical applications of EPR: overview and perspectives. *NMR Biomed.* **2004,** *17* (5), 335.
(95) Ranguelova, K.; Mason, R. P. The fidelity of spin trapping with DMPO in biological systems. *Magn. Reson. Chem.* **2011,** *49* (4), 152.
(96) Takayanagi, T.; Kimiya, H.; Ohyama, T. Formation of artifactual DMPO-OH spin adduct in acid solutions containing nitrite ions. *Free Radic. Res.* **2017,** *51* (7-8), 739.
(97) Leinisch, F.; Jiang, J.; DeRose, E. F.; Khramtsov, V. V.; Mason, R. P. Investigation of spin-trapping artifacts formed by the Forrester-Hepburn mechanism. *Free Radic. Biol. Med.* **2013,** *65* (Supplement C), 1497.

(98) Yamada, K.-i.; Mito, F.; Matsuoka, Y.; Ide, S.; Shikimachi, K.; Fujiki, A.; Kusakabe, D.; Ishida, Y.; Enoki, M.; Tada, A.et al. Fluorescence probes to detect lipid-derived radicals. *Nat Chem Biol* **2016,** *12* (8), 608.
(99) Goldring, C.; Casini, A. F.; Maellaro, E.; Del Bello, B.; Comporti, M. Determination of 4-hydroxynonenal by high-performance liquid chromatography with electrochemical detection. *Lipids* **1993,** *28* (2), 141.
(100) Esterbauer, H.; Zollern, H. Methods for determination of aldehydic lipid peroxidation products. *Free Radical Biology and Medicine* **1989,** *7* (2), 197.
(101) Spickett, C. M. The lipid peroxidation product 4-hydroxy-2-nonenal: Advances in chemistry and analysis(). *Redox Biology* **2013,** *1* (1), 145.
(102) Bruemmer, K. J.; Brewer, T. F.; Chang, C. J. Fluorescent probes for imaging formaldehyde in biological systems. *Curr. Opin. Chem. Biol.* **2017,** *39* (Supplement C), 17.
(103) d'A. Heck, H.; White, E. L.; Casanova-Schmitz, M. Determination of formaldehyde in biological tissues by gas chromatography/mass spectrometry. *Biol. Mass Spectrom.* **1982,** *9* (8), 347.
(104) Tong, Z.; Han, C.; Luo, W.; Wang, X.; Li, H.; Luo, H.; Zhou, J.; Qi, J.; He, R. Accumulated hippocampal formaldehyde induces age-dependent memory decline. *Age* **2013,** *35* (3), 583.
(105) Brewer, T. F.; Chang, C. J. An Aza-Cope Reactivity-Based Fluorescent Probe for Imaging Formaldehyde in Living Cells. *J. Am. Chem. Soc.* **2015,** *137* (34), 10886.
(106) Roth, A.; Li, H.; Anorma, C.; Chan, J. A Reaction-Based Fluorescent Probe for Imaging of Formaldehyde in Living Cells. *J. Am. Chem. Soc.* **2015,** *137* (34), 10890.
(107) Bruemmer, K. J.; Walvoord, R. R.; Brewer, T. F.; Burgos-Barragan, G.; Wit, N.; Pontel, L. B.; Patel, K. J.; Chang, C. J. Development of a General Aza-Cope Reaction Trigger Applied to Fluorescence Imaging of Formaldehyde in Living Cells. *Journal of the American Chemical Society* **2017,** *139* (15), 5338.
(108) Brewer, T. F.; Burgos-Barragan, G.; Wit, N.; Patel, K. J.; Chang, C. J. A 2-aza-Cope reactivity-based platform for ratiometric fluorescence imaging of formaldehyde in living cells. *Chemical Science* **2017,** *8* (5), 4073.
(109) Wang, T.; Douglass, E. F.; Fitzgerald, K. J.; Spiegel, D. A. A "Turn-On" Fluorescent Sensor for Methylglyoxal. *J. Am. Chem. Soc.* **2013,** *135* (33), 12429.
(110) Chaplen, F. W. R.; Fahl, W. E.; Cameron, D. C. Evidence of high levels of methylglyoxal in cultured Chinese hamster ovary cells. *Proc. Natl. Acad. Sci. U. S. A.* **1998,** *95* (10), 5533.
(111) Tang, Y.; Kong, X.; Xu, A.; Dong, B.; Lin, W. Development of a Two-Photon Fluorescent Probe for Imaging of Endogenous Formaldehyde in Living Tissues. *Angew. Chem. Int. Ed.* **2016,** *55* (10), 3356.
(112) Yuen, L. H.; Saxena, N. S.; Park, H. S.; Weinberg, K.; Kool, E. T. Dark Hydrazone Fluorescence Labeling Agents Enable Imaging of Cellular Aldehydic Load. *ACS Chem. Biol.* **2016,** *11* (8), 2312.

(113) Chen, J.; Zeng, L.; Xia, T.; Li, S.; Yan, T.; Wu, S.; Qiu, G.; Liu, Z. Toward a Biomarker of Oxidative Stress: A Fluorescent Probe for Exogenous and Endogenous Malondialdehyde in Living Cells. *Anal. Chem.* **2015,** *87* (16), 8052.
(114) Kato, D.; Boatright, K. M.; Berger, A. B.; Nazif, T.; Blum, G.; Ryan, C.; Chehade, K. A. H.; Salvesen, G. S.; Bogyo, M. Activity-based probes that target diverse cysteine protease families. *Nat. Chem. Biol.* **2005,** *1* (1), 33.
(115) Liu, Y.; Patricelli, M. P.; Cravatt, B. F. Activity-based protein profiling: The serine hydrolases. *Proceedings of the National Academy of Sciences* **1999,** *96* (26), 14694.
(116) Weerapana, E.; Simon, G. M.; Cravatt, B. F. Disparate proteome reactivity profiles of carbon electrophiles. *Nat. Chem. Biol.* **2008,** *4* (7), 405.
(117) Weerapana, E.; Wang, C.; Simon, G. M.; Richter, F.; Khare, S.; Dillon, M. B. D.; Bachovchin, D. A.; Mowen, K.; Baker, D.; Cravatt, B. F. Quantitative reactivity profiling predicts functional cysteines in proteomes. *Nature* **2010,** *468* (7325), 790.
(118) Bar-Peled, L.; Kemper, E. K.; Suciu, R. M.; Vinogradova, E. V.; Backus, K. M.; Horning, B. D.; Paul, T. A.; Ichu, T.-A.; Svensson, R. U.; Olucha, J.et al. Chemical Proteomics Identifies Druggable Vulnerabilities in a Genetically Defined Cancer. *Cell 171* (3), 696.
(119) Go, Y.-M.; Jones, D. P. Redox compartmentalization in eukaryotic cells. *Biochimica et Biophysica Acta (BBA) - General Subjects* **2008,** *1780* (11), 1273.
(120) Hensley, K. In *Detection of Blotted Proteins: Methods and Protocols*; Kurien, B. T.;Scofield, R. H., Eds.; Springer New York: New York, NY, 2015, DOI:10.1007/978-1-4939-2718-0_11 10.1007/978-1-4939-2718-0_11.
(121) Mateos, R.; Lecumberri, E.; Ramos, S.; Goya, L.; Bravo, L. Determination of malondialdehyde (MDA) by high-performance liquid chromatography in serum and liver as a biomarker for oxidative stress: Application to a rat model for hypercholesterolemia and evaluation of the effect of diets rich in phenolic antioxidants from fruits. *J. Chromatogr. B* **2005,** *827* (1), 76.
(122) Siegel, D.; Meinema, A. C.; Permentier, H.; Hopfgartner, G.; Bischoff, R. Integrated Quantification and Identification of Aldehydes and Ketones in Biological Samples. *Anal. Chem.* **2014,** *86* (10), 5089.
(123) Nakamura, A.; Goto, S. Analysis of Protein Carbonyls with 2, 4-Dinitrophenyl Hydrazine and Its Antibodies by Immunoblot in Two-Dimensional Gel Electrophoresis. *The Journal of Biochemistry* **1996,** *119* (4), 768.
(124) Levine, R. L.; Wehr, N.; Williams, J. A.; Stadtman, E. R.; Shacter, E. In *Stress Response: Methods and Protocols*; Walker, J. M.;Keyse, S. M., Eds.; Humana Press: Totowa, NJ, 2000, DOI:10.1385/1-59259-054-3:15 10.1385/1-59259-054-3:15.
(125) Stankowski, J.; Codreanu, S.; Liebler, D.; McLaughlin, B. *Analysis of Protein Targets by Oxidative Stress Using the OxyBlot and Biotin–Avidin-Capture Methodology*, 2011.

(126) Baraibar, M. A.; Hyzewicz, J.; Rogowska-Wrzesinska, A.; Bulteau, A.-L.; Prip-Buus, C.; Butler-Browne, G.; Friguet, B. Impaired energy metabolism of senescent muscle satellite cells is associated with oxidative modifications of glycolytic enzymes. *Aging (Albany NY)* **2016,** *8* (12), 3375.
(127) Fenaille, F.; Tabet, J.-C.; Guy, P. A. Immunoaffinity Purification and Characterization of 4-Hydroxy-2-nonenal- and Malondialdehyde-Modified Peptides by Electrospray Ionization Tandem Mass Spectrometry. *Anal. Chem.* **2002,** *74* (24), 6298.
(128) Le Boulch, M.; Ahmed, E. K.; Rogowska-Wrzesinska, A.; Baraibar, M. A.; Friguet, B. Proteome oxidative carbonylation during oxidative stress-induced premature senescence of WI-38 human fibroblasts. *Mech. Ageing Dev.* **2017**,
(129) Tamarit, J.; de Hoogh, A.; Obis, E.; Alsina, D.; Cabiscol, E.; Ros, J. Analysis of oxidative stress-induced protein carbonylation using fluorescent hydrazides. *J. Proteomics* **2012,** *75* (12), 3778.
(130) Maier, C. S.; Chavez, J.; Wang, J.; Wu, J. Protein adducts of aldehydic lipid peroxidation products: identification and characterization of protein adducts using an aldehyde/keto reactive probe in combination with mass spectrometry. *Methods Enzymol.* **2010,** *473*, 305.
(131) Soreghan, B. A.; Yang, F.; Thomas, S. N.; Hsu, J.; Yang, A. J. High-Throughput Proteomic-Based Identification of Oxidatively Induced Protein Carbonylation in Mouse Brain. *Pharm. Res.* **2003,** *20* (11), 1713.
(132) Codreanu, S. G.; Zhang, B.; Sobecki, S. M.; Billheimer, D. D.; Liebler, D. C. Global Analysis of Protein Damage by the Lipid Electrophile 4-Hydroxy-2-nonenal. *Molecular & Cellular Proteomics : MCP* **2009,** *8* (4), 670.
(133) Spiess, P. C.; Deng, B.; Hondal, R. J.; Matthews, D. E.; van der Vliet, A. Proteomic profiling of acrolein adducts in human lung epithelial cells. *J. Proteomics* **2011,** *74* (11), 2380.
(134) Galligan, J. J.; Smathers, R. L.; Fritz, K. S.; Epperson, L. E.; Hunter, L. E.; Petersen, D. R. Protein Carbonylation in a Murine Model for Early Alcoholic Liver Disease. *Chem. Res. Toxicol.* **2012,** *25* (5), 1012.
(135) Dalle-Donne, I.; Carini, M.; Orioli, M.; Vistoli, G.; Regazzoni, L.; Colombo, G.; Rossi, R.; Milzani, A.; Aldini, G. Protein carbonylation: 2,4-dinitrophenylhydrazine reacts with both aldehydes/ketones and sulfenic acids. *Free Radic. Biol. Med.* **2009,** *46* (10), 1411.
(136) Landar, A.; Zmijewski, J. W.; Dickinson, D. A.; Le Goffe, C.; Johnson, M. S.; Milne, G. L.; Zanoni, G.; Vidari, G.; Morrow, J. D.; Darley-Usmar, V. M. Interaction of electrophilic lipid oxidation products with mitochondria in endothelial cells and formation of reactive oxygen species. *American Journal of Physiology - Heart and Circulatory Physiology* **2006,** *290* (5), H1777.
(137) Zmijewski, J. W.; Landar, A.; Watanabe, N.; Dickinson, D. A.; Noguchi, N.; Darley-Usmar, V. M. Cell signalling by oxidized lipids and the role of reactive oxygen species in the endothelium. *Biochem. Soc. Trans.* **2005,** *33* (Pt 6), 1385.

(138) Higdon, A. N.; Dranka, B. P.; Hill, B. G.; Oh, J.-Y.; Johnson, M. S.; Landar, A.; Darley-Usmar, V. M. Methods for imaging and detecting modification of proteins by reactive lipid species. *Free Radic. Biol. Med.* **2009,** *47* (3), 201.
(139) Landar, A.; Shiva, S.; Levonen, A.-L.; Oh, J.-Y.; Zaragoza, C.; Johnson, Michelle S.; Darley-Usmar, Victor M. Induction of the permeability transition and cytochrome c release by 15-deoxy-Δ(12,14)-prostaglandin J(2) in mitochondria. *Biochem. J* **2006,** *394* (Pt 1), 185.
(140) Tallman, K. A.; Kim, H.-Y. H.; Ji, J.-X.; Szapacs, M. E.; Yin, H.; McIntosh, T. J.; Liebler, D. C.; Porter, N. A. Phospholipid−Protein Adducts of Lipid Peroxidation: Synthesis and Study of New Biotinylated Phosphatidylcholines. *Chem. Res. Toxicol.* **2007,** *20* (2), 227.
(141) Szapacs, M. E.; Kim, H.-Y. H.; Porter, N. A.; Liebler, D. C. Identification of Proteins Adducted by Lipid Peroxidation Products in Plasma and Modifications of Apolipoprotein A1 with a Novel Biotinylated Phospholipid Probe. *J. Proteome Res.* **2008,** *7* (10), 4237.
(142) Vila, A.; Tallman, K. A.; Jacobs, A. T.; Liebler, D. C.; Porter, N. A.; Marnett, L. J. Identification of Protein Targets of 4-Hydroxynonenal Using Click Chemistry for ex Vivo Biotinylation of Azido and Alkynyl Derivatives. *Chem. Res. Toxicol.* **2008,** *21* (2), 432.
(143) Codreanu, S. G.; Ullery, J. C.; Zhu, J.; Tallman, K. A.; Beavers, W. N.; Porter, N. A.; Marnett, L. J.; Zhang, B.; Liebler, D. C. Alkylation Damage by Lipid Electrophiles Targets Functional Protein Systems. *Molecular & Cellular Proteomics : MCP* **2014,** *13* (3), 849.
(144) Kim, H.-Y. H.; Tallman, K. A.; Liebler, D. C.; Porter, N. A. An Azido-Biotin Reagent for Use in the Isolation of Protein Adducts of Lipid-derived Electrophiles by Streptavidin Catch and Photorelease. *Molecular & Cellular Proteomics : MCP* **2009,** *8* (9), 2080.

CHAPTER 2

*DEVELOPMENT OF T-REX: A TRANSPOSABLE PLATFORM TO STUDY REDOX SIGNALING

Introduction

The **t**argetable **r**eactive **e**lectrophiles and o**x**idants (T-REX) platform uses a proximity-driven approach to selectively modify a redox-sensing protein and decode the functional consequences of this single redox signaling event (**Figure 2.1**)[1-4]. First, a HaloTag domain is genetically fused to a protein-of-interest (POI). The POI can be a known redox sensor or any protein whose redox-sensitivity is being evaluated. The T-REX method uses a bifunctional molecule that consists of (i) a photocaged precursor to a reactive LDE, and (ii) a chloroalkane recognition unit[1-4]. The HaloTag™ enzyme covalently conjugates to the recognition unit with very high specificity and selectivity, with an apparent second order rate constant of 2.7×10^6 $M^{-1}s^{-1}$.[5] The linker between the photocaged precursor and the chloroalkane recognition unit renders the molecule solvent exposed. Illumination with a low-powered ultraviolet (UV) light (365 nm) rapidly and efficiently uncages the reactive LDE ($t_{1/2}$ < 0.5 min) in the microenvironment of the POI. Importantly, each molecule of the photocaged precursor generates a stoichiometric amount of the reactive redox signal.

*Sections of this Chapter were published previously. "T-REX on-demand redox targeting: a toolset for functional discoveries and validations"; **Saba Parvez**, Marcus Long, Hongyu Lin, Yi Zhao, Joseph A. Haegele, Vanha N. Pham, Dustin K. Lee and Yimon Aye; *Nature Protocols,* **2016**, 11, 2328–2356 (Underlined: First-author)

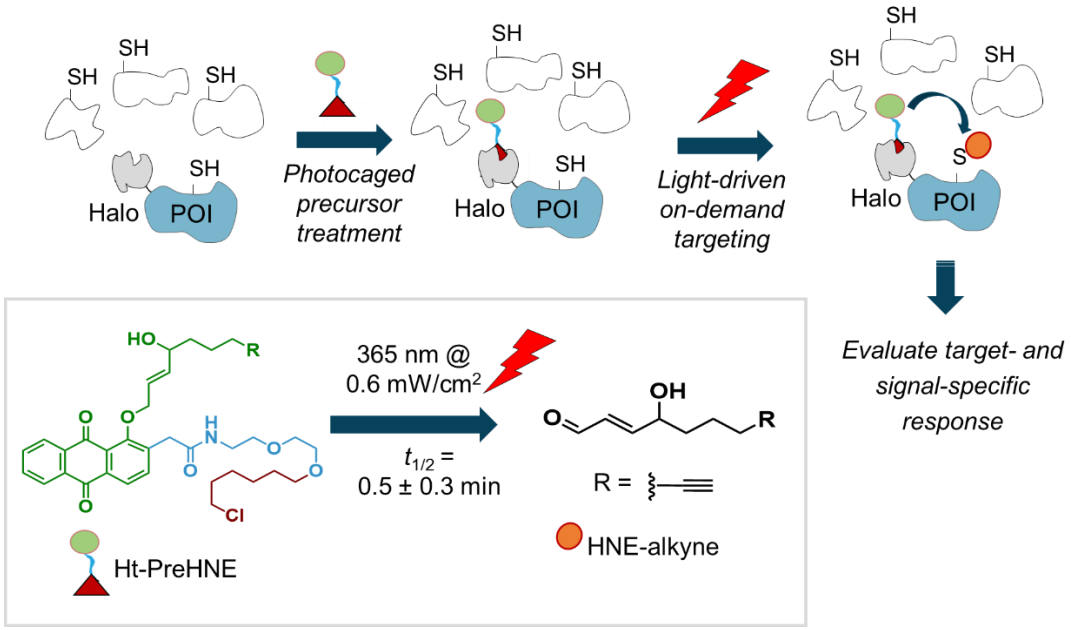

Figure 2.1: Workflow of T-REX: T-REX is a unique tool that uses proximity-driven approach to selectively label a protein-of-interest (POI) with a desired LDE. The platform uses a bifunctional photocaged precursor to an LDE (HaloTag™ targetable precursor to HNE in this case, Ht-PreHNE) (see Inset). One part of the bifunctional molecule consists of a hexyl chloride linker (brown) that can covalently conjugate with high specificity and affinity to a HaloTag™ (gray) genetically encoded to a POI (blue). The other part consists of a reactive LDE caged using an anthraquinone core (green). The precursor generates the reactive LDE on-demand upon illumination with a low power UV lamp. In biological systems, T-REX enables decoding the functional consequences of a single redox event. The workflow consists of treating a biological system expressing a Halo-POI with the photocaged precursor, rinsing away any unbound precursor, and subsequent on-demand uncaging of the LDE in proximity to the POI. Signaling consequences resulting from the LDE modification of a privileged redox sensor POI can be evaluated using downstream biological readouts.

Results

HaloTag™ targetable precursor to HNE (Ht-PreHNE) is efficiently uncaged **in cells*

HEK293T cells expressing Halo domain were treated with Ht-PreHNE. After incubation in a humidified atmosphere at 37 °C for 2.5 h, cells were rinsed three times at 30-min intervals to remove any excess unbound precursor. Subsequently, HNE was released by shining UV light on the cells for varying time. Release efficiency was

measured after lysing the cells and conjugating Cy5 azide to the alkyne handle of Ht-PreHNE (**Figure 2.1**). The samples were analyzed using in-gel fluorescence to measure signal intensity on Halo. Results show that (i) Ht-PreHNE covalently conjugates to Halo in cells (ii) Ht-PreHNE is efficiently uncaged upon UV light illumination (**Figure 2.2**). The $t_{1/2}$ is calculated to be 0.5 ± 0.3 min.

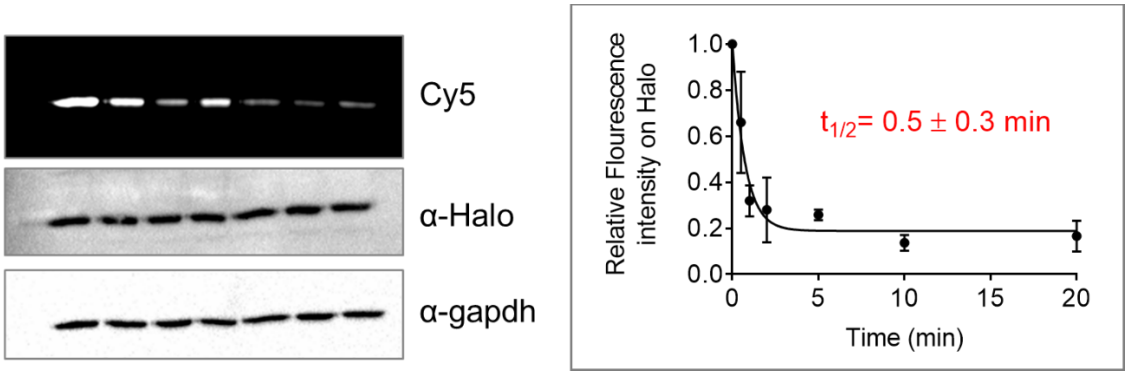

Figure 2.2: Ht-PreHNE covalently conjugates to HaloTag expressed in mammalian cells. The photocaged precursor is also efficiently uncaged to generate the reactive aldehyde. *Inset*: 50% of the precursor is uncaged within 1 min of light illumination on whole cells.

**Low-powered UV light illumination is non-perturbing to cells*

Prolonged exposure of cells to high intensity UV radiation has mutagenic effect[6] and triggers immunological and inflammatory pathway activation[7]. Typically, high energy radiation (< 320 nm) and long exposure time are required for these effects[7]. Although T-REX method requires illumination with only low-powered UV light (365 nm, 0.5 mW/cm^2), we wanted to validate that this level of exposure is non-intrusive and does not upregulate stress-responsive pathways in mammalian cells. We used two independent approaches. First, we measured time-dependent phosphorylation of

Histone H2A.X (γ-H2AX), a well-known marker of DNA damage in cells[8], using immunofluorescence (IF, data collected by Dr. Marcus Long) (**Figure 2.3A**). We also used a luciferase-based reporter assay to report on the transcriptional activity of NF-κB, an established stress-response pathway in mammalian cells[9] (**Figure 2.3B**). IF data showed no significant upregulation in DNA damage after 20 min of light illumination. MitomycinC[10], an inducer of DNA damage and Aphidicolin[11], a small molecule inhibitor of DNA replication, showed significant upregulation of γ-H2AX levels. Additionally, no significant NF-κB pathway activation was observed after UV light illumination of cells for 20 min. Phorbol myristate ester (PMA), an activator of the NF-κB pathway[12], treated cells showed 1.5-fold upregulation compared to untreated control.

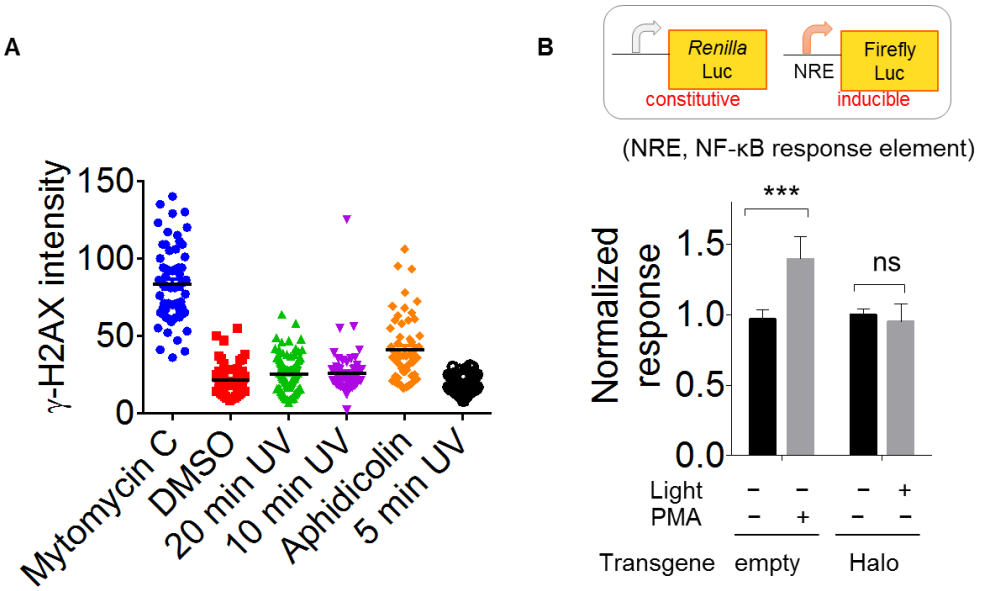

Figure 2.3: UV light illumination does not cause DNA damage or activate stress response in HEK293T cells (**A**) Quantitation of IF data demonstrate that UV light for up to 20 min does not increase γ-H2AX levels in cells. Mitomycin C and Aphidicolin, small molecules that induce DNA damage, are used as positive controls. (**B**) *Inset*:

Experimental setup of luciferase-based reporter assay to measure the transcriptional activity of NF-κB. Firefly luciferase is under the control of NF-κB response element (NRE). Constitutively expressing *Renilla* luciferase under CMV reporter is used as a normalization control. No significant increase in NF-κB activity was measured after 20 min of light exposure in cells expressing the two reporter constructs. PMA, an activator of NRE is used as a positive control. $n > 3$. *** denotes $p < 0.001$.

**T-REX enables modification of a single-target protein in mammalian cells*

We next examined whether T-REX can successfully modify Keap1, an established electrophile-sensitive protein[13-15] and a key regulator of the Nrf2/AR signaling axis (See Chapter 3 for discussion) (**Figure 2.4**). HEK293T cells expressing HaloTagged-TEV-Keap1 (Halo-Keap1 from hereon) were treated with the Ht-PreHNE. The Tobacco Etch Virus (TEV) protease cleavage site allows separation of the Halo domain and Keap1 protein upon treatment with TEV protease[16] and therefore enables detection of Keap1-selective modification after T-REX. After rinsing away any unbound Ht-PreHNE, cells were illuminated with UV light for 20 min. The labeling efficiency of Keap1 was determined by first lysing the cells, separating the Keap1 protein from the Halo domain using TEV protease, and subsequent copper-assisted click chemistry[17] to conjugate Cy5 azide to the alkyne-functionalized uncaged HNE (and any unreleased Ht-PreHNE still bound to Halo domain) (**Figure 2.4A**). The data clearly demonstrated that Keap1 is selectively modified by HNE using the T-REX platform (**Figure 2.4B**). Comparison of proteome labeling with bolus dosing method (25 μM HNE-alkyne for 30 min, rightmost lane) on the same gel demonstrated the tremendous improvement in selectivity in target modification achieved by T-REX.

Additionally, T-REX enables quantitation of the extent of modification of the target protein. The targeting efficiency is determined using the following equation:

$$\left[\frac{Cy5(x)/\,WB(x)}{Cy5(y) - Cy5(z)/\,WB(y)}\right] X\ 100\%$$

Where Cy5(x) is the amount of Cy5 signal from Keap1 after photouncaging, WB(x) is the western blot signal intensity from the protein, Cy5(y) is the amount of Cy5 signal from the fused Halo-Keap1 protein before light illumination, Cy5(z) is the Cy5 signal from Halo domain post light shining (residual unreleased Ht-PreHNE), and WB(y) is the western blot signal from the fused Halo-Keap1 protein. In Figure 2.2, the targeting efficiency was calculated to be ~25–30%.

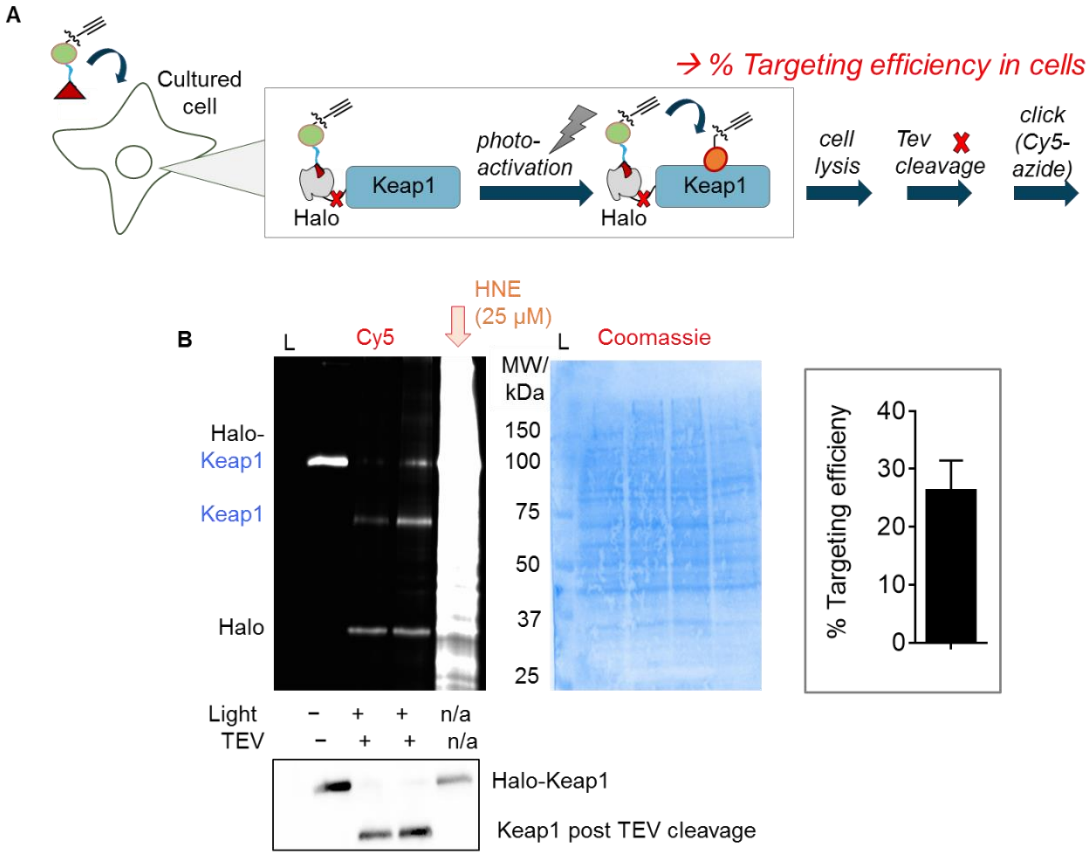

Figure 2.4: (**A**) General workflow of T-REX in mammalian cells. Cells expressing Halo-Keap1 are treated with Ht-PreHNE and incubated for 2.5 h. Cells are then washed 3 times at an interval of 30-min to wash away any excess unbound Ht-PreHNE. UV

light illumination uncages the reactive electrophile resulting in modification of Keap1. Targeting efficiency is analyzed after cell lysis, TEV protease-mediated separation of Halo and Keap1 protein, Click chemistry with Cy5 azide and subsequent SDS-PAGE and in-gel fluorescence analysis. ✘ TEV protease cleavage site. (**B**) In-gel fluorescence to show selective targeting of Keap1 using T-REX. L: Molecular weight ladder. Bolus dosing samples were prepared by treating cells with 25 μM HNE-alkyne for 30 min. *Inset*: Quantitation of % targeting efficiency. N = 4. Data is presented as Mean ± s.d.

Halo and Keap1 fusion is required for HNE modification of Keap1 using T-REX

We next investigated the mechanism of HNE delivery to Keap1. One can envisage the following possibilities (i) Photoliberation results in a rapid accumulation of the electrophile in the coordination sphere of the target protein. The reactive electrophile then covalently conjugates with the target protein in a quasi-intramolecular way (ii) photouncaging of the precursor generates an increased global increase in HNE in cells. Because Keap1 is overexpressed in these cells it reacts with the reactive electrophile due to mass action. To investigate these two possibilities, we set-up a "Split system". We co-transfected cells with two separate plasmids for expressing Halo-GFP (**Figure 2.5A**) and Keap1(No HaloTag). T-REX was performed as described above. The targeting efficiency of Keap1 with HNE-alkyne in the "split system" was evaluated against the efficiency obtained when Halo-Keap1 was expressed as a fused protein. In-gel fluorescence data showed that fusion of Halo and Keap1 proteins was required for efficient delivery of HNE to Keap1 (**Figure 2.5B**). A significant reduction in targeting efficiency was observed when the Halo and Keap1 proteins were expressed as two separate protein suggesting that HNE delivery to Keap1 is quasi-intramolecular (Option I above)

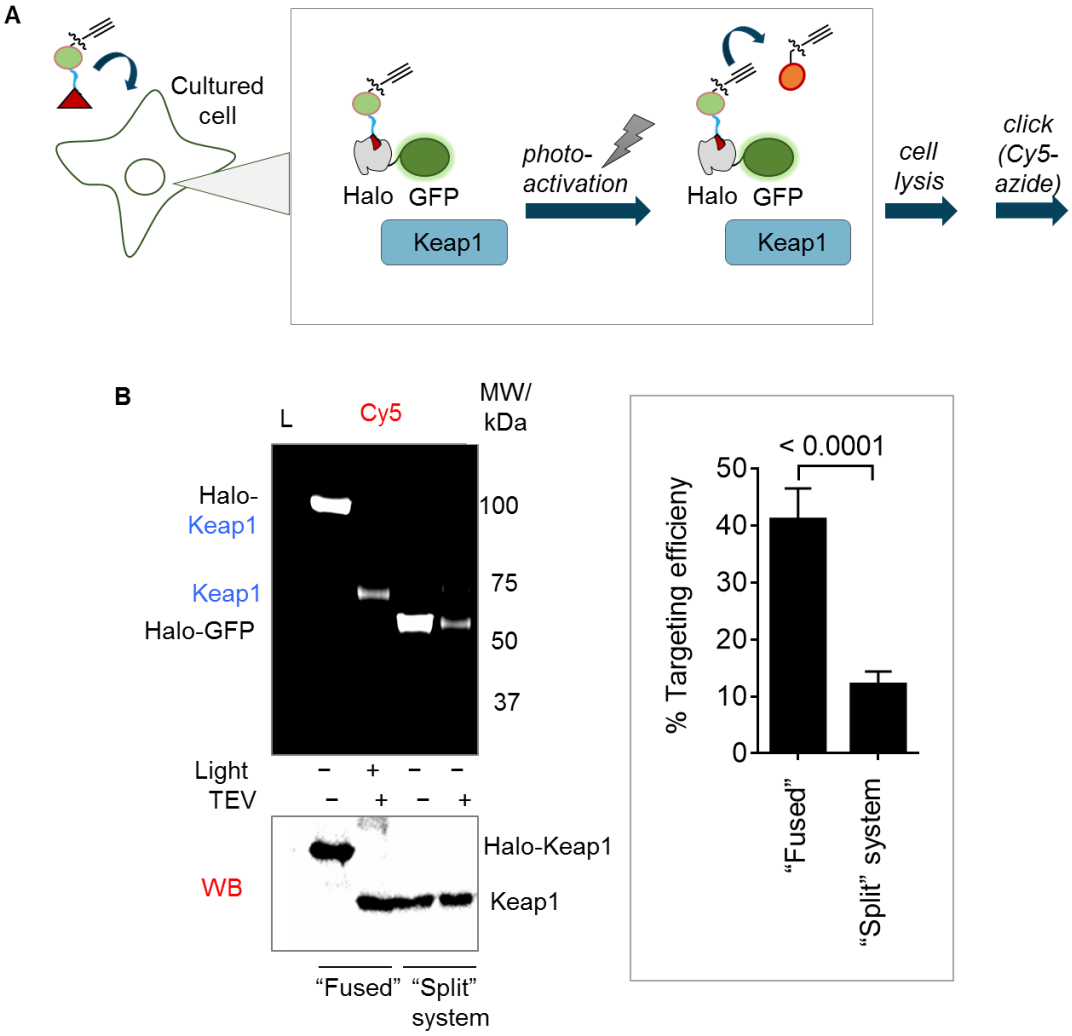

Figure 2.5: (**A**) Workflow of "split-system". HEK293T cells were co-transfected with plasmids for expressing Halo-GFP and Keap1 ("Split" system). T-REX was performed as described above. Targeting efficiency was analyzed after cell lysis, Click chemistry with Cy5 azide, and subsequent SDS-PAGE and in-gel fluorescence analysis. (**B**) In-gel fluorescence data show that fusion of Halo and Keap1 protein ("fused") is required for efficient HNE delivery. "Split" system show considerable reduced Cy5 signal intensity on Keap1 after photouncaging of Ht-PreHNE compared to "fused" samples. L: Molecular weight ladder. *Inset*: Quantitation of % targeting efficiency. N = 6. Data is presented as Mean ± s.d.

---

*Sections of this Chapter were published previously. "T-REX on-demand redox targeting: a toolset for functional discoveries and validations"; **Saba Parvez**, Marcus Long, Hongyu Lin, Yi Zhao, Joseph A. Haegele, Vanha N. Pham, Dustin K. Lee and Yimon Aye; *Nature Protocols,* **2016**, 11, 2328–2356 (Underlined: First-author)

After validating that T-REX can successfully be used to modify specific proteins in mammalian cells, we wanted to test whether the platform is transposable to other model organisms. We first tested whether T-REX is compatible in *E.coli*. *E. coli* and other prokaryotes are responsive to redox signals[18], and trigger upregulation of several detoxification genes upon oxidative stress[19]. Recently, oxidative stress response in E. coli is shown to affect the mitochondrial stress response of host organisms such as *C. elegans* [20]. *E. coli* are also one of the most user-friendly model systems.

Bacteria were transformed with pet28a-Halo-Keap1 plasmid. Growing *E. coli* cultures containing the plasmid were induced using 0.5 mM Isopropyl β-D-1-thiogalactopyranoside (IPTG) at 19 °C overnight. The overnight culture was subsequently diluted in LB-media and the cells were treated with 25 μM Ht-PreHNE for 2 h while shaking them at 200 r.p.m at 19 °C. Cells were then washed 4 times using PBS, resuspended in PBS, illuminated with light for 30 min while shaking at ~100 r.p.m at room temperature. Subsequently, cells were lysed, incubated with TEV protease, conjugated with Cy5 azide using click chemistry. Targeting of Keap1 was analyzed using SDS-PAGE and in-gel fluorescence. As in the case of mammalian cells, Ht-PreHNE did not show adverse effects on the growth rate of *E. coli*, the precursor was able to permeate the bacterial cells within 2 h. Finally, the selective labeling of Keap1 was also successful in *E. coli* and showed a significant improvement in minimizing off-target spectrum compared to bolus dosing (**Figure 2.6**).

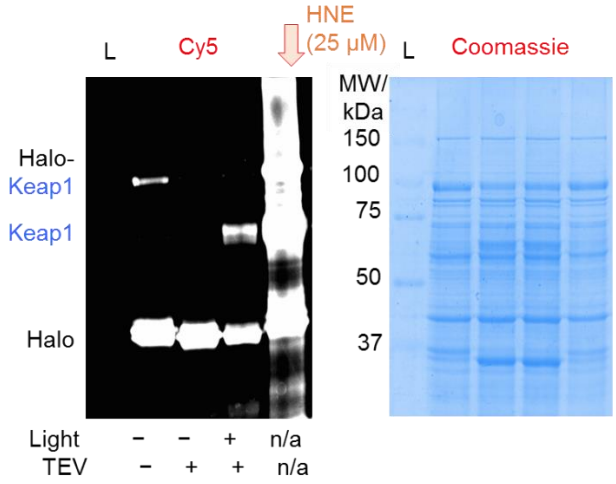

Figure 2.6: In-gel fluorescence shows selective targeting of Keap1 using T-REX in *E. coli* cells. L: Molecular weight ladder. Bolus dosing samples were prepared by treating bacteria with 25 μM HNE-alkyne for 30 min. Coomassie gels shows equal protein loading.

*Danio rerio (zebrafish) is an ideal **vertebrate** model system to study redox signaling*

Next, we tested whether the platform is compatible with more complex organisms. We assessed the feasibility of transposing T-REX to zebrafish. Our goal of transposing T-REX to zebrafish was inspired by the fact that most investigations in the realm of redox signaling has focused on work in cell culture[21,22]. Although these studies have been critical in our understanding of redox signaling, studies in mammalian cell culture do not recapitulate the nuances of a whole organism. Multicellular organisms rely on complex intercellular and interorgan communications for growth and survival. These signaling networks and their associated phenotypes are impossible to recapitulate *in vitro* and in cell culture. Studies in mice have been highly informative[23-25]. However, mouse and similar complex transgenic models are difficult to generate and can take considerable effort to maintain and at significant expense. Comparatively, zebrafish genetic manipulation is easy and reliable, maintenance is significantly cheaper, and the

high fecundity of the organism supports high-throughput methods[26-28]. Additionally, external fertilization and optical transparency of the embryos at early developmental stage is ideal for opto-chemical techniques[29] such as T-REX.

***Z-REX: T-REX is transposable to Danio rerio (zebrafish)*

Z-REX consists of the following steps (1) Generation of a Halo-POI plasmid in a vector compatible for *in vitro* transcription, (2) microinjection of zebrafish embryos with *in vitro* transcribed mRNA to transiently express the Halo-POI, (3) treatment with the photocaged precursor and light-assisted release of the reactive electrophile signal resulting in modification of the target protein.

1. *Plasmid generation*

To successfully validate Z-REX, we generated the following two plasmids in pcs2+8 vector backbone: Halo-TEV-Keap1-2xHA (Halo-Keap1) and Halo-2xHA-P2A-TEV-Keap1-2xHA(Halo-P2A-Keap1). The use of the epitope tags (two tandem HA tags) allows detection of the protein via western blot even when protein expression is minimal. Additionally, the epitope tag also allows us to discriminate the ectopically expressing human Keap1 in zebrafish from the native Keap1 protein (non HaloTagged). Halo-P2A-Keap1 was constructed to ensure that HNE delivery to Keap1 is orchestrated intra-molecularly during Z-REX. P2A is a self-cleaving peptide from porcine teschovirus A that results in the generation of a stoichiometric amount of the two

[30] A

This section is part of a paper currently under revision. Z-REX: Shepherding Reactive Electrophiles to Specific Proteins and Recording the Resultant Functional Redox Responses in Developing Larval Fish"; Marcus Long, **Saba Parvez, Jesse Poganik, and Yimon Aye*; *Nature Protocols,* In revision (Underlined: First-author)

To transfer the DNA coding for Halo-POI, and simultaneously introduce C-terminal 2xHA tag into pCS2+8, the following sequence was performed (**Figure 2.7A**) (i) Halo-Keap1 was amplified by polymerase chain reaction (PCR) using primers that anneal in the forward direction to the N-terminus of Halo and the reverse direction to the C-terminus of Keap1 (**Table 2.1**). The Halo primer has a 5´-flanking region that can anneal to the pCS2+8 plasmid. The forward extender primer contains a Kozak sequence [CCACC(ATG)] and this must be retained to ensure translation); the reverse primer has a 5´-flanking sequence that introduces 2xHA (YPYDVPDYA) tag. (ii) The product of the first PCR reaction, after PCR clean up, was "extended" sequentially using two sets of forward and reverse primers that ultimately give a PCR product that has around 40–60 bp overlap with the destination vector. (iii) The product of these sequential reactions was then used to prime a PCR reaction of linearized, empty pCS2+8 plasmid. The resulting product, was transformed into *E. coli*. Colonies with the desired insert were screened by colony PCR and sequenced for sequence verification.

Halo-P2A-Keap1 was generated using the following steps (**Figure 2.7B**): (1) TEV-Keap1 was amplified by PCR using primers that anneal in the forward direction to the TEV cleavage site and the reverse direction to the C-terminus of Keap1 (**Table 2.1**). The TEV forward primer has a 5´-flanking region that can anneal to gene encoding P2A cleavage site. The reverse primer has a 5´-flanking sequence that introduces 2xHA (YPYDVPDYA) tag. Simultaneously, Halo domain was amplified using a set of primers that anneal in the forward direction to the N-terminus of Halo (and has a 5´-flanking region that can anneal to the pCS2+8 plasmid) and the reverse direction to the C-terminus of Halo (and has a 5´-flanking sequence that overlaps with the gene encoding

for P2A peptide) (ii) The product of the first PCR reactions, after PCR clean up, were "extended" separately using the primers in Table 2.1 (iii) The product of these 'extension' reactions was then joined using a PCR reaction and subsequently (iv) inserted in a linearized empty pCS2+8 plasmid. The resulting product, was transformed into *E. coli*. Colonies with the desired insert were screened by colony PCR and sequenced for sequence verification.

To generate the mRNA, the genes were first amplified using RNA fwd and RNA Rev primers (**Table 2.1**). The amplified products were used as templates to generate the mRNA for the two plasmids using a commercially available SP6-mMessage mMachine *in vitro* transcription kit.

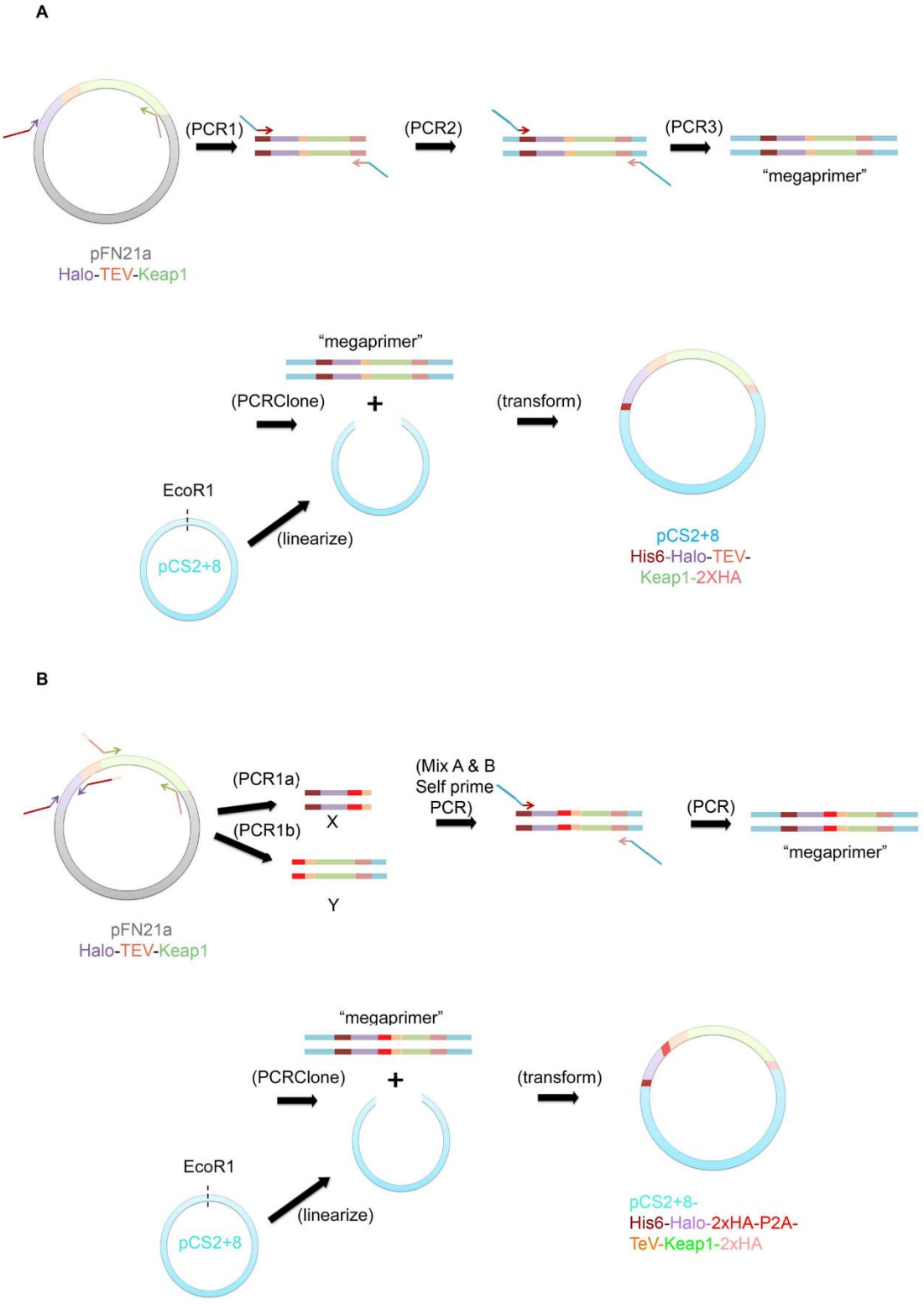

Figure 2.7: Schematic showing the steps for generating (**A**) His_6-Halo-Keap1-2xHA and (**A**) His_6-Halo-2xHA-P2A-Keap1-2xHA plasmids in pcs2+8 vector.

Table 2.1 Primers for cloning His_6-Halo-TEV-Keap1-2xHA and His_6-Halo-2xHA-P2A-TEV-Keap1-2xHA**.**

Primers for cloning His_6-Halo-TEV-Keap1-2xHA		
	Primers for gene amplification	His_6-Halo-Fwd: CATGGGCAGCAGCCATCATCATCATCATCATGGGTCAGGGATGGCAGAAATCGGTACTGG Keap1-HA-Rev: CCGGCGTAGTCTGGGACGTCGTAAGGATAGCTGCCACAGGTACAGTTCTGCTGGTCAATC
	Extension primers 1: (Kozak sequence (**CCAC(ATG**)) is bolded)	pCS2+8-Fwd extender (1): AGGTGACACTATAGAATACAAGCTACTTGTTCTTTT**CCACCATG**GGCAGCAGCCATCATC Keap1-2x HA-Rev extender (1): TCCAAGCGTAATCTGGAACATCGTATGGGTAGCTGCCGGCGTAGTCTGGGACGTCGTAAG
	Extension primers 2:	pCS2+8-Fwd-extender (2): GTCGGAGCAAGCTTGATTTAGGTGACACTATAGAATACAAGCTACTTGTTCTTTT**CCACC** HA-pCS2+8-Rev-extender (2): CGGCCTTTAATTAATGGCGCGCCACTAGTTTATTTTTTCCAAGCGTAATCTGGAACATCG
Primers for cloning His_6-Halo-2xHA-P2A-TEV-Keap1-2xHA		
	Primers for gene amplification (Halo)	His_6-Halo-Fwd (*same as above*): CATGGGCAGCAGCCATCATCATCATCATCATGGGTCAGGGATGGCAGAAATCGGTACTGG

	Primers for gene amplification (Keap1)	Halo-HA-Rev: ATGGGTAGCTGCCGGCGTAGTCTGGGACGTC GTAAGGATAGCCGGAAATCTCGAGCGTCG P2A-Tev-fwd: GCTGGAGACGTGGAGGAGAACCCTGGACCT GGCAGCGAGCCAACCACTGAGGATCTGTAC Keap1-HA-Rev (*same as above*): CCGGCGTAGTCTGGGACGTCGTAAGGATAG CTGCCACAGGTACAGTTCTGCTGGTCAATC
	Extension primers 1: (Kozak sequence (**CCAC(ATG**)) is bolded)	pCS2+8-Fwd extender (1) (*same as above*): AGGTGACACTATAGAATACAAGCTACTTGTT CTTTT**CCACC**ATGGGCAGCAGCCATCATC 2xHA-P2A Rev extender: AAGTTAGTAGCTCCGCTTCCGGCGTAATCTG GAACATCGTATGGGTAGCTGCCGGCGTAG P2A-fwd extender: CGCC GGAAGCGGAGCTACTAACTTCAGCCTGCTGA AGCAG GCTGGAGACGTGGAGGAGAA Keap1-2xHA-Rev extender (1) (*same as above*): TCCAAGCGTAATCTGGAACATCGTATGGGTA GCTGCCGGCGTAGTCTGGGACGTCGTAAG
Primers for amplifying gene-of-interest for *in vitro* transcription	RNA-fwd: GACGTAAATGGGCGGTAGGCG RNA-Rev: CATGATTACGCCAAGCGCGC	

2. *Microinjection of mRNA in zebrafish embryos and validation of protein expression (performed by Dr. Marcus Long)*

After successful cloning of the gene-of-interests in pcs2+8 vector and subsequent *in vitro* transcription to generate the mRNA, we tested the expression of the HaloTagged proteins in zebrafish. Fish embryos at the 1–4 cell stage were injected with the desired mRNA (**Figure 2.8A**). Next, the embryos were incubated at 28.5 °C and allowed to develop for another 24–30 h before evaluation of protein expression. Expression of Halo-Keap1 and Halo-P2A-Keap1 was determined using IF against the 2xHA epitope tag or a commercially-available antibody raised against human Keap1. Anti-Keap1 antibody also recognized the endogenous zebrafish Keap1 proteins (**Figure 2.8B–C**). IF results showed that the successful expression of both Halo-Keap1 and Halo-P2A-Keap1 proteins in the injected zebrafish embryos (**Figure 2.8B**). Moreover, the level of expression of Halo-Keap1 and Halo-P2A-Keap1 were similar to each other, and comparable to the endogenous zebrafish Keap1 protein levels (**Figure 2.8C *Inset***).

To perform Z-REX, embryos were treated with ~5μM Ht-PreHNE in 10% Hank's buffer immediately after injection with the desired mRNA (**Figure 2.8A**). Subsequently, the embryos were incubated at 28.5 °C and allowed to develop for another 24–30 h. Next, the fish were rinsed three times with 10% Hank's at 30-min intervals. Photouncaging was performed for 4 min using a UV lamp (365 nm, 0.5 mW/cm^2). To ensure that the photocaged precursor and UV light illumination are not harmful to the embryos, we tested their viability after 24 h growth (**Figure 2.9**).

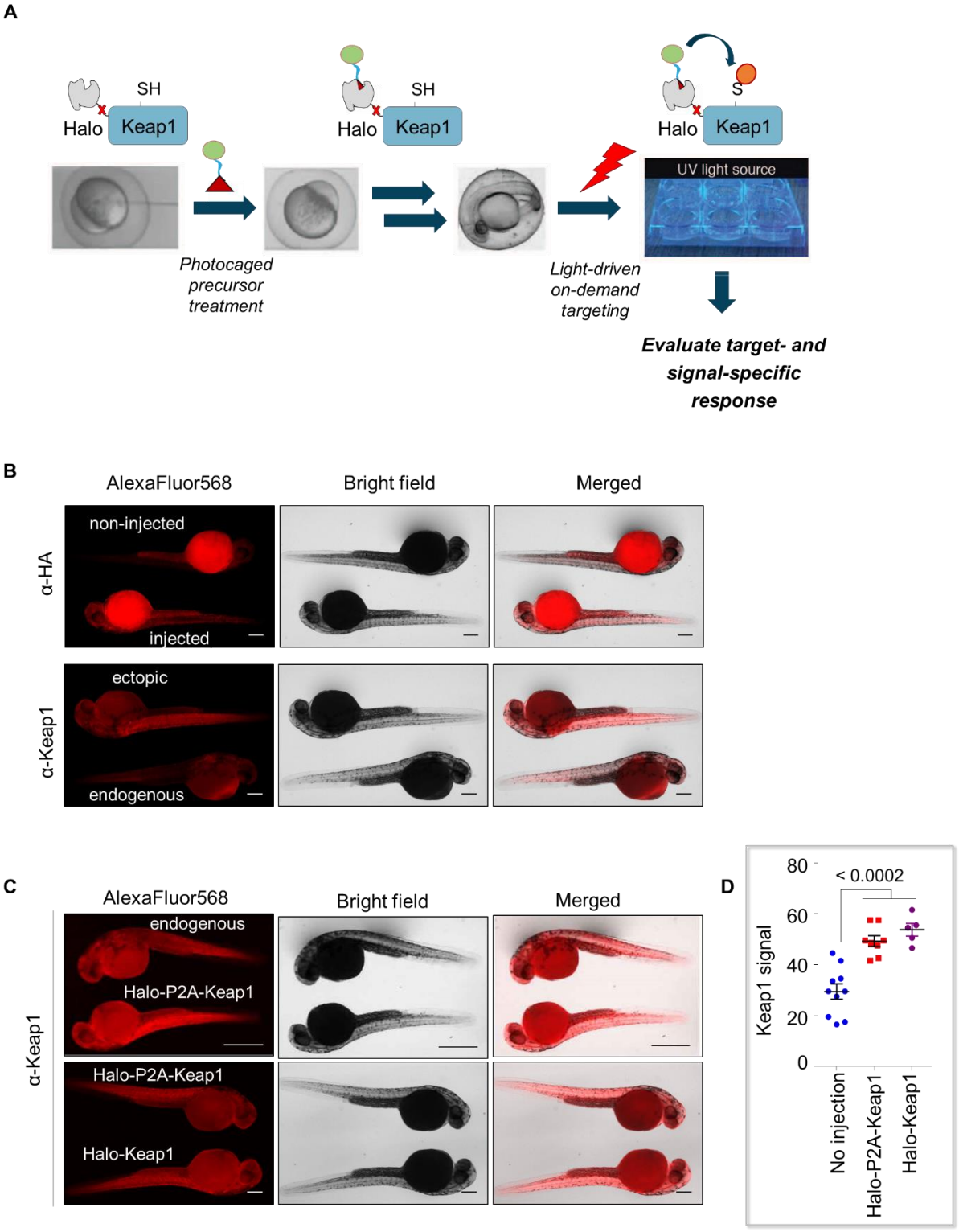

Figure 2.8: (**A**) Workflow of Z-REX. Zebrafish embryos at 1–4 cell stage were injected with the mRNA for expressing the desired transgene. Immediately after injection, embryos were treated with ~5 μM Ht-PreHNE in 10% Hank's buffer and incubated at

28.5 °C for 24–30 h. Subsequently, the larvae were washed 3x over 1.5 h with Hank's buffer to remove excess and unbound photocaged precursor. Phtouncaging was performed by placing a 6-well plate containing the embryos in 10% Hank's buffer under a UV lamp for 4 min. Subsequently, downstream analysis was performed as needed. (**B–C**) Validating the expression of Halo-Keap1 and Halo-P2A-Keap1 in injected fish embryos using IF. Transgene expression was either probed using the 2xHA epitope tag (**B**, *top panel*) or using a mouse polyclonal α-Keap1 antibody. A anti-mouse IgG AlexaFluor568 secondary antibody was used for detecting protein expression. (**D**) Quantitation of Keap1 signal intensity in non-injected fish embryos and those injected with Halo-Keap1 or Halo-P2A-Keap1 mRNA.

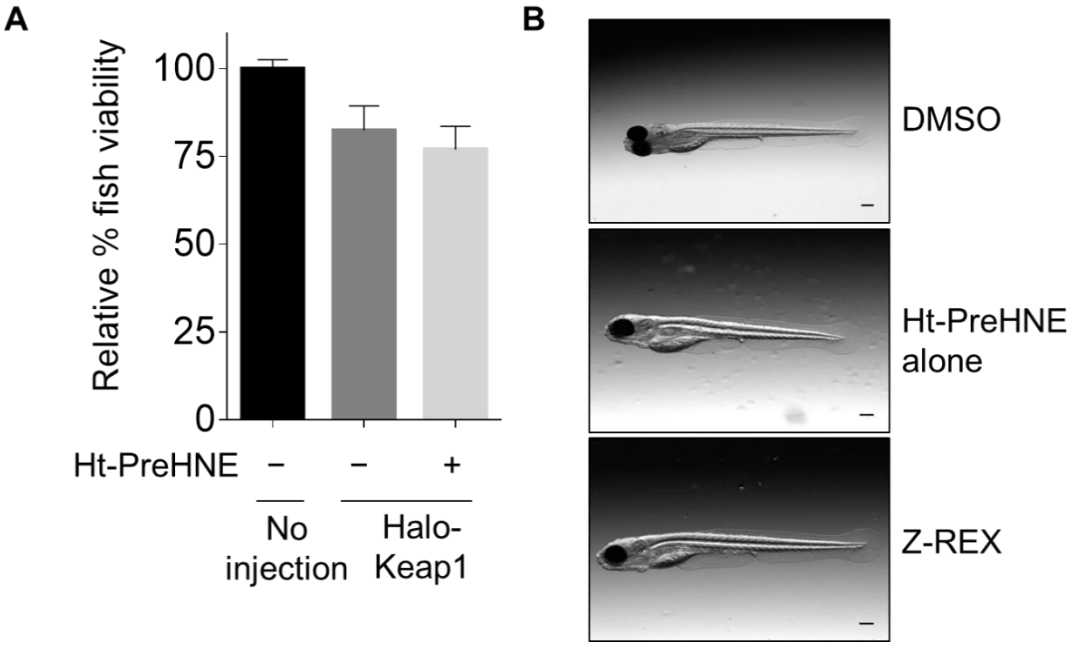

Figure 2.9: Photocaged precursor compounds are non-invasive **(A)** Ht-PreHNE does not show any significant toxicity/teratogenicity compared to non-injected fish. **(B)** Ht-PreHNE is non-teratogenic. Fish embryos were treated with 6 μM Ht-PreHNE at 1–4 cell-stage. After 24 h, Z-REX was performed, and fish were allowed to develop for another 72 h before imaging.

3. Validating HNE modification of Halo-Keap1(performed by Dr. Marcus Long)

After demonstrating that Z-REX is non-invasive to fish development, we next assessed whether the method can successfully label a target protein selectively. Z-REX

was performed as described above on Halo-Keap1 or Halo-P2A-Keap1 injected fish embryos. To determine labeling, embryos were chilled on ice immediately after light illumination. The embryos were manually dechorionated, and deyolked. Next, we washed the embryos three times with 1 X PBS to remove yolk proteins. Subsequently, the yolk-free embryos were either flash frozen for later analysis or lysed in 50 mM Hepes buffer (pH 7.6). Lysate was treated with TEV protease, click chemistry was performed with Biotin-azide (instead of the Cy5 azide in case of in-gel fluorescence analysis). Subsequently, modified proteins were enriched using streptavidin-agarose beads. Halo-Keap1 mRNA injected fish embryos show a significant enrichment of Keap1 protein (**Figure 2.10**) demonstrating that Z-REX can modify a redox-sensitive target protein. Additionally, no enrichment was observed under various controls. Importantly, no significant enrichment of Keap1 was observed in embryos injected with Halo-P2A-Keap1 mRNA (**Figure 2.10**) under identical condition to those of Halo-Keap1 mRNA injected fish. As in the case of mammalian cells, this data unequivocally demonstrates that HNE-delivery to Keap1 is quasi-intramolecular and requires fusion of the two proteins for efficient delivery. Moreover, HNE modification of Keap1 in zebrafish, where the overexpression level of the protein is comparable to endogenous zebrafish Keap1 (as opposed to in mammalian cells where expression levels are >10 times to that of endogenous protein), suggests that T-REX/Z-REX-mediated HNE delivery to proteins is determined by their “kinetic privilege” rather than mass action.

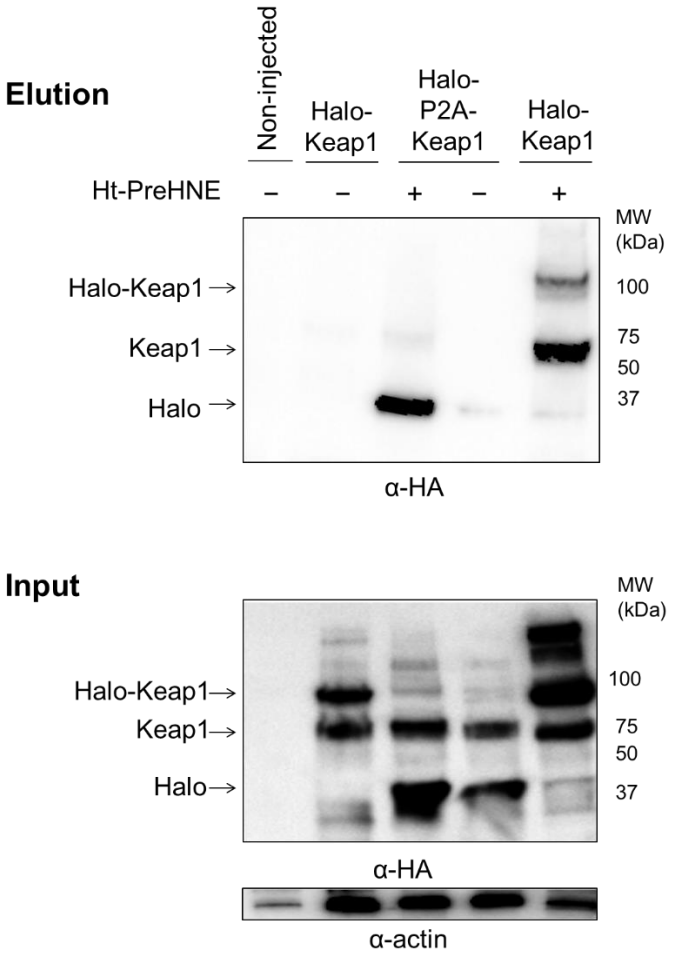

Figure 2.10: Z-REX enables LDE modification of Keap1 through proximity enhancement. Fusion of Halo and Keap1 domains is required for LDE delivery to Keap1. Post Z-REX, zebrafish larvae are lysed, and Halo and Keap1 domains separated using TEV protease. Copper-assisted click chemistry in lysate couples biotin-azide to the alkyne handle on the LDE and is followed by enrichment using streptavidin agarose beads and subsequent western blot analysis. Keap1 enrichment post Z-REX shows protein modification only when Halo-Keap1 is expressed as a fusion protein. No labeling of Keap1 is observed in fish injected with Halo-P2A-Keap1 mRNA. *Top*: Elution blot. The Halo band is detected in Halo-2xHA-P2A-TEV-Keap1-2xHA (Halo-P2A-Keap1 injected fish embryos. *Bottom*: Input lanes to demonstrate comparable loading.

Experimental Setup

Cell Culture and Transfection: HEK-293 cells were cultured in DMEM-Glutamax (Invitrogen 41090-036) supplemented with 10% v/v FBS (100 nm-triple filtered, Hyclone SH30071.03), 5% NEAA (Invitrogen A11140-050) and 5% pyruvate (Invitrogen 11360-070) in the presence of 1X penicillin-streptomycin antibiotics (Invitrogen 15140-122). All cells were cultivated in adherent culture plates (Corning) in a humidified atmosphere of 5% CO_2 at 37 ^oC and harvested by trypsinization (Invitrogen 25300-054). Transient transfection was performed at 50–60% confluency using Mirus TransIT-2020 (Mirus MIR5400) for HEK-293 according to the manufacturer's protocol.

T-REX in mammalian cells: HEK 293T cells were maintained in 1X MEM+ Glutamax™ media supplemented with 10% FBS, 1X NEAA, 1X sodium pyruvate and 1X Pen-Strep. Cells were grown in humidified, 5% CO_2 incubator at 37 °C. For in-gel fluorescence analysis and western blot, ~ 0.7–0.8 $X10^6$ HEK 293T cells were seeded in 8 cm^2 tissue culture dishes. 24 h later, cells were transfected using TransIT-2020 transfection reagent using manufacturer's recommendation. The subsequent steps were performed under red light. 24–36 h post transfection, monolayer of cells were treated with 25 μM Ht-PreHNE in serum-free media and incubated for 2.5 h. Cells were gently rinsed with serum-free media three times every 30 min over the next 1.5 h. Meanwhile, UV lamps were turned on 20 min prior to UV irradiation time to warm up the lamp. For samples designated for light exposure, the lids from the dishes were removed and the monolayered cells were placed under 365 nm UV light for 20 min. The cells were harvested, washed two times with ice-cold PBS and frozen in liquid nitrogen.

Cell lysis and western blotting: Whole cell lysates were prepared by three times rapid freeze thaw in ice-cold 50mM HEPES buffer (pH 7.6), 1% Nonidet P-40 and 0.3mM TCEP. Cell extract was clarified by centrifugation at 16,000Xg for 8min at 4C. Total protein concentration in lysate was determined using Bradford Assay. For Nrf2 stabilization experiments, whole cell lysate was prepared in 1X RIPA buffer (50mM Tris (pH 7.4), 150mM NaCl, 1% (v/v) Nonidet P-40, 0.5% (w/v) Deoxycholate, 0.1% (w/v) SDS, 1mM orthovanadate and Roche protease inhibitor).

In-gel fluorescence assay: All steps were performed in dark or under red light. Cells from 8cm^2 plates were lysed in 30 µL of buffer containing 50 mM HEPES (pH 7.6), 1% Nonidet P–40 and 0.3 mM TCEP by rapid freeze-thaw (x3). Cells debris was removed by centrifugation at 18,000x g for 8 min at 4 °C. Protein concentration of the clarified lysate was determined using Bradford assay. A portion of the lysate protein was made up to 25 µL final volume containing, in final concentrations, 50 mM HEPES (pH 7.6), 1.0 mg/mL lysate protein, 0.3 mM TCEP, and 0.2 mg/mL TEV protease. The sample was incubated at 37 °C for 45 min, and subsequently subjected to Click reaction[31]. In a final volume of 30 µL, the click reaction mix consisted of 1.7 mM TCEP, 5% t-BuOH, 1% SDS, 1mM $CuSO_4$, 0.1 mM Cu(TBTA), 10 µM Cy5 azide and the lysate from above. The samples were incubated at 37 °C for 30 min and subsequently quenched with 5 µL of 4X Laemmeli dye containing 6% βME. After additional 5-min incubation at 37 °C, 25 µL of the lysate was resolved by SDS-PAGE. After electrophoresis, the gel was rinsed 3X with ddH_2O with 5-min each rinse on a shaker and imaged on a Biorad Chemi-doc-MP Imager. Where applicable, the gel was transferred to a PVDF membrane for western blot analysis.

T-REX in E. coli: BL21 codon plus (DE3) RIL *E. coli* cells were transformed with pet28a-Halo-Keap1 plasmid, and plated on LB-kanamycin plate. The plate was incubated overnight at 37 °C. Single colonies were picked and inoculated into 5 mL of LB-kanamycin-chloroamphenicol media (50 µg/mL of Kanamycin, 30 µg/mL chloroamphenicol). The flask was shaken at 200 rpm at 37 °C overnight. Next, the 5 mL overnight culture was diluted into another 5 mL LB-kanamycin media to a final OD of 0.1–0.2, and the culture flask was shaken at 200 rpm at 37 °C until the A_{600} value reached 0.6–0.8. The culture was induced with with 0.5 mM isopropyl-β-D-thiogalactopyranoside (IPTG; Goldbio at 19 °C. Shake the culture at 19 °C overnight at 200 rpm. After overnight growth, cells were diluted to O.D of 0.6–0.8 in fresh LB-KAN media. Cells were treated with 25 µM Ht-PreHNE for 2 hours while shaking at 200 rpm at 19 °C. 1 mL of cell suspension was transfer into a microcentrifuge tube, the pellet collected after centrifugation at 5,000 x g for 5 min. The pellets were 5 times by resuspending in 1 mL PBS and centrifuging to collect the pellet. After the fifth rinse, cells were resuspended in 500 µL PBS and irradiated by placing the samples under 365 nm UV light source for 30 min at room temperature, while constantly shaking the samples at 80–100 rpm. The samples were incubated for an additional 10 min post light shining and subsequently harvested by centrifugation at 5,000 x g, for 5 min.

E. coli cell lysis and in-gel fluorescence: To lyse *E. coli* cells, cell pellet was resuspended in 100 µL lysis buffer consisting of 50 mM HEPES pH 7.6, 2 mM TCEP, 1% Nonidet p-40, 150 µg/ mL Lysozyme, 5 µg/ mL DNAse-I and incubated for 20 min at room temperature with agitation. The cellular debris was removed by centrifugation

(18,000 x g, 8 min) at 4 °C. Click chemistry with Cy5 azide on the clarified lysate was performed as described above and the samples analyzed using SDS-PAGE analysis.

Fish husbandry and crossing: All procedures conform to the National Institutes of Health guidelines regarding animal experimentation and were approved by Cornell University's Institutional Animal Care and Use committees. Animals were maintained, and embryos were obtained according to standard fish husbandry procedures.

Fish injection and Z-REX: For injection in fish embryos, mRNA for Halo-Keap1 and Halo-P2A-Keap1 was generated. First, the desired genes were amplified using RNA-fwd and RNA-rev primers. mRNA was generated using an mMessage mMachine SP6 *in vitro* transcription kit (Ambion, AM1340) as per manufacturer's protocol except the reaction was scaled up for two preps.

Fertilized eggs at the 1–4 cell stage were injected with 2 nl mRNA (1.3–1.6 mg/ml) into the yolk sack. Immediately after injection, embryos were pooled, and separated into two petri dishes (10 cm) filled with 30 mL 10% Hank's salt solution with methylene blue and penicillin (100 U/ml) / streptomycin (100 µg/ml). To one set was added the photocaged precursor to designated LDE at a final concentration of 6 µM and to the other equal volume of DMSO in the dark. Embryos were maintained at 28 °C in the dark for 28 h after which time fish larva were washed in 10% Hank's solution with no methylene blue/antibiotic (3 times for 30 min each). Larvae were moved to 6-well plates. Half of the larvae (Ht-PreLDE-treated or -untreated) were exposed to light for 4 min the other half of each set was not. For bolus dosing, treatment of larvae with LDEs

was staggered such that the harvest time was the same for all samples including larvae that underwent Z-REX (34 hpf).

Immunofluorescence in whole zebrafish: To assess protein expression in zebrafish, larvae at 34 hours post fertilization (hpf) were dechorionated, washed twice in ice-cold PBS and fixed in 4% paraformaldehyde in 1X PBS for at least overnight with gentle rocking at 4 °C. Fixed larvae were permeabilized with chilled methanol at –20 °C for 4 h–overnight. Fish were then washed 2 times with PBS-0.1%Tween-1% DMSO for 30 min each with gentle rocking, then blocked in PBS-0.1%Tween containing 2% BSA and 10% FBS, then stained with anti-HA (rat monoclonal, Sigma H3663) or anti-Keap1 (mouse polyclonal; abcam; ab119403) primary antibodies overnight at 4 °C in blocking buffer. Subsequently, the larvae were washed twice (30 min each wash), re-blocked for 1 h at room temperature, and incubated with the AlexaFluor 568-conjugated fluorescent secondary antibodies (Abcam, ab15053 (anti-rat) ab175472(anti-mouse)) in blocking buffer for 1.5 h at room temperature with gentle rocking, and then washed three times. Fish were imaged on 2% agarose plates on a Leica M205-FA equipped with a stereomicroscope. Quantitation of IF data was performed using ImageJ/FIJI (NIH).

Click chemistry and enrichment of modified proteins after Z-REX: Casper zebrafish expressing Halo-Keap1 were treated with either the photocaged precursor with the indicated LDEs (~120 per condition). Photocaged precursors were added to the fish water after injection of Halo-Keap1 mRNA at a final concentration of 6 μM and Z-REX was performed as specified above. Immediately after Z-REX, larvae were

dechorionated and deyolked manually at 4 °C, washed twice with cold PBS to remove yolk proteins, and washed once with cold 50 mM Hepes (pH 7.6). The zebrafish pellet was flash frozen in liquid nitrogen and stored at −80 °C until lysis. Fish pellet was resuspended in 50 mM Hepes (pH 7.6), 1% Triton X-100, 0.1 mg/ml soybean trypsin inhibitor, and 2X Roche protease inhibitor. Lysis was performed by vortexing with Zirconia beands for 20s and subsequent 3 times freeze-thaw. Lysate protein was collected after centrifugation at 21,000 × g for 10 min, and concentration determined using Bradford dye relative to BSA standard. 30–50 μg of the lysate protein was removed, quenched with Laemmli buffer and saved as input. The remaining lysate was diluted to 1 mg/ml with 50 mM Hepes (pH 7.6) and 0.2 mM TCEP, TEV protease was added at a final concentration of 0.2 mg/ml, and the sample incubated at 37 °C for 30 min. Next, 5% *t*-BuOH was added to the sample. A stock solution containing 10% SDS, 10 mM $CuSO_4$, 1 mM Cu-TBTA, 1 mM biotin-azide and 20 mM TCEP (made as a 100 mM stock in 500 mM HEPES pH 7.5) was prepared and added to the sample such that the final concentration are as follows: 1% SDS, 1 mM $CuSO_4$, 0.1 mM Cu-TBTA, 0.1 mM biotin-azide, and 2 mM TCEP. The mixture was mixed thoroughly and incubated at 37 °C for 15 min, after which another 1 mM TCEP was added, mixed, and the sample incubated for additional 15 min. Protein precipitation was performed by adding EtOH (prechilled at −20 °C) at a final concentration of 75% (v/v), vortexing the sample, and incubating at −80 °C for at least overnight. Precipitated protein was collected by centrifugation at 21,000 × g at 4 °C for 2 h, washed twice with prechilled EtOH (twice), once with 75% EtOH in water, and an additional wash with prechilled acetone. Precipitate was air-dried and subsequently redissolved in 8% LDS in 50 mM HEPES

(pH 7.6), 1 mM EDTA by sonication at 50 °C and vortexing. The solubilized lysate protein was collected following centrifugation and diluted in 50 mM Hepes (pH 7.6) to give a final concentration of 0.5% LDS. The sample was added to pre-washed streptavidin high-capacity resin and incubated at 4–6 h at rt. The supernatant was removed following a low-speed centrifugation (1000 ×g), and the beads washed thrice with 50 mM Hepes (pH 7.6) containing 0.5% LDS. Bound proteins were eluted by boiling beads in 2x laemmli buffer with 6% βME at 98 °C. Samples were analyzed using SDS-PAGE followed by western blot as specified below.

SDS-PAGE and western blot: Up to 30 µl of input or elution samples were separated on a 10% polyacrylamide gel using SDS-PAGE. The gel was subsequently transferred to a PVDF membrane at 4 °C in ice-cold transfer buffer containing 25mM Tris, 192 mM Glycine, and 15% Methanol (v/v). Membrane was blocked in 5% milk for 2 h at rt, incubated with primary antibody in 1% milk for 5 h at rt, washed three times with Tris Buffer Saline (100 mM tris, pH 7.6, 150 mM NaCl) containing 0.2% Tween-20 (TBST). Where applicable, the membrane was incubated with secondary antibody in 1% milk for 5 h at rt, washed twice with TBST, followed by an additional wash with TBS. Pierce ECL western blotting substrate was used for detection of the desired protein bands.

Data quantitation and analysis: Imaging data was quantitated using ImageJ (NIH).

References

(1) Fang, X.; Fu, Y.; Long, M. J. C.; Haegele, J. A.; Ge, E. J.; Parvez, S.; Aye, Y. Temporally Controlled Targeting of 4-Hydroxynonenal to Specific Proteins in Living Cells. *J. Am. Chem. Soc.* **2013,** *135* (39), 14496.

(2) Lin, H.-Y.; Haegele, J. A.; Disare, M. T.; Lin, Q.; Aye, Y. A Generalizable Platform for Interrogating Target- and Signal-Specific Consequences of Electrophilic Modifications in Redox-Dependent Cell Signaling. *J. Am. Chem. Soc.* **2015,** *137* (19), 6232.

(3) Parvez, S.; Fu, Y.; Li, J.; Long, M. J. C.; Lin, H.-Y.; Lee, D. K.; Hu, G. S.; Aye, Y. Substoichiometric Hydroxynonenylation of a Single Protein Recapitulates Whole-Cell-Stimulated Antioxidant Response. *J. Am. Chem. Soc.* **2015,** *137* (1), 10.

(4) Parvez, S.; Long, M. J. C.; Lin, H.-Y.; Zhao, Y.; Haegele, J. A.; Pham, V. N.; Lee, D. K.; Aye, Y. T-REX on-demand redox targeting in live cells. *Nat. Protocols* **2016,** *11* (12), 2328.

(5) Los, G. V.; Encell, L. P.; McDougall, M. G.; Hartzell, D. D.; Karassina, N.; Zimprich, C.; Wood, M. G.; Learish, R.; Ohana, R. F.; Urh, M.et al. HaloTag: A Novel Protein Labeling Technology for Cell Imaging and Protein Analysis. *ACS Chem. Biol.* **2008,** *3* (6), 373.

(6) Sinha, R. P.; Hader, D.-P. UV-induced DNA damage and repair: a review. *Photochemical & Photobiological Sciences* **2002,** *1* (4), 225.

(7) Clydesdale, G. J.; Dandie, G. W.; Muller, H. K. Ultraviolet light induced injury: Immunological and inflammatory effects. *Immunology And Cell Biology* **2001,** *79*, 547.

(8) Sharma, A.; Singh, K.; Almasan, A. In *DNA Repair Protocols*; Bjergbæk, L., Ed.; Humana Press: Totowa, NJ, 2012, DOI:10.1007/978-1-61779-998-3_40 10.1007/978-1-61779-998-3_40.

(9) Simon, M. M.; Aragane, Y.; Schwarz, A.; Luger, T. A.; Schwarz, T. UVB Light Induces Nuclear Factor κB (NFκB) Activity Independently from Chromosomal DNA Damage in Cell-Free Cytosolic Extracts. *Journal of Investigative Dermatology* **1994,** *102* (4), 422.

(10) Lee, Y.-J.; Park, S.-J.; Ciccone, S. L. M.; Kim, C.-R.; Lee, S.-H. An in vivo analysis of MMC-induced DNA damage and its repair. *Carcinogenesis* **2006,** *27* (3), 446.

(11) Baranovskiy, A. G.; Babayeva, N. D.; Suwa, Y.; Gu, J.; Pavlov, Y. I.; Tahirov, T. H. Structural basis for inhibition of DNA replication by aphidicolin. *Nucleic Acids Research* **2014,** *42* (22), 14013.

(12) Hellweg, C. E.; Arenz, A.; Bogner, S.; Schmitz, C.; Baumstark-Khan, C. Activation of Nuclear Factor κB by Different Agents. *Annals of the New York Academy of Sciences* **2006,** *1091* (1), 191.

(13) Zhang, D. D. Mechanistic studies of the Nrf2-Keap1 signaling pathway. *Drug Metab Rev* **2006,** *38*.

(14) Itoh, K.; Mimura, J.; Yamamoto, M. Discovery of the negative regulator of Nrf2, Keap1: a historical overview. *Antioxidants & redox signaling* **2010,** *13*.

(15) Eggler, A. L.; Savinov, S. N. Chemical and biological mechanisms of phytochemical activation of Nrf2 and importance in disease prevention. *Recent advances in phytochemistry* **2013,** *43*, 121.
(16) Kapust, R. B.; Tözsér, J.; Fox, J. D.; Anderson, D. E.; Cherry, S.; Copeland, T. D.; Waugh, D. S. Tobacco etch virus protease: mechanism of autolysis and rational design of stable mutants with wild-type catalytic proficiency. *Protein Engineering, Design and Selection* **2001,** *14* (12), 993.
(17) Kolb, H. C.; Finn, M. G.; Sharpless, K. B. Click Chemistry: Diverse Chemical Function from a Few Good Reactions. *Angewandte Chemie International Edition* **2001,** *40* (11), 2004.
(18) Farr, S. B.; Kogoma, T. Oxidative stress responses in Escherichia coli and Salmonella typhimurium. *Microbiological Reviews* **1991,** *55* (4), 561.
(19) Greenberg, J. T.; Demple, B. A global response induced in Escherichia coli by redox-cycling agents overlaps with that induced by peroxide stress. *J Bacteriol* **1989,** *171* (7), 3933.
(20) Govindan, J. A.; Jayamani, E.; Zhang, X.; Mylonakis, E.; Ruvkun, G. Dialogue between E. coli free radical pathways and the mitochondria of C. elegans. *Proceedings of the National Academy of Sciences* **2015,** *112* (40), 12456.
(21) Paulsen, C. E.; Carroll, K. S. Cysteine-Mediated Redox Signaling: Chemistry, Biology, and Tools for Discovery. *Chem. Rev.* **2013,** *113* (7), 4633.
(22) Long, M. J. C.; Poganik, J. R.; Ghosh, S.; Aye, Y. Subcellular Redox Targeting: Bridging in Vitro and in Vivo Chemical Biology. *ACS Chem. Biol.* **2017,** *12* (3), 586.
(23) Itoh, K.; Chiba, T.; Takahashi, S.; Ishii, T.; Igarashi, K.; Katoh, Y.; Oyake, T.; Hayashi, N.; Satoh, K.; Hatayama, I.et al. An Nrf2/Small Maf Heterodimer Mediates the Induction of Phase II Detoxifying Enzyme Genes through Antioxidant Response Elements. *Biochemical and Biophysical Research Communications* **1997,** *236* (2), 313.
(24) Chan, K.; Lu, R.; Chang, J. C.; Kan, Y. W. NRF2, a member of the NFE2 family of transcription factors, is not essential for murine erythropoiesis, growth, and development. *Proceedings of the National Academy of Sciences of the United States of America* **1996,** *93* (24), 13943.
(25) de Haan, J. B.; Bladier, C.; Griffiths, P.; Kelner, M.; O'Shea, R. D.; Cheung, N. S.; Bronson, R. T.; Silvestro, M. J.; Wild, S.; Zheng, S. S.et al. Mice with a Homozygous Null Mutation for the Most Abundant Glutathione Peroxidase, Gpx1, Show Increased Susceptibility to the Oxidative Stress-inducing Agents Paraquat and Hydrogen Peroxide. *Journal of Biological Chemistry* **1998,** *273* (35), 22528.
(26) Das, B. C.; McCormick, L.; Thapa, P.; Karki, R.; Evans, T. Use of zebrafish in chemical biology and drug discovery. *Future Medicinal Chemistry* **2013,** *5* (17), 2103.
(27) Dooley, K.; Zon, L. I. Zebrafish: a model system for the study of human disease. *Current Opinion in Genetics & Development* **2000,** *10* (3), 252.
(28) Basu, S.; Sachidanandan, C. Zebrafish: A Multifaceted Tool for Chemical Biologists. *Chemical Reviews* **2013,** *113* (10), 7952.

(29) Kowalik, L.; Chen, J. K. Illuminating developmental biology through photochemistry. *Nature Chemical Biology* **2017,** *13*, 587.
(30) Kim, J. H.; Lee, S.-R.; Li, L.-H.; Park, H.-J.; Park, J.-H.; Lee, K. Y.; Kim, M.-K.; Shin, B. A.; Choi, S.-Y. High Cleavage Efficiency of a 2A Peptide Derived from Porcine Teschovirus-1 in Human Cell Lines, Zebrafish and Mice. *PLOS ONE* **2011,** *6* (4), e18556.
(31) Kolb, H. C.; Finn, M. G.; Sharpless, K. B. Click chemistry: diverse chemical function from a few good reactions. *Angew. Chem. Int. Ed. Engl.* **2001,** *40*, 2004.

CHAPTER 3

*ESTABLISHING SUFFICIENCY IN REDOX SIGNALING USING T-REX

Introduction

In enzyme-mediated cellular signaling such as phosphosignaling, it is well recognized that modification stoichiometry as low as 10% of a protein is sufficient to trigger biological outcome[1]. Low-occupancy modifications likely function through gain-of-function or dominant loss-of-function[2]. However, establishing whether low-occupancy ***redox*** modification of a specific protein is sufficient to trigger a biological response has been extremely challenging. Traditional bolus dosing approach to study redox signaling use an excess of reactive signals and have little to no control on the stoichiometry of protein modification making it impossible to establish sufficiency of redox modification required for a functional outcome. Importantly, it is also unclear whether modification of a single protein by redox signals is sufficient to elicit a phenotypic response or alternatively, modifications of several redox-sensitive targets simultaneously are required for a functional response. Because T-REX generates at most a stoichiometric amount of the redox signal in proximity to a given protein, it is perfectly suited to answer these important biological questions. Thus, we used T-REX to investigate whether selective modification of Keap1, a key modulator of the Nrf2/AR signaling axis**,** is sufficient to activate the antioxidant response pathway.

---

*This Chapter was published previously. "Substoichiometric hydroxynonenylation of a single protein recapitulates whole-cell-stimulated antioxidant response"; **Saba Parvez**, Yuan Fu, Jiayang Li, Marcus, J. C. Long, Hongyu Lin, Dustin K. Lee, Gene S. Hu and Yimon Aye* *Journal of the American Chemical Society*, **2015**, 137, 10-13 (Underlined: First-author)

Keap1, with 27 cysteines (human Keap1) in a 70 kDa protein, is a quintessential redox-sensor in mammalian cells. Even before the discovery of Keap1, it was noted that chemical inducers of phase II detoxification genes, constituted a wide array of structurally diverse compounds. However, despite the structural diversity, all these compounds were Michael acceptors capable of sulfhydryl reactivity[3]. The discovery of Keap1, a cysteine-rich protein, as the modulator of phase II detoxification response validated this claim. Of the 27 cysteines, 10 are in proximity to positively-charged amino acids which may enhance the reactivity of these cysteines by lowering the pKa and stabilizing the thiolate anion.

Keap1 is a substrate adaptor protein for the Cullin3-based Cullin-RING ubiquitin ligase (CUL3). Keap1 binds its substrate through an ETGE binding motif. A number of Keap1 interacting proteins have been characterized[4], including Nrf2. Nrf2, a transcription factor, is the key protein regulating the expression of a battery of cytoprotective and detoxification genes under the control of antioxidant response element (ARE) (**Figure 3.1**)[5]. Under basal conditions, Keap1 sequesters Nrf2 in the cytosol. Low steady-state levels of Nrf2 are maintained by CUL3-mediated constitutive ubiquitination of the transcription factor assisted by Keap1[6-8]. It is proposed that oxidative and electrophilic modifications of Keap1 disrupt the interaction between Keap1/Nrf2 and induce Nrf2 accumulation. Nrf2 reportedly then translocates to the nucleus, heterodimerizes with small Maf proteins, and induces transcriptional activation of ARE-responsive genes.

We chose to study the Nrf2/AR pathway using T-REX mainly because of the following reasons (1) Keap1 is a validated electrophile sensor proteins (2) Majority of the 27 human or mouse Keap1 cysteines has been claimed to be responsible for redox sensing roles, different cysteines being modified using different electrophiles/oxidants or under different treatment conditions[9-13] (3) Nrf2/AR signaling pathway is also regulated by multiple different redox-sensitive proteins, including GSK3β, Nrf2, PTEN etc., many of which get simultaneously modified using bolus dosing conditions[5] (**Figure 3.1**). We thus posited to use Nrf2/AR as a model signaling pathway to answer the question of sufficiency in redox signaling.

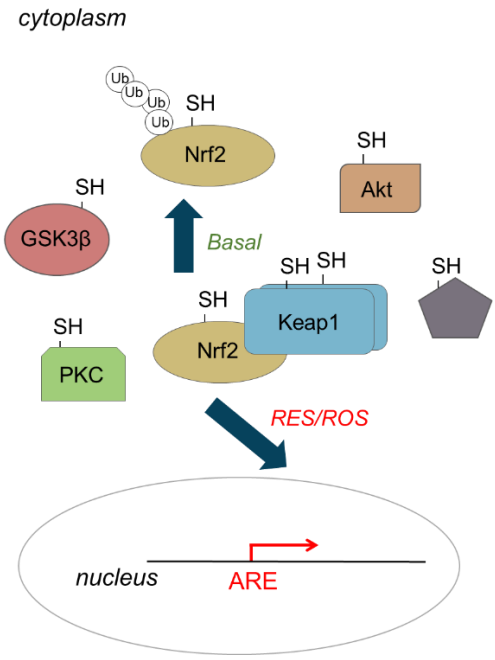

Figure 3.1 Schematic of the Nrf2/AR signaling axis. Nrf2 is a transcription factor and master regulator of the antioxidant response element (ARE). Under non-stimulated conditions Nrf2 is constitutively ubiquitylated by the action of Keap1, an adaptor protein, and Cul3-E3 ligase (not shown). Reactive oxygen and electrophilic species (ROS/RES) treatment is proposed to modify Keap1, which results in dissociation of the Keap1-Nrf2 complex, and the consequent translocation of the transcription factor to the nucleus and upregulation of ARE. Nrf2 is also regulated by a host of other proteins,

many of which are redox-sensitive. Bolus dosing methods modify many of these proteins simultaneously making it extremely challenging to understand whether modification a single target protein is sufficient to trigger a functional redox response. T-REX, because it allows selective modification of a single target protein is well suited to deconvolute this (and other) complex signaling network.

Results

Halo-Keap1 is functional

Because T-REX requires tagging the protein of interest with a HaloTag™, we first tested whether Halo-Keap1 maintained its functions. We used two different methods (1) In-cell imaging to assess the ability of Halo-Keap1 to anchor Nrf2 in the cytosol, and (2) Gel filtration analysis to assess binding of recombinant Halo-Keap1 to Nrf2. Ectopic GFP-Nrf2 expression resulted in an increase in fluorescence intensity both in the cytosol and the nucleus (**Figure 3.2A**). Co-expression of Halo-Keap1 resulted in cytosolic anchoring of GFP-Nrf2 demonstrating that Halo-Keap1 can successfully bind to Nrf2 and inhibit its translocation to the nucleus. Similar, results were obtained when GFP-Nrf2 was overexpressed in HEK293T cells stably expressing Halo-Keap1.

We next tested whether recombinantly purified human Halo-Keap1 can interact with human His_6-Nrf2. Human His_6-Keap1, His_6-Halo-Keap1, and His_6-Nrf2 were purified from *E.coli* to >95% purity (purification and gel filtration analysis of recombinant proteins was done by Dr. Jiayang Li with assistance from Dustin Lee) (**Figure 3.2B**). His_6-Keap1 or His_6-Halo-Keap1 was combined with His_6-Nrf2 in a 2:1 ratio and injected on an analytical size exclusion chromatography column and the

retention time of the elution peaks corresponding to the proteins were monitored (**Figure 3.2C-D**). Both His_6-Keap1 (**Figure 3.2C**) and His_6-Halo-Keap1 (**Figure 3.2D**) successfully bound His_6-Nrf2 as evidenced from the shift in retention time of the complex. Estimating the molecular weight using protein size standards revealed that His_6-Keap1(**Figure 3.2C**, 24.0 min; 210 kDa) and His_6-Halo-Keap1 (**Figure 3.2D**, 21.7 min; 357 kDa) formed homodimers. The discrepancy between the expected molecular weights of His_6-Keap1 (144 kDa) and His_6-Halo-Keap1 (214 kDa) dimers to those observed in gel filtration analysis has been previously reported[14]. The same is true for observed molecular weight differences in His_6-Nrf2[15].

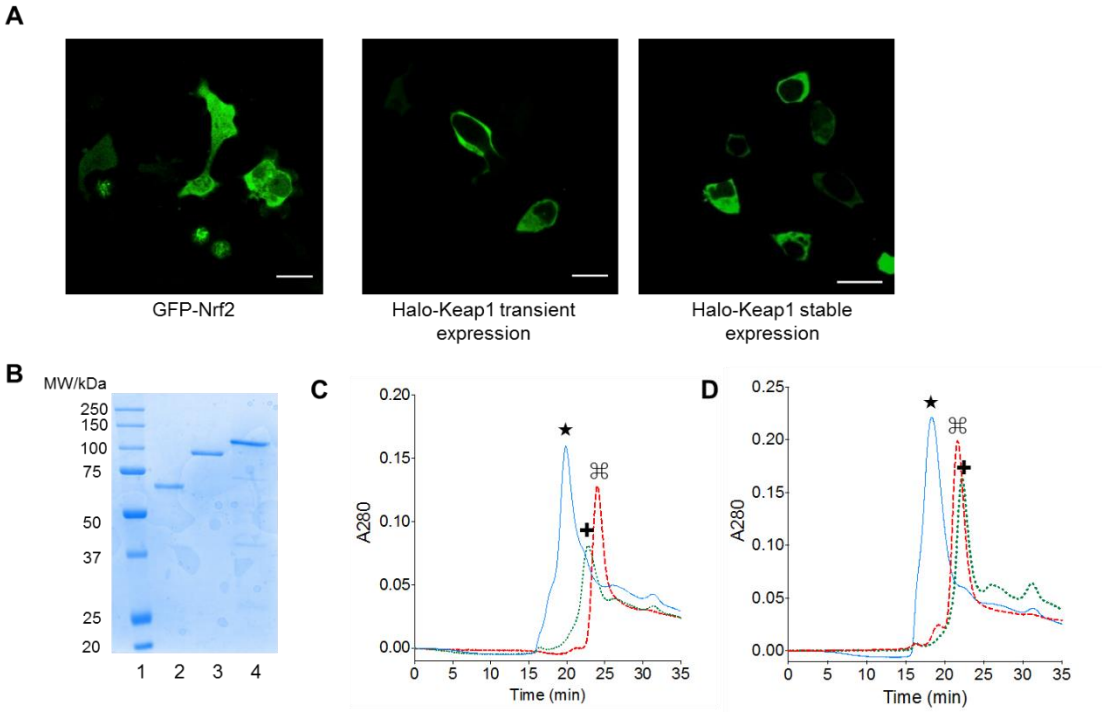

Figure 3.2 Halo Tagging Keap1 is non-invasive and does not affect its function. (A) *left panel:* HEK293T cells overexpressing GFP-Nrf2 show fluorescence both in the cytosol and the nucleus; *middle panel:* transient co-expression of Halo-Keap1 renders GFP-Nrf2 cytosolic; *right panel:* HEK293T cells stably expressing Halo-Keap1 are also able to inhibit nuclear translocation of transiently expressed GFP-Nrf2. **(B)** SDS-PAGE analysis of recombinant human proteins. Lane 1, MW ladder. Lane 2, His_6-Keap1 (72

kDa). Lane 3, His_6-Halo-Keap1 (107 kDa). Lane 4, His_6-Nrf2 (70 kDa). Nrf2 has been previously reported to migrate at an apparent MW of ~95−110 kDa. **(C-D)** Gel filtration analyses show that Halo-Keap1 behaves similarly as Keap1, in dimerization and binding to Nrf2. In both Figures 3.1C and D, solid blue (—) traces designate corresponding Keap1–Nrf2 (**C**) and (Halo-Keap1)–Nrf2 (**D**) complexes. Dotted green (…) designates Nrf2 as a standard. Dashed red (---) traces respectively designate Keap1 (**C**) and Halo-Keap1 (**D**) as standards. In the left panel, ★: 19.9 min, 541 kDa (2:1 Keap1: Nrf2); ✚: 22.5 min, 298kDa (Nrf2 alone); and ⌘: 24.0 min, 210 kDa (Keap1 dimer alone). Note: retention time of Keap1 dimer is known to deviate from the theoretical value predicted based on MW. In the right panel, ★: 18.3 min, 782 kDa (2:1 Halo-Keap1: Nrf2); ✚: 22.5 min, 298 kDa (Nrf2 alone); and ⌘: 21.7 min, 357 kDa (Halo-Keap1 dimer alone). MWs were extracted from GE Healthcare MW standard curve.

TREX selectively modifies Keap1 in vivo

After validating that Halo-Keap1 is functional we next tested whether T-REX can selectively modify Keap1 in cells. Halo-Keap1 expressing HEK293T cells were treated with 25 μM Ht-PreHNE, incubated at 37 °C in the dark for 2.5 h, washed 3 times to remove excess unbound Ht-PreHNE. HNE was released by shining 365 nm UV light on the samples for 20 min. Cells were harvested after an additional 10 min incubation. In-gel fluorescence was used to determine the modification efficiency of Keap1. We used Cy5 azide to conjugate to the alkyne functionalized Ht-PreHNE and the released HNE using copper-assisted click-chemistry. The modification efficiency of Keap1 was calculated to be 30%-50%. Interestingly, despite the co-overexpression of Halo-Keap1 and myc-Nrf2, labeling was identified solely on Keap1 to the limit of detection (**Figure 3.3A**). Unsurprisingly, bolus treatment with 25 μM HNE alkyne resulted in indiscriminate labeling of several proteins in addition to multivalent modification of overexpressed Halo-Keap1 protein. Thus, T-REX significantly minimizes the off-targets observed during bolus dosing.

Performing T-REX *in vitro* (data collected by Dr. Jiayang Li) with Halo-Keap1 and His_6-Nrf2 (added in a 2:1 ratio) and molar equivalent of Ht-PreHNE to Halo-Keap1 further underscored the importance of Keap1 as the primary electrophilic sensor. Despite the presence of both Halo-Keap1 and His_6-Nrf2 *in vitro*, efficient labeling with the released HNE alkyne was only observed on Keap1. (**Figure 3.3B**).

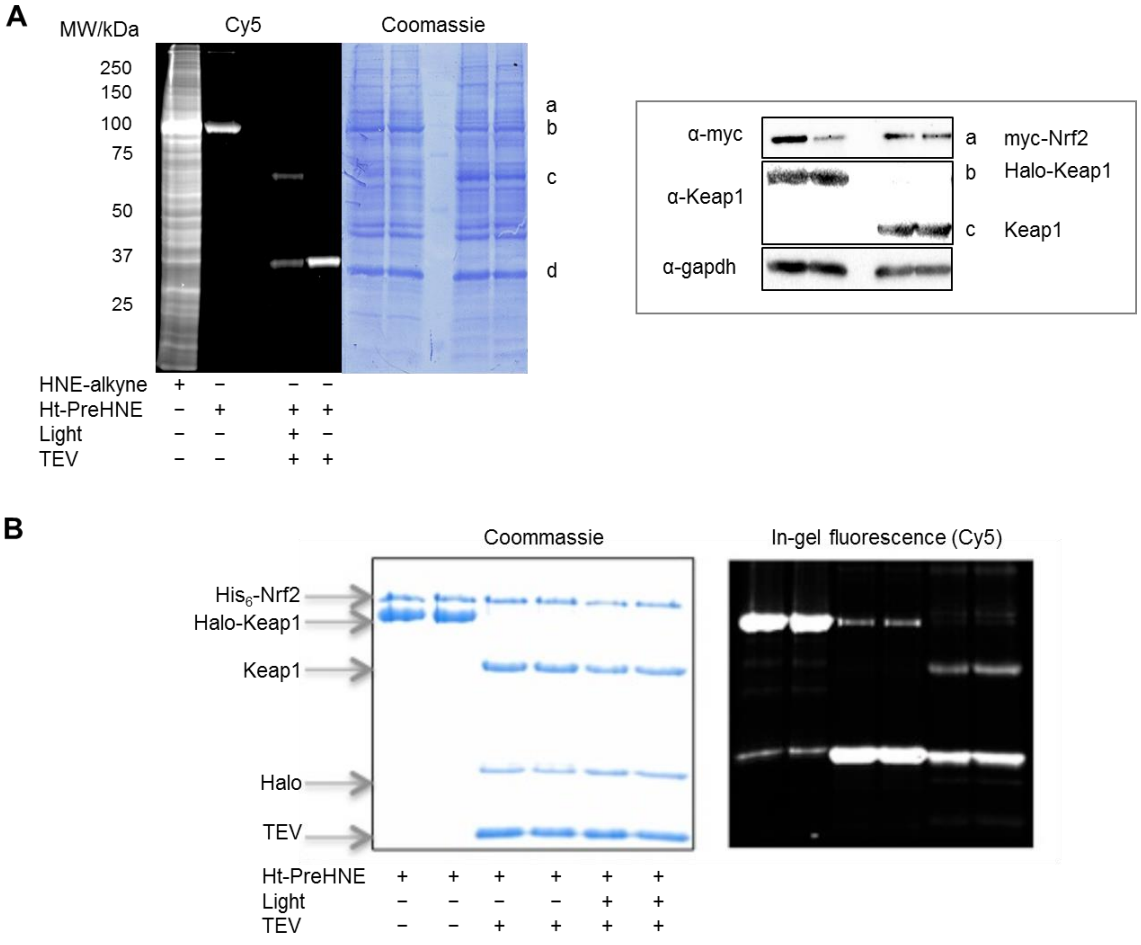

Figure 3.3 T-REX enables low stoichiometry modification of Keap1 with HNE. (A) Keap1-specific HNEylation in HEK-293 cells expressing Halo-Keap1 and myc-Nrf2 enabled by T-REX. Global HNE-alkyne treatment (25 μM) is nonspecific (left-most lane of the "Cy5" gel). a, b, c, and d markers designate myc-Nrf2, Halo-Keap1, Keap1, and Halo, respectively. Keap1-specific targeting efficiency in this representative data set is 34%. Coomassie-stained PVDF and western blot (inset) are also shown. TEV, Tobacco Etch Virus cysteine protease, enables separation of Halo and Keap1 domains.

(B) T-REX with recombinant proteins. Modification is only observed on Keap1 post light shining.

Keap1-selective modification with HNE results in Nrf2 stabilization

Because Keap1 assists in the ubiquitination of Nrf2 and its subsequent degradation, we assessed whether modification of Keap1 results in increased Nrf2 protein levels. Using western blot analysis, we first validated that HEK293T cells overexpressing Halo-Keap1 and myc-Nrf2 showed increased Nrf2 protein levels upon bolus treatment with HNE. Consistent with literature, the stabilization of Nrf2 was fast and achieved maximal upregulation within an hour of treatment with HNE (**Figure 3.4A*, left panel*).** Interestingly, Keap1-alone modification with HNE using T-REX also resulted in a significant stabilization of the ectopically expressing myc-Nrf2 (**Figure 3.4A*, right panel*)** within similar time frame. No significant Nrf2 protein level changes were observed under various T-REX controls demonstrating that short exposure to low-powered UV light and treatment with the photocaged precursor to HNE are non-invasive and does not activate the Nrf2/AR pathway.

Next, to identify whether intramolecular delivery of HNE to Keap1 is required for Nrf2 stabilization, we co-expressed GFP-Halo, His_6-Keap1, and myc-Nrf2. After performing T-REX, we assessed Nrf2 stabilization. As demonstrated in **Figure 3.4B**, no significant Nrf2 stabilization was observed in this case. Thus, T-REX results in Nrf2 stabilization by intramolecular delivery of HNE to Keap1. We were also curious to identify the mechanism of Nrf2 stabilization. There are two conflicting propositions regarding the mechanism of Nrf2 stabilization: (1) Keap1 modification with

electrophiles/oxidants results in dissociation of Keap1-Nrf2 complex and consequent increase in Nrf2 protein levels (2) Keap1 modification results in inability of Keap1 to ubiquitinate the bound Nrf2. In this second case, the bound Nrf2 does not dissociate. In fact, it stays bound and prevents newly synthesized Nrf2 from binding to Keap1 thereby increasing Nrf2 protein levels. To test these two hypotheses, we treated pre-bound recombinant Halo-Keap1: Nrf2 (2:1) complex with HNE and compared the binding profile using gel filtration analysis (**Figure 3.4C,** data collected by Dr. Jiayang Li). No observable dissociation of Halo-Keap1/Nrf2 complex was observed upon electrophile treatment suggesting that the latter of the two hypotheses is more plausible.

To ensure that Nrf2 stabilization was not a result of inhibition of proteasomal machinery, we probed for the small subunit of human ribonucleotide reductase (hRNR2), another protein with similar half-life as human Nrf2 (~3 h). No change in hRNR2 level was observed after T-REX (**Figure 3.4D*, left panel***) even though significant stabilization of Nrf2 was observed in the same samples, demonstrating that T-REX does not affect the proteasomal degradation pathway. Treatment with 20 nM Bortezomib, a known proteasome inhibitor, however, increased the levels of both ectopically expressing myc-Nrf2 and endogenous hRNR2 (**Figure 3.4D, *right panel*)**.

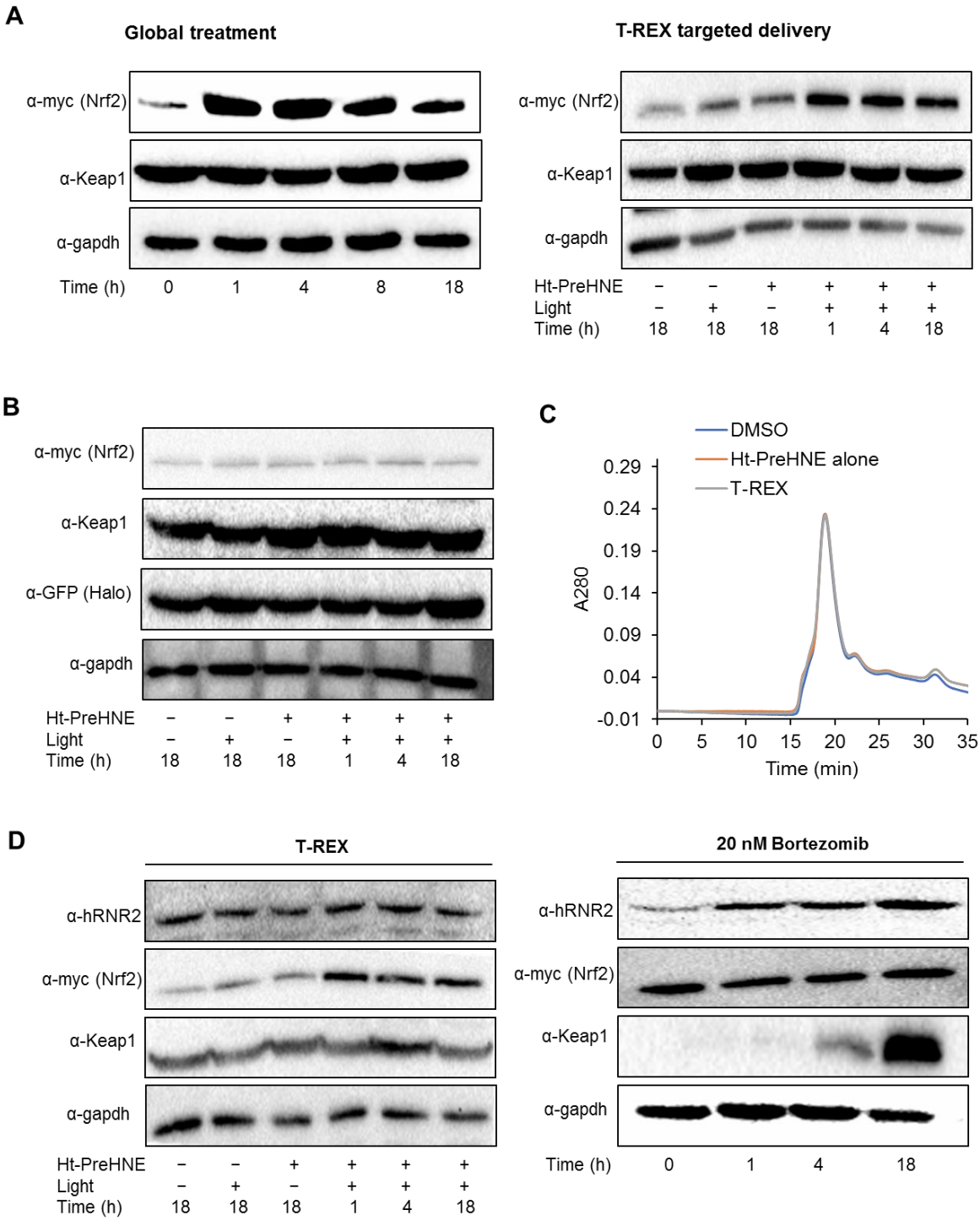
A
Global treatment
T-REX targeted delivery
α-myc (Nrf2)
α-Keap1
α-gapdh
Time (h) 0 1 4 8 18
Ht-PreHNE – – + + + +
Light – + – + + +
Time (h) 18 18 18 1 4 18
B
α-myc (Nrf2)
α-Keap1
α-GFP (Halo)
α-gapdh
Ht-PreHNE – – + + + +
Light – + – + + +
Time (h) 18 18 18 1 4 18
C
DMSO
Ht-PreHNE alone
T-REX
A280
0.29
0.24
0.19
0.14
0.09
0.04
-0.01
0 5 10 15 20 25 30 35
Time (min)
D
T-REX
20 nM Bortezomib
α-hRNR2
α-myc (Nrf2)
α-Keap1
α-gapdh
Ht-PreHNE – – + + + +
Light – + – + + +
Time (h) 18 18 18 1 4 18
Time (h) 0 1 4 18

Figure 3.4 Intramolecular delivery of HNE to Keap1 results in Nrf2 stabilization. **(A)** Bolus treatment of HEK293T cells expressing Halo-Keap1 and myc-Nrf2 with 25 μM HNE results in a rapid increase in myc-Nrf2 protein levels (*left panel*). T-REX assisted Keap1-seletive HNEylation also results in upregulation of myc-Nrf2 levels in cells (*right panel*). Time designates incubation time post treatment with bolus HNE or post light shining during T-REX. **(B)** Similar Nrf2 stabilization is not observed in cells subjected to T-REX but expressing Halo and Keap1 separately. **(C)** Gel filtration analyses showing that Nrf2 stabilization is not due to Nrf2 dissociating from the Keap1/Nrf2 complex post HNE modification. HNE modified Halo-Keap1 still forms complex with recombinant His_6-Nrf2. **(D)** Nrf2 stabilization is also not a result of proteasomal inhibition. Keap1-alone HNEylation stabilizes myc-Nrf2, whereas another unrelated, yet proteasomally regulated protein, hRNR2 with a half-life similar to Nrf2 is unaffected (*left panel*). Treatment with 20 nM Bortezomib, a proteasome inhibitor, results in a time-dependent stabilization of both hRNR2 and myc-Nrf2 (*right panel*).

HNEylation of Keap1 increases both cytosolic and nuclear Nrf2 levels

We next asked whether Nrf2 stabilization resulted in increased translocation of Nrf2 to the nucleus. We used cell fractionation and fluorescence imaging as two independent methods to assess change in nuclear localization of Nrf2 upon T-REX. Cells expressing Halo-Keap1 and myc-Nrf2 were fractionated after Keap1 modification with HNE using T-REX. Cell fractionation data demonstrated that there was an increase in overall levels of myc-Nrf2 both in the cytosol and nucleus rather than selective translocation of stabilized Nrf2 (**Figure 3.5A**). Quantitation of Immunofluorescence (IF) data measuring the ratio of nuclear myc-Nrf2 to total myc-Nrf2 also substantiated the outcome observed by cell fractionation method (**Figure 3.5B**).

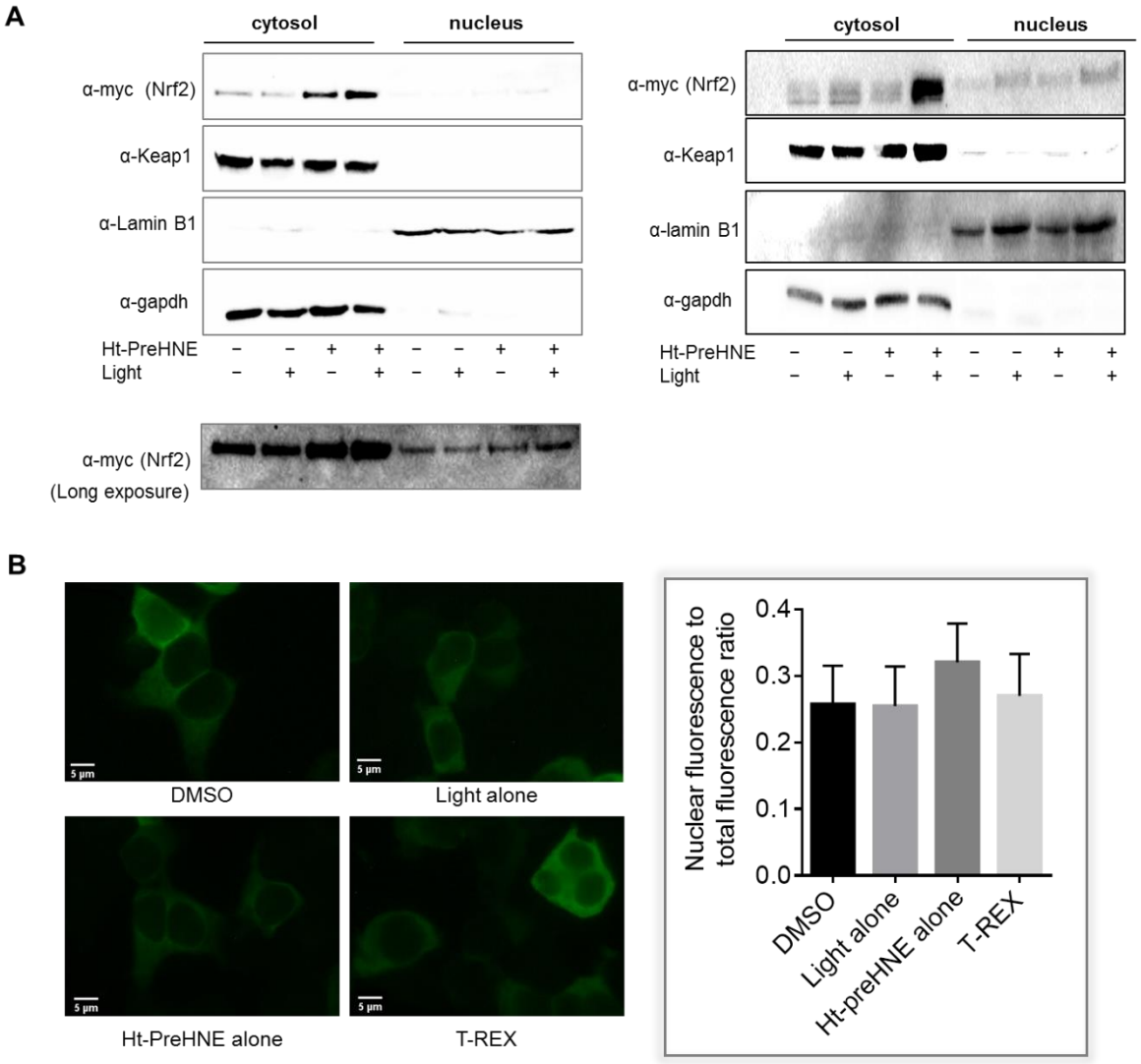

Figure 3.5 Keap1-selective HNEylation results in an increase of cytosolic and nuclear Nrf2. (A) Nuclear/cytosol fractionation analysis subsequent to T-REX-assisted Keap1-specific HNEylation shows that Nrf2 does not selectively accumulate in the nucleus. Rather there is an increase in overall levels of Nrf2 in both the cytosol and the nucleus. Lamin B and GAPDH respectively serve as nuclear and cytosol markers (and loading controls). Two sets of representative data are shown. **(B)** The outcomes were independently validated by immunofluorescence analysis. HEK-293 cells transiently expressing myc-Nrf2 and stably expressing Halo-Keap1 were subjected to the indicated conditions against controls and subsequently fixed and immunostained using anti-myc primary and FITC-conjugated secondary antibodies. Representative images are shown with scale bars, 5 μm. *Inset*: Image-J quantitation of IF data shows no significant change in nuclear:total Nrf2 ratio in HEK293T cells post T-REX.

Low stoichiometry HNEylation of Keap1 is sufficient to trigger AR pathway activation

We looked further downstream to assess whether Nrf2 stabilization leads to increase in transcriptional activity of Nrf2. We used multiple approaches to answer this question. First, we used a luciferase-based reporter assay that reports on the transcriptional activity of Nrf2. The reporter consists of a firefly luciferase under the control of ARE promoter. A constitutively expressing *Renilla* luciferase under CMV promoter is used as a normalization control. Our data revealed that selective modification of Keap1 at low stoichiometry using T-REX is sufficient to upregulate AR to extent similar to that observed under bolus dosing method (**Figure 3.6A**). The level of AR induction we observed is comparable to previously reported values. In-gel fluorescence analyses also showed that the HNE signal on Keap1 persisted over time the time course of the experiment (**Figure 3.6B**). Additionally, consistent with lack of labeling when Halo and Keap1 are expressed as non-fused proteins (**Figure 3.6C**), no AR upregulation was observed in cells expressing GFP-Halo, His_6-Keap, and myc-Nrf2 under otherwise identical conditions to T-REX samples (**Figure 3.6B**).

We further demonstrated the increase in transcriptional activity of Nrf2 using quantitative reverse transcriptase-PCR (qRT-PCR) analysis to probe for changes in endogenous Nrf2-regulated genes (data collected in collaboration with Dr. Yuan Fu) (**Figure 3.6C**). NQO1, HO-1, Trx, and GCLM1, established ARE-driven genes, were upregulated relative to GAPDH post T-REX. We also showed an increase in protein levels of NQO1 using western blot (in collaboration with Dr. Yuan Fu) (**Figure 3.6D**). These data collectively provide direct experimental evidence that substoichiometric

HNEylation on a single target is sufficient to stimulate physiologic responses in the same way enzyme-assisted modifications such as phosphorylation do.

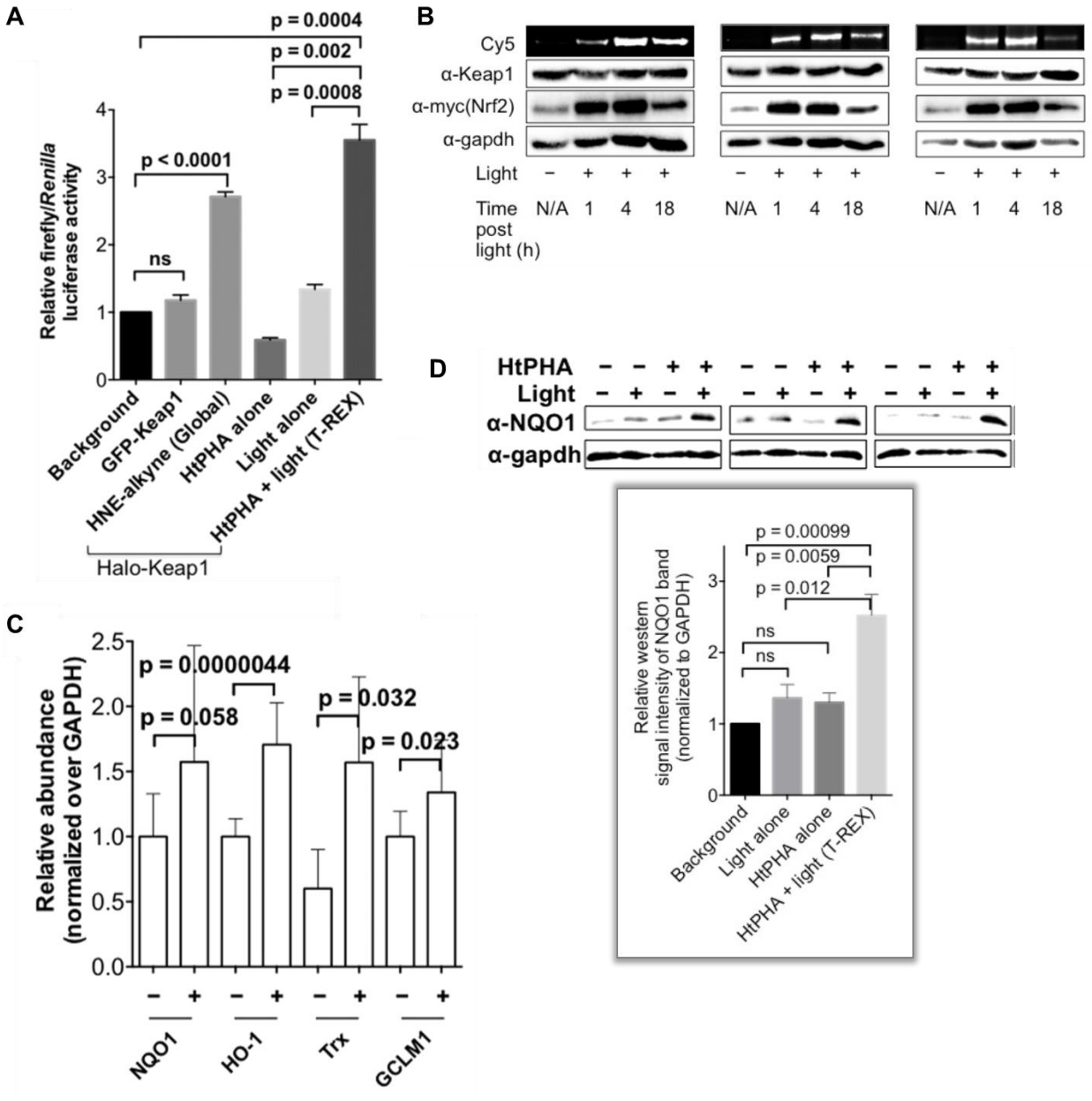

Figure 3.6 Keap1-selective HNEylation results in upregulation of the Nrf2/AR response. (A) Keap1-selective HNE modification results in ARE induction measured using a dual luciferase reporter assay. Firefly luciferase is under the control of ARE promoter which is normalized to *Renilla* luciferase intensity under constitutively expressing CMV promoter. The level of ARE induction upon T-REX is similar to that

observed with HNE bolus dosing. Additionally, no AR induction was observed when T-REX was performed in cells where Halo and GFP-Keap1 were expressed as non-fused proteins. **(B)** HNE-alkyne signal remains on Keap1 over the time course of the western blot and ARE-luciferase assays shown in Figures **3.4A** and **3.6A**. Results from three independent experiments are shown. Time post light indicates incubation time after 20-min light exposure. **(C)** Relative transcript levels of various endogenous ARE-regulated genes induced subsequent to T-REX HNEylation in HEK-293T cells analyzed by qRT-PCR. **(D)** Upregulation of endogenous NQO1 protein post T-REX HNEylation of Keap1. Three representative western blots are shown. *Inset:* Quantitation of western blot using ImageJ.

Keap1 is a promiscuous sensor of electrophiles

We were interested to find out whether certain cysteine residues of Keap1 serve as gatekeeper residues for HNE sensing. We used mass spectrometry to identify the cysteine residues that get labeled in *in vitro* and in cells (**Figure 3.7A and Appendix I,** data was collected in collaboration with Dr. Yuan Fu). Bolus treatment of Halo-Keap1 expressing cells with 100 μM HNE modified four unique cysteines, C23, C226, C273, and C368. Only C23, and C368 were HNEylated upon treatment with 25 μM HNE. A unique set of cysteines were identified to be HNEylated upon T-REX in cells. C513 and C518 were the modified residues under this condition. Interestingly, T-REX *in vitro* modified C226 and C368. Bolus dosing with 1.1 equivalent HNE of recombinant Halo-Keap1 identified the following six HNEylated cysteine residues, C77, C151, C226, C273, C319, and C368 (**Figure 3.7A**). The difference in modification sites identified under different conditions likely arises from difference in Keap1 conformation, difference in protein microenvironment *in vitro* vs in cells, as well contributions from various cellular partners. Unsurprisingly, majority of the 27 Cys residues of human and mouse Keap1 proteins has been reportedly modified *in vitro* with various electrophiles[12].

We next mutagenized each of the cysteine residues identified to be HNEylated using T-REX either *in vitro* or in cells to the corresponding serine residues. We then assessed the targeting efficiency on these mutants as well as assessed Nrf2 stabilization in cells expressing the mutants upon T-REX (**Figure 3.7B-C**). Our data demonstrated that C513S/C518S, and C226S/C368S mutants and the respective double mutants were labeled with HNE as efficiently as the wild type Halo-Keap1. Additionally, modification of the mutant proteins also led to Nrf2 stabilization to similar extents to those of wild type protein modification (**Figure 3.7B-C**). These data likely suggest that Keap1 is a promiscuous sensor of electrophiles, and that multiple cysteines can respond to HNE signal.

A

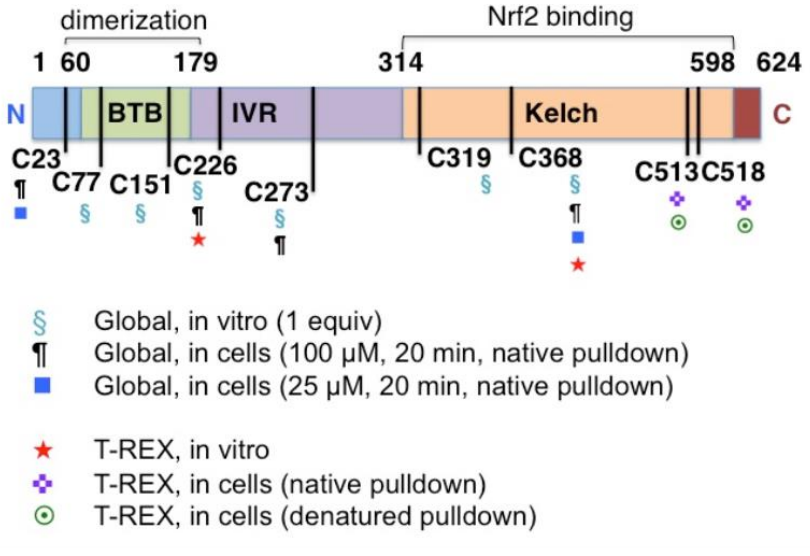
dimerization
Nrf2 binding
1 60 179 314 598 624
N
BTB
IVR
Kelch
C
C23 C77 C151 C226 C273 C319 C368 C513 C518
§ Global, in vitro (1 equiv)
¶ Global, in cells (100 μM, 20 min, native pulldown)
■ Global, in cells (25 μM, 20 min, native pulldown)
★ T-REX, in vitro
✣ T-REX, in cells (native pulldown)
⊙ T-REX, in cells (denatured pulldown)

B

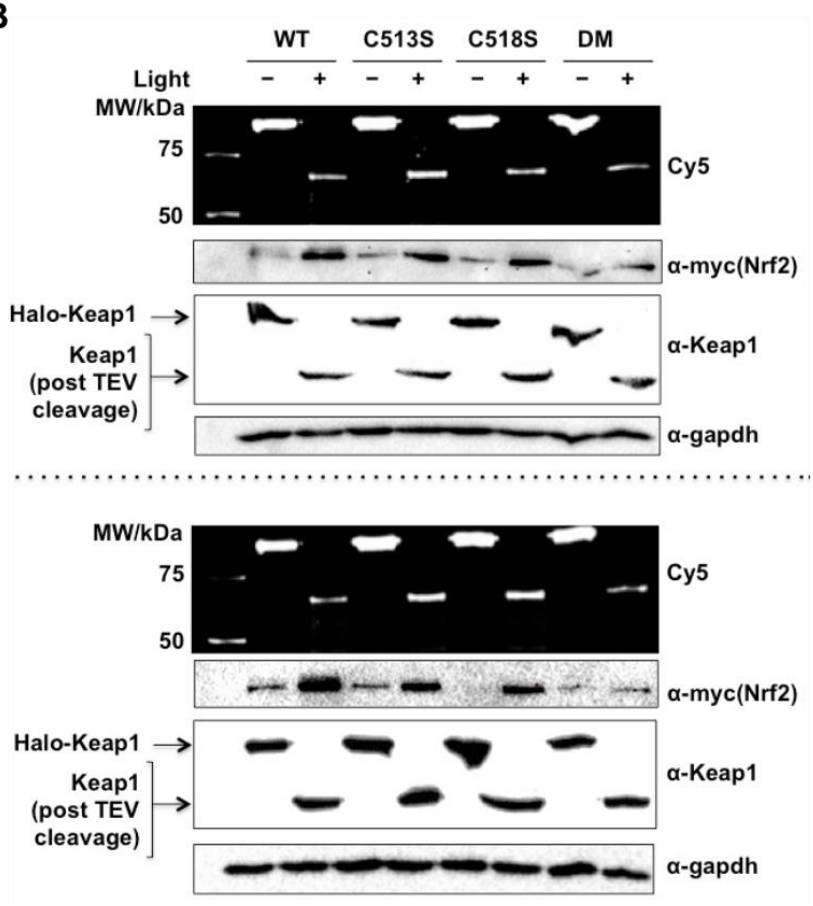
WT C513S C518S DM
Light – + – + – + – +
MW/kDa
75
50
Cy5
α-myc(Nrf2)
Halo-Keap1
Keap1 (post TEV cleavage)
α-Keap1
α-gapdh
MW/kDa
75
50
Cy5
α-myc(Nrf2)
Halo-Keap1
Keap1 (post TEV cleavage)
α-Keap1
α-gapdh

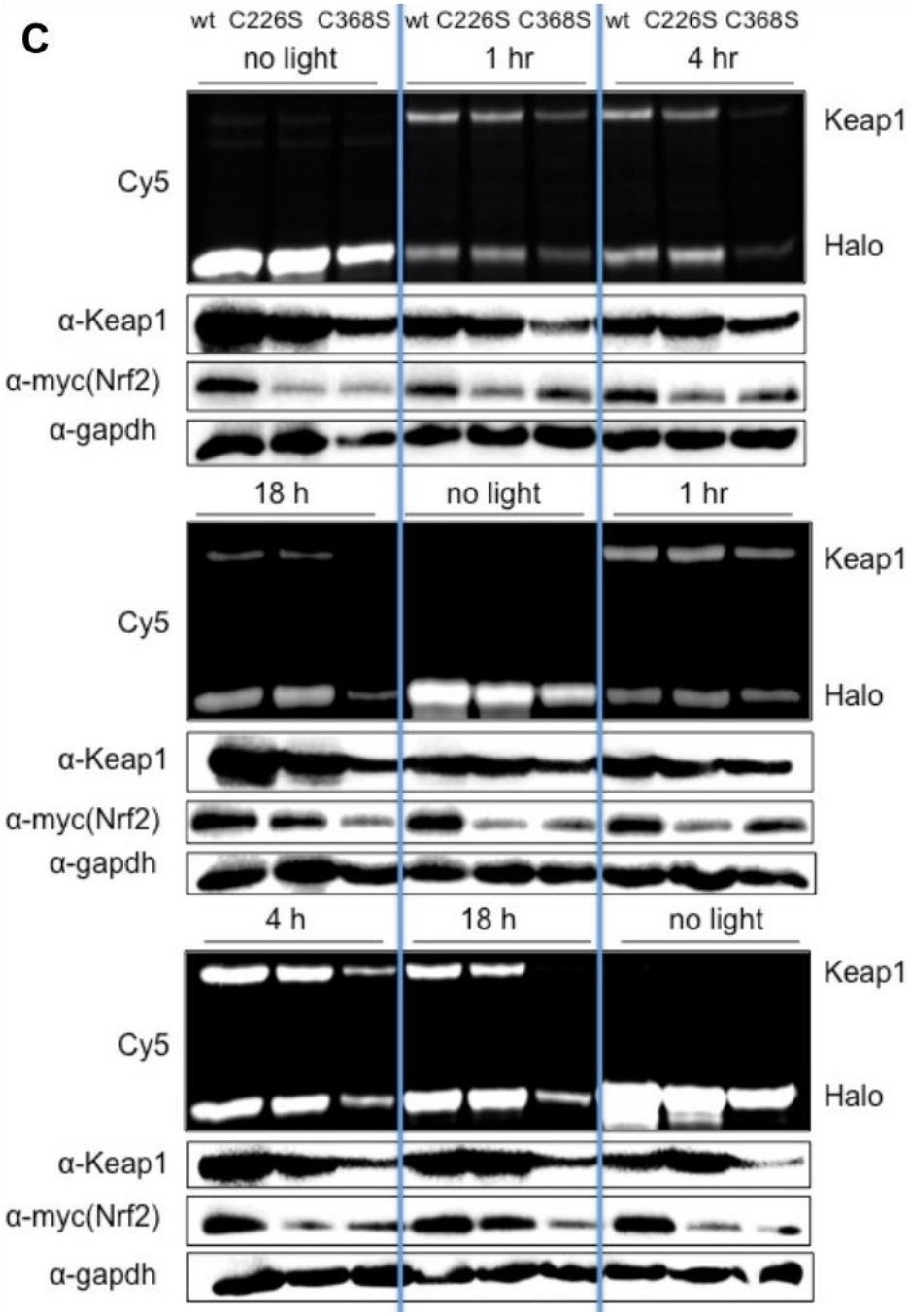

Figure 3.7 Keap1 is a promiscuous sensor of HNE. (A) Different cysteines are modified with HNE depending on the condition of treatment. Bolus treatment with HNE in cells results in a different set of cysteines being modified compared to in vitro treatment. Similarly, different set of cysteines are modified upon T-REX in vitro compared to in cells. The difference in cysteine residues is likely a result of conformation difference of Halo-Keap1 in vitro and in cells. **(B)** C513S and C518S mutants, and **(C)** C226S and C368S mutants are as efficiently labeled as with HNE as

the wild type protein. The mutants also can upregulate Nrf2 protein suggesting that Keap1 is a promiscuous sensor to HNE.

Discussion

Understanding the molecular underpinnings of cellular communication has been at the cornerstone of modern drug discovery efforts[16,17]. In canonical form of cellular signaling such as phosphosignaling, the involvement of enzymes (kinases and phosphatases) has provided biochemical tractability in understanding the consequences of individual enzyme-catalyzed posttranslational modification (PTM) events[18]. However, despite significant efforts our understanding of how non-enzymatic PTMs, such as those mediated by reactive redox signals, play roles in cell signaling has remained limited[19]. This is in part due to lack of tools to study the functional ramifications of individual redox signaling events in biological systems. Current approaches using bolus dosing have provided a wealth of information regarding stress-response pathways[19-22]. However, these approaches modify a large number of proteins simultaneously triggering multiple redox-linked pathways[19-21,23]. Thus, bolus dosing methods are less amenable for the study of physiological redox signaling whereby modifications of individual redox-sensitive proteins are perhaps sufficient to trigger biological response. Additionally, conventional approaches do not provide information on the stoichiometry of modification on an individual or a set of targets required to elicit a biological outcome.

Here, we reported the use of a unique redox-targeting platform (T-REX) to understand the functional ramifications of low stoichiometry redox modification of redox-sensitive proteins. As a proof-of-concept, we demonstrated that

substoichiometric modification of Keap1, an important electrophile-responsive protein and a negative regulator of the druggable Nrf2/AR signaling pathway, results in activation of signaling response. Importantly, we showed that the level of AR activation achieved by target-specific modification of Keap1 is comparable to that obtained by bolus dosing methods where a plethora of other redox-sensitive targets are also modified. In summary, our results clearly demonstrate that T-REX is a unique platform that allows not only the selective modification of redox-sensitive proteins on-demand but also assess the functional outcome of this modification in a cellular context. To our knowledge, the findings presented in this chapter demonstrate for the first time that low-occupancy modification of a single protein is sufficient to trigger an efficient biological response. This knowledge is unattainable using bolus dosing methods.

Experimental Setup

Cell culture and T-REX: Cell culture conditions and T-REX in mammalian cells are described in Chapter 2

*Generation of stably transfected cells***:** HEK-293 cells were transfected with pMIR-DsRed-IRES-HaloKeap1 plasmid according to the Mirus protocol. Upon reaching full confluence, the cells were incubated with fresh media containing puromycin at 2 μg/mL, and growth was continued changing media every 4^{th} day. Upon regaining full confluence (over ~1-2 weeks period), the cells were transferred into a small flask (e.g., 25 cm^2) and cultivation was continued at the same concentration of puromycin. Western blot and FACS analysis were performed subsequently.

Cell lysis and western blotting: Whole cell lysates was prepared by three times rapid freeze thaw in ice-cold 50mM HEPES buffer (pH 7.6), 1% Nonidet P-40 and 0.3mM TCEP. Cell extract was clarified by centrifugation at 16,000Xg for 8min at 4C. Total protein concentration in lysate was determined using Bradford Assay. For Nrf2 stabilization experiments, whole cell lysate was prepared in 1X RIPA buffer (50mM Tris (pH 7.4), 150mM NaCl, 1% (v/v) Nonidet P-40, 0.5% (w/v) Deoxycholate, 0.1% (w/v) SDS, 1mM orthovanadate and Roche protease inhibitor).

Immunofluorescence: Cells were grown to 70% confluent in 6 well plates with coverslips coated in 0.1% Gelatin. The media was aspirated and cells washed once with 1X PBS buffer. To fix cells, 2% Paraformaldehyde freshly prepared in PBS was added to each well and incubated for 35 min at 4C. The fixative was aspirated and washed with PBS three times with 5 minutes incubation at 4C per wash. Blocking and permeabilization was performed for 20 min at 4C with 3% BSA, 0.2% Triton X-100 in PBS. Cells were incubated with anti-c-myc antibody (1:100) in incubation buffer (1% BSA, 0.02% Triton X-100 in PBS) for 45 min at room temperature followed by 35 min incubation with mouse IgG conugated to FITC (1:500). Cells were rinsed 3 times with PBS after each incubation period. DAPI was prepared fresh by adding 10uL of 0.005% in 15 mL PBS and added to the wells for 1.5 min in dark. Coverslips were washed with once with PBS, placed on slides with mounting medium stored till imaged using a Zeiss 510 meta confocal fluorescence microscope. Image analysis was performed using ImageJ.

*ARE dual luciferase assay***:** Cignal Antioxidant Response Reporter (luc) Kit (CCS-5020L) was from Qiagen and Dual Luciferase reporter Assay system was from Promega (E1910) were used according to the manufacturer's protocol.

Cell fractionation **:** Cell fractionation protocol was adapted from *Nature Protocols, 8 (3) 2013*[24]. Cells from 8cm^2 plate were suspended in 50 µL Buffer A containing 20mM Tris (pH 7.6) 0.1 mM EDTA, 2 mM $MgCl_2$.6H2O, 0.5 mM NaF and 0.5mM sodium orthovanadate and Roche cocktail protease inhibitor. The cell suspension was incubated for 2 min at room temperature followed by 10 min on ice. 1% final concentration of Nonidet P-40 was added to the cell suspension and mixed with 200uL pipet. The cell lysate was centrifuged at 500xg for 3 min at 4C and 80% of the supernatant was extracted. The remaining white nuclear pellet was washed three time with 200 µL Buffer A containing 1% Nonidet P-40. The nuclear pellet was resuspended in 20 µL Buffer B containing 20 mM HEPES (pH 7.9), 400mM NaCl, 25% (v/v) glycerol, 1 mM EDTA, 0.5 mM NaF, 0.5 mM sodium orthovanadate, 0.5 mM DTT and Roche. Pellet was lysed by 2 times rapid freeze thaw followed by 20 min incubation on ice. The supernatant was collected after centrifuging at 20,000Xg for 20 min. Protein concentration was determined using Bradford dye.

His-tag pull down: HEK 293T cells were split in 2 X 60 cm^2 plate. After the cells reached 60% confluence, the media were aspirated and replaced with fresh 8 mL complete media. Cells were transfected with 7.5 µg of the designated Halo clone and 30 µL PEI in 600 µL in Opti-MEM media for 24–36 h after which the cells were treated with 25 µM Ht-PreHNE for 2.5 h. Rinsing and light shining protocol were as described

above. Cells were harvested, pooled, washed twice with chilled 1X DPBS and flash frozen. Cell lysis was performed in 500 µL of lysis buffer containing in final concentrations 50 mM HEPES (pH 7.6), 100 mM NaCl, 1% Nonidet P-40, 10 mM Imidazole, 5 mM βME and Roche protease inhibitor by a rapid freeze-thaw (x3). Lysate was clarified by centrifugation at 18,000 x g for 8 min at 8 °C. Total protein concentration was determined using Bradford assay using BSA as a standard. Lysate was diluted to 1.5 mg/mL in lysis buffer and incubated with 50 µL bed volume of His60 nickel resin (pre-equilibrated with lysis buffer) for 1 h at 4 °C with end-over-end rotation. The resin was then washed (x3), each time for 5 min with 500 µL wash buffer containing in final concentrations 50 mM HEPES (pH 7.6), 100 mM NaCl, 0.5% Nonidet P-40, 20 mM imidazole and 5 mM βME. The bound protein was eluted sequentially with 30 µL of elution buffer 1 (50 mM HEPES, 100 mM NaCl, 60 mM imidazole, 5 mM βME), elution buffer 2 (50 mM HEPES, 100 mM NaCl, 100 mM Imidazole, 5 mM βME) and finally with elution buffer 3 (50 mM HEPES, 100 mM NaCl, 150 mM imidazole, 5 mM βME). The samples were subjected to SDS-PAGE and stained with colloidal blue (Coomassie G-250) stain.

In-gel trypsin digestion of SDS gel bands: The enriched Halo-Akt3 protein band from the SDS-PAGE gel above was cut and subjected to in-gel digestion with trypsin (Promega) followed by extraction of the tryptic peptide as reported previously[25]. The excised gel pieces were washed consecutively in 200 µL distilled water, 100 mM ammonium bicarbonate (Ambic, pH 7.8)/acetonitrile (1:1) and acetonitrile (ACN). The gel pieces were reduced with 70 µL of 5 mM TCEP in 50 mM Ambic solution (pH 7.8)

for 45 min at room temperature and alkylated with 100 µL of 55 mM Iodoacetamide in 100 mM Ambic at room temperature in the dark for 60 min. After wash steps as described above, the gel slices were dried and rehydrated with 50 µL trypsin in 50 mM Ambic, 10% ACN (20 ng/µL) at 37 °C for 16 h. The digested peptides were extracted twice with 70 µl of 50% ACN, 5% formic acid (FA) and once with 70 µl of 90% ACN, 5% FA. Extracts from each sample were combined and lyophilized.

Protein Identification by nano LC/MS/MS Analysis: The in-gel tryptic digests were reconstituted in 20 µL of 0.5% FA for nanoLC-ESI-MS/MS analysis, which was carried out by an Orbitrap Elite mass spectrometer (Thermo-Fisher Scientific, San Jose, CA) equipped with a "CorConneX" nano ion source device (CorSolutions LLC, Ithaca, NY). The Orbitrap was interfaced with a Dionex UltiMate3000RSLCnano system (Thermo, Sunnyvale, CA). The gel extracted peptide samples (5 µL) were injected onto a PepMap C18 trap column-nano Viper (5 µm, 100 µm x 2 cm, Thermo) at 20 µL/min flow rate for on-line desalting and then separated on a PepMap C18 RP nano column (3 µm, 75 µm x 25 cm, Thermo) which was installed in the nano device with a 10-µm spray emitter (NewObjective, Woburn, MA). The Orbitrap calibration and nanoLC-MS/MS operation were as described previously[26]. Peptides were eluted with a 90-min gradient of 5% to 38% ACN in 0.1% FA at a flow rate of 300 nL/min, followed by a 5-min ramping to 95% ACN-0.1% FA and a 7-min hold at 95% ACN-0.1% FA. The Orbitrap Elite was operated in positive ion mode with nano spray voltage set at 1.5 kV and source temperature at 250 °C.

The instrument was operated in parallel data-dependent acquisition (DDA) under FT-IT mode using FT mass analyzer for one MS survey scan from m/z 375 to 1800 with a resolving power of 120,000 (fwhm at m/z 400) followed by MS/MS scans on top 15 most intensive peaks with multiple charged ions above a threshold ion count of 10,000 in FT mass analyzer. External calibration using Ultramark 1621 for both FT mass analyzer and IT mass analyzer is performed. Dynamic exclusion parameters and normalized collisional energy were set same as previously[26,27]. All data were acquired under Xcalibur 2.2 operation software (Thermo-Fisher Scientific).

LC-MS/MS data analysis: The DDA raw files for CID MS/MS only were subjected to database searches using Proteome Discoverer (PD) 1.4 software (Thermo Fisher Scientific, Bremen, Germany) with the Sequest HT algorithm. The database search was conducted against a human UniProt database containing 160,672 entries with two-missed trypsin cleavage sites allowed. The peptide precursor tolerance was set to 10 ppm and fragment ion tolerance was set to 0.6 Da. Variable modification of cysteine carboxymethylation, methionine oxidation, N-terminal acetylation and deamidation of asparagine/glutamine were set along with HNE alkyne (152.08 Da) and reduced HNE alkyne (154.10 Da) as well as their dehydrated HNE alkyne (134.07 Da) and dehydrated and reduced HNE alkyne (136.09 Da) on cysteine and all of these modifications also on histidine and lysine residues. Only high confidence peptides defined by Sequest HT with a 1% FDR by Percolator were considered for the peptide identification. All MS/MS spectra for identified Cam (carbamidomethylation) and HNE Cys modified peptides

from initial database searching were manually inspected and validated using Xcalibur 2.2.

References

(1) Wu, R.; Haas, W.; Dephoure, N.; Huttlin, E. L.; Zhai, B.; Sowa, M. E.; Gygi, S. P. A large-scale method to measure absolute protein phosphorylation stoichiometries. *Nat Meth* **2011,** *8* (8), 677.

(2) Lin, H.; Du, J.; Jiang, H.; Begley, T. P. In *Wiley Encyclopedia of Chemical Biology*; John Wiley & Sons, Inc., 2007

(3) Talalay, P.; De Long, M. J.; Prochaska, H. J. Identification of a common chemical signal regulating the induction of enzymes that protect against chemical carcinogenesis. *Proceedings of the National Academy of Sciences of the United States of America* **1988,** *85* (21), 8261.

(4) Hast, B. E.; Goldfarb, D.; Mulvaney, K. M.; Hast, M. A.; Siesser, P. F.; Yan, F.; Hayes, D. N.; Major, M. B. Proteomic analysis of ubiquitin ligase KEAP1 reveals associated proteins that inhibit NRF2 ubiquitination. *Cancer research* **2013,** *73* (7), 2199.

(5) Hayes, J. D.; Dinkova-Kostova, A. T. The Nrf2 regulatory network provides an interface between redox and intermediary metabolism. *Trends in Biochemical Sciences 39* (4), 199.

(6) Itoh, K.; Wakabayashi, N.; Katoh, Y.; Ishii, T.; O'Connor, T.; Yamamoto, M. Keap1 regulates both cytoplasmic-nuclear shuttling and degradation of Nrf2 in response to electrophiles. *Genes to Cells* **2003,** *8* (4), 379.

(7) Kobayashi, A.; Kang, M.-I.; Okawa, H.; Ohtsuji, M.; Zenke, Y.; Chiba, T.; Igarashi, K.; Yamamoto, M. Oxidative Stress Sensor Keap1 Functions as an Adaptor for Cul3-Based E3 Ligase To Regulate Proteasomal Degradation of Nrf2. *Molecular and Cellular Biology* **2004,** *24* (16), 7130.

(8) Zhang, D. D.; Lo, S.-C.; Cross, J. V.; Templeton, D. J.; Hannink, M. Keap1 Is a Redox-Regulated Substrate Adaptor Protein for a Cul3-Dependent Ubiquitin Ligase Complex. *Molecular and Cellular Biology* **2004,** *24* (24), 10941.

(9) Zhang, D. D. Mechanistic studies of the Nrf2-Keap1 signaling pathway. *Drug Metab Rev* **2006,** *38*.

(10) Holland, R.; Fishbein, J. C. Chemistry of the Cysteine Sensors in Kelch-Like ECH-Associated Protein 1. *Antioxidants & redox signaling* **2010,** *13* (11), 1749.

(11) Itoh, K.; Mimura, J.; Yamamoto, M. Discovery of the negative regulator of Nrf2, Keap1: a historical overview. *Antioxidants & redox signaling* **2010,** *13*.

(12) Bryan, H. K.; Olayanju, A.; Goldring, C. E.; Park, B. K. The Nrf2 cell defence pathway: Keap1-dependent and -independent mechanisms of regulation. *Biochem. Pharmacol.* **2013,** *85* (6), 705.

(13) Eggler, A. L.; Savinov, S. N. Chemical and biological mechanisms of phytochemical activation of Nrf2 and importance in disease prevention. *Recent advances in phytochemistry* **2013,** *43*, 121.

(14) Small, E.; Eggler, A.; Mesecar, A. D. Development of an efficient E. coli expression and purification system for a catalytically active, human Cullin3–RINGBox1 protein complex and elucidation of its quaternary structure with Keap1. *Biochemical and Biophysical Research Communications* **2010,** *400* (4), 471.
(15) Lau, A.; Tian, W.; Whitman, S. A.; Zhang, D. D. The Predicted Molecular Weight of Nrf2: It Is What It Is Not. *Antioxidants & Redox Signaling* **2013,** *18* (1), 91.
(16) Sebolt-Leopold, J. S.; English, J. M. Mechanisms of drug inhibition of signalling molecules. *Nature* **2006,** *441* (7092), 457.
(17) Ohren, J. F.; Sebolt-Leopold, J. S. Inhibitors of Bcr-abl... breaking new ground again. *Nat. Chem. Biol.* **2006,** *2* (2), 63.
(18) Jensen, O. N. Modification-specific proteomics: characterization of post-translational modifications by mass spectrometry. *Curr. Opin. Chem. Biol.* **2004,** *8* (1), 33.
(19) (Eds.); Jacob, C.; Winyard, P. G. Redox Signaling and Regulation in Biology and Medicine. **2009 Wiley-VCH**,
(20) Wall, S. B.; Smith, M. R.; Ricart, K.; Zhou, F.; Vayalil, P. K.; Oh, J. Y.; Landar, A. Detection of electrophile-sensitive proteins. *Biochim. Biophys. Acta* **2014,** *1840* (2), 913.
(21) Rudolph, T. K.; Freeman, B. A. Transduction of redox signaling by electrophile-protein reactions. *Sci Signal* **2009,** *2* (90), re7.
(22) Owen, E. E. Redox Metabolism and Longevity Relationships in Animals and Plants: . *Talor & Francis Group* **2009**.
(23) Marnett, J. D. W. a. L. J. Alterations in Gene Expression Induced by the Lipid Peroxidation Product, 4-Hydroxy-2-nonenal. *Chem. Res. Toxicol* **2005,**.
(24) Rosner, M.; Schipany, K.; Hengstschlager, M. Merging high-quality biochemical fractionation with a refined flow cytometry approach to monitor nucleocytoplasmic protein expression throughout the unperturbed mammalian cell cycle. *Nature protocols* **2013,** *8* (3), 602.
(25) Yang, Y.; Thannhauser, T. W.; Li, L.; Zhang, S. Development of an integrated approach for evaluation of 2-D gel image analysis: impact of multiple proteins in single spots on comparative proteomics in conventional 2-D gel/MALDI workflow. *Electrophoresis* **2007,** *28* (12), 2080.
(26) Yang, Y.; Qiang, X.; Owsiany, K.; Zhang, S.; Thannhauser, T. W.; Li, L. Evaluation of different multidimensional LC-MS/MS pipelines for isobaric tags for relative and absolute quantitation (iTRAQ)-based proteomic analysis of potato tubers in response to cold storage. *J. Proteome Res.* **2011,** *10* (10), 4647.
(27) Hochrainer, K.; Racchumi, G.; Zhang, S.; Iadecola, C.; Anrather, J. Monoubiquitination of nuclear RelA negatively regulates NF-kappaB activity independent of proteasomal degradation. *Cell. Mol. Life Sci.* **2012,** *69* (12), 2057.

CHAPTER 4

*T-REX AS A DISCOVERY TOOL: IDENTIFYING PRIVILEGED REDOX SENSORS

Introduction

A major drawback of currently available methods to profile lipid-derived electrophile (LDE)-sensitive proteins in cells is that the methods require bolus treatment with a huge excess of the LDE under study[1-7]. Treatment of cells and model organisms with high concentrations of the LDE most likely alters the redox state of the cell/organism and eventually triggers apoptosis[8]. Therefore, profiling true redox-sensors that are endogenously relevant under these conditions is not ideal. Another important consideration is that bolus dosing-dependent methods yield a high background of proteins that are likely not important sensors in cellular context[2,4]. This is because covalent modification of proteins with LDE is a function of concentration of the LDE as well the duration of treatment. An ideal sensor protein in a signaling context, however, should have the ability to respond to endogenously relevant amounts of a given redox signal and within a time frame consistent with signaling conditions. These proteins are likely 'kinetically privileged sensors' with the ability to respond to endogenous levels of redox signals. A number of factors including solvent accessibility[9] and the microenvironment of the sensing residue can impart such privilege[10,11].

---

*This Chapter was published previously. "Akt3 is a privileged first responder in isozyme-specific electrophile response"; Marcus Long, **Saba Parvez**, Yi Zhao, Sanjna L. Surya, Yiran Wang, Sheng Zhang, and Yimon Aye*; *Nature Chemical Biology,* **2017**, 13, 333–338 (Underlined: First-author)

Traditional bolus dosing methods are biased against detecting such sensor proteins because treatment with a large amount of LDEs results in modification of several other proteins as well. Thus, identifying true 'privileged sensors' in the noise generated from other contaminating proteins becomes a challenging task. Profiling experiments done by titrating a range of LDE concentrations may alleviate some of the problems associated with bolus dosing methods[1,6,12]. However, additional factors such as cellular abundance of the protein, cell permeability of the LDE, reaction of the LDE with the plasma membrane and membrane-bound proteins, cellular metabolism/excretion etc. complicate the analysis of results obtained from such profiling methods.

Because T-REX enables the generation of a stoichiometric amount of a given LDE in close proximity to a POI, it is an ideal tool to quantitatively assess redox-sensitivities of known proteins and to discover novel 'privileged first-responders' to an LDE. HaloTag™ human and mouse full-length open reading frame clone libraries are also commercially available facilitating such discovery efforts (Kazusa Collection, Promega). With this ability in hand, we recently screened a small HaloTag™ kinase library for possible identification of 'privileged redox sensors'. Our library of ~20 select kinases and their isoforms identified Akt3, an isoform of the oncogenic serine/threonine kinase Akt, as a novel sensor to the endogenous electrophilic signal HNE. Low-occupancy modification of Akt3 with HNE resulted in downregulation in kinase activity of the enzyme with downstream functional consequences in mammalian cells as well as in zebrafish.

Results**

T-REX screen identifies Akt3 as a privileged sensor of HNE

We set up a small throughput screen of select kinases and their isoforms to test their redox sensing ability. HaloTagged kinase were transfected in HEK293T cells. 24 hours post-transfections, T-REX was performed as specified earlier using Ht-PreHNE as the T-REX caged compound. Protein labeling by HNE-alkyne was assessed using in-gel fluorescence by conjugating Cy5 azide to the HNE-alkyne labeled proteins via Click chemistry (data collected in collaboration with Dr. Marcus Long). Our screen identified Akt2 and Akt3 as possible sensors of HNE (**Figure 4.1A**). Interestingly, no HNE modification was identified on Akt1. Additionally, none of the other kinases showed any significant labeling although expression levels of two of the proteins (PI3KCA, and p38) were also lower. Nonetheless, we decided to perform validation of the distinct HNE labeling of the three Akt kinase isoforms. In-gel fluorescence analysis validated the findings of the screen and demonstrated that HNE efficiently labels Akt3, with targeting efficiency of ~20% (**Figure 4.1B–C**). Akt2 and Akt1 were significantly less sensitive to HNE modification upon T-REX.

We used another independent approach to validate these findings. Instead of click conjugation with Cy5 azide for fluorescent detection, we conjugated the HNE-alkyne labeled proteins with Biotin azide and used streptavidin beads for subsequent enrichment of the modified proteins. This method also substantiated the finding of the screen revealing Akt3 as the unique HNE-sensitive isoform amongst the Akt kinases (**Figure 4.1 D**).

** All fish experiments were performed in collaboration with Dr. Marcus Long. Fish injection with plasmids/mRNA, treatment with various compounds, and Z-REX were performed by Dr. Marcus Long. Unless otherwise specified, all downstream fish experiments were performed by Saba Parvez. Data collected by Dr. Marcus Long are specified throughout the text.

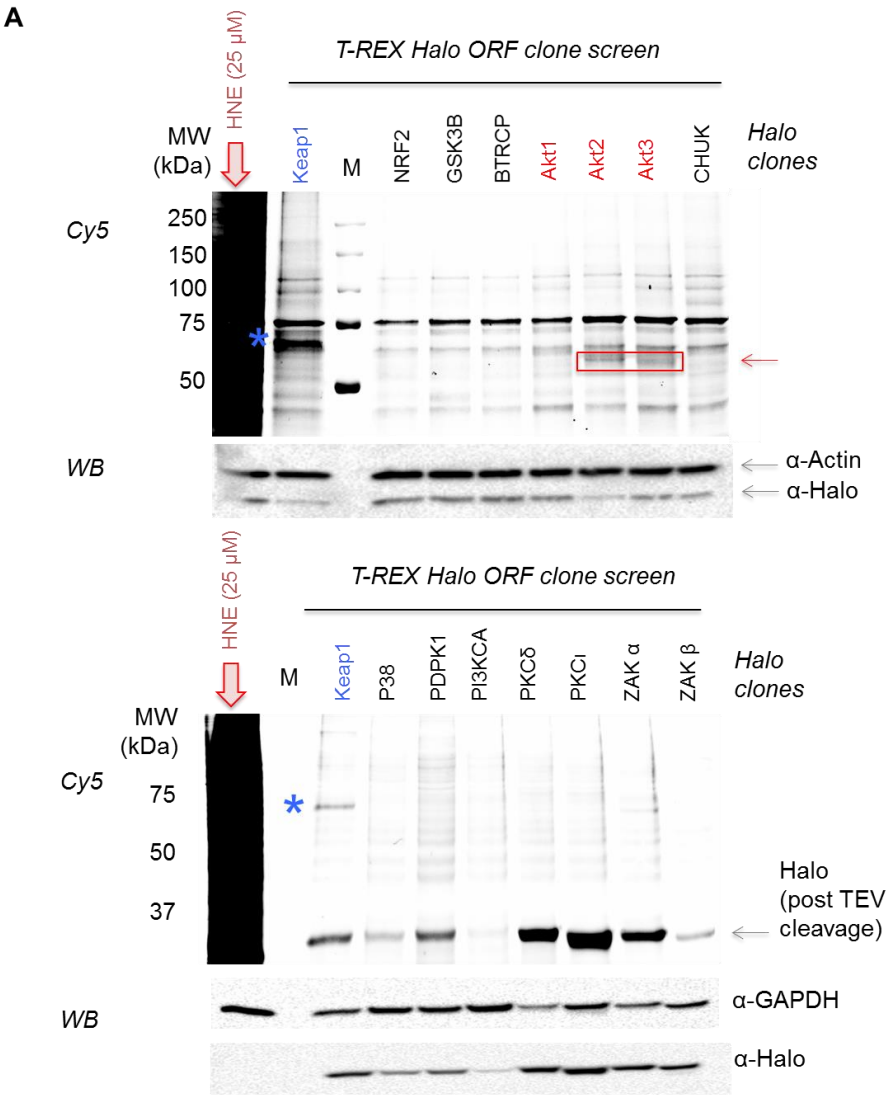
A
T-REX Halo ORF clone screen
HNE (25 µM)
MW (kDa)
Keap1
M
NRF2
GSK3B
BTRCP
Akt1
Akt2
Akt3
CHUK
Halo clones
Cy5
250
150
100
75
50
WB
α-Actin
α-Halo
T-REX Halo ORF clone screen
HNE (25 µM)
M
Keap1
P38
PDPK1
PI3KCA
PKCδ
PKCι
ZAK α
ZAK β
Halo clones
MW (kDa)
Cy5
75
50
37
Halo (post TEV cleavage)
WB
α-GAPDH
α-Halo

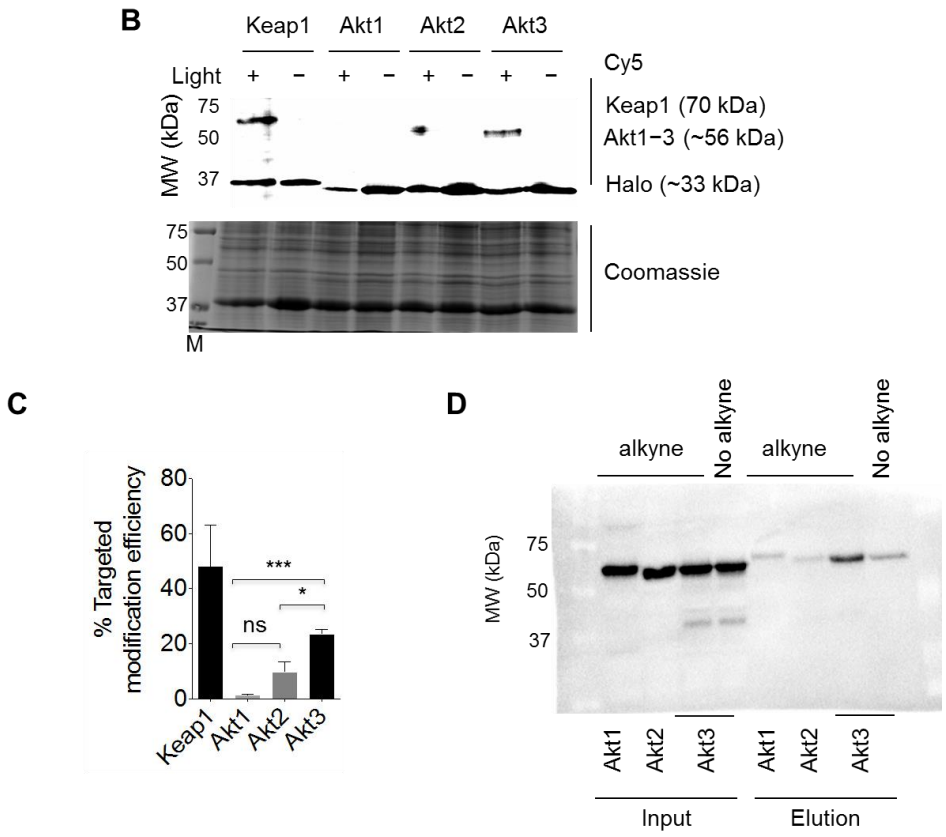

Figure 4.1 Akt3 is a first-responding isozyme to reactive native lipid signals (**A**) HaloTagged kinase isozymes and other postulated redox-sensor POIs based on available proteomics profiling data derived from global LDE flooding methods were selected as potential targets. T-REX subsequent and in-gel fluorescence analysis was performed on HaloTagged kinases. Two representative gels from the screen (Top and Bottom) are shown. The rapid throughput processing procedure adopted at the screening stages resulted in low-quality background signals and variations. Subsequent validation must thus be performed (see **Fig. 1B**–**D**). "M" designates MW ladder. Expected MW's (kDa): Keap1, 70 (diagnostic positive control, marked by *); NRF2, 68 (note: NRF2 runs at ~110); GSK3B, 47; BTRCP, 68; Akt1, Akt2, Akt3, 57; CHUK, 90; P38, 38; PDPK1, 63; Pi3KCA, 120; PKCδ, 87; PKCι, 87; ZAK-α, 90; and ZAK-β, 47. Top gel identified Akt2 and Akt3 as potential sensors from the screen (red arrow). Individual protein expression was unoptimized in these screens and analyzed by western blot (WB) using antibody to HaloTag. Either actin (Top) or GAPDH (Bottom) was used as loading control. Cy5-signal associated with cleaved HaloTag can be seen in the Bottom gel (grey arrow) which arises from the remaining photocaged precursor covalently bound to HaloTag due to incomplete photouncaging. (**B**) Validation of Akt3 as a first HNE-responder. Keap1 was used for comparison. *Top:* Cy5 signal from samples treated with or without light, followed by TEV-protease treatment. M designates MW (molecular weight)-ladder. *Bottom:* Coomassie (**C**) Quantitation: the Cy5 signal intensity on the band corresponding to POI MW in the samples exposed to light was normalized by the

signal intensity on Halo on the corresponding samples not exposed to light. Error bars designate s.d (**D**) Orthogonal validation using Click coupling with biotin-azide followed by streptavidin enrichment subsequent to T-REX-enabled targeted-HNE(alkyne)-modification in live cells. "No alkyne" corresponds to probe that had no-alkyne functionalization, controlling for any non-specific binding/biotinylation.

C119 of Akt3 is the unique HNE sensing residue

Having established that Akt3 is a novel HNE sensor, we sought to find out the residue(s) on Akt3 that endow it with HNE sensing ability. We used mass spectrometry to identify the HNE sensing residue on Akt3. Our results identified C119 of Akt3 as being modified with reduced HNE upon T-REX (**Figure 4.2A and Appendix II**). Comparison with other Akt isoforms revealed that C119 is located in a flexible linker of the enzyme. Akt isoforms share >70% sequence homology. Interestingly, the linker region of the enzyme is the most divergent between the isoforms, which may explain the differential HNE sensitivity of the isoforms. Consistent with this hypothesis, C119 of Akt3 is not conserved across the three isoforms. Akt2, interestingly, possesses a Cys124 residue in the flexible linker region instead. Earlier reports have identified this residue as site of sulfenic acid modification upon treatment of fibroblast cells with growth factors implying that different isoforms of a protein have evolved to respond to oxidative or electrophilic signals[13]. In accordance with C119 being the HNE sensing residue on Akt3, C119S mutants had significantly reduced HNE-sensitivity compared to the wild-type (WT) protein as judged using in-gel fluorescence (**Figure 4.2B**).

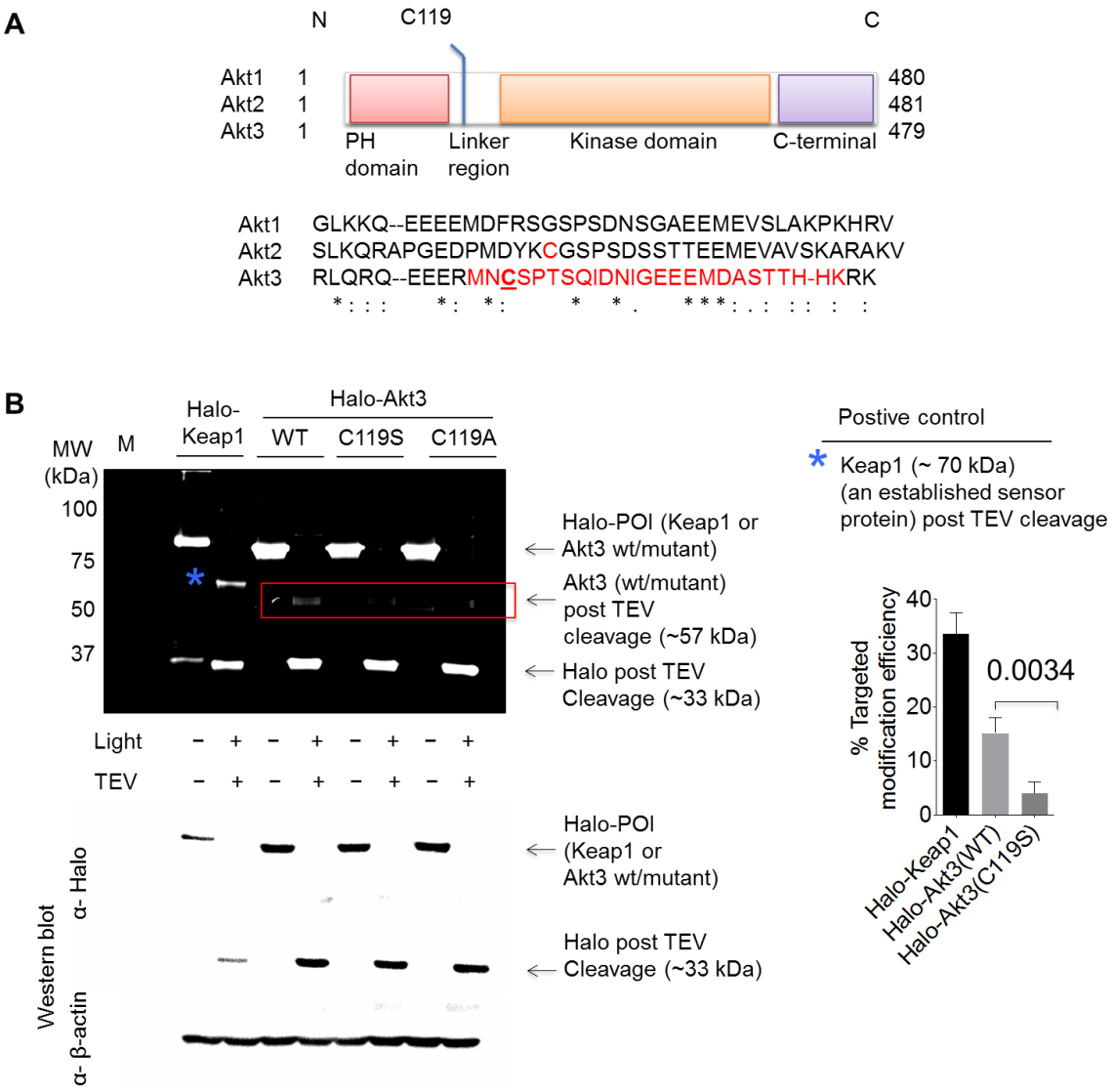
A
N
C119
C
Akt1 1
Akt2 1
Akt3 1
480
481
479
PH domain
Linker region
Kinase domain
C-terminal
Akt1 GLKKQ--EEEEMDFRSGSPSDNSGAEEMEVSLAKPKHRV
Akt2 SLKQRAPGEDPMDYKCGSPSDSSTTEEMEVAVSKARAKV
Akt3 RLQRQ--EEERMNCSPTSQIDNIGEEEMDASTTH-HKRK
B
MW (kDa)
M
Halo-Keap1
Halo-Akt3
WT
C119S
C119A
100
75
50
37
Halo-POI (Keap1 or Akt3 wt/mutant)
Akt3 (wt/mutant) post TEV cleavage (~57 kDa)
Halo post TEV Cleavage (~33 kDa)
Light
TEV
Western blot
α- Halo
α- β-actin
Halo-POI (Keap1 or Akt3 wt/mutant)
Halo post TEV Cleavage (~33 kDa)
Postive control
Keap1 (~ 70 kDa) (an established sensor protein) post TEV cleavage
% Targeted modification efficiency
40
30
20
10
0
0.0034
Halo-Keap1
Halo-Akt3(WT)
Halo-Akt3(C119S)

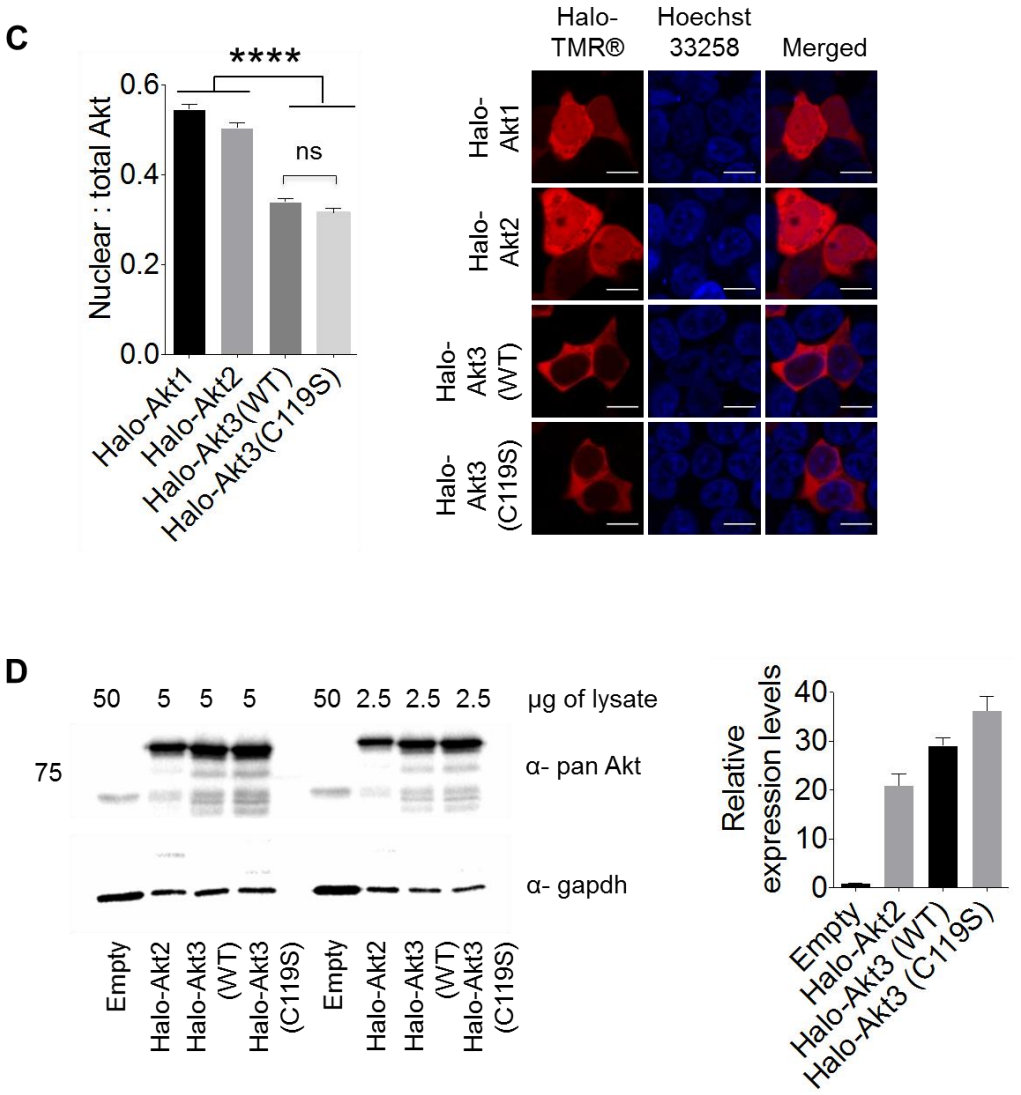

Figure 4.2 C119 of Akt3 is the unique HNE-sensing residue. (**A**) Domain composition of Akt isoforms: the linker region displays the highest divergence in amino acid sequence (shown) among the three isozymes. C124 of Akt2 (in red) is sensitive to H_2O_2[19]. We identified C119 (underlined) of Akt3 to be the site of HNE(alkyne)-modification on the tryptic peptide shown in red. (**B**) In-gel fluorescence shows attenuated targeting efficiency of C119S/C119A HNE-insensitive mutants compared to Akt3 wild type (WT). The percentage targeting efficiency was calculated as described in Chapter 2). M designates the lane in which MW ladder was loaded. For quantitation, n = 5 independent biological replicates. Error bars indicate s.e.m. (**C**) Localization of ectopically expressing HaloTagged kinases. HEK293T cells overexpressing the HaloTagged kinases were treated with Halo-TMR (3.0 µM) for 3 h in serum-free media, then washed and analyzed by live cell imaging. For nuclear stain, cells were incubated with 1 µg/mL Hoechst-33258 dye in complete media for 30 min prior to imaging. Inset

on the left shows quantitation (Halo-Akt1: n = 51, Halo-Akt2: n = 54, Halo-Akt3: n = 91, and Halo-Akt3(C119S): n = 68; cells from two independent plates at different passage numbers). (**D**) Comparison of the expression levels of HaloTagged kinase isoforms in mammalian cells. Th expression levels are 20–30 fold relative to the endogenous total Akt levels.

We next assessed whether Akt3 HNE sensing ability had any functional relevance in a cellular and organismal context. First, we demonstrated successful expression of all three HaloTagged Akt isoforms in mammalian HEK293T cells. HaloTMR® ligand, which binds to the Halo domain was used to track the localization of each of the isoforms. Interestingly, while Halo-Akt1 and Halo-Akt2 were expressed both in the cytosol and the nucleus, Halo-Akt3 (both the WT and the C119S mutants) were exclusively cytosolic (**Figure 4.2C**). The cytosolic and nuclear localization of Akt1 and Akt2 isoforms is in agreement with previous reports although the authors looked at endogenous Akt rather than overexpressed isoforms[14]. Akt3, however, was reported to be largely nuclear in this study. The difference in reported literature and our results may stem from different cell lines used in these studies (HEK293T vs MDAMB-231). Consistent with this hypothesis, another group has demonstrated the mainly cytosolic localization of the ectopic Akt3 isoform in retinal ganglion cells[15]. None-the-less, Akt3 WT and C119S had similar localization. We also compared the overexpression levels of the two redox-sensing isoforms. Halo-Akt2 and Halo-Akt3 (WT and C119S) has similar overexpression levels and ~20–30 fold above endogenous pan-Akt levels (**Figure 4.2D**). Since C119S mutant is correctly regulated and stable, we conclude that C119 is the unique HNE sensor residue on Akt3.

HNE modification of Akt3 downregulates its kinase activity in cells

After successful identification of the HNE-sensing residue of Akt3, we investigated the downstream ramifications of Akt3 HNEylation in whole cells. One of the key benefits of T-REX is that downstream signaling ramifications caused by specific LDE modifications of sensitive proteins can be assayed easily. Akt3(C119S)—the mutant hypomorphic for HNE-delivery—served as an ideal 'negative control', enabling better dissection of on-target redox responses from off-target effects. We used a known ratiometric FRET-based "Akt activity reporter (AktAR)" biosensor[16] (**Fig. 4.3A**) that measures Akt activity directly and can detect relatively small changes in Akt activity. Briefly, the biosensor construct constitutes a CFP/YFP-FRET-pair separated by a linker region that integrates a substrate peptide sequence favored by all Akt isoforms and a FHA2-protein-binding domain. This latter domain binds selectively to the phosphorylated substrate peptide. Co-expression of the individual HaloTagged Akt2 and Akt3 (both WT and C119S) with the reporter resulted in increased FRET from CFP to YFP relative to an empty vector (**Figure 4.3B**), validating activity of the expressed proteins.

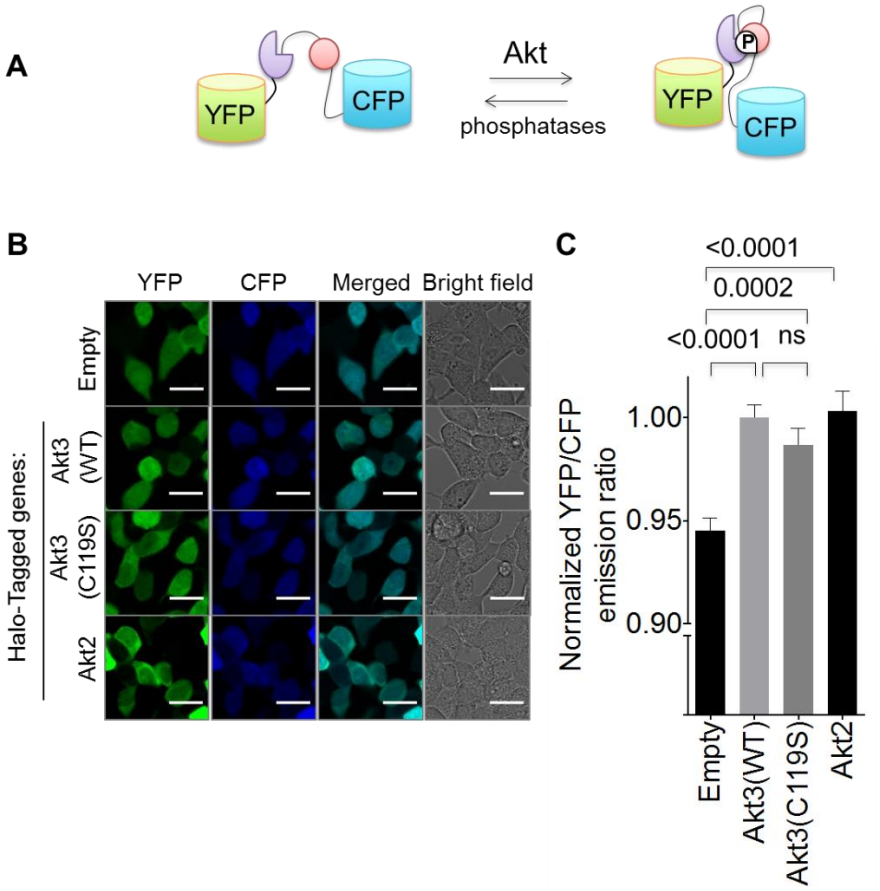

Figure 4.3 (**A**) Schematic of the FRET-based Akt activity reporter (AktAR)[24]. Phosphorylation of a peptide substrate (pink) by Akt isozymes allows a phospho-peptide binding domain (purple) to bind the phosphorylated substrate resulting in an increase in FRET (**B**) HEK293T cells were transfected with a pFN21a empty vector or that encoding one of the indicated Halo-Tagged transgenes and the AktAR plasmid using Mirus 2020. Post 36-h transfection, cells were analyzed by imaging. Overexpression of all three genes results in an increase in ratiometric FRET signal, indicating that all three kinase variants are active. Representative images. Scale bar 20 µm. (b) Quantitation: error bars indicate s.e.m (n>90 from two independent plates at different passage numbers)**.**

We then performed T-REX on cells co-expressing the Halo-Akt isoforms and the FRET reporter construct (**Figure 4.4**). We observed a decrease in FRET in cells expressing Halo-Akt3 (WT) in response to T-REX implying that there is a decrease in kinase activity of the enzyme upon HNE modification (**Figure 4.4A, E**). Our results

were strengthened by the lack of FRET response in cells expressing Halo-Akt3(C119S) (**Figure 4.4B, E**). This data validates that the drop in FRET response after T-REX in case of WT expressing cells is a result of HNEylation of Akt3 at C119 residue. Cells expressing Halo-Akt2 also did not show any significant downregulation of kinase activity (**Figure 4.4C, E**), demonstrating a unique HNE-sensing role of Akt3 amongst the three isoforms. Interestingly, co-expression of Halo-PTEN, another known redox-sensitive protein[17-20] that negatively regulates the Akt-pathway, and the FRET reporter resulted in an increase in FRET response after T-REX (**Figure 4.4D–E)**. These data collectively demonstrate that the Akt pathway is prone to regulation by redox signals.

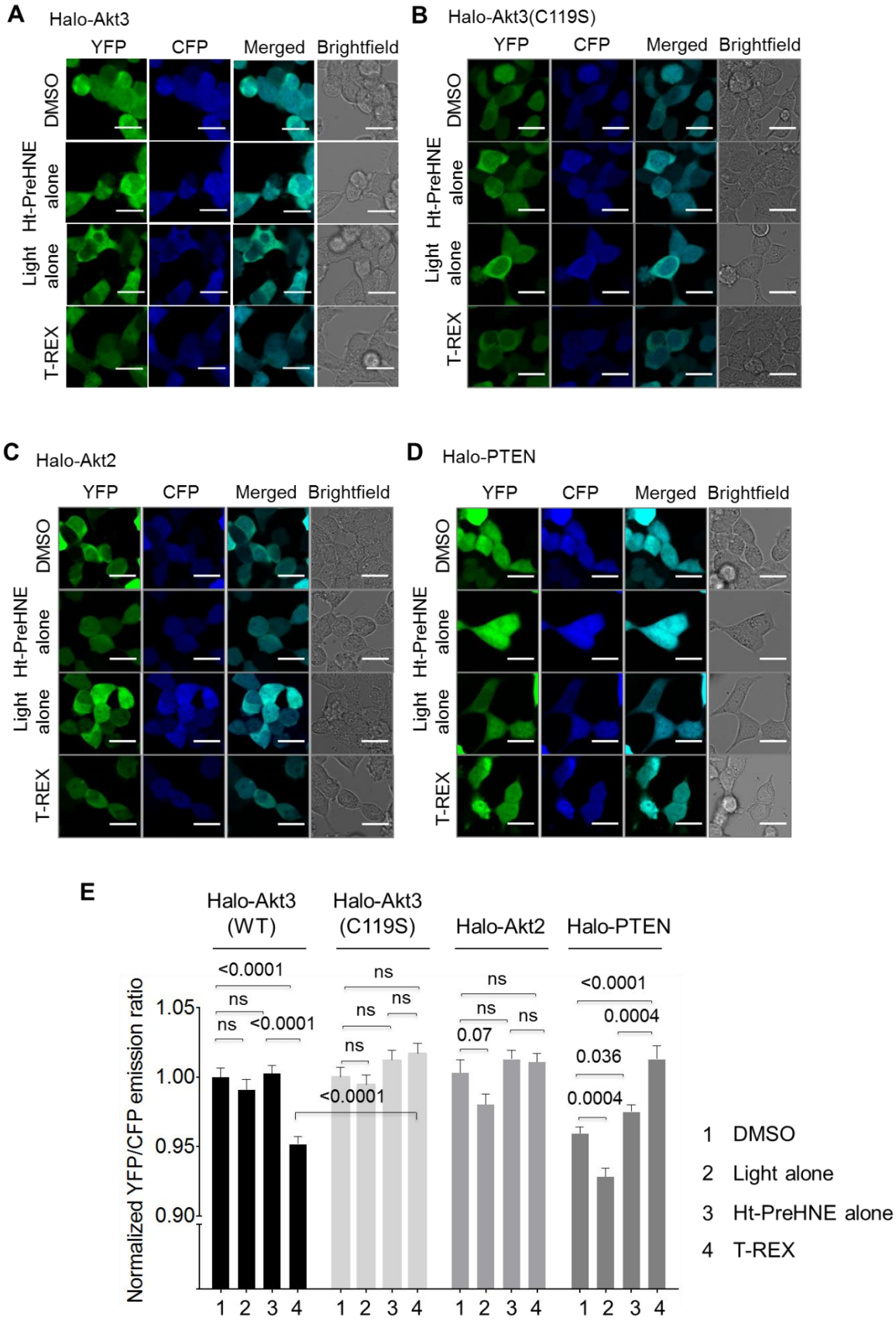
A
Halo-Akt3
YFP
CFP
Merged
Brightfield
DMSO
Ht-PreHNE alone
Light alone
T-REX
B
Halo-Akt3(C119S)
C
Halo-Akt2
D
Halo-PTEN
E
Halo-Akt3 (WT)
Halo-Akt3 (C119S)
Halo-Akt2
Halo-PTEN
Normalized YFP/CFP emission ratio
1.05
1.00
0.95
0.90
<0.0001
ns
0.07
0.036
0.0004
1 DMSO
2 Light alone
3 Ht-PreHNE alone
4 T-REX

Figure 4.4. HEK293T cells transfected with AktAR reoporter plasmid and (**A**) Halo-Akt3(WT), (**B**) Halo-Akt3(C119S), (**C**) Halo-Akt2, and (**D**) Halo-PTEN, and (**c**), were subjected to T-REX-assisted HNE-targeting. After 8–10 h, cells were excited using an Argon laser (458 nm). Images were obtained using cyan (463–498 nm) and yellow (525–620 nm) channels. Scale bar: 20 μm (**E**) Quantitation of YFP/CFP ratio of individual cells in **A**–**D** using Image-J. Error bars designate s.e.m. with n = Akt3(wt) (197, 124, 205, 185); Akt3(C119S) (242, 243, 252, 240); Akt2 (107, 103, 103, 104); and PTEN (94, 38, 52, 43) for DMSO, light alone, Ht-PreHNE alone, and T-REX, respectively, where n designates number of cells quantitated per condition from two independently replicated sets at different passage numbers.

To set these results relative to the maximal response tolerated by this system, we directly compared ratiometric-FRET-quenching observed in T-REX to that observed upon treatment with two different pan-Akt-kinase inhibitors [MK-2206 and afuresertib (GSK2110183)] under otherwise identical conditions (Halo-Akt3 transfected and serum-starved) (**Figure 4.5**) (data collected by Dr. Marcus Long). A time- and dose-dependent titration revealed that the maximum change in the system, for both inhibitors, was ~30% (**Figure 4.5B**). This was reached within 3 h after treatment. This plateau was maintained for 24 h, and was the same for both inhibitors, strongly indicating that ~30% is the maximal dynamic range of this assay relative to serum-containing conditions.

Because AktAR assays are typically set up under serum-starved conditions and so are T-REX experiments, we also showed that serum starvation still allowed measurements of FRET changes in both wt- and mutant-expressing cells following treatment with MK-2206 as the representative pan-Akt-inhibitor (**Figure 4.5A–B**). In general, serum starvation caused a maximal 15% drop in signal after > 3 h treatment that remained constant over 24 h (**Figure 4.5B**), and the decrease in fluorescence caused by MK-2206 was independent of serum starvation. Thus, the maximal dynamic range

under T-REX conditions is 15%. Comparison with the maximum FRET decrease achieved by this assay demonstrated that under T-REX condition on the WTHalo-Akt3, the extent of Akt3-activity downregulation achieved was 20–30% of the maximum; whereas the kinase activity of the HNE-sensing-defective mutant, Akt3(C119S), was unperturbed. Although, the magnitude of activity suppression is modest (20–30%) (**Figure 4.5E**), it is consistent with the targeting efficiency observed on the protein (~20%, **Figure 4.1C**).

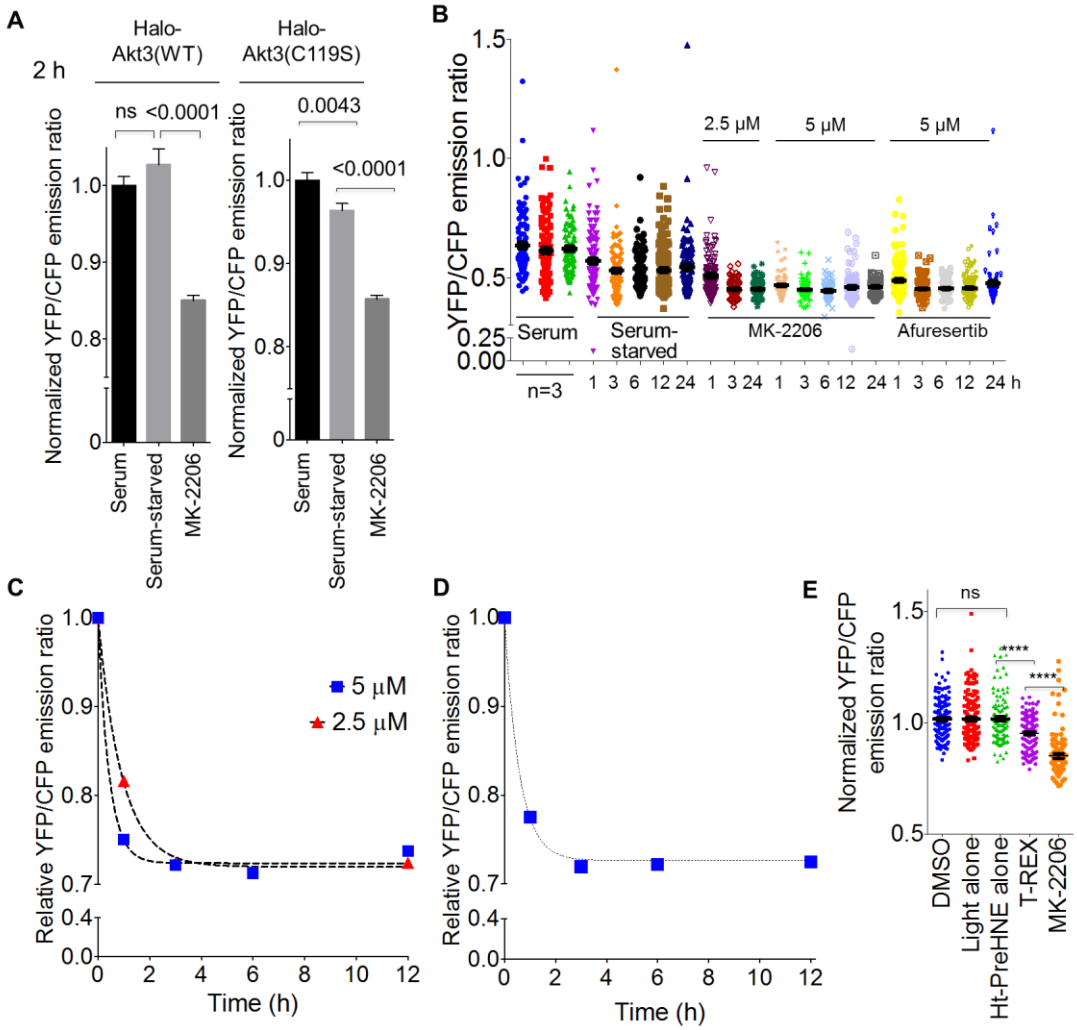

Figure 4.5 (**A**) Quantitation of AktAR FRET response in cells expressing either Halo-Akt3(WT) or halo-Akt3(C119S) under serum-starvation or treated with MK-2206, a pan-Akt inhibitor. (**B**) Same as in (**A**) but cells were either left in serum (triplicate samples), or serum starved, or serum starved and treated with the indicated pan-Akt inhibitor at the dose and incubation time (x-axis) shown. Samples were staggered such that all samples were ready to image 1 h apart starting from the shortest time point. Error bars are s.e.m. (**C**) Time course of dose- and time-dependent changes in fluorescence caused by MK-2206 and (**D**) afuresertib (**E**) Replot of the ratiometric-FRET-signal change upon T-REX relative to its controls and the drop caused by MK-2206. From this plot we ascertained that T-REX causes 20–30% of the maximal possible drop in ratiometric FRET signal. Errors indicate s.e.m.

HNEylation occupancy on a POI is a function of photouncaging efficiency [the percentage of reactive HNE signal liberated from Ht-PreHNE bound to Halo under the assay conditions; typically > ~60% after 4-min light-exposure in cells] and targeting efficiency (the percentage of liberated HNE signal delivered to POI). In the case of Akt3, the targeting efficiency is ~20% implying that the HNEylation occupancy is 12% (20% of 60%). The downregulation in kinase activity of the WT Akt3 is ~20–30%. The discrepancy in occupancy and reduction in kinase activity can be accounted for by the known dominant-negative effects that can occur for Akt[21,22], which predicts that inhibition would be higher than absolute occupancy.

HNEylation of Akt3 does not change its phosphorylation levels

To understand the mechanism of Akt3 activity downregulation, we investigated the phosphorylation levels of Akt3 after T-REX. Akt enzyme has at least two distinct phosphorylation sites[23]. Akt isoforms are reportedly phosphorylated at Thr308 (Thr305 in Akt3) by PDK1 (3-phosphoinositide-dependent protein kinase-1). The PH domains of PDK1 and Akt bind to PIP3. The PIP3-dependent recruitment of the two enzymes to

the plasma membrane, and their colocalization enables phosphorylation of Akt by PDK1. Akt is also phosphorylated at Ser473 by mammalian target of rapamycin complex 2 (mTORC2). Phosphorylation of both sites is required for full activation of the enzyme. Recent reports have suggested that phosphorylation of Akt at Thr308 better reflects the protein kinase activity in certain malignancies[24]. We therefore assessed the Thr305 phosphorylation levels on Akt3 (data collected in collaboration with Dr. Marcus Long). Additionally, the Akt3 isoform (Akt3 isoform 2) used in this study lacks the Ser473 (Ser474) phosphorylation site prompting us to investigate the Thr305 levels. As expected, treatment of cells expressing the HaloTagged kinases with serum stimulated phosphorylation at the Thr305 site. Both the WT and C119S mutants were similarly phosphorylated, and responded similarly to a stimulant (serum) and the MK-2206 pan Akt inhibitor (**Figure 4.6A**). Selective HNEylation of Akt3, however, did not alter the total Thr305 phosphorylation levels (**Figure 4.6B**). This implies that HNEylation of Akt3 does not perturb upstream signaling events such as its interaction with PDK1.

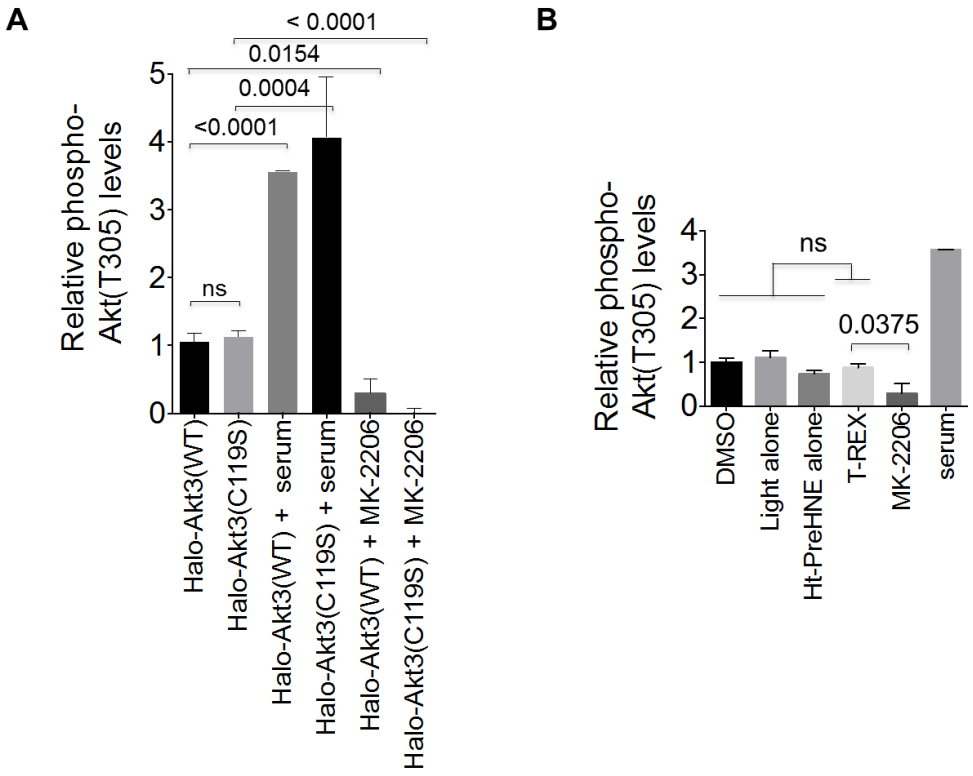

Figure 4.6 Akt3-targeted HNEylation does not change Akt3 phosphorylation at Thr305. (**A**) HEK293T cells were transfected with a pFN21a plasmid encoding Halo-Akt3 (either WT or C119S mutant). After 36 h, cells were either left in serum-containing media, starved, or treated with the stated inhibitor for 10 h. After this time, levels of phosphorylated ectopic Akt3 were assessed using ELISA (plate coated with mouse anti-Halo) detecting with a phospho-T305-Akt3 antibody (rabbit). Note: C119S and wt Akt3 were similarly phosphorylated, further consistent with them having similar kinase activity and being similarly regulated. (**B**) T-REX on Akt3(WT) does not change the T305 phosphorylation levels. MK-2206 and serum stimulation work as expected.

HNEylation of Akt3 downregulates FOXO phosphorylation

To assess the downstream biological consequences of Akt3 modification with HNE, we used three independent analyses. First, we used ELISA to quantitate phosphorylation of ectopically expressing FOXO3a, a transcription factor and an established target of Akt[23]. FOXO is reportedly phosphorylated by Akt upon activation of the kinase[25-27]. Akt-mediated phosphorylation inhibits the translocation of the

transcription factor and a consequent repression of its transcriptional activity (**Figure 4.7A**). Our results (collected by Dr. Marcus Long) demonstrated that phosphorylation of FOXO3a at Thr32 is decreased upon HNEylation of Akt3 (**Figure 4.7B**). No significant drop in phosphorylation at Thr32 of FOXO3a was observed after performing T-REX on cells expressing the Halo-Akt3 C119S mutant, even though both the mutants and the WT could respond to MK-2206 efficiently.

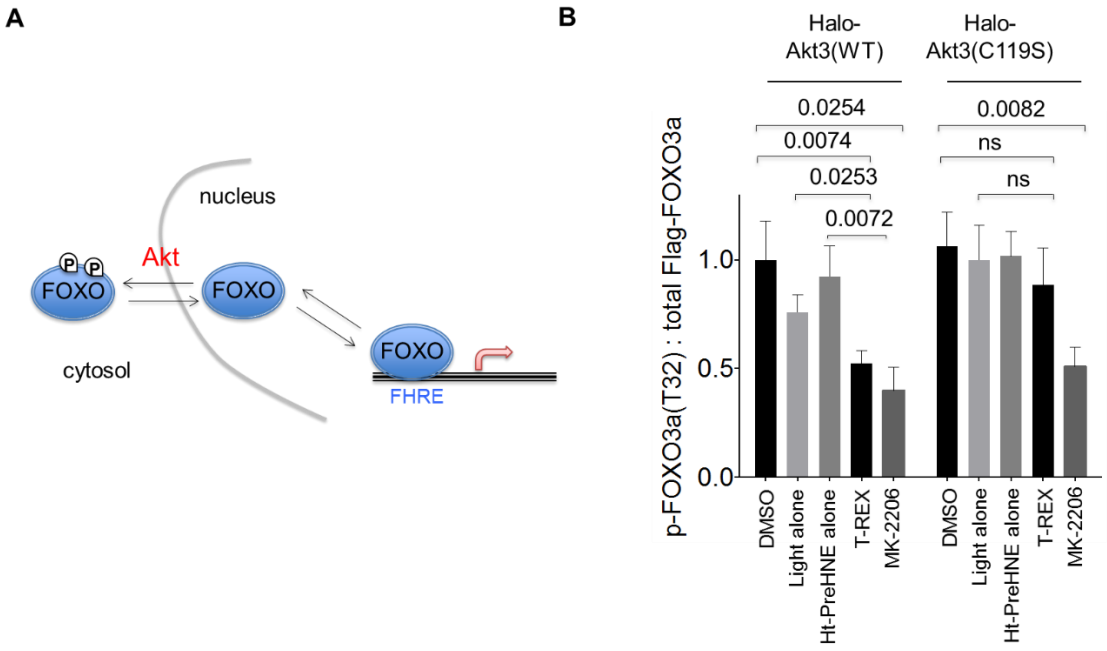

Figure 4.7 (**A**) Schematic of FOXO regulation by Akt kinases. Phosphorylation of FOXO by Akt is reported to inhibit its nuclear translocation, consequently a suppression in transcriptional activity. FHRE: Fork head response element. (**B**) HNEylation-dependent kinase activity downregulation of Akt3 results in decrease in phosphorylation of FOXO3a at Thr32. HEK293T cells were co-transfected with the Halo-Akt3 plasmid and a plasmid encoding FLAG-FOXO3a. After T-REX experiments, lysates were added to an ELISA plate pre-coated with goat anti-FLAG and ectopic-phospho-FOXO3a was assessed using a specific phospho-T24/T32 FOXO1a/3a antibody (rabbit). Error bars indicate s.e.m.

Second, we measured the nuclear translocation of FOXO after TREX-mediated downregulation in Akt3 kinase activity using IF (data collected by Dr. Marcus Long). As expected, overexpression of Halo-Akt3 resulted in cytosolic localization of ectopically expressing FOXO1a (**Figure 4.8A**). Halo-Akt3 WT expressing cells showed a significant increase in the total nuclear levels of FOXO1a after T-REX (**Figure 4.8B**). The C119S mutant hypomorphic for HNE sensing had no observable change in nuclear translocation of FOXO1a under otherwise identical conditions (**Figure 4.8B–C)**. Some differences in basal nuclear levels of FOXO1a were observed between WT and the C119S transfected cells (**Figure 4.8B**), even though our kinase activity data using the FRET reporter plasmid demonstrated that both the WT and mutants are active (**Figure 4.8C**). We also validated that the change is nuclear localization of FOXO is not induced by any change in localization of Halo-Akt3 after T-REX (**Figure 4.8D**).

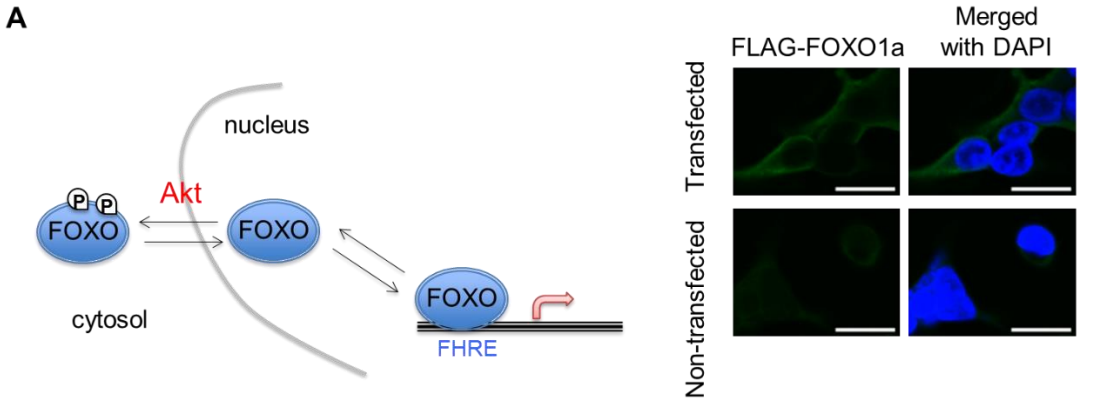
A
nucleus
Akt
P
P
FOXO
FOXO
FOXO
cytosol
FHRE
FLAG-FOXO1a
Merged with DAPI
Transfected
Non-transfected

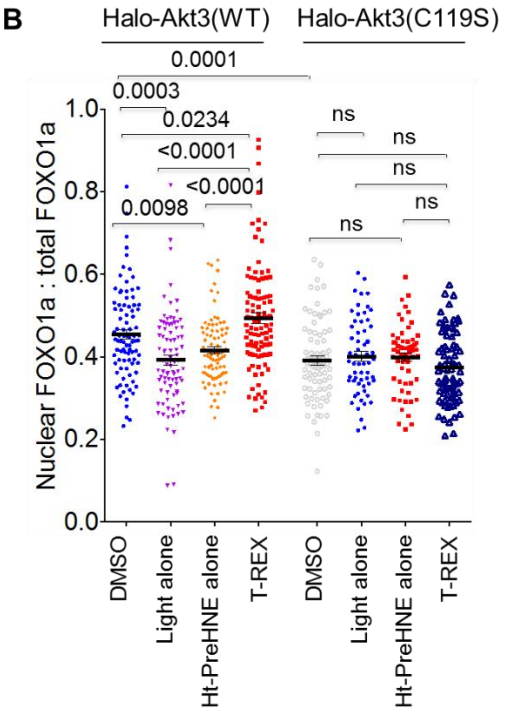
B
Halo-Akt3(WT)
Halo-Akt3(C119S)
0.0001
0.0003
0.0234
<0.0001
<0.0001
0.0098
ns
ns
ns
ns
ns
Nuclear FOXO1a : total FOXO1a
1.0
0.8
0.6
0.4
0.2
0.0
DMSO
Light alone
Ht-PreHNE alone
T-REX
DMSO
Light alone
Ht-PreHNE alone
T-REX

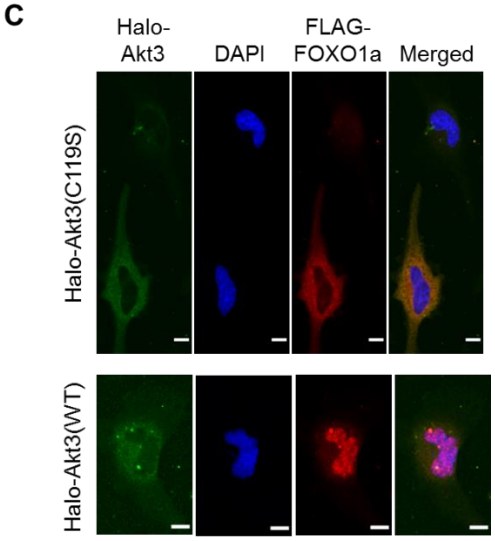
C
Halo-Akt3
DAPI
FLAG-FOXO1a
Merged
Halo-Akt3(C119S)
Halo-Akt3(WT)

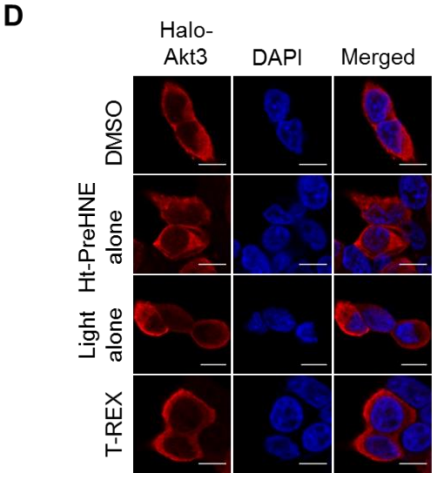
D
Halo-Akt3
DAPI
Merged
DMSO
Ht-PreHNE alone
Light alone
T-REX

Figure 4.8. Targeted HNEylation of Akt3 (only wt and not C119S) stimulates FOXO nuclear translocation. (**A–C**) HeLa cells were transfected with a pFN21a vector encoding the indicated transgene and a plasmid encoding FLAG-FOXO1a using Mirus 2020 for 36 h. After this time, cells were subjected to the indicated conditions, then after 8 h, cells were fixed with methanol (–20 ^{o}C) for 20 min, then blocked/permeabilized; stained with the stated antibodies [Halo (Ms) and FLAG (Rb)] and secondary antibodies (Ms-FITC/Rb-AlexaFlour®-647). Cells were then analyzed by imaging. (**A**) Successful detection of ectopically expressing FLAG-FOXO1a. Scale bar: 20 μm. (**B**) Quantitation of nuclear FOXO/total FOXO for each condition. Error bars represent s.e.m. (**C**) Representative images from these experiments. Scale bar: 5 μm. (**D**) T-REX conditions did not visibly alter Akt3 localization in HEK293T cells. 8 h post light exposure, cells were fixed with formaldehyde, permeabilized, blocked with BSA and incubated with rabbit polyclonal α-Halo. Halo protein was visualized using AlexaFluor®647-linked secondary antibody to rabbit IgG. DAPI was used for nuclear stain. Scale bar: 10 μm.

Finally, we also measured the transcriptional activity of FOXO using a luciferase-based reporter plasmid. As expected, co-transfection of HaloTagged Akt isoforms and firefly luciferase plasmid under the Forkhead response element (FHRE) promoter (Constitutively expressing *Renilla* luciferase was used as a normalization control), showed suppression of FOXO transcriptional activity (**Figure 4.9A–B**). This data further validates that HaloTagged Akt2 and Akt3 are functional and that elevated Akt-activity can be detected in this assay. Consistent with T-REX-mediated HNE modification of Akt3 (WT), upregulation of FOXO transcriptional activity was observed in cells expressing Halo-Akt3 (WT) but not the C119S mutant or Halo-Akt2 isoform.

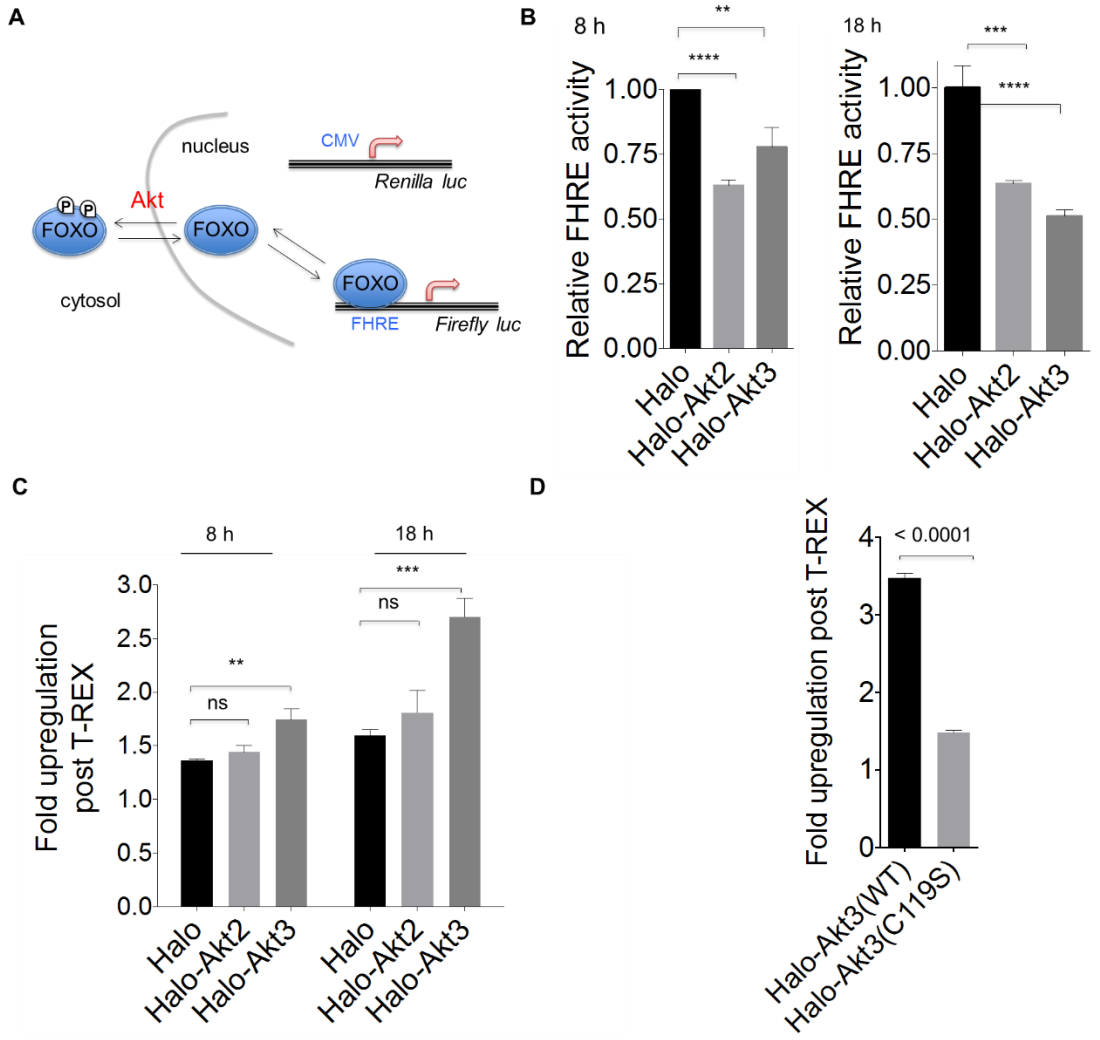

Figure 4.9 Akt3-specific modification with lipid signal activates FOXO transcriptional activity. (**A**) Schematic of the FOXO reporter assay. Akt-catalyzed phosphorylation of FOXO renders it cytosolic. Akt inactivation thus promotes nuclear translocation of FOXO and consequent activation of Firefly luciferase under Fork-Head Response Element (FHRE)-promoter driven firefly luciferase. Constitutively expressing Renilla luciferase is used as an internal control. (**B**) Overexpression of Halo-Akt2 and Halo-Akt3 in HEK 293T cells downregulates FOXO transcriptional activity compared to Halo alone control suggesting HaloTagging preserves the functionality of the kinases and that the reporter assay is suitable for the measurements of both Akt2 and Akt3 activities. Times indicate time post UV irradiation. No light samples were also incubated for the same duration (**C**) Akt3-specific targeting with HNE using T-REX in HEK 293T cells results in FOXO transactivation. No statistically significant activation was observed for Halo-Akt2 compared to Halo alone control (**D**) No significant change in FOXO transcriptional activity was observed in cells expressing Halo-Akt3(C119S) compared to those expressing Halo-Akt3(WT) 18 h after T-REX.

HNEylation of Akt3 upregulates apoptosis signaling pathway in cells

Akt is an oncogene and a negative regulator of the apoptotic pathway[23,28,29]. It negatively regulates p53[29] and FOXO[28], important tumor suppressors and regulators of apoptosis signaling[23]. Because T-REX suppresses Akt kinase activity we investigated whether downregulation in the kinase activity of the enzyme triggered apoptotic signaling in mammalian cells. Consistent with increases in transcriptional activity of FOXO, we measured an increase in capase3/7 activity in cells expressing Halo-Akt3(WT) but not Halo-Akt3 (C119S), subsequent to T-REX (**Figure 4.10**).

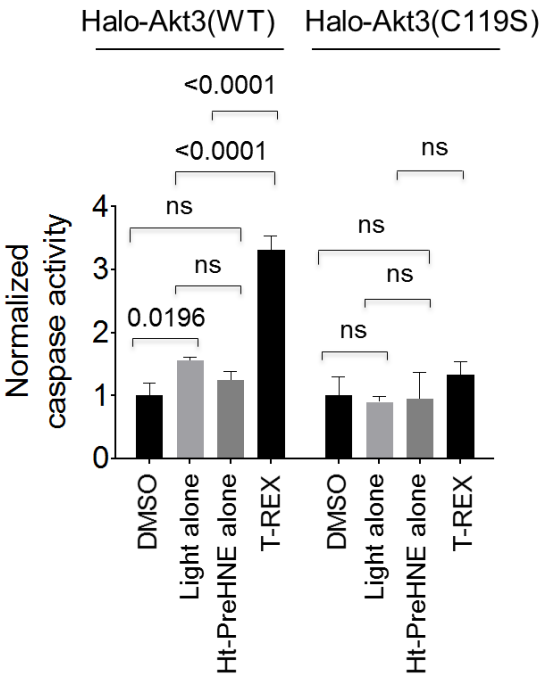

Figure 4.10 HEK293T cells were transfected with FHRE::firefly luciferase/ pCMV::*Renilla* luciferase (40:1) and a pFN21a vector encoding the indicated transgene (1:1) using Mirus 2020. After 36-h post transfection, cells were subjected to the indicated conditions and left for 18 h. After this time, cells were lysed in passive lysis buffer and caspase activity was assayed by measuring release of AMC from Ac-DEVD-AMC continuously on a plate reader for 2 h. A steady-state rate was maintained through this time. Consequentially *Renilla* luciferase activity was measured using the stop-and-

glo assay kit. The caspase activity was normalized to the *Renilla* luciferase activity to give the normalized caspase activity. Data show mean with s.e.m.

Akt3-specific HNE modification occurs in zebrafish

We then assessed whether HNEylation of Akt3 is relevant in the context of whole organism. We first tested the expression of HaloTagged Akt isoforms in zebrafish. mRNA for HaloTagged kinases was *in vitro* transcribed and zebrafish embryos were injected at 1–4 cells stage. Whole mount IF using Halo antibody showed expression of Halo-Akt2 and Halo-Akt3 (both WT and C119S) (data collected by Dr. Marcus Long) (**Figure 4.11A–B**). The expression levels of Halo-Akt2 and Halo-Akt3 isoforms were comparable (**Figure 4.11B**). As in the case of Halo-Keap1 (Chapter 2), we also validated that Z-REX does not affect the viability of the Halo-Akt3 (WT and C119S) mRNA fish embryos (**Figure 4.12A–B**). Consistent with our earlier analyses, no significant change in viability of the embryos was observed either upon injection of mRNA of various Akt isoform or under Z-REX conditions. Treatment with 5 μM of MK-2206 and Afuresertib, inhibitors of Akt signaling pathway, did reduce the viability of the embryos (**Figure 4.12A–B**) (data collected in collaboration with Dr. Marcus Long).

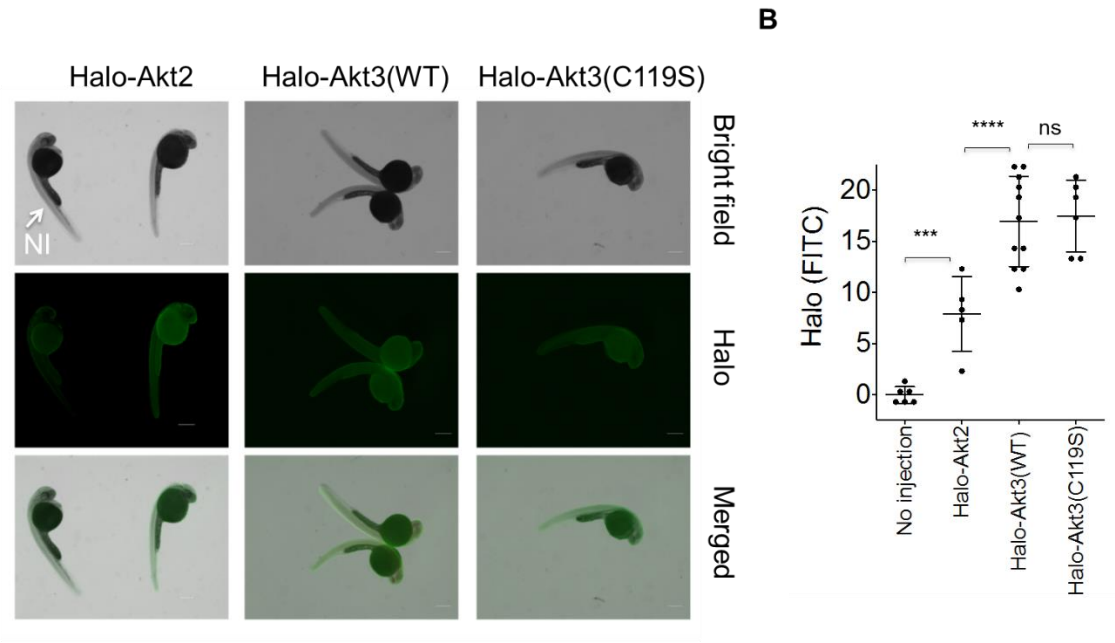

Figure 4.11 (**A**) Expression level comparison of the indicated transgenes. NI, non-injected fish. (**B**) Quantitation of relative fluorescence intensity using anti-halo (Rb) primary antibody followed by a secondary anti-rabbit-FITC antibody. Error bars indicate s.d. Scale bar, 300 µm.

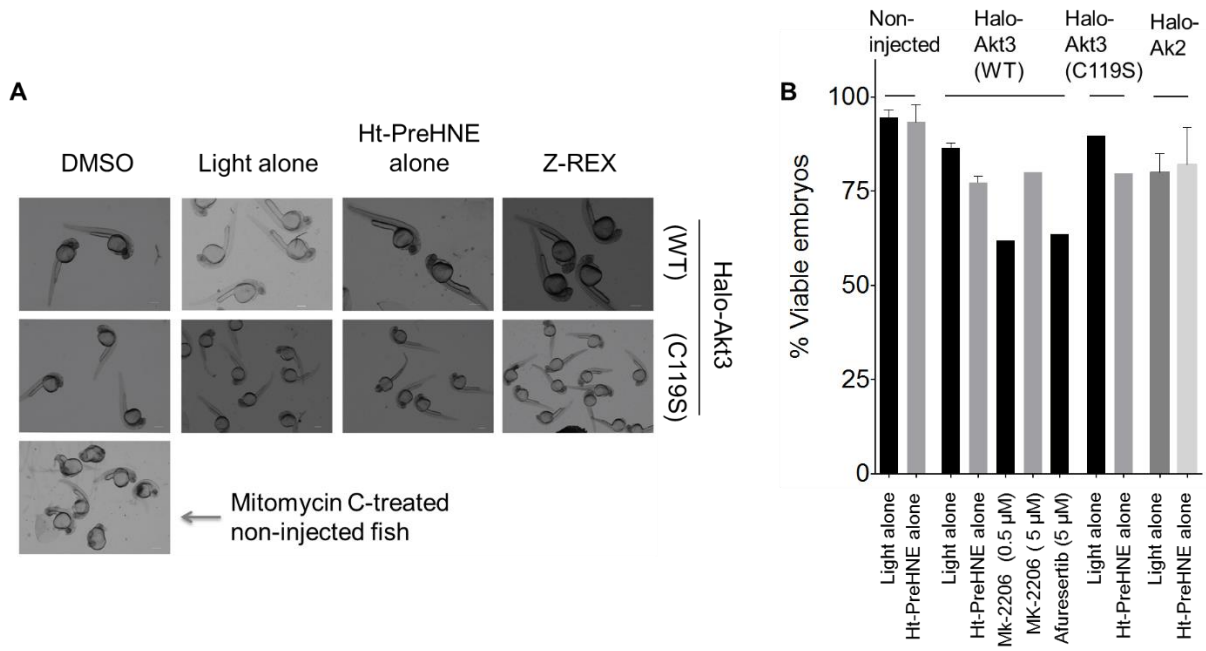

Figure 4.12 As show in Chapter 2, T-REX is well tolerated in zebrafish (**A**) Casper zebrafish embryos were injected directly into the yolk sac at the 1–2 cell stage with mRNA encoding Halo-Akt3 (either wt or C119S) and subjected to the indicated conditions 36 hpf. At 40 hpf, fish were dechorionated, transferred to 2% agarose plates, and imaged on a Leica M205-FA using a 1x pan apo lens. Scale bar, 300 µm. (**B**) T-REX conditions are non-invasive to fish viability and development.

Having established that Z-REX is non-invasive, we proceeded to demonstrate successful labeling of Akt3 by HNE in zebrafish. First, we showed that Ht-PreHNE (treated in fish water) can permeate the fish embryos and successfully label Halo-Akt3 in whole fish. Treatment with a fluorescent competitive ligand to the Halo conjugation site (HaloTMR®), showed no fluorescent signal if the embryos were pretreated with Ht-PreHNE, suggesting that the photocaged precursor occupies 100% of the Halo binding site on the HaloTagged enzyme (**Figure 4.13A**). We then assessed HNE modification of Akt3 using Z-REX (data collected by Dr. Marcus Long). Modified

protein in whole zebrafish was enriched subsequent to click conjugation of HNE(alkyne)-modified Akt3 with Biotin azide. A significant enrichment of Akt3 was observed compared to controls demonstrating successful modification of Akt3 by HNE after Z-REX (**Figure 4.13B**).

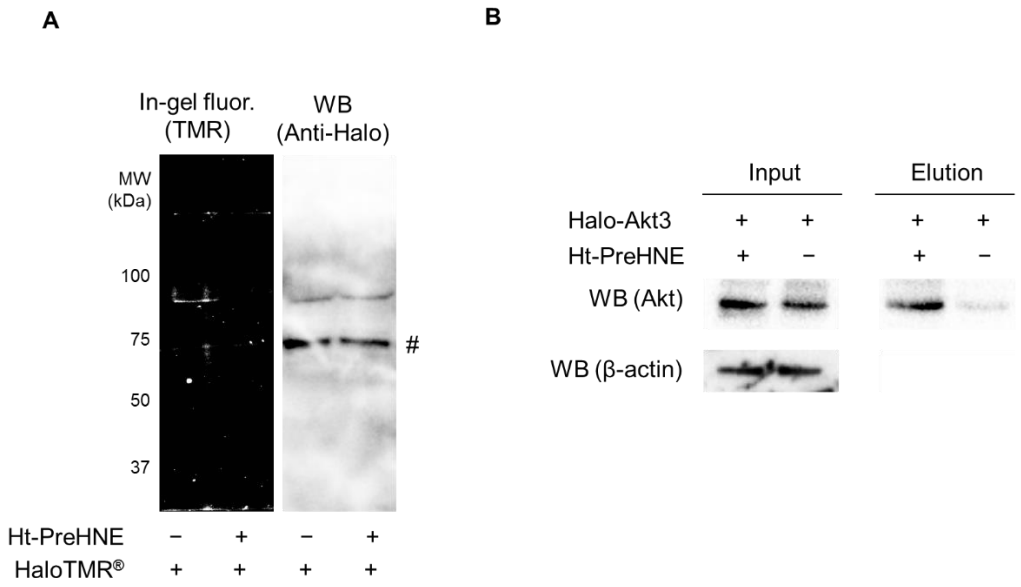

Figure 4.13 T-REX successfully and selectively modifies Akt3 in zebrafish (**A**) Fish injected with mRNA encoding Halo-Akt3 express the full-length protein. Pre-treatment of Halo-Akt3 expressing embryos with Ht-preHNE renders a competitive HaloTMR® ligand unable to bind to Halo-Akt3. *Left panel*: Fluorescent gel, *Right panel*: Western blot. # indicates a non-specific band. (**B**) Akt3 is HNE-modified in zebrafish embryos. Post execution of T-REX in fish, dechorionated and deyolked fish were lysed and subjected to alkyne-bion-azide-Click coupling and HNE-modified protein was enriched using streptavidin agarose beads. β-actin serves as a loading control.

Modification of Akt3 at C119 affects downstream signaling in whole fish

We finally investigated the functional outcome of Akt3-specific HNEylation in whole zebrafish. We used two independent techniques. First, we used the FRET Akt activity reporter plasmid to measure kinase activity of Akt isoform after Z-REX in the

whole organism. Zebrafish embryos were co-injected with plasmid DNA of the reporter plasmid and the mRNA for HaloTagged enzyme. Plasmid DNA injection results in a mosaic expression of the FRET reporter in zebrafish somatic cells[30] (**Figure 4.14A**). mRNA injection, on the other hand, results in ubiquitous and uniform expression as shown above (**Figure 4.11**). Consistent with in-cell data, performing Z-REX in whole fish and quantitating the FRET response in individual somatic cells demonstrated a decrease in FRET reporter response suggesting a downregulation in Akt3 kinase activity (**Figure 4.14B**) (data collected by Dr. Marcus Long). This effect was independent from the concentration of the Ht-PreHNE used for treatment as long as the precursor completely occupied the binding site of Halo-Akt3. More importantly, no decrease in FRET response was observed in fish embryos injected with Halo-Akt3(C119S) mRNA unequivocally demonstrating that the response is residue-specific. Additionally, as expected the two pan-Akt inhibitors showed a drop in FRET response (**Figure 4.15**) (data collected by Dr. Marcus Long) consistent with the fold-decrease observed in cells.

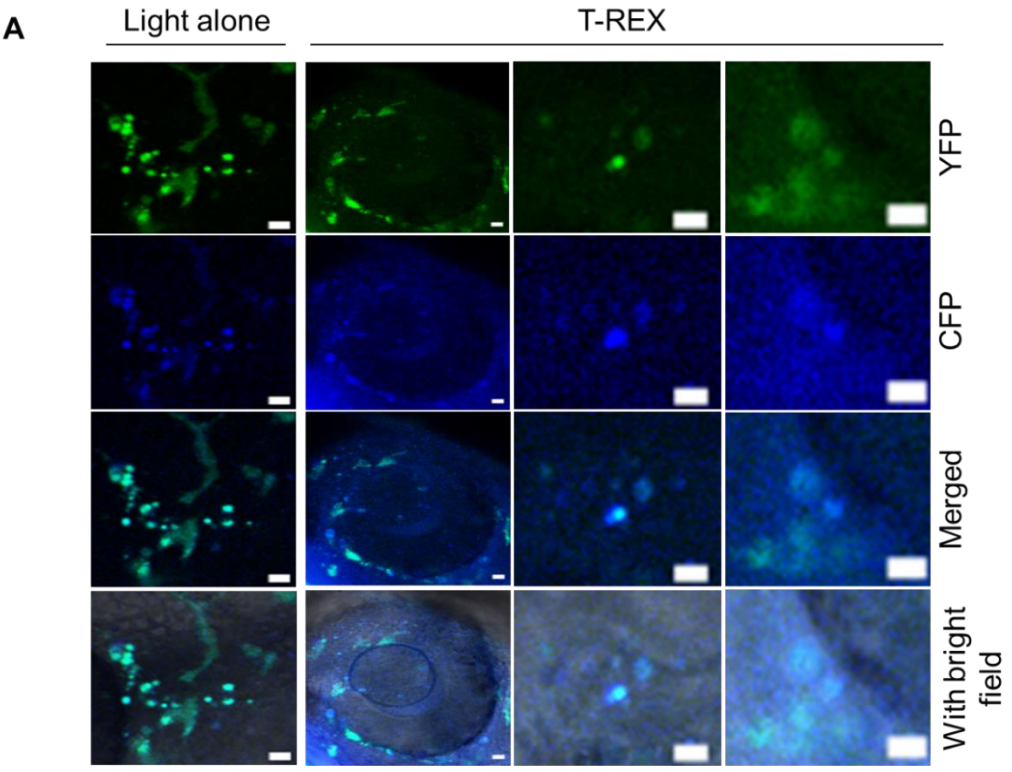
A
Light alone
T-REX
YFP
CFP
Merged
With bright field
B
Halo-Akt3 (WT)
Halo-Akt3 (C119S)
Normalized YFP/CFP emission ratio
ns
0.0119
<0.0001
<0.0001
DMSO
Light alone
Ht-PreHNE alone
T-REX
6 μM
1 μM

Figure 4.14 (**A**) Representative images showing mosaic expression of the AktAR FRET reporter 24–30 h post-injection of the plasmid DNA in zebrafish embryos. Scale bar: 10 μm (**B**) Quantitation of CFP and YFP fluorescence in fish co-injected with Halo-Akt3 mRNA and AktAR plasmid DNA. YFP/CFP ratiometric image quantification of individual somatic cells cells from n=5 independent embryos indicate Akt3-C119-specific HNEylation in wt-fish embryos enabled by T-REX downregulates the kinase activity; these effects were ablated in Akt3(C119S) mutant. Error bars are s.e.m.

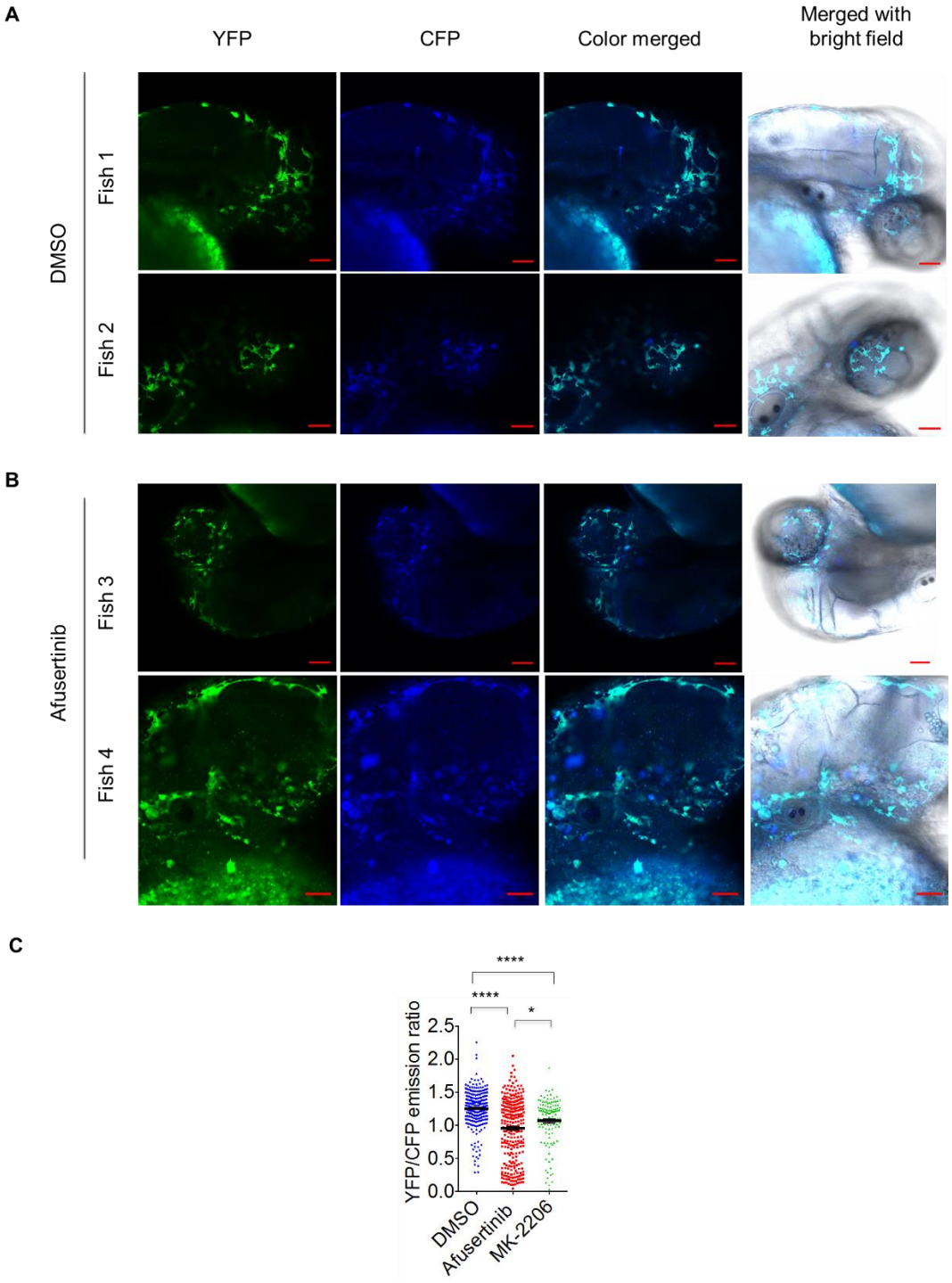

Figure 4.15 (**A–B**) Representative images showing mosaic expression of the AktAR FRET reporter 24–30 h post-injection of the plasmid DNA in zebrafish embryos. Fish expressing the AktAR plasmids and Halo-Akt3 were treated with 5 µM each of either MK-2206 (**A**) or Afuresetib (**B**) Scale bar: 10 µm (**B**) Quantitation of CFP and YFP fluorescence shows decrease in FRET ratio upon treatment with inhibitors. Error bars are s.e.m.

Finally, we also measured the transcript levels of endogenous genes regulated by p53 and FOXO, transcription factors negatively regulated by Akt. We measured the transcript levels of catalase, bcl-6, and bax1, genes regulated by the p53 and FOXO signaling axes. Consistent with our data showing relatively low expression of Halo-Akt-(wt/C119S) protein with respect to endogenous global Akt protein expression, basal levels of downstream Akt-controlled genes were unchanged in Halo-Akt3-(wt/C119S) injected fish relative to controls (**Figure 4.16A**). None-the-less, we found that relative to β-actin, T-REX promoted induction of known downstream Akt targets only when Akt3-WT was selectively targeted (**Figure 4.16B**). While all of these downstream transcripts are regulated by both Akt2 and Akt3, replicating identical experiments with either Halo-Akt2 or the hypomorphic mutant Halo-Akt3(C119S), in place of Halo-Akt3 did not activate those genes (**Figure 4.16C–D**).

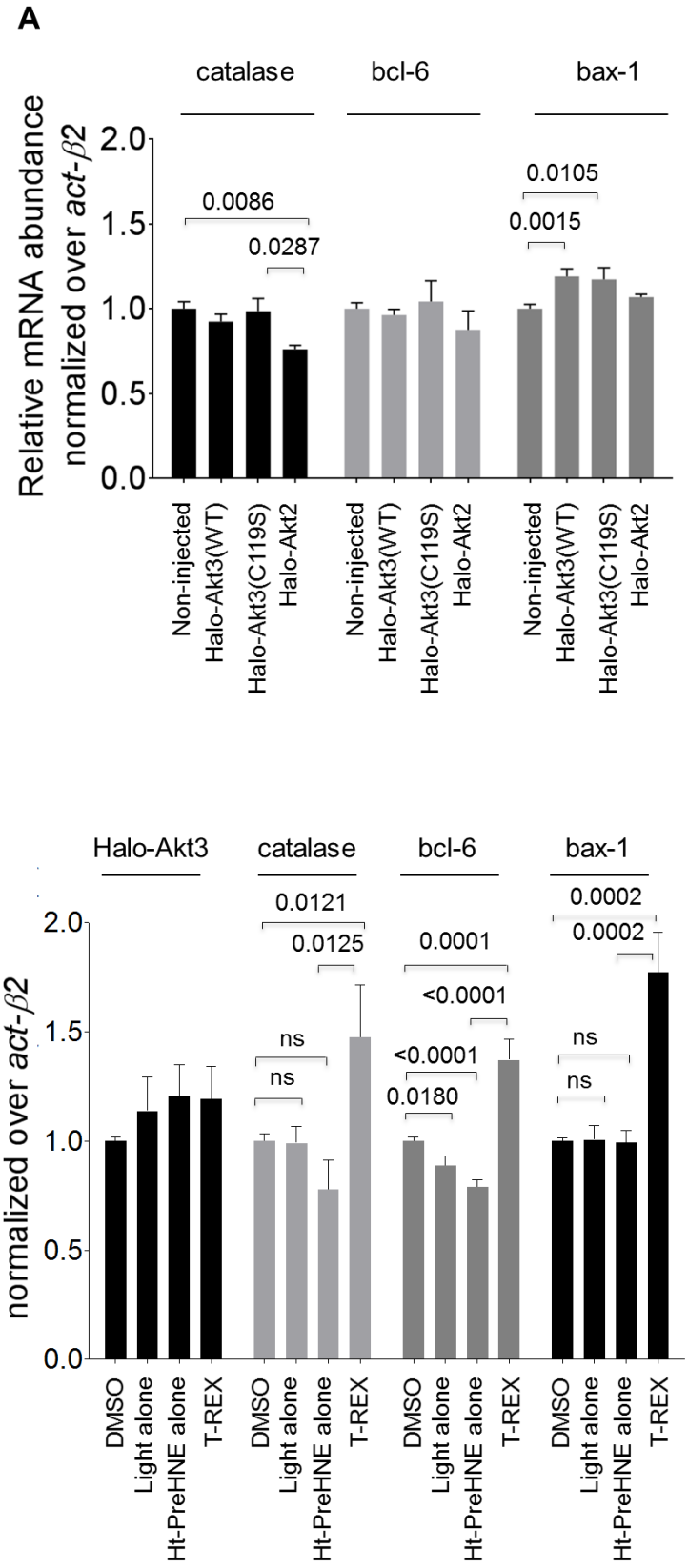
A
catalase
bcl-6
bax-1
Relative mRNA abundance normalized over act-β2
2.0
1.5
1.0
0.5
0.0
0.0086
0.0287
0.0105
0.0015
Non-injected
Halo-Akt3(WT)
Halo-Akt3(C119S)
Halo-Akt2
B
Halo-Akt3
catalase
bcl-6
bax-1
0.0121
0.0125
0.0001
<0.0001
0.0002
0.0002
ns
ns
<0.0001
0.0180
ns
ns
DMSO
Light alone
Ht-PreHNE alone
T-REX

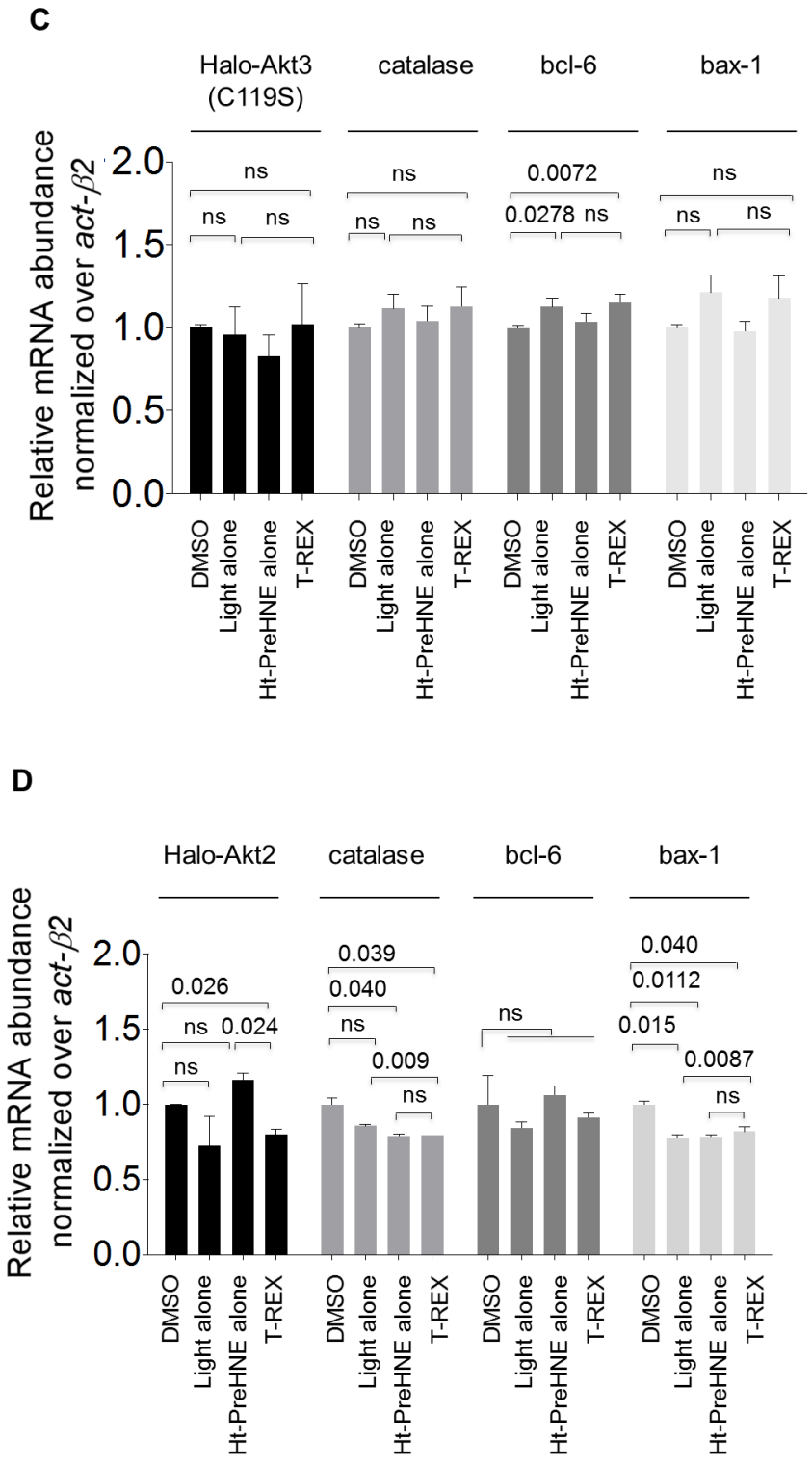
C
Halo-Akt3 (C119S)
catalase
bcl-6
bax-1
Relative mRNA abundance normalized over act-β2
2.0
1.5
1.0
0.5
0.0
ns
ns
ns
ns
ns
ns
0.0072
0.0278
ns
ns
ns
DMSO
Light alone
Ht-PreHNE alone
T-REX
D
Halo-Akt2
catalase
bcl-6
bax-1
Relative mRNA abundance normalized over act-β2
0.026
ns
0.024
ns
0.039
0.040
ns
0.009
ns
ns
0.040
0.0112
0.015
0.0087
ns

Figure 4.16 (**A**) Akt3 is an established upstream antagonist of FOXO and p53. Overexpression of HaloTagged Akt kinase isoforms did not alter the basal transcript levels of catalase and Bcl6 (driven by FOXO), and Bax-1 (regulated by p53), respectively (**B**) Akt3-specific HNEylation-dependent kinase-activity downregulation upregulates transcriptional activities of FOXO and p53 tumor suppressors. Error bars designate s.e.m. (**C–D**) These changes were not observed for Halo-Akt3(C119S) or Halo-Akt2.

Discussion

Isoform-specific regulatory patterns of proteins are critical in controlling a wide-array of cellular responses including cell proliferation, growth and survival. This is exemplified in the case of Akt, an oncogenic kinase and a major signaling hub in mammals[23]. Accumulating evidence suggests the three isoforms of Akt–Akt1, Akt2, and Akt3–have unique roles in the regulation of cellular processes despite sharing ~80% amino acid sequence homology[31-34]. Multifactorial mechanisms such as expression levels[35], subcellular localization[36], substrate preferences[31], and posttranslational modifications[13,37] are believed to underlie the isoform-specific signaling actions and disease phenotypes governed by Akt isoforms. However, our understanding of the molecular underpinnings of how highly homologous protein isoforms are regulated in cells has remained limited in part due to functional redundancy among different isoforms. Specifically, in the realms of non-canonical redox signaling paradigm, studying isoform-specific regulations in a cellular or organismal context has proven to be incredibly challenging.

Here, we used T-REX, a unique redox targeting tool, to screen kinases for their redox-sensing ability and ultimately their ability to translate the redox signal in a functional redox response. We unexpectedly discovered isoform-specific redox-sensing

ability of Akt. Akt3 was identified as a sensor for a model lipid-derived electrophile, HNE. We identified a cysteine (Cys119) residue in the flexible linker region of Akt3 isoform that endows it with HNE-sensing ability. Interestingly, Akt2 has another cysteine (Cys124) residue in the linker region that has been previously characterized as an oxidant-sensitive cysteine. Specifically, Cys124 was found to be oxidized to sulfenic acid upon treatment of NIH-3T3 cells with PDGF[13]. In the case of both Akt2 and Akt3, oxidative and electrophilic modification of the corresponding cysteine residues in the linker region attenuated their kinase activity. These data together suggest Akt isoforms have evolved to sense distinct native redox signals presumably by diversifying or acquiring new function within their linker regions. We further demonstrated that downregulation in kinase activity of Akt3 by low occupancy HNE modification is sufficient to trigger downstream signaling responses in mammalian cells as well as in zebrafish. Our discovery promises development of novel therapeutics that tap into the electrophile/oxidant-responsivity of specific kinase isoforms. In summary, we demonstrated here that T-REX is a powerful tool to identify novel privileged redox sensors. Commercial availability of the entire mouse and human HaloTag ORFeome will certainly aid in future discovery efforts of more privileged redox sensors.

Experimental Setup

Materials: All procedures related to zebrafish studies conform to the National Institutes of Health guidelines regarding animal experimentation and were approved by Cornell University's Institutional Animal Care and Use committees. Casper strain zebrafish were used for the experiments.

All primers were from IDT. Phusion HotStart II polymerase was from Thermo Scientific. All restriction enzymes were from NEB. All Halo clones in pFN21a vector (Kazusa Collection) and HaloTag®-TMR ligand were from Promega. Trizol RNA purification kit and Superscript III Reverse transcriptase were from Life Technologies. iQ SYBR Green Supermix was from BioRad. Complete EDTA free protease inhibitor was from Roche. 1X RIPA buffer was from Santa Cruz biotech. 1X Bradford dye was from BioRad. TALON metal affinity resin and His60 nickel resin were from Clonetech. Pre-HNE and HaloTag-targetable photocaged precursor HNE alkyne (Ht-PreHNE) were synthesized as described previously[38,39,16]. Cy5 azide and Cu(TBTA) were from Lumiprobe. Dithiothreitol (DTT), streptomycin sulfate, isopropyl β-D-1-thio-galactopyranoside (IPTG), TCEP-HCl, Coelenterazine, and D-Luciferin were from Goldbio Biotechnology. Coenzyme A was from Avanti Polar lipids. *trans*-1,2-Diaminocyclohexane-N,N,N',N'-tetraacetic acid monohydrate (CDTA) was from Alfa Aesar. 2-(4-aminophenyl)-6-methylbenzothiazole (APMBT) was from Enamine. Adenosine triphosphate disodium salt hydrate (ATP) was from Fisher. Biotin-dPEG®$_{11}$-azide was from Quanta Biodesign. MK-2206.2HCl (S1078) and Afuresertib (S7521) were from Selleckchem. A 10 mM stock of the inhibitors were prepared in

DMSO and stored in aliquots in −80 °C. Streptavidin sepharose beads were from GE Healthcare. Bovine Serum Albumin (BSA) powder was from Thermo Scientific. All other chemicals were from Sigma. BL21 (DE3)-RIL codon plus cells were from Stratagene. The plasmid for recombinant expression of TEV protease (pRK793, Addgene #8827), FOXO reporter plasmid FHRE-Luc (Addgene #1789), FLAG-FOXO-1a plasmid (Addgene #12148), FLAG-FOXO-3a plasmid (Addgene #8360), and the empty pCS2+8 vector (Addgene #34931) were from Addgene. HEK 293T cells were from American Type Culture Collection (ATCC). Cell line was validated to be free of mycoplasma contamination using MycoGuard™ Mycoplasma PCR detection kit (Genecopoeia™, MPD-T-050). 1X DPBS, 1X Trypsin (TrypLe), 100X NEAA, 100X sodium pyruvate, 100X Penicillin-Streptomycin and 1X MEM+Glutamax media were from Life Technologies. Fetal Bovine Serum (FBS) was from Sigma (F2442). TransIT 2020 transfection reagent was from Mirus Bio LLC. Polyethylenimine, linear, MW 25,000 (PEI, 23966-1) was from Polysciences, Inc. All tissue-culture treated plasticware was from CellTreat. 365 nm UV lights were from Spectroline (for handheld size, ENF240C) and Thermo Fisher (if larger surface area is needed, XX-15N). For T-REX experiments, the lamps were positioned above confluent monolayer of cells or zebrafish embryos in 6-well plates such that the power of UV irradiation was ~ 5 mW/ cm^2 (as measured by a hand-held power sensor (Spectroline, XDS-1000). For all confocal imaging experiments, a Zeiss LSM710 confocal microscope was used. Quantitation of fluorescence intensity was performed using Image-J software (NIH, version 1.50g). In-gel fluorescence analysis and imaging of western blots and Coomassie stained gel were performed using BioRad Chemi-Doc MP Imaging system. Densitometric quantitation

was performed using Image-J (NIH). Cy5 excitation source was epi illumination and 695/55 emission filter was used. Cell counting was done by Countess II FL (A25750). His_6-TEV S219V protease was recombinantly expressed and purified from BL21(DE3)-RIL cells using TALON resin. Quantitative PCR (qRT-PCR) was performed using MyiQ™ Single-Color Real-Time PCR Detection System (Bio-Rad 170-9740). Dual luciferase assay was performed using a BioTek Cytation™ 3 Cell Imaging Multi-mode reader with dual reagent injectors.

Construction of plasmids: Ligase-free cloning was used to clone various plasmids for expression in mammalian cells and in zebrafish. Halo ORFeome clone library in pFN21a vector was purchased from Promega. To sub-clone the Halo fusion genes in pCS2+8 vector and insert a His_6 tag at the N-terminus, the gene of interest (GOI) was cloned out from the original plasmid using the indicated forward (fwd-1) and reverse primers (rev-1). The resultant PCR product was extended using the indicated fwd-2, and rev-2 primers. An additional extension step was performed on the resulting product using fwd-3 and rev-2 primers. The resultant "megaprimer" was inserted into empty pCS2+8 vector (Addgene #34931) linearized with ClaI restriction enzyme (NEB). To make pCS2+8 His_6-Halo-(TEV)- Akt3(C119S) mutant, Akt3(wt) was amplified from the original plasmid using the indicated forward (fwd-1) and reverse primers (rev-1). The resultant PCR product was extended using the indicated fwd-2 and rev-2 extender primers. The resultant "megaprimer" was inserted into pCS2+8 His_6-Halo- Akt3(wt) after linearizing with ClaI restriction enzyme. To insert 2X FLAG peptide at the C-terminus of pCS2+8 His_6-Halo-Akt3(wt), the gene of interest was amplified as

described above except that the indicated forward and reverse primers were used. All plasmid sequences were verified by sequencing the entire gene at the genomics facility of Cornell Institute of Biotechnology. Plasmids were purified using EZ-10 spin column plasmid DNA miniprep kits (Bio Basic, BS614).

Table 4.1: Primers used for the construction of human, His_6-Halo-TEV-Akt2, His_6-Halo-TEV-Akt3(wt), His_6-Halo-TEV-Akt3 (C119S), and His_6-Halo-TEV-Akt3 (WT/C119S) 2X FLAG in pCS2+8 vector and primers for qRT-PCR analysis of Akt-regulated downstream gene expression. Note: "TEV" here refers to TEV-protease cleavage site.

Entry	**Plasmid**	**Primers**
(1)	His_6-Halo-TEV-Akt2	Fwd-1 CATGGGCAGCAGCCATCATCATCATCATCATGGGTC AGGGATGGCAGAAATCGGTACTGG Fwd-2 AGGTGACACTATAGAATACAAGCTACTTGTTCTTTT CCACCATGGGCAGCAGCCATCATC Fwd-3 GTCGGAGCAAGCTTGATTTAGGTGACACTATAGAA TACAAGCTACTTGTTCTTTTCCACC Rev-1 CGGCCTTTAATTAATGGCGCGCCACTAGTTTATTTT TTCCACTCGCGGATGCTGGCCGAG Rev-2 TCGAGAGGCCTTGAATTCCAATCGATGTCCGGCGAT CGCTGGCCGGCCTTTAATTAATGG

(2)	His_6-Halo-TEV-Akt3(wt)	Fwd-1 CATGGGCAGCAGCCATCATCATCATCATCATGGGTC AGGGATGGCAGAAATCGGTACTGG Fwd-2 AGGTGACACTATAGAATACAAGCTACTTGTTCTTTT CCACCATGGGCAGCAGCCATCATC Fwd-3 GTCGGAGCAAGCTTGATTTAGGTGACACTATAGAA TACAAGCTACTTGTTCTTTTCCACC Rev-1 GGCCGGCCTTTAATTAATGGCGCGCCACTAGTTTAT TTTTTCCAGTTACCCAGCATGC Rev-2 TCGAGAGGCCTTGAATTCCAATCGATGTCCGGCGAT CGCTGGCCGGCCTTTAATTAATGG
(3)	His_6-Halo-TEV-Akt3(C119S)	Fwd-1 AGAAGAGGAGAGAATGAATAGTAGTCCAACTTCAC AAATTGATAATAT Fwd-2 TATCCAGGCTGTAGCAGACAGACTGCAGAGGCAAG AAGAGGAGAGAATGAATAGTAGTCC

		Rev-1 GGCCGGCCTTTAATTAATGGCGCGCCACTAGTTTAT TTTTTCCAGTTACCCAGCATGC Rev-2 TCGAGAGGCCTTGAATTCCAATCGATGTCCGGCGAT CGCTGGCCGGCCTTTAATTAATGG
(4)	His_6-Halo- TEV- Akt3(WT/C11 9S)-2X FLAG	Fwd-1 CATGGGCAGCAGCCATCATCATCATCATCATGGGTC AGGGATGGCAGAAATCGGTACTGG Fwd-2 AGGTGACACTATAGAATACAAGCTACTTGTTCTTTT CCACCATGGGCAGCAGCCATCATC Fwd-3 GTCGGAGCAAGCTTGATTTAGGTGACACTATAGAA TACAAGCTACTTGTTCTTTTCCACC Rev-1 TCTTTGTAGTC CTTGTCGTCATCGTCTTTGTAGTC GCTGCC GTTACCCAGCATGCCACAA Rev-2 CGCGCCACTAGTTTATTTTTTCCACTTGTCGTC ATCG TCTTTGTAGTCCTTGTCGTCATC Rev-3

		GATGTCCGGCGATCGCTGGCCGGCCTTTAATTAATG GCGCGCCACTAGTTTATTTTTTCC
(5)	Primers for amplifying HaloTag genes for *in-vitro* transcription	RNA fwd GACGTAAATGGGCGGTAGGCG RNA Rev CATGATTACGCCAAGCGCGC
(6)	qPCR primers	human_akt3_fwd ACCGCACACGTTTCTATGGT human_akt3_Rev TGGCCATCTTTGTCCAGCAT human_akt2_fwd CCTGCCCTTCTACAACCAGG human_akt2_Rev TCCTTCTTAAGCAGCCCAGC ZF_Catalase_fwd ACGATGACAACGTGACCCAA ZF_Catalase_Rev ATCAGGTTTTGCACCATGCG ZF_Bcl6_fwd CCAGTTCAACAGACCCGCTA ZF_Bcl6_Rev TGAGCAACCTGCACGAATCT ZF_Bax_Fwd CGATACGGGCAGTGGCAAT

		ZF_Bax_Rev TCACTTCAGCATCCCTGTCG ZF_ Actinβ2_Fwd TCACTTTGAGCTCCTCCACACG ZF_Actinβ2_Rev ATCCATGGCTGAACTTGGGTTTG

T-REX in mammalian cells: HEK 293T cells were maintained in 1X MEM+ Glutamax™ media supplemented with 10% FBS, 1X NEAA, 1X sodium pyruvate and 1X Pen-Strep. Cells were grown in humidified, 5% CO_2 incubator at 37 °C. For in-gel fluorescence analysis and western blot, ~ 0.7–0.8 $X10^6$ HEK 293T cells were seeded in 8 cm^2 tissue culture dishes. 24 h later, cells were transfected using TransIT-2020 transfection reagent using manufacturer's recommendation. The subsequent steps were performed under red light. 24–36 h post transfection, monolayer of cells were treated with either 12 μM Ht-PreHNE or indicated concentrations (25 μM in the case of Halo-PTEN activity reporter assays) in serum-free media and incubated for 2.5 h. Cells were gently rinsed with serum-free media three times every 30 min over the next 1.5 h. Meanwhile, UV lamps were turned on 20 min prior to UV irradiation time to warm up the lamp. For samples designated for light exposure, the lids from the dishes were removed and the monolayered cells were placed under 365 nm UV light for 3–20 min (FRET assay and FOXO reporter assay in mammalian cells: 3 min; FRET assay and samples for qRT-PCR in zebrafish: 5 min; MS samples and In-gel fluorescence samples:

20 min)[39]. The cells were harvested, washed two times with ice-cold PBS and frozen in liquid nitrogen.

Western blotting: Cells were lysed in 1X RIPA buffer containing in final concentrations 1X Roche EDTA-free Protease inhibitor, 1 mM sodium orthovanadate and 1 mM PMSF, by rapid freeze-thaw (x3). Cell debris was removed, and the supernatant was collected after centrifugation at 18,000x g for 8 min at 4 °C. Protein concentration was determined using Bradford assay. 30–50 µg of total lysate was resolved by SDS-PAGE and the gel was transferred onto a PVDF membrane at 100 V for 1 h at 4 °C or at 40 V overnight at 4 °C. Membrane was blocked with 5% BSA and probed with various antibodies at the indicated dilutions.

In-gel fluorescence assay: As described in Chapter 2.

Biotin azide pull down from mammalian lysate: HEK 293T cells were split in 60 cm^2 plate. After the cells reached 60% confluence, the old media were aspirated and replaced with fresh 8 mL complete media. Cells were transfected with 7.5 µg of the designated plasmids encoding the HaloTag fusion gene and 30 µL 1 mg/mL PEI in 600 µL in Opti-MEM media for 24–36 h after which the cells were treated with 25 µM Ht-PreHNE or without alkyne (control) for 2.5 h. Rinsing and light shining protocol were as described above. Cells were harvested, washed twice with chilled 1X DPBS and flash frozen. Cell lysis was performed in 200 µL of lysis buffer containing in final concentrations 50 mM HEPES (pH 7.6), 150 mM NaCl, 1% Nonidet P-40 and 0.3 mM TCEP by rapid freeze-thaw (x3). Lysate was clarified by centrifugation at 18,000x g for 8 min at 4 °C. Total protein concentration was determined using Bradford assay using BSA as a standard.

TEV protease at a final concentration of 0.2 mg/mL was added to the lysate and incubated at 37 °C for 45 min. The lysate was subsequently diluted to 2 mg/mL with a buffer made up of 50 mM HEPES (pH 7.6) and 0.3 mM TCEP, and subjected to Click reaction with biotin azide for 30 min at 37 °C. The final concentrations of each components were: 1% SDS, 5% t–BuOH, 200 µM Biotin azide, 2 mM TCEP, 0.9 mM $CuSO_4$ and 0.1 mM Cu(TBTA). The lysate proteins were precipitated by adding 4 volumes of EtOH pre-chilled at −20 °C. The sample was vortexed and incubated at −80 °C overnight (or at least 4 h). The precipitant was collected by centrifugation at 18,000x g for 30 min at 4 °C and washed twice with pre-chilled MeOH then acetone. The pellet was resuspended in 50 µL of 50 mM HEPES (pH 7.6), 4% LDS and 0.5 µM EDTA and dissolved by vortexing and heating at 42 °C for 5 min. LDS was diluted to a final concentration of 0.5% by diluting the sample with 350 µL of 50 mM HEPES (pH 7.6) and added to 50 µL bed volume of Streptavidin sepharose beads pre-equilibrated with 50 mM HEPES (pH 7.6) and 0.5% LDS. The sample was incubated with beads for 2–3 h at room temperature by end-over-end rotation after which the supernatant was removed post-centrifugation at 500x g for 3 min. The beads were washed three times with 500 µL of 50 mM HEPES (pH 7.6) with 0.5% LDS with end-over-end rotation at room temperature for 30 min during each wash. The bound protein was eluted by boiling the beads at 98 °C for 10 min with 30 µL of Laemmeli dye containing 6% βME. The sample was subjected to SDS-PAGE and transferred to a PVDF membrane for western blot analysis.

FRET assay in live mammalian cells: 0.4–0.5 $X10^6$ HEK 293T cells were split into 4 X 35 mm glass-bottomed dishes. After 24 h, cells from each plate were transfected with 750 ng of AktAR reporter plasmid and 750 ng of the designated HaloTag fusion gene plasmid in pFN21a vector, using TransIT 2020. 24 h post transfection, cells were treated with 25 μM Ht-PreHNE or the equivalent final volume of DMSO in serum-free media and incubated for 2.5 h. Cells were gently rinsed with serum-free media three times every 30 min over the next 1.5 h. Meanwhile, UV lamps were turned on 10 min prior to UV irradiation time to warm up the lamp. For samples designated for light exposure, the lids from the dishes were removed and the monolayered cells were placed under 365 nm UV light for 3 min. The lids were replaced and the cells incubated for additional 8-10 h before imaging. FRET imaging was performed using a Zeiss LSM 710 confocal microscope as previously described. Briefly, 458 nm argon laser was used for excitation. The signals in cyan channel (463–498 nm) and yellow channel (525–620 nm) were recorded. For quantitation, the mean CFP and YFP signal intensity was measured using Image-J software by drawing a freehand circle around the cells and ratio image was calculated. Graphing and data analysis (Student's t-test) was performed using Prism software.

ELISA: Antibody was bound to the plate at the stated concentration (1-3 μg/mL) in sodium bicarbonate buffer pH 9.6 for at least 24 h in a 96 well white plate (80 μL per plate) at 4 ^{o}C. Maximum incubation time was 48 h. After this time, incubation buffer was removed, washed once with TBS-Tween (100 mM Tris, 150 mM NaCl, 0.03% Tween-20) and then blocked in 5% BSA in TBS-Tween (280 μL per plate) for 3-5 h at

rt. After this time, BSA was washed away two times using TBS-Tween, then wells were filled with 150 μL blocking buffer (1.1 % BSA, 5 mM sodium orthovanadate, 20 mM NaF). Cells were lysed in 50 mM HEPES pH 7.6, 1 % NP-40, 5 mM sodium orthovanadate, 20 mM NaF and 2X ROCHE complete minus EDTA protease inhibitors. 30 μg each lysate (quantified by Bradford relative to BSA) was added to each well (approximately 30 μL lysate, but always equal amounts of total lysate buffer was added for each set). For a number of individual data points (usually those yielding the most protein), the amount of lysate loaded was doubled in separate wells and the value recorded was ultimately compared to the value obtained for 1X lysate. This was shown to give equal signal (proving saturation conditions wherein the amount of phosphorylated protein detected reflects the ratio of phosphorylated to non-phosphorylated protein in the lysate). This was incubated at 4 ^{o}C overnight. After this time, wells were washed with TBS-Tween 3 times, then primary antibody was added in 1.1 % BSA in TBS-Tween overnight at 4 ^{o}C. After this time, wells were washed (primary antibody could be recycled, but this was not done for the data in this manuscript) and HRP-conjugated secondary antibody was added in 1% Milk in TBS-Tween. After 1 h at rt, wells were washed 3 times with TBS-Tween, for 15 min, then once with TBS for 20 min after which time 50 μL TBS was added to each well. HRP was detected using an autoinjector program on a Biotek citation 3 plate reader. Femto ELISA substrate was used, injecting 50 μL Femto ELISA substrates 1 and 2 per well. Signals were calculated relative to well coated in antibody and treated with untransfected lysate. Usually this gave signals very close to those observed for treatment with inhibitor.

Table 4.2: Summary of antibodies used for WB, ELISA and IF.

Antibody	Application	Catalog number; Supplier	Dilution WB/ELISA	Dilution IF
Mouse monoclonal anti-β-Actin	WB	A4700; Sigma	1:30000	-
Rabbit polyclonal anti-Halo	WB	G9281; Promega	1:1000	1:200
Monoclonal anti-gapdh- peroxidase	WB	G92296; Sigma	1:30000	-
Secondary antibody to rabbit IgG, HRP linked	WB	7074; Cell Signaling Technology	1:3000-6000	-
Secondary antibody to mouse HRP linked	WB	Ab6789; Abcam	1:5000	-
Donkey Anti-rabbit IgG AlexaFluor® 647	IF	Ab150075; Abcam	1:800	-
Rabbit Monoclonal anti-phospho-Akt (T308) (D25E6) (Note: for Akt3, the residue is T305)	ELISA (detection of antibody-bound protein)	13038; Cell Signaling Technology	1:1000	-
Rabbit Monoclonal anti-Akt (pan) (C67E7)	WB/ IF	4691; Cell Signaling Technology	1:1000	1:200
Anti-DDDDK tag antibody	ELISA (bound to plate)	Ab1257; AbCam	1-3 ug/ml	1:200

				(validated using cell-based IF for specificity)
Mouse monoclonal anti-Halo	ELISA (bound to plate) /IF	G9211; Promega	3 ug/ml	1:200
Donkey anti goat-FITC	IF	AB97109 AbCam	-	1:800
Mouse monoclonal anti-phospho FOXO1a/3a T24/32	ELISA (detection of antibody-bound protein)	9464; Cell Signaling Technology	1:1000	-
Donkey anti Rabbit-AlexaFluor® 594	IF	AB150064 AbCam	-	1:800

Luciferase assay: 0.5–0.6 X10^5 HEK 293T cells were seeded in each well of a 48-well plate. 24 h later, the cells were transfected with 120 ng of the designated HaloTag fusion gene plasmid and 120 ng of FHRE::Firefly luciferase: pCMV::Renilla luciferase (40:1) mix, by using TransIT–2020 transfection agent. 24 h post-transfection, cells were treated with DMSO or 25 µM Ht-PreHNE for 2.5 h, rinsed three times and irradiated with 365 nm UV light for 3 min. The cells were incubated for either 8 or 18 h. For dual luciferase assay, cells in each well were gently washed with 1X DPBS and lysed in 65 µL of 1X passive lysis buffer that contained in final concentrations 25 mM Tris (pH 7.8), 2 mM 1,2- CDTA, 2 mM DTT, 1 mg/mL BSA, 1 % Triton X-100, and 10%

Glycerol. 20 µL lysate was transferred to a white opaque 96-well plate (Corning). Firefly luciferase was read after adding 50 µL of Firefly substrate (75 mM HEPES pH 8.0, 4 mM $MgSO_4$, 20 mM DTT, 0.1 mM EDTA, 0.53 mM ATP, 0.27 mM Coenzyme-A, 0.47 mM D-Luciferin Firefly). Subsequently, 50 µL of Stop and Glow substrate (7.5 mM sodium acetate pH 5.0, 400 mM sodium sulfate, 10 mM CDTA, 15 mM sodium pyrophosphate, 0.025 mM APMBT (2-(4-Aminophenyl)-6-methylbenzothiazol), 5.5 µM Coelenterazine) was added and Renilla luciferase activity was measured.

Caspase assay in mammalian cells: 0.5–0.6 $X10^5$ HEK 293T cells were seeded in each well of a 48-well plate. 24 h later, the cells were transfected with 120 ng of the designated HaloTag fusion gene plasmid and 120 ng of 40:1 FHRE::firefly luciferase : pCMV::Renilla luciferase, using TransIT–2020 transfection agent. 24 h post-transfection, cells were treated with DMSO or 25 µM Ht-PreHNE for 2.5 h, rinsed three times and irradiated with 365 nm UV light for 3 min. The cells were incubated for 18 h after which the cells were trypsinized, washed two times and lysed in 65 µL of 1X passive lysis buffer (see Luciferase assay protocol). 20 µL of the lysate was transferred to a white opaque 96-well plate (Corning). Firefly luciferase and Renilla luciferase activities (the latter was used for normalization) were measured as described (see Luciferase assay protocol). 25 µL of the remaining lysate was transferred to a black opaque 96-well plate (Corning) for measuring caspase activity. 100 µL caspase substrate containing 50mM HEPES (7.4), 100mM NaCl, 0.1% CHAPS, 10mM DTT, 1mM EDTA, 10% glycerol and 15 µM Ac-DEVD-AMC was added to each well and

the release of AMC was measured continuously by fluorescence for 2 h at 37 °C using a plate reader with excitation at 380 nm and emission at 440 nm.

In vitro transcription: All genes were cloned into pCS2+8 vector. Prior to *in vitro* transcription, the genes were PCR amplified using RNA fwd and Rev primers. *In vitro* transcription was performed using a mMessage mMachine SP6 transcription kit per manufacturer's suggestion.

Fish injection and T-REX: Fertilized eggs at the 1–2 cell stage from casper zebrafish were injected with mRNA (1.6 mg/ml) into the yolk sack. Immediately after injection, embryos were pooled, and separated into two petri dishes (10 cm) filled with 30 mL 10% Hank's salt solution with methylene blue and penicillin (100 U/ml) / streptomycin (100 µg/ml). To one set was added the HaloTag-targetable photocaged precursor to HNE (Ht-preHNE, hereafter) (<15 µM) and the other DMSO in the dark. Fish were maintained at 28 ^{o}C in the dark for 28 h after which time fish were washed in 10% Hank's solution with no methylene blue/antibiotic (3 times for 30 min each). Fish were moved to 6-well plates. Half of the embryos (Ht-preHNE-treated or -untreated) were irradiated with UV light for 5 min the other half of each set was not. Embryos were left for 8 h after which time they were euthanized, washed with cold 1X DPBS and dechorionated (and deyolked if protein analysis was to be undertaken) then either lysed using (for qRT-PCR) Trizol together with vortexing with glass beads; or (for protein analysis) resuspended in 50 mM Hepes, 1% triton X-100 and lysed by freeze-thawing followed by vortexing with zirconia beads (3 times).

FRET reporter assay in fish: Embryos at the 1-cell stage were injected with a mixture of mRNA (1.4 mg/ml) and reporter plasmid (30 µg/ml) into the single cell of fertilized eggs. Immediately after injection, embryos were pooled, and separated into two petri dishes (10 cm) filled with 30 ml 10% Hank's salt solution with methylene blue and penicillin (100 U/ml) / streptomycin (100 µg/ml). To one set was added Ht-preHNE (at indicated concentrations) and the other DMSO in the dark. In cases where inhibition of Akt was analysed, another set of fish embryos were treated with the designated concentrations of the inhibitor. Fish were maintained at 28 $^{\circ}$C in the dark for 28 h after which time fish were washed in 10% Hank's solution with no methylene blue (3 times with 30 min in between each wash). After this time fish were moved to 6-well plates. The two sets of embryos for T-REX were exposed to UV light for 5 min. Embryos were left for 5 h after which time they were placed on ice. Embryos were then screened for expression of fluorescence and those expressing the fluorescence reporter were imaged using confocal microscopy on a Leica 710 microscope using a 10X water lens with 1.7-fold magnification. 5–6 embryos were imaged each set and around 9–15 z-stacks were taken each time. Fish were irradiated with 458 nm laser and YFP and CFP emission fluorescence was collected with band pass emission filters (525–620 nm and 463–498 nm, respectively). CFP and YFP fluorescence was quantified using Image-J taking the signals of the surrounding area as a local background in a procedure similar to the established ratio image generation method in zebrafish[40]. Around 250 separate cells were quantified for each condition.

Whole-mount IF: Fish were treated as described. Approximately 24 hpf, they were dechorionated and fixed in 4% PFA for 24-48 h with gentle rocking at 4^{o}C. After this time, PFA was removed and replaced with methanol and stored at –20^{o}C for 24 h. Fish were then washed 2 times with PBS-0.1%Tween-1%DMSO for 30 min each, then blocked in 10% FBS/2% BSA in PBS-0.1%Tween, then stained with the appropriate primary antibody overnight at 4^{o}C in blocking buffer, then washed 2x(30 min) and stained with the appropriate fluorescent secondary antibodies for 1.5 h at rt. Fish were imaged on 2% agarose plates either on a Zeiss LSM700 confocal microscope or a Leica M205-FA equipped with a stereomicroscope.

Biotin azide pull down from fish: Around 250–300 zebrafish embryos injected with the designated mRNA and treated under T-REX condition were manually dechorionated and deyolked immediately post UV irradiation at 4 ^{o}C. The embryos were washed 3X with 50 mM HEPES (pH 7.6) to remove residual yolk proteins. The embryos were lysed in 100 µL of lysis buffer containing in final concentrations 50 mM HEPES (pH 7.6), 150 mM NaCl, 1% Nonidet P-40, 0.3 mM TCEP and 2X Roche cOmplete, mini, EDTA-free protease inhibitor (Roche Life Sciences), 0.2 mg/mL soybean trypsin inhibitor by rapid freeze-thaw (x3) and vortexing with zirconia beads (Bio spec 0.7 mm beads; 11079107zx). Lysate was clarified by centrifugation at 18,000x g for 8 min at 4 °C. Total protein concentration was determined using Bradford assay using BSA as a standard. TEV protease at a final concentration of 0.2 mg/mL was added to the lysate and incubated at 37 °C for 45 min. The lysate was subsequently diluted to 2 mg/mL with a buffer made up of 50 mM HEPES (pH 7.6), 0.3 mM TCEP, and 2X Roche

protease inhibitor and subjected to Click reaction [1% SDS, 5% t–BuOH, 200 µM Biotin azide, 2 mM TCEP, 0.9 mM $CuSO_4$ and 0.1 mM Cu(TBTA)] for 30 min at 37 °C. Click reaction condition and subsequent pull-down protocol is identical to that reporter above for mammalian cells.

qRT-PCR analyses in fish extracts: qRT-PCR analysis was performed as previously described[41]. Briefly, 7–10 fish embryos (24 hpf) were homogenized in 1 mL TRIzol by vortexing with glass beads for 2 min. Total RNA was extracted and purified using TRIzol® Plus RNA Purification kit (Life Technologies, 1218355) per manufacturer's suggestion. Around 600 ng of the total isolated RNA was reverse transcribed using SuperScript® III Reverse Transcriptase (Life Technologies, 18080093). qRT-PCR analysis was performed with iQ™ SYBR® Green Supermix (Bio-Rad, 170-8880) on a MyiQ™ Single-Color Real-Time PCR Detection System (Bio-Rad, 170-9740). In a total volume of 20 µL the PCR reaction mix contained, in final concentrations, 1X iQ™ SYBR® Green Supermix, 0.35 µM each of the forward and reverse primers and 20 ng of template cDNA. The qPCR program was set for 3 min at 95 °C followed by 45-repeat cycles comprising heating at 95 °C for 10 s and at 55 °C for 30 s. The expected products were of ~100–150 bp in size. The primers used for each gene are specified in **Table 4.1**. All primers were validated as specified previously[41].

Live-cell Imaging: Cells were grown to 70% confluence in 35 mm glass-bottomed dishes and transfected with HaloTagged Akt plasmids. 24 h post-transfection, cells were incubated in dark at 37 °C incubator with 3 µM HaloTMR® ligand for 3 h in serum free

media. Subsequently cells were washed 3 times with serum free media and incubated for 30 min with complete media containing, in final concentration, 1 μg/mL Hoechst 33258 dye (Thermo Scientific). Cells were rinsed 2 times with complete media and imaged using a Zeiss LSM 710 meta confocal fluorescence microscope. Image analysis was performed using Image-J (NIH).

References

(1) Weerapana, E.; Wang, C.; Simon, G. M.; Richter, F.; Khare, S.; Dillon, M. B. D.; Bachovchin, D. A.; Mowen, K.; Baker, D.; Cravatt, B. F. Quantitative reactivity profiling predicts functional cysteines in proteomes. *Nature* **2010,** *468* (7325), 790.

(2) Wang, C.; Weerapana, E.; Blewett, M. M.; Cravatt, B. F. A chemoproteomic platform to quantitatively map targets of lipid-derived electrophiles. *Nat Meth* **2014,** *11* (1), 79.

(3) Vila, A.; Tallman, K. A.; Jacobs, A. T.; Liebler, D. C.; Porter, N. A.; Marnett, L. J. Identification of Protein Targets of 4-Hydroxynonenal Using Click Chemistry for ex Vivo Biotinylation of Azido and Alkynyl Derivatives. *Chem. Res. Toxicol.* **2008,** *21* (2), 432.

(4) Codreanu, S. G.; Zhang, B.; Sobecki, S. M.; Billheimer, D. D.; Liebler, D. C. Global Analysis of Protein Damage by the Lipid Electrophile 4-Hydroxy-2-nonenal. *Molecular & Cellular Proteomics : MCP* **2009,** *8* (4), 670.

(5) Kim, H.-Y. H.; Tallman, K. A.; Liebler, D. C.; Porter, N. A. An Azido-Biotin Reagent for Use in the Isolation of Protein Adducts of Lipid-derived Electrophiles by Streptavidin Catch and Photorelease. *Molecular & Cellular Proteomics : MCP* **2009,** *8* (9), 2080.

(6) Codreanu, S. G.; Ullery, J. C.; Zhu, J.; Tallman, K. A.; Beavers, W. N.; Porter, N. A.; Marnett, L. J.; Zhang, B.; Liebler, D. C. Alkylation Damage by Lipid Electrophiles Targets Functional Protein Systems. *Molecular & Cellular Proteomics : MCP* **2014,** *13* (3), 849.

(7) Yang, J.; Tallman, K. A.; Porter, N. A.; Liebler, D. C. Quantitative Chemoproteomics for Site-Specific Analysis of Protein Alkylation by 4-Hydroxy-2-Nonenal in Cells. *Anal. Chem.* **2015,** *87* (5), 2535.

(8) Dalleau, S.; Baradat, M.; Gueraud, F.; Huc, L. Cell death and diseases related to oxidative stress:4-hydroxynonenal (HNE) in the balance. *Cell Death Differ.* **2013,** *20* (12), 1615.

(9) Long, M. J. C.; Aye, Y. Privileged Electrophile Sensors: A Resource for Covalent Drug Development. *Cell Chemical Biology* **2017,** *24* (7), 787.

(10) Truong, T. H.; Ung, P. M.-U.; Palde, P. B.; Paulsen, C. E.; Schlessinger, A.; Carroll, K. S. Molecular Basis for Redox Activation of Epidermal Growth Factor Receptor Kinase. *Cell chemical biology* **2016,** *23* (7), 837.
(11) Peralta, D.; Bronowska, A. K.; Morgan, B.; Dóka, É.; Van Laer, K.; Nagy, P.; Gräter, F.; Dick, T. P. A proton relay enhances H2O2 sensitivity of GAPDH to facilitate metabolic adaptation. *Nature Chemical Biology* **2015,** *11*, 156.
(12) Weerapana, E.; Simon, G. M.; Cravatt, B. F. Disparate proteome reactivity profiles of carbon electrophiles. *Nat. Chem. Biol.* **2008,** *4* (7), 405.
(13) Wani, R.; Qian, J.; Yin, L.; Bechtold, E.; King, S. B.; Poole, L. B.; Paek, E.; Tsang, A. W.; Furdui, C. M. Isoform-specific regulation of Akt by PDGF-induced reactive oxygen species. *Proc. Natl. Acad. Sci. U. S. A.* **2011,** *108* (26), 10550.
(14) Santi, S. A.; Lee, H. The Akt isoforms are present at distinct subcellular locations. *American Journal of Physiology - Cell Physiology* **2010,** *298* (3), C580.
(15) Miao, L.; Yang, L.; Huang, H.; Liang, F.; Ling, C.; Hu, Y. mTORC1 is necessary but mTORC2 and GSK3β are inhibitory for AKT3-induced axon regeneration in the central nervous system. *eLife* **2016,** *5*, e14908.
(16) Gao, X.; Zhang, J. Spatiotemporal Analysis of Differential Akt Regulation in Plasma Membrane Microdomains. *Mol. Biol. Cell* **2008,** *19* (10), 4366.
(17) Leslie, N. R.; Bennett, D.; Lindsay, Y. E.; Stewart, H.; Gray, A.; Downes, C. Redox regulation of PI 3-kinase signalling via inactivation of PTEN. *The EMBO Journal* **2003,** *22* (20), 5501.
(18) Cho, S.-H.; Lee, C.-H.; Ahn, Y.; Kim, H.; Kim, H.; Ahn, C.-Y.; Yang, K.-S.; Lee, S.-R. Redox regulation of PTEN and protein tyrosine phosphatases in H2O2-mediated cell signaling. *FEBS Letters* **2004,** *560* (1-3), 7.
(19) Fang, X.; Fu, Y.; Long, M. J. C.; Haegele, J. A.; Ge, E. J.; Parvez, S.; Aye, Y. Temporally Controlled Targeting of 4-Hydroxynonenal to Specific Proteins in Living Cells. *J. Am. Chem. Soc.* **2013,** *135* (39), 14496.
(20) Parvez, S.; Long, M. J. C.; Lin, H.-Y.; Zhao, Y.; Haegele, J. A.; Pham, V. N.; Lee, D. K.; Aye, Y. T-REX on-demand redox targeting in live cells. *Nat. Protocols* **2016,** *11* (12), 2328.
(21) Zhou, B. P.; Hu, M. C.; Miller, S. A.; Yu, Z.; Xia, W.; Lin, S. Y.; Hung, M. C. HER-2/neu blocks tumor necrosis factor-induced apoptosis via the Akt/NF-kappaB pathway. *J. Biol. Chem.* **2000,** *275* (11), 8027.
(22) Dudek, H.; Datta, S. R.; Franke, T. F.; Birnbaum, M. J.; Yao, R.; Cooper, G. M.; Segal, R. A.; Kaplan, D. R.; Greenberg, M. E. Regulation of neuronal survival by the serine-threonine protein kinase Akt. *Science* **1997,** *275* (5300), 661.
(23) Manning, B. D.; Cantley, L. C. AKT/PKB Signaling: Navigating Downstream. *Cell* **2007,** *129* (7), 1261.
(24) Vincent, E. E.; Elder, D. J. E.; Thomas, E. C.; Phillips, L.; Morgan, C.; Pawade, J.; Sohail, M.; May, M. T.; Hetzel, M. R.; Tavaré, J. M. Akt phosphorylation on Thr308 but not on Ser473 correlates with Akt protein

kinase activity in human non-small cell lung cancer. *British Journal of Cancer* **2011,** *104* (11), 1755.
(25) Greer, E. L.; Brunet, A. FOXO transcription factors at the interface between longevity and tumor suppression. *Oncogene* **2005,** *24*, 7410.
(26) Calnan, D. R.; Brunet, A. The FoxO code. *Oncogene* **2008,** *27*, 2276.
(27) Santo, E. E.; Stroeken, P.; Sluis, P. V.; Koster, J.; Versteeg, R.; Westerhout, E. M. FOXO3a Is a Major Target of Inactivation by PI3K/AKT Signaling in Aggressive Neuroblastoma. *Cancer Research* **2013,** *73* (7), 2189.
(28) Franke, T. F.; Hornik, C. P.; Segev, L.; Shostak, G. A.; Sugimoto, C. PI3K/Akt and apoptosis: size matters. *Oncogene* **2003,** *22*, 8983.
(29) Ogawara, Y.; Kishishita, S.; Obata, T.; Isazawa, Y.; Suzuki, T.; Tanaka, K.; Masuyama, N.; Gotoh, Y. Akt Enhances Mdm2-mediated Ubiquitination and Degradation of p53. *Journal of Biological Chemistry* **2002,** *277* (24), 21843.
(30) Köster, R. W.; Fraser, S. E. Tracing Transgene Expression in Living Zebrafish Embryos. *Developmental Biology* **2001,** *233* (2), 329.
(31) Sanidas, I.; Polytarchou, C.; Hatziapostolou, M.; Ezell, Scott A.; Kottakis, F.; Hu, L.; Guo, A.; Xie, J.; Comb, Michael J.; Iliopoulos, D.et al. Phosphoproteomics Screen Reveals Akt Isoform-Specific Signals Linking RNA Processing to Lung Cancer. *Molecular Cell 53* (4), 577.
(32) Tschopp, O.; Yang, Z.-Z.; Brodbeck, D.; Dummler, B. A.; Hemmings-Mieszczak, M.; Watanabe, T.; Michaelis, T.; Frahm, J.; Hemmings, B. A. Essential role of protein kinase Bγ (PKBγ/Akt3) in postnatal brain development but not in glucose homeostasis. *Development* **2005,** *132* (13), 2943.
(33) Cho, H.; Mu, J.; Kim, J. K.; Thorvaldsen, J. L.; Chu, Q.; Crenshaw, E. B.; Kaestner, K. H.; Bartolomei, M. S.; Shulman, G. I.; Birnbaum, M. J. Insulin Resistance and a Diabetes Mellitus-Like Syndrome in Mice Lacking the Protein Kinase Akt2 (PKBβ). *Science* **2001,** *292* (5522), 1728.
(34) Chen, W. S.; Xu, P.-Z.; Gottlob, K.; Chen, M.-L.; Sokol, K.; Shiyanova, T.; Roninson, I.; Weng, W.; Suzuki, R.; Tobe, K.et al. Growth retardation and increased apoptosis in mice with homozygous disruption of the akt1 gene. *Genes & Development* **2001,** *15* (17), 2203.
(35) Lee, R. S.; House, C. M.; Cristiano, B. E.; Hannan, R. D.; Pearson, R. B.; Hannan, K. M. Relative Expression Levels Rather Than Specific Activity Plays the Major Role in Determining In Vivo AKT Isoform Substrate Specificity. *Enzyme Research* **2011,** *2011*, 18.
(36) Gonzalez, E.; McGraw, T. E. Insulin-modulated Akt subcellular localization determines Akt isoform-specific signaling. *Proceedings of the National Academy of Sciences* **2009,** *106* (17), 7004.
(37) Okano, J.-i.; Gaslightwala, I.; Birnbaum, M. J.; Rustgi, A. K.; Nakagawa, H. Akt/Protein Kinase B Isoforms Are Differentially Regulated by Epidermal Growth Factor Stimulation. *Journal of Biological Chemistry* **2000,** *275* (40), 30934.
(38) Lin, H. Y.; Haegele, J. A.; Disare, M. T.; Lin, Q.; Aye, Y. A generalizable platform for interrogating target- and signal-specific consequences of

electrophilic modifications in redox-dependent cell signaling. *J. Am. Chem. Soc.* **2015,** *137* (19), 6232.
(39) Parvez, S.; Long, M. J. C.; Lin, H.-Y.; Zhao, Y.; Haegele, J. A.; Pham, V. N.; Lee, D. K.; Aye, Y. T-REX™ On-demand redox targeting: a toolset for functional discoveries and validations. *Nat. Protoc.* **2016,** *11*, 2328.
(40) Kardash, E.; Bandemer, J.; Raz, E. Imaging protein activity in live embryos using fluorescence resonance energy transfer biosensors. *Nat. Protoc.* **2011,** *6* (12), 1835.
(41) Parvez, S.; Fu, Y.; Li, J.; Long, M. J.; Lin, H. Y.; Lee, D. K.; Hu, G. S.; Aye, Y. Substoichiometric hydroxynonenylation of a single protein recapitulates whole-cell-stimulated antioxidant response. *J. Am. Chem. Soc.* **2015,** *137* (1), 10.

CHAPTER 5

PARALOG-SPECIFIC REGULATORY ROLES OF ZEBRAFISH KEAP1

Introduction

Zebrafish is a popular organism for the study of vertebrate gene function[1-5]. The ease of genetic modification (overexpression and knockdown), coupled with transparency of the developing embryo makes it especially suited to study the effects of genetic manipulation on organ/animal development. Systematic genetic screens have identified many genes, loss-of-function of which results in phenotypes that are also found in human diseases[1-3,6]. An interesting feature of the zebrafish genome is that the model organism often has two paralogs of human genes. This is because zebrafish belongs to teleost class of vertebrates that underwent whole-genome duplication[7]. This duplication event has presented opportunities to gain additional insights into gene functions that are not obtainable using mammalian counterparts.

The Nrf2/AR signaling axis is evolutionarily conserved in zebrafish, showing high functional homology with the mammalian Keap1[8], Nrf2[9], and the antioxidant response element (ARE)[10]. However, because of genome duplication, zebrafish possesses two paralogs of Keap1(ZfKeap1a and ZfKeap1b)[8], and Nrf2 (ZfNrf2a, ZfNrf2b)[9]. The two Keap1 paralogs are demonstrated to have complementary roles in regulating AR[11]. Similarly, the two Nrf2 paralogs also show distinct roles in transcriptional regulation of ARE-controlled genes[9]. Most studies to understand the functional roles of ZfKeap1 and ZfNrf2 paralogs are conducted using bolus dosing approach in a genetically manipulated background (either knock-down or

overexpression of specific paralogs)[8,9,11]. While these studies are useful, the redox signal-induced state of a redox-sensing protein is hard to mimic using bolus dosing. Downstream phenotypes from bolus dosing likely arise from simultaneous modifications of multiple redox-sensing regulators. Z-REX, on the other hand, enables targeted modification of a protein-of-interest, with the ability to shed light on the signal-induced state of a protein in regulating biological processes. Here, we sought to characterize the Nrf2/AR signaling pathway in zebrafish upon selective modification of ectopically expressing human Keap1 using Z-REX, with the aim of identifying novel regulators of the Nrf2/AR signaling pathway. We used Z-REX coupled with morpholino-induced knockdown of the two paralogs of ZfKeap1 and ZfNrf2 to parse out the complex regulatory roles of these proteins in controlling the zebrafish Nrf2/AR signaling axis.

Results*

Halo-Keap1(human)is functional in zebrafish

As shown in Chapter 2, injection of Halo-Keap1 mRNA in zebrafish at 1–4 cell stage resulted in ubiquitous expression of the protein at a level similar to endogenous zebrafish Keap1. We next sought to validate that Halo-Keap1 is indeed functional in whole fish. We used two independent readouts: a specific transgenic AR-reporter strain "*Tg(-3.5gstp1:GFP)/it416b*" [hereafter *Tg(gstp1:GFP)*][12] and by qRT-PCR in Casper fish.

* All fish experiments were performed in collaboration with Dr. Marcus Long. Fish injection with plasmids/mRNA, treatment with various compounds, and Z-REX were performed by Dr. Marcus Long. Unless otherwise specified, all downstream fish experiments were performed by Saba Parvez. Data collected by Dr. Marcus Long are specified throughout the text.

Both readouts demonstrated that Halo-Keap1 overexpression results in a drop in basal AR response in the zebrafish embryos (**Figure 5.1**). Intriguingly, we observed differential AR response in the head *vs* the tail. We found that ubiquitous expression of Halo-Keap1 in *Tg(gstp1:GFP)* fish led to AR-downregulation selectively in the tail (**Figure 5.1A**). This spatially-selective response was also observed in an independent Halo-Keap1-mRNA-injected Casper non-reporter fish by qRT-PCR, where the tail showed a more prominent AR-attenuation (**Figure 5.1B**).

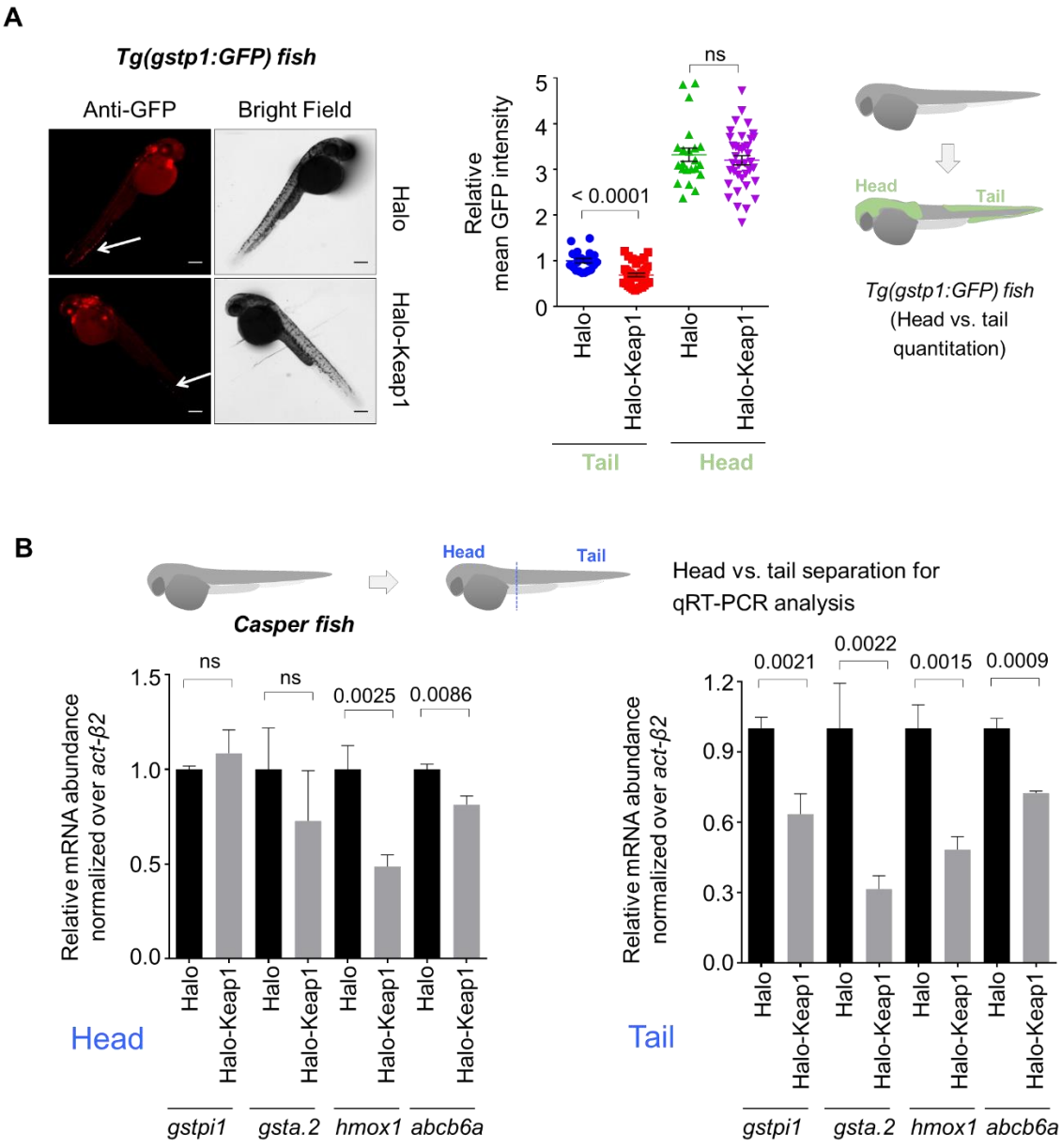

Figure 5.1 Halo-Keap1 (human) (Halo-Keap1 from hereon) is functional in zebrafish. (**A**) Ectopic expression of Halo-Keap1donwregulates AR in *Tg(gstp1:GFP)* fish compared to Halo overexpression. Interestingly, the AR downregulation is primarily observed in the tail with the head being unresponsive to Halo-Keap1 overexpression (B) the results from *Tg(gstp1:GFP)* fish are validated using qRT-PCR. The head and tail of fish larvae were separated, total RNA was isolated separately, and the transcript levels of each antioxidant response element (ARE)-regulated genes were analyzed.

Both Nrf2a and Nrf2b paralogs regulate basal AR

To further investigate the tissue-specific AR response, we examined zebrafish where either of the two ZfNrf2 paralogs was knocked-down using morpholinos (MOs). The morphants showed similar AR downregulation selectively in the tail (**Figure 5.2A–B**). Additionally, overexpression of Halo-Keap1 in the Nrf2 morphants did not show further suppression of AR, demonstrating that Keap1 and Nrf2 reside on the same signaling axis (**Figure 5.2C**). These data collectively demonstrated that AR is less responsive to changes in the head than in the tail of zebrafish embryos. The data from Nrf2 morphants also justified use of the reporter fish in studying AR signaling. We, therefore, proceeded to investigate the effect of Keap1-specific redox signaling in zebrafish.

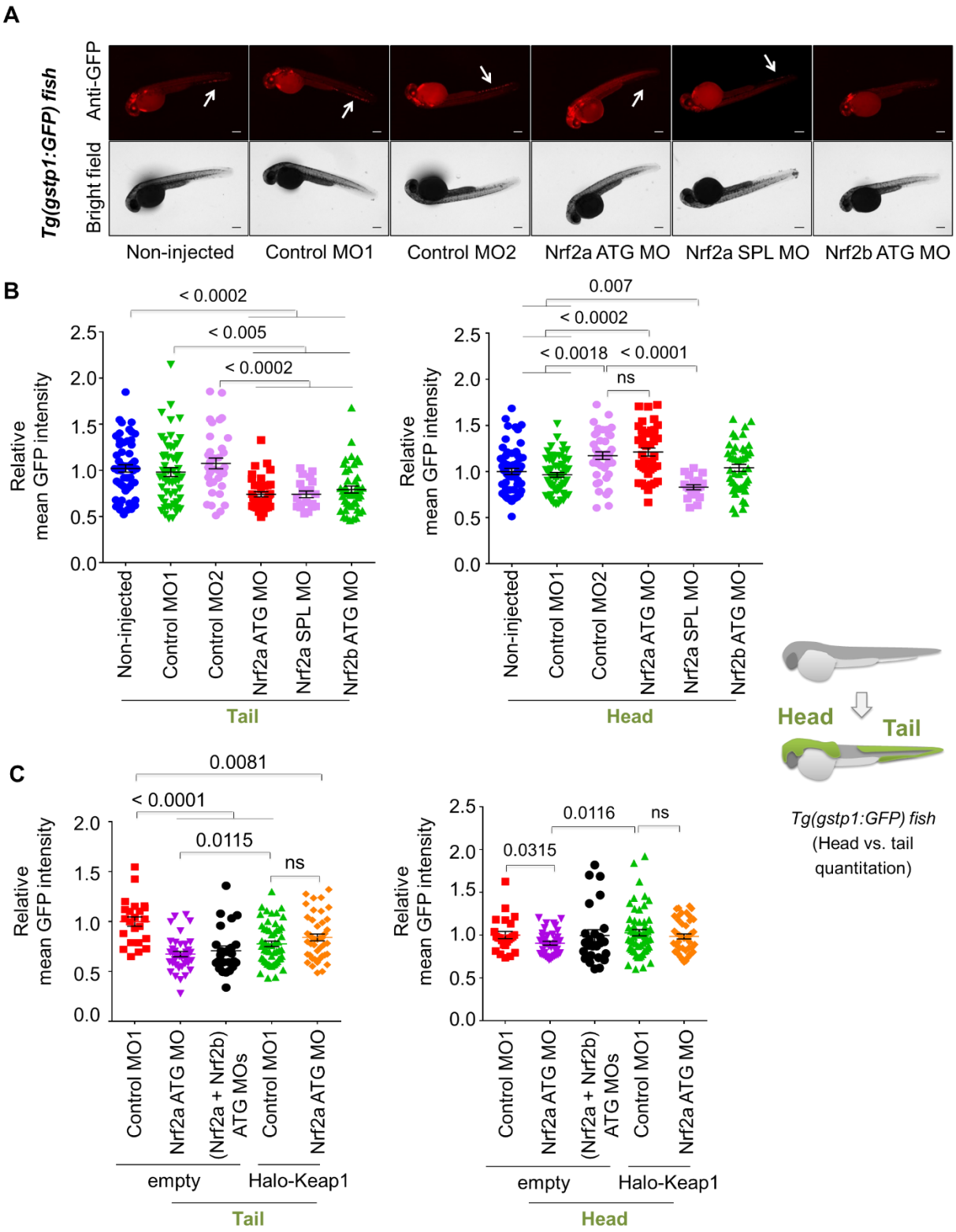
A
Tg(gstp1:GFP) fish
Anti-GFP
Bright field
Non-injected
Control MO1
Control MO2
Nrf2a ATG MO
Nrf2a SPL MO
Nrf2b ATG MO
B
Relative mean GFP intensity
< 0.0002
< 0.005
< 0.0002
0.007
< 0.0002
< 0.0018
< 0.0001
ns
Tail
Head
Head
Tail
Tg(gstp1:GFP) fish
(Head vs. tail quantitation)
C
0.0081
< 0.0001
0.0115
ns
0.0315
0.0116
ns
empty
Halo-Keap1
(Nrf2a + Nrf2b) ATG MOs

Figure 5.2 (**A**) Representative images of *Tg(gstp1:GFP)* fish injected with various Nrf2 morpholinos (MOs). Injection of either Nrf2a or Nrf2b MOs resulted in suppression of AR response. ATG MOs target the region flanking the start codon. Splice (SPL) MOs target intron-exon junctions resulting in improper splicing and consequent translation of a defunct protein. (**B**) Quantitation of data in (**A**) showing significant AR suppression in the tails of Nrf2a/b injected *Tg(gstp1:GFP)* fish. Consistent with the data in **Figure 5.1**, AR in the head of the fish is not responsive to Nrf2a/b knock down. (**C**) Consistent with previous reports[13,14], Halo-Keap1 overexpression in Nrf2a MO injected fish show epistasis demonstrating that both the regulators act on the same signaling axis.

Selective modification of Keap1 using Z-REX upregulates AR

Heterozygous reporter fish embryos were generated by crossing homozygous reporter *Tg(gstp1:GFP)* fish with wild-type. The embryos were injected with Halo-Keap1 mRNA and treated with 6 μM Ht-PreHNE immediately following injection. Z-REX was performed as specified in Chapter 2. We found that Z-REX-targeted Keap1-HNEylation resulted in ~1.5-fold AR-upregulation (tail-specific) at 34 hpf, following light-exposure at 30 hpf (**Figure 5.3A**). Whole-fish treatment with HNE (25 μM) at the same 30 hpf, followed by 4 h incubation, elicited similar AR-fold-upregulation also selectively in the tail (**Figure 5.3A**).

We next validated AR upregulation in fish after Z-REX or bolus dosing using qRT-PCR method to measure the upregulation of endogenous AR-driven genes (**Figure 5.3B**). Three representative genes associated with drug metabolism under control of Nrf2 [GST isoforms, HMOX1 and ABCB6 [15]] were activated to similar levels between Z-REX and bulk HNE-treatment, and AR modulation was most prominent in the tail (**Figure 5.3B**) although both Z-REX and bolus dosing with HNE mounted a weak but measurable AR in the head.

A

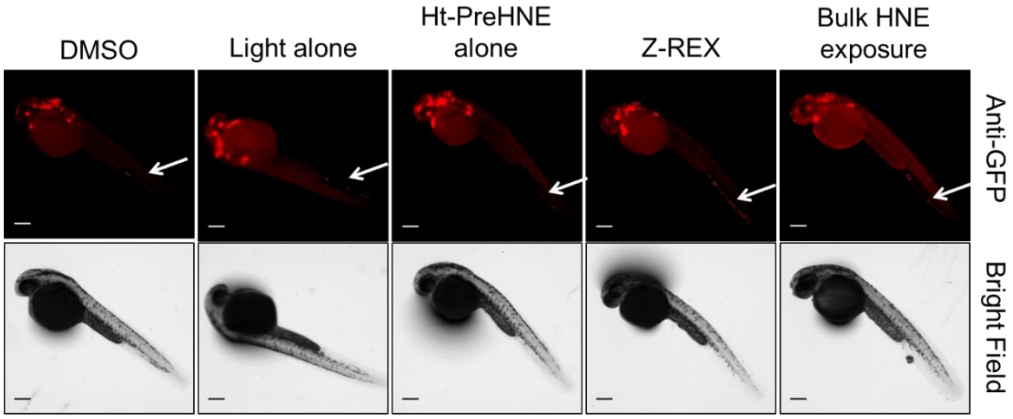
DMSO
Light alone
Ht-PreHNE alone
Z-REX
Bulk HNE exposure
Anti-GFP
Bright Field

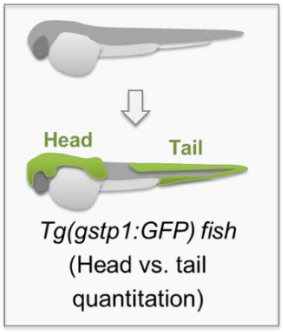
Head
Tail
Tg(gstp1:GFP) fish
(Head vs. tail quantitation)

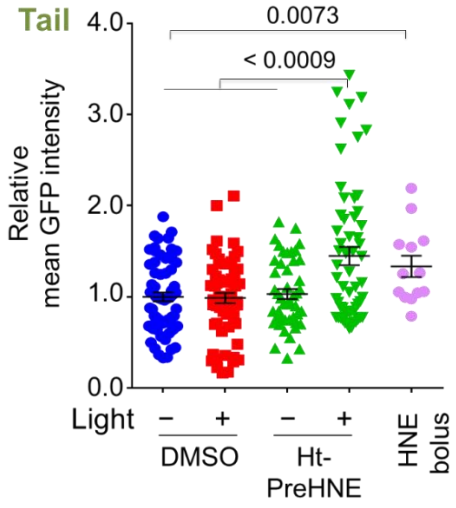
Tail
0.0073
< 0.0009
Relative mean GFP intensity
4.0
3.0
2.0
1.0
0.0
Light
DMSO
Ht-PreHNE
HNE bolus

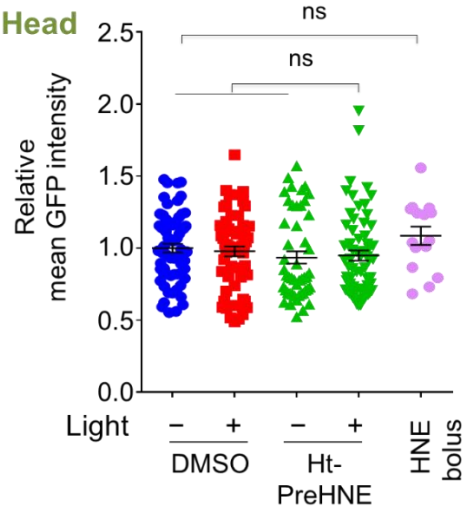
Head
ns
ns
Relative mean GFP intensity
2.5
2.0
1.5
1.0
0.5
0.0
Light
DMSO
Ht-PreHNE
HNE bolus

B

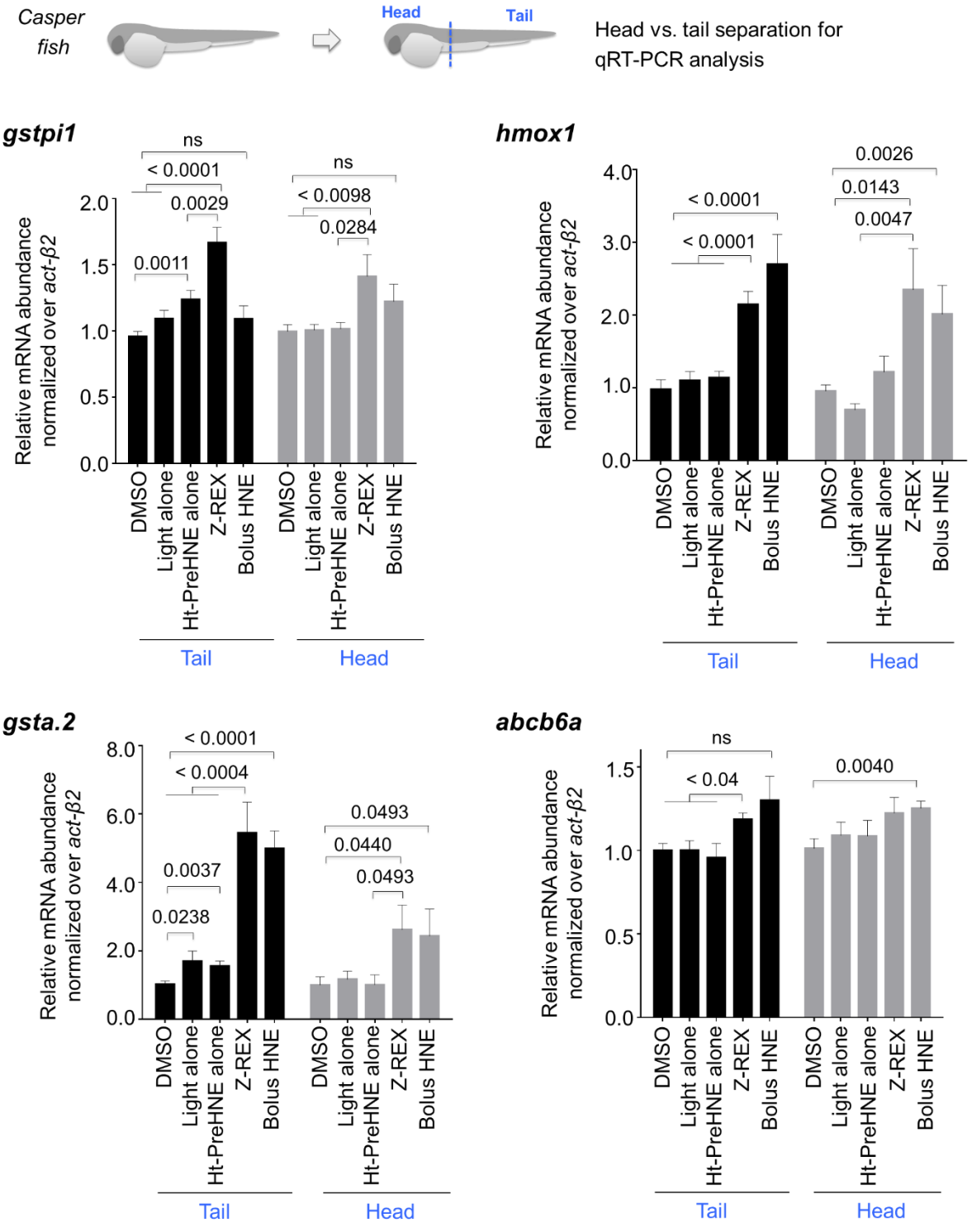
Casper fish
Head
Tail
Head vs. tail separation for qRT-PCR analysis
gstpi1
Relative mRNA abundance normalized over act-β2
ns
< 0.0001
0.0029
0.0011
ns
< 0.0098
0.0284
DMSO
Light alone
Ht-PreHNE alone
Z-REX
Bolus HNE
Tail
Head
hmox1
0.0026
0.0143
0.0047
< 0.0001
< 0.0001
gsta.2
< 0.0001
< 0.0004
0.0037
0.0238
0.0493
0.0440
0.0493
abcb6a
ns
< 0.04
0.0040

Figure 5.3 (**A**) *Top:* Representative images of *Tg(gstp1:GFP)* fish showing AR upregulation selectively in the tail after Z-REX. No significant upregulation was observed in fish under various Z-REX control conditions. Bolus treatment with 25 μM HNE for 2 h also induces AR upregulation in the reporter fish. *Bottom:* Quantitation of data showing significant AR upregulation in the tails of *Tg(gstp1:GFP)* fish after Z-REX. Consistent with the data in **Figure 5.1** and **Figure 5.2**, AR in the head of the fish is not responsive to Z-REX-mediated upregulation (**B**) Independent validation using qRT-PCR of Z-REX-mediated AR upregulation in the tails of zebrafish. Casper zebrafish were injected with Halo-Keap1. 2 h post Z-REX, the head and tail of the embryos were split, RNA isolated separated, and the transcript levels quantified.

Z-REX upregulates AR through quasi-intramolecular HNEylation of Keap1

To ensure that AR upregulation is a consequence of Keap1-specific HNEylation, we compared the extent of AR upregulation observed after Z-REX in fish injected with either Halo-Keap1 or Halo-P2A-Keap1 mRNA (**See Chapter 2**). As demonstrated in Chapter 2, fusion of Halo and Keap1 proteins is required for delivery of HNE to Keap1. Here, we validated that the Keap1-selective HNEylation is required for downstream AR upregulation as well. No significant AR upregulation was observed in the tails of *Tg(gstp1:GFP)* fish expressing Halo-P2A-Keap1 (**Figure 5.4A**). In contrast, Halo-Keap1 mRNA injected fish showed significant AR upregulation. Importantly, both Halo-Keap1 and Halo-P2A-Keap1 injected fish showed similar AR upregulation when treated with Tecfidera, an electrophilic AR inducer and an FDA-approved drug for the treatment of relapsing remitting multiple sclerosis. The data from transgenic fish was also corroborated by qRT-PCR results where significant attenuation in AR-regulated genes was observed in Halo-P2A-Keap1 expressing fish after Z-REX. (**Figure 5.4B**).

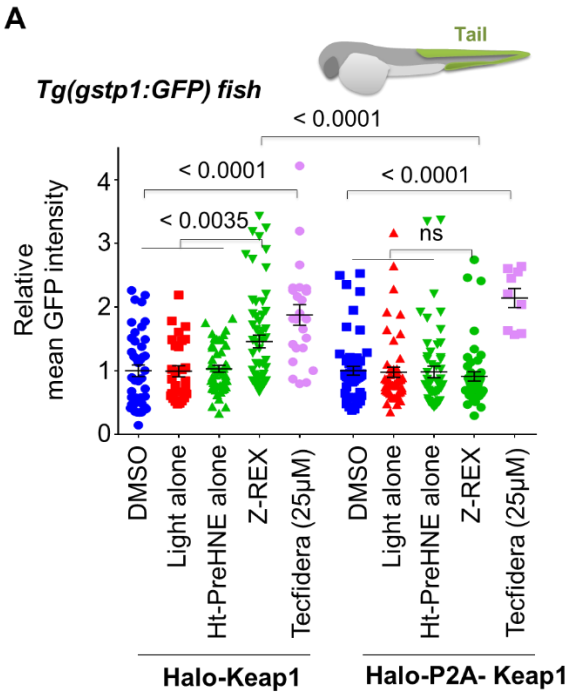
A
Tail
Tg(gstp1:GFP) fish
< 0.0001
< 0.0001
< 0.0001
< 0.0035
ns
Relative mean GFP intensity
0
1
2
3
4
DMSO
Light alone
Ht-PreHNE alone
Z-REX
Tecfidera (25μM)
DMSO
Light alone
Ht-PreHNE alone
Z-REX
Tecfidera (25μM)
Halo-Keap1
Halo-P2A- Keap1

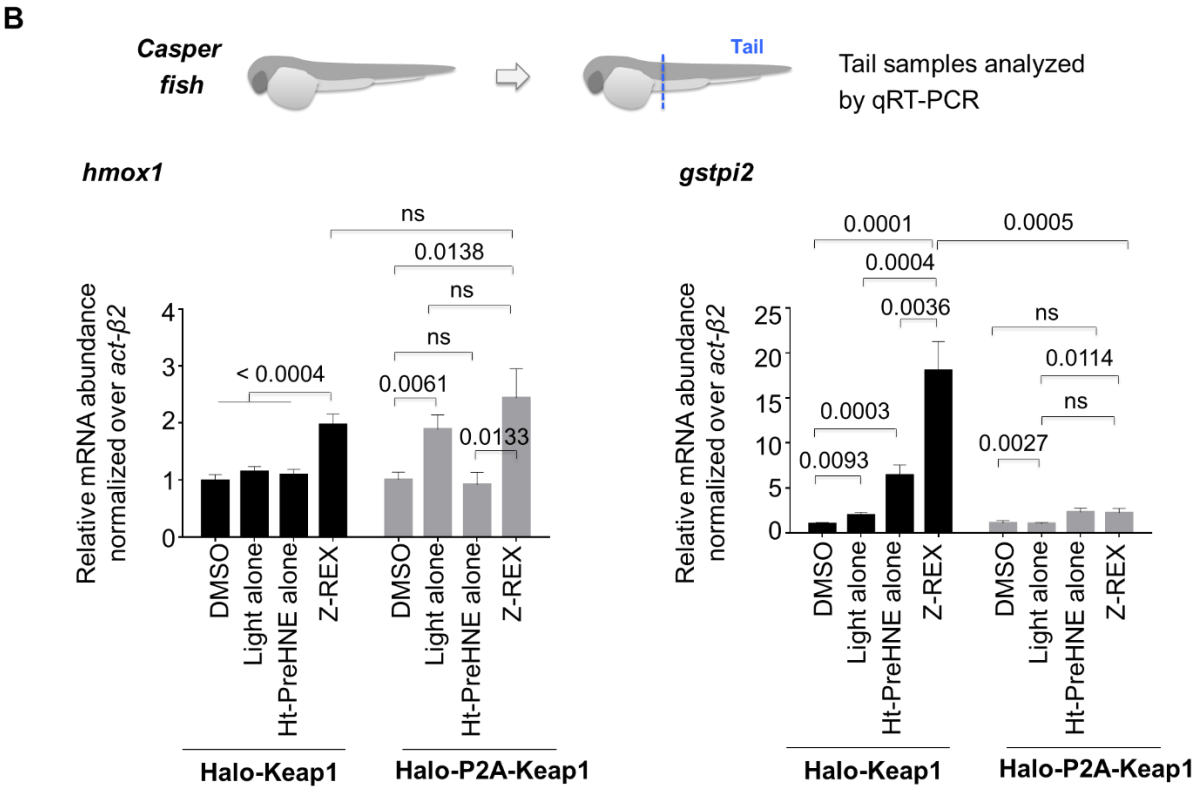
B
Casper fish
Tail
Tail samples analyzed by qRT-PCR
hmox1
Relative mRNA abundance normalized over act-β2
ns
0.0138
ns
ns
< 0.0004
0.0061
0.0133
0
1
2
3
4
DMSO
Light alone
Ht-PreHNE alone
Z-REX
DMSO
Light alone
Ht-PreHNE alone
Z-REX
Halo-Keap1
Halo-P2A-Keap1
gstpi2
Relative mRNA abundance normalized over act-β2
0.0001
0.0005
0.0004
0.0036
ns
0.0114
ns
0.0003
0.0093
0.0027
0
5
10
15
20
25
DMSO
Light alone
Ht-PreHNE alone
Z-REX
DMSO
Light alone
Ht-PreHNE alone
Z-REX
Halo-Keap1
Halo-P2A-Keap1

Figure 5.4 (**A**) Quantitation of the tails of *Tg(gstp1:GFP)* fish shows significant AR upregulation after Z-REX in fish injected with Halo-Keap1. No AR upregulation was observed in fish injected with Halo-P2A-Keap1 mRNA instead. The P2A self-cleaving peptide results in a 1:1 expression of "split" Halo and Keap1 proteins. (**B**) Validation of the results in (**A**) using qRT-PCR. Casper zebrafish were injected with either Halo-Keap1 or Halo-P2A-Keap1 mRNA. 2 h post Z-REX, the head and tail of the embryos were split, RNA isolated separated, and the transcript levels quantified of two ARE-regulated genes. Collectively, the data demonstrate that fusion of Halo and Keap1 is required for HNEylation of Keap1 (Chapter 2) and consequent AR upregulation.

Structurally-homologous LDEs show similar AR upregulation post Z-REX

We were curious to understand how Keap1 labeling contributed to overall AR for other structurally-homologous native LDEs bearing linear alkyl chains (**Figure 5.5A**). Recently, we had reported the development of an electrophile toolbox comprising of various LDEs and their photocaged precursors [16,17]. All these compounds were shown to modify Keap1 in cells resulting in AR upregulation. Of these compounds, 4-hydroxy-dodecenal (HDE [identified in human urine[18] and heated oils[19]], 4-dehydroxy-nonenal (dHNE, also decenal) [another endogenously-generated LDE with age-dependent rise in production[20]], and decenone (DE) [an FDA-approved food additive with natural occurrence in certain fruits and mushrooms[21]] were chosen as representatives to test their effect on AR upregulation *in vivo*. Using *Tg(gstp1:GFP)* fish, we found that all linear LDEs elicited similar AR-upregulation in fish tail upon Z-REX (**Figure 5.5B**). qRT-PCR analysis of endogenous AR-driven genes following Z-REX with the linear LDEs similarly showed that targeted Keap1 modification by HNE and analogous LDEs in fish gave broadly similar upregulation of these genes (**Figure 5.5C**).

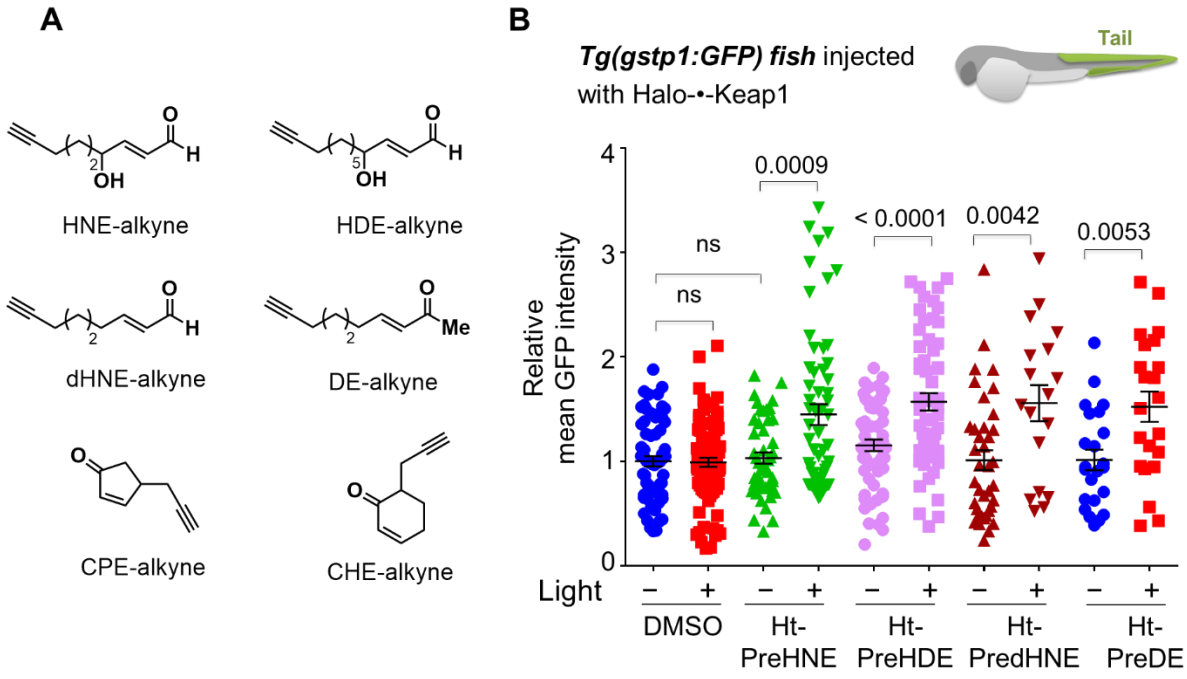
A
HNE-alkyne
HDE-alkyne
dHNE-alkyne
DE-alkyne
CPE-alkyne
CHE-alkyne
B
Tg(gstp1:GFP) fish injected with Halo-•-Keap1
Tail
Relative mean GFP intensity
0.0009
ns
ns
< 0.0001
0.0042
0.0053
Light
DMSO
Ht-PreHNE
Ht-PreHDE
Ht-PredHNE
Ht-PreDE

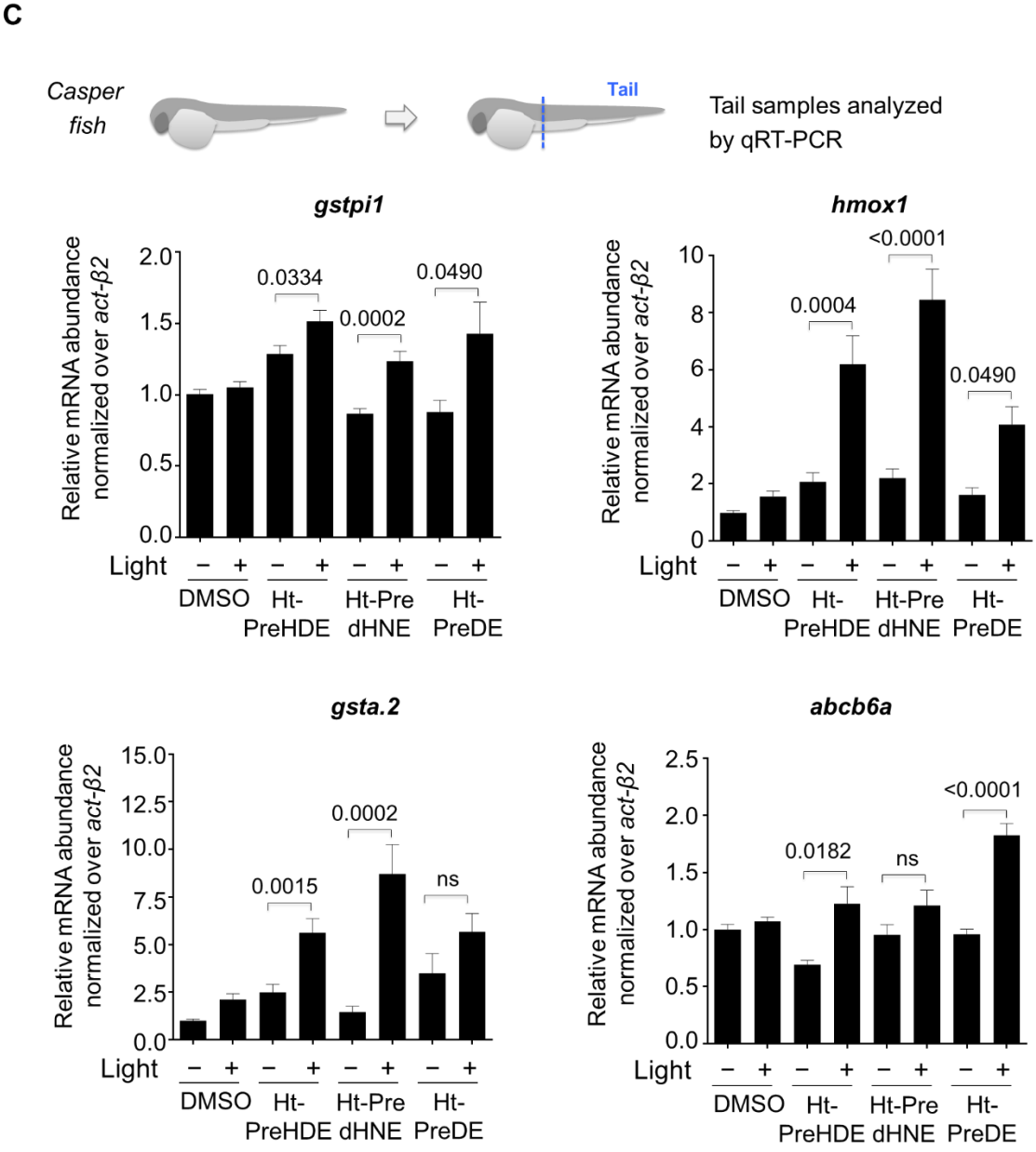

Figure 5.5 (**A**) Structures of LDEs used in the study. Synthesis of the alkyne-functionalized LDEs and their photocaged precursor has been reported[22]. The linear LDEs are generated in biological systems. The cyclic LDEs CHE-alkyne and CPE-alkyne are the reactive moieties of bioactive electrophiles such as Bardoxolone methyl and 15d-PGJ_2, respectively (**B**) Three linear LDEs yield similar AR fold upregulation (in tails) upon selective modification of Keap1 in *Tg(gstp1:GFP)* zebrafish embryos. (**C**) Validation of the results in (**B**) using qRT-PCR. Consistent with the results in (**B**), upregulation of ARE-driven genes post Z-REX is similar across LDEs of varying chain-length and reactivity.

We also looked at two cyclic-enone-based non-native RES, cyclopentenone (CPE) and cyclohexenone (CHE) (**Figure 5.4A**). Both the electrophiles have previously been shown to modify Keap1 in mammalian cells resulting in upregulation of AR. The fold AR activation was found to be similar to those observed upon Keap1 HNEylation[22]. Interestingly, in fish, photocaged-CPE/CHE-probe-alone controls themselves resulted in AR-upregulation (**Figure 5.6**) precluding further assessment of downstream signaling response. We hypothesize that cyclic ether-bearing components of Ht-PreCPE and Ht-PreCHE interfere with other signaling pathway(s) that crosstalk with AR in the complex arena of the developing fish.

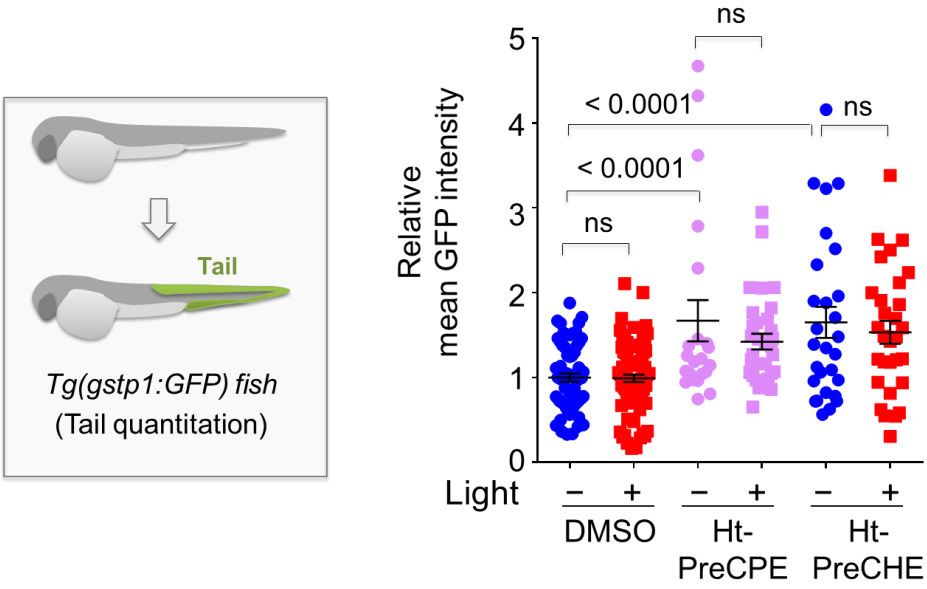

Figure 5.6 The photocaged precursors of CPE and CHE, Ht-PreCPE and Ht-PreCHE respectively, result in upregulation of AR in the tails of *Tg(gstp1:GFP)* zebrafish embryos (even without light illumination).

We thus focused on the native linear chain LDEs and evaluated the extent of Keap1-specific modification under Z-REX in each case. Using Click-biotin-pulldown following Z-REX *in vivo*, HDE and dHNE labeled Keap1 to the extent similar to that achieved with HNE (**Figure 5.7A**, data collected by Dr. Marcus Long). These findings explain the similar magnitude of AR-outputs observed with Z-REX. Importantly, using Ht-PredHNE as an example, we showed that Halo-P2A-Keap1 was hypomorphic for Z-REX-mediated AR (**Figure 5.7B**). This observation provided compelling evidence that Z-REX supports output specifically stemming from on-target LDE-modifications.

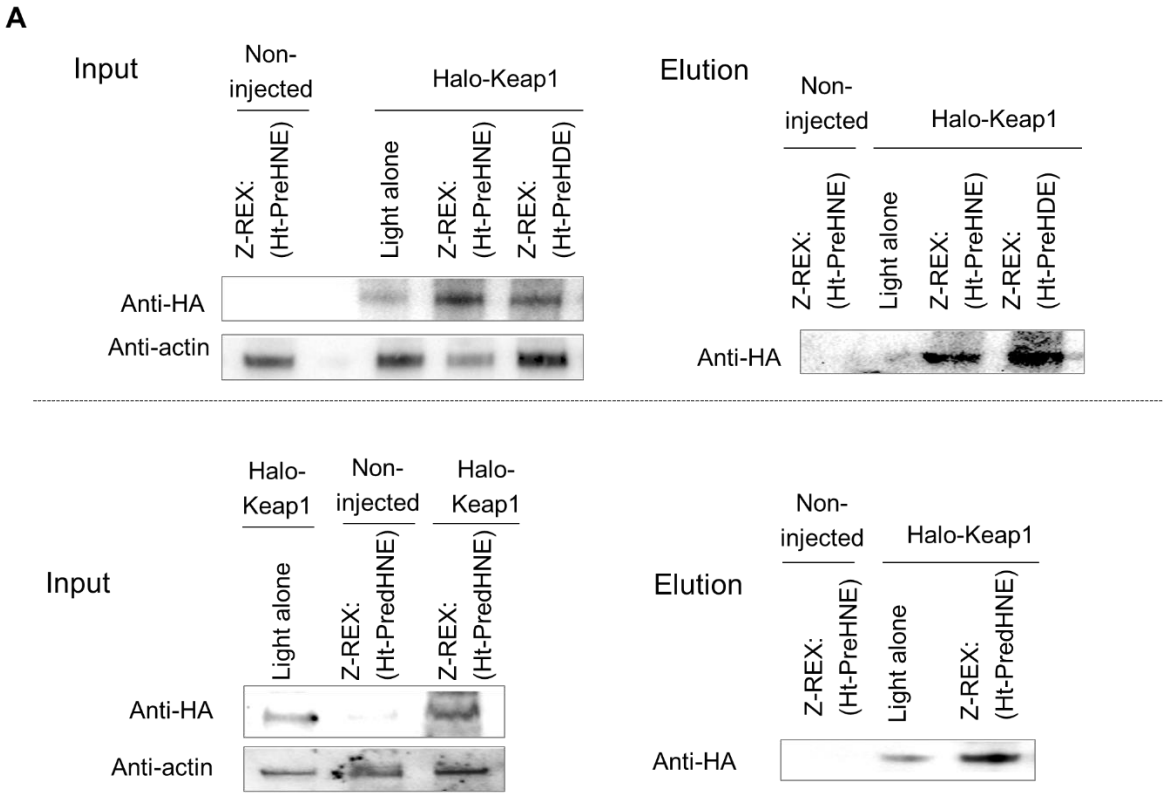

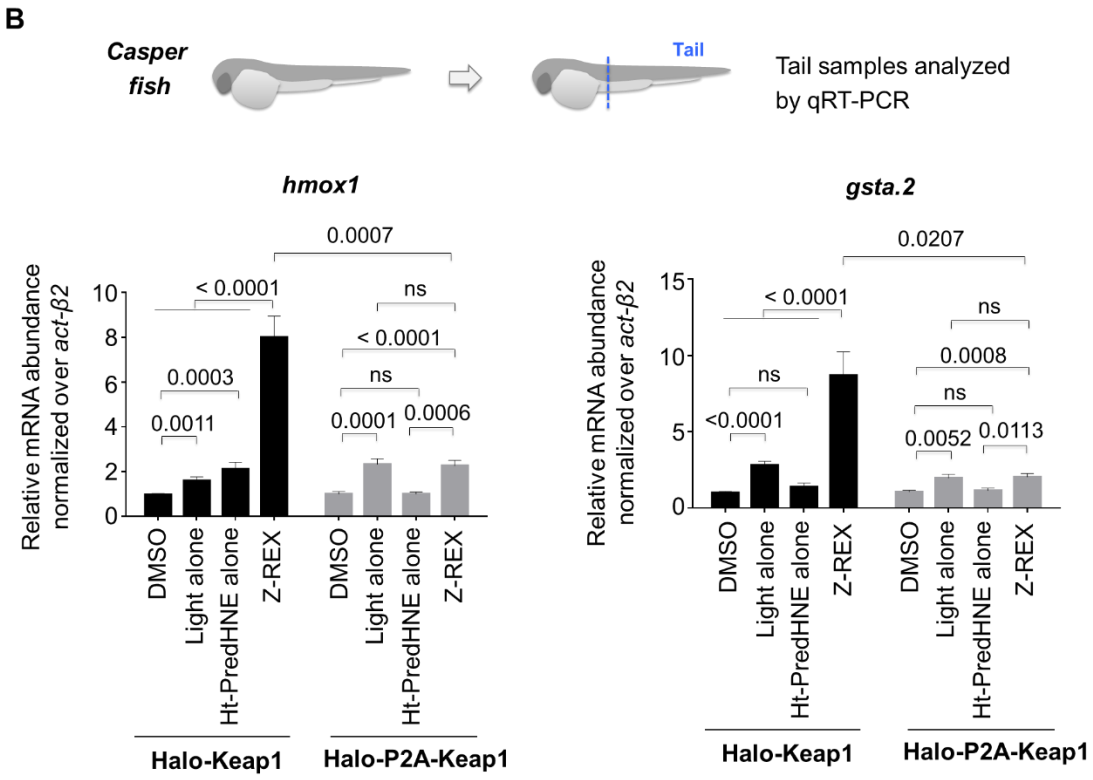

Figure 5.7 (**A**) LDEs structurally-homologous to HNE show similar extent of labeling on Keap1 explaining the overall similar fold activation observed in *Tg(gstp1:GFP)* fish after Z-REX. LDE(alkyne functionalized)-modified Keap1was pulled-down following Z-REX using biotin-azide click and subsequent streptavidin beads enrichment. (**B**) Consistent with data in **Figure 5.4B**, quasi-intramolecular delivery of LDEs is required for upregulation of ARE-regulated endogenous genes.

Bolus dosing with various electrophiles upregulates AR selectively in the tail

We next compared the extent of AR upregulation observed after Z-REX to that obtained using bolus dosing with various electrophiles. *Tg(gstp1:GFP)* fish were treated with 25 μM of the compounds and AR upregulation was measured. The data demonstrated that all electrophiles showed AR upregulation albeit different fold upregulations were observed upon bolus dosing with the electrophiles (**Figure 5.8**).

Interestingly, linear α,β-unsaturated aldehydes gave higher fold AR upregulation compared to enone-based electrophiles. Sulforaphane, an electrophilic compound found in cruciferous vegetables, showed no measurable AR upregulation. We propose that the different levels of AR upregulation observed upon bolus dosing with electrophiles are due to multifactorial effects such as differential pharmacokinetics (uptake, metabolism, excretion etc), different reactivities, and different on- and off-target spectrum of the electrophiles. Nonetheless, except sulforaphane all the electrophiles showed selective AR upregulation in the tail. No significant AR change was detected in the heads of *Tg(gstp1:GFP)* fish.

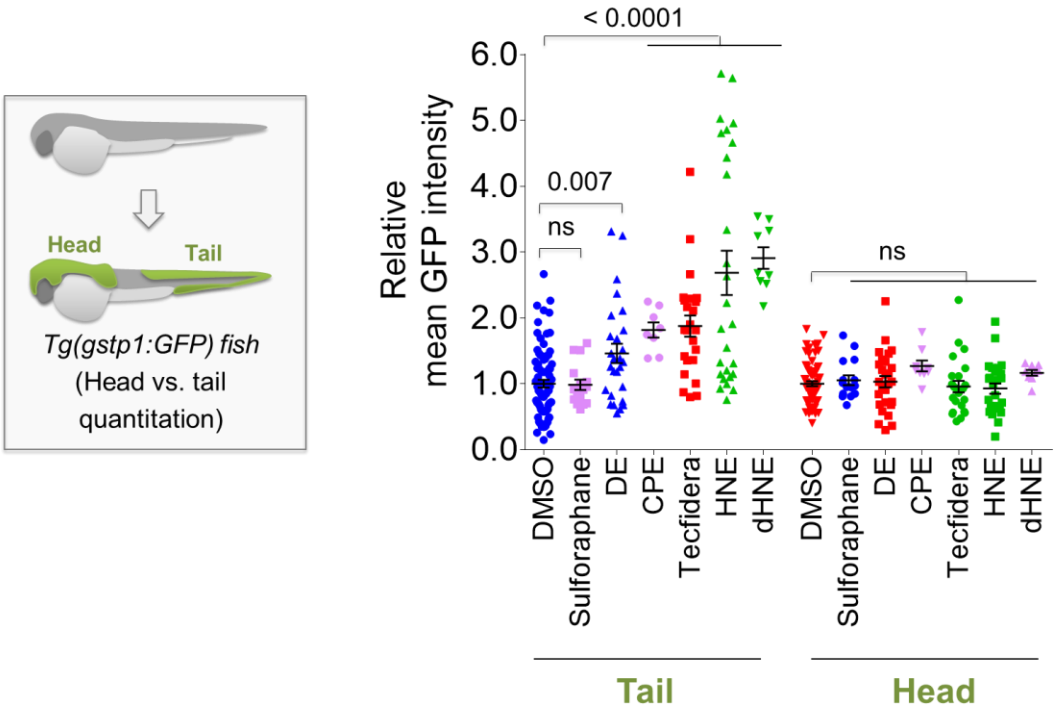

Figure 5.8 Bolus dosing with various electrophiles results in electrophile-specific AR response in the tails of *Tg(gstp1:GFP)* fish. Reactive aldehydes seem to show higher upregulation of AR compared to enone-based electrophiles. Sulforaphane was unable to upregulate AR. Nonetheless, AR activation was only observed in the tails of *Tg(gstp1:GFP)* fish.

Distinct ZfNrf2 and ZfKeap1 expression levels in tail vs head

Next, we sought to understand the reason behind tail-selective AR upregulation upon Z-REX and bolus dosing. Different electrophiles have been shown to require distinct Keap1 paralogs to elicit AR upregulation[8,11]. We were curious whether the locale-specific AR upregulation was due to differential expression and localization of Keap1 and Nrf2 paralogs. We used qRT-PCR to compare the levels of endogenous paralogs of Keap1 and Nrf2. Interestingly, qRT-PCR data showed distinct expression of the two paralogs of Keap1 and Nrf2 in the head *vs* the tail of zebrafish. Keap1b, a negative regulator of the AR pathway, was found to have lower expression levels in the tail relative to the head (**Figure 5.9A**). On the other hand, the levels of Nrf2 (both ZfNrf2a and ZfNrf2b), positive regulators of the AR response, were significantly higher in the tail than in the head (**Figure 5.9B**). This data may explain why the tail is more responsive to electrophile treatment compared to the head.

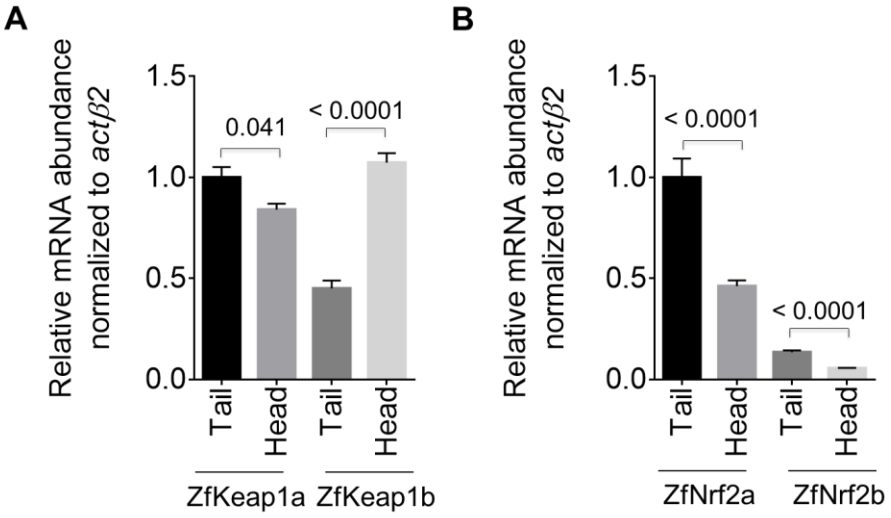

Figure 5.9 Paralogs of ZfKeap1 (**A**) and ZfNrf2 (**B**) have differential expression in the tail and the head. Transcripts levels of Keap1b, a negative regulator of the AR pathway

is more abundant in the head whereas the transcript levels of ZfNrf2a and ZfNrf2b, positive regulator of the pathway, are higher in the tail of zebrafish embryos at 34–36 hpf.

Keap1a and Keap1b have distinct AR-regulatory roles

We sought to validate these finding by selective knock-down of the ZfKeap1 and ZfNrf2 paralogs. As expected ZfNrf2a and ZfNrf2b morphants had reduced basal AR upregulation compared to control MO injected fish. This effect was more pronounced in the tail than the head. ZfKeap1a and ZfKeap1b morphants did not show a significant basal change in AR (**Figure 5.10A**). Next, we treated *Tg(gstp1:GFP)* fish injected with ZfKeap1/ZfNrf2-paralog-specific morpholinos with dHNE and measured the level of electrophile-induced AR upregulation. Interestingly, we observed different fold activation in the morphants compared to the fish injected with control morpholinos (**Figure 5.10B**). ZfNrf2a morphants had significantly attenuated fold AR upregulation suggesting that ZfNrf2a is the primary transcription factor responsible for electrophile-induced AR upregulation. ZfNrf2b morphants, however, showed increased AR upregulation compared to control MO injected fish. This may suggest that under electrophile-stimulated condition ZfNrf2b may act as a suppressor for AR signaling. This is interesting given that both ZfNrf2a and ZfNrf2b are activators of AR signaling pathway under non-induced condition. Interestingly, one study had previously proposed the negative regulatory role of ZfNrf2b under electrophile-stimulated conditions[9]. We also identified differential regulation of electrophile-induced AR by ZfKeap1 paralogs. ZfKeap1b knockdown showed reduced AR fold upregulation relative to control MO injected fish. ZfKeap1a morphants, however, showed increased AR fold upregulation

suggesting that ZfKeap1a is a suppressor of electrophile-induced AR. Like ZfNrf2 paralogs, both ZfKeap1 and ZfKeap1b are negative regulators of the AR pathways under non-stimulated conditions. These data collectively suggest that electrophile-modified zebrafish Nrf2 and Keap1 proteins behave differently than unmodified ones, and further highlighting that electrophile-modified proteins act as new signaling variants of their unmodified counterparts.

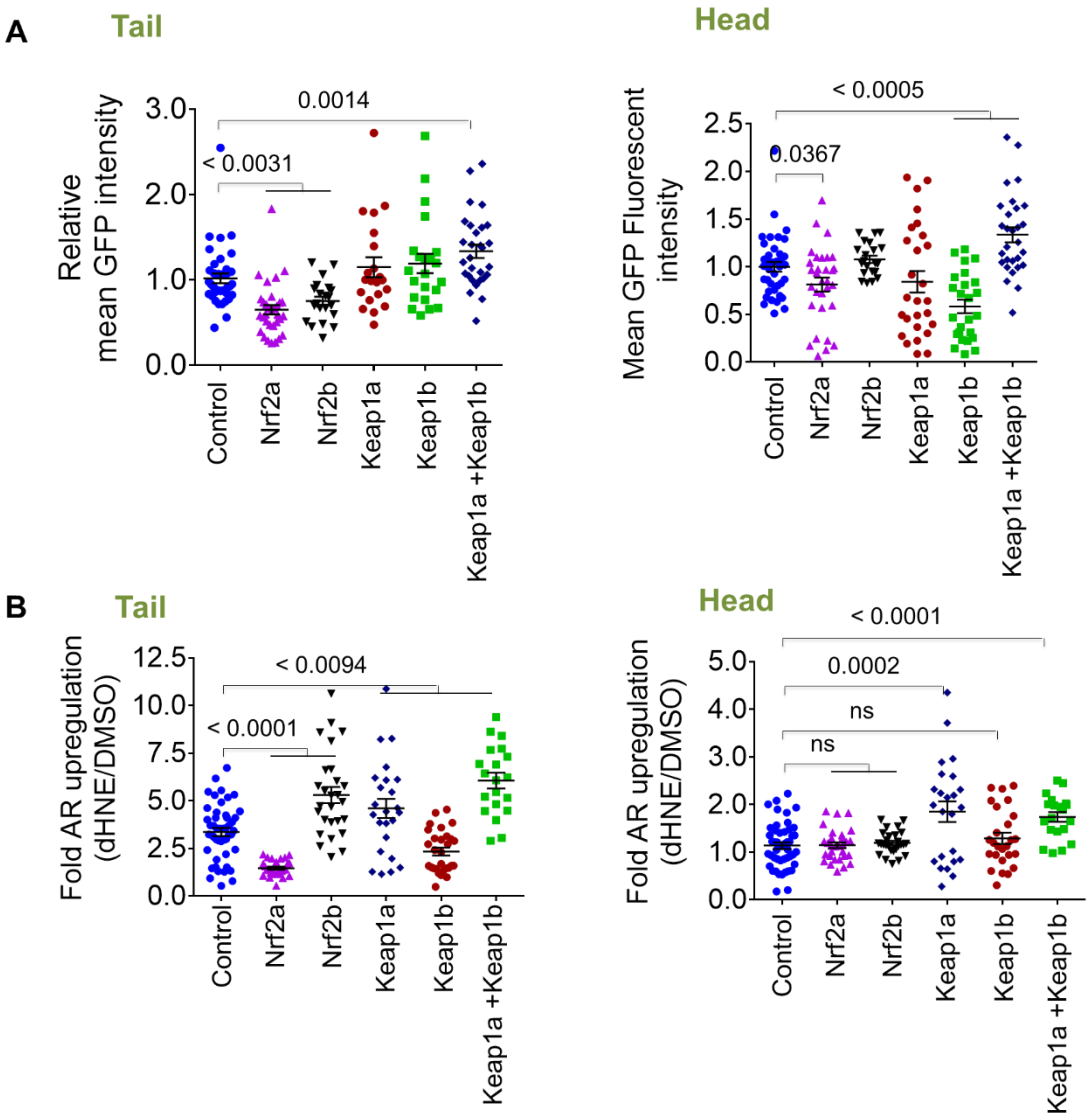

Figure 5.10 *Tg(gstp1:GFP)* fish were injected with the indicated morpholinos (MOs) and either the basal (**A**) or dHNE-induced (**B**) AR upregulation was quantitated. (**A**) Consistent with ZfNrf2 being positive regulator of the AR pathway, ZfNrf2a/b morphants showed reduced basal AR in the tail. ZfKeap1 morphants, however, did not show a significant change in basal AR. Knock-down of both ZfKeap1a and ZfKeap1b showed increase basal AR suggesting both paralogs negatively regulate the AR pathway (**B**) Quantitating the relative fold change after electrophile treatment (dHNE/DMSO) revealed that different paralogs regulate AR differently. This regulation is also electrophile-induced.

Discussion

Genome duplication has been proposed to be an important factor in evolutionary success of organisms. The existence of two copies of the same gene allows one copy to gain additional functions by beneficial mutations while the other copy preserves the original function[7]. Additionally, the two copy of the genes may evolve complementary functions[7] in a process termed as 'subfunctionalization'. The duplicated genome in the teleost zebrafish provides a unique opportunity to understand functional partitioning between gene duplicates. In redox signaling, gene/genome duplication event may provide a unique prospect to identify and characterize redox-sensitive residues with functional importance in regulating biological processes. For example, in the case of Keap1, a promiscuous sensor of electrophiles and oxidants, interrogation into functional partitioning between the two zebrafish paralogs may help identify residues capable of sensing different electrophiles and oxidants. In our study, we have identified electrophile modification-specific signaling roles of the two ZfKeap1 paralogs. We identified ZfKeap1b as a sensor of electrophilic signals. Knockdown of ZfKeap1b attenuated AR fold upregulation compared to control morpholino injected fish suggesting that ZfKeap1b sensing function is required for AR pathway activation in

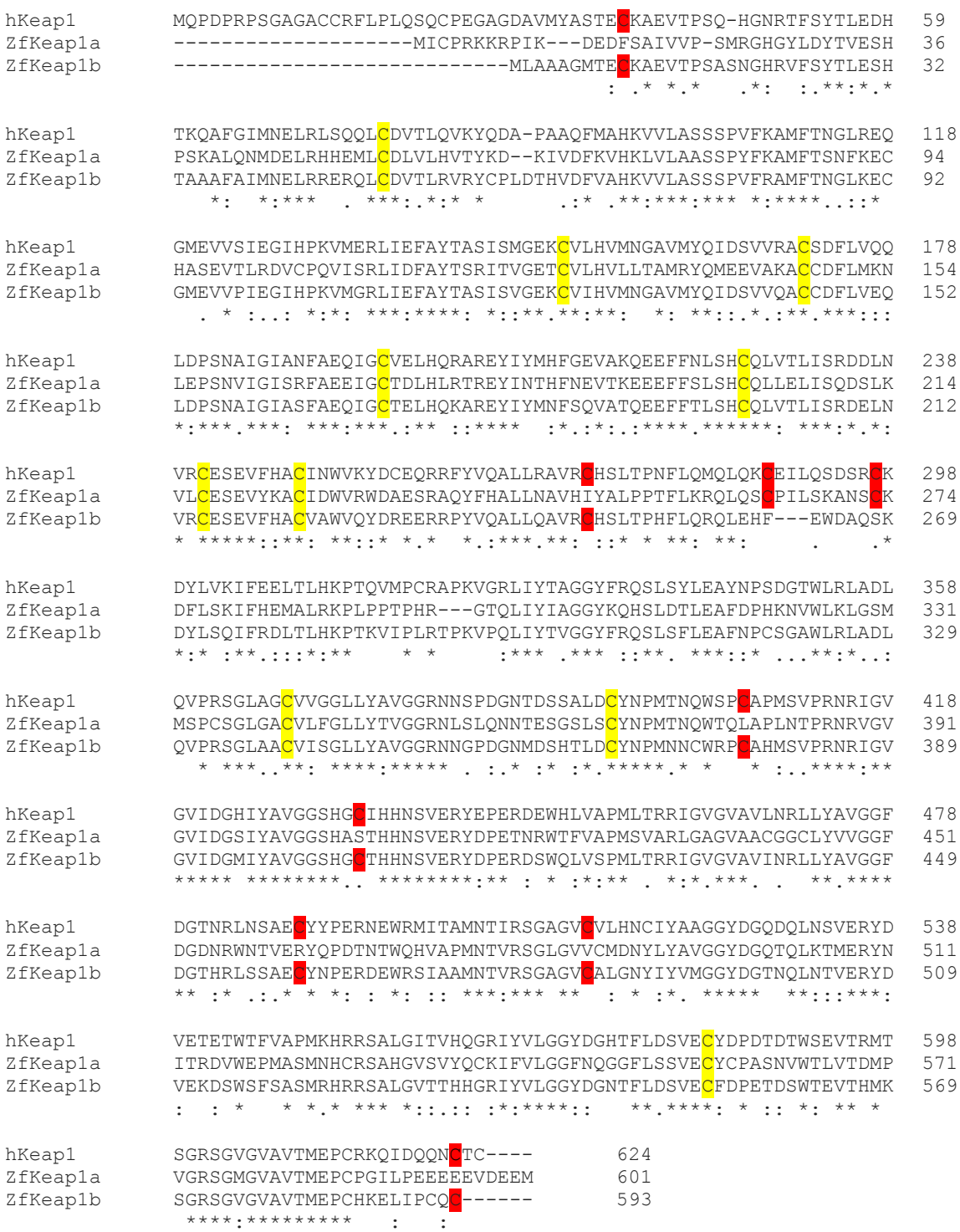

Figure 5.11 Amino acid sequence alignment of ZfKeap1a and ZfKeap1b paralogs to human Keap1 protein. Cysteine residues conserved across all three proteins are highlighted in yellow. Cysteine residues that are conserved between human Keap1 and

only one paralog of ZfKeap1 protein are highlighted in red. Sequence alignment was performed using Clustal Omega.

response to electrophile treatment. Interestingly, we also discovered an electrophile modification-dependent negative regulatory function of ZfKeap1a paralog. ZfKeap1a morphants showed enhanced fold upregulation compared to control MO injected fish upon electrophile treatment. The next step would be to identify the electrophile-sensing residues on ZfKeap1a and ZfKeap1b paralogs. Sequence alignment of ZfKeap1 paralogs to that of human Keap1 protein (**Figure 5.11**) shows that many of the proposed redox-sensitive cysteines in human Keap1 are partitioned between the two ZfKeap1 paralogs. An interesting hypothesis would be that the human Keap1 contains both the positive- and negative-regulatory cysteine such that AR activation is finely tuned in response to oxidative and electrophilic signals. Thus, the next step will be identifying these redox-sensing cysteines. A simple proposal would be to make the human Keap1 protein more like either ZfKeap1a or ZfKeap1b by mutating the residues unique to each of the two paralogs. This will allow identification of cysteines on Keap1 that enables the protein to either upregulate/downregulate AR in response to electrophilic signals.

Experimental Setup

Plasmids: Generation of Halo-Keap1 and Halo-P2A-Keap1 plasmids is described in Chapter 2. Fish injection and Z-REX protocols are also as described in Chapter 2.

Set up for IF and qRT-PCR in Tg(gstp1:GFP) and casper fish, respectively:

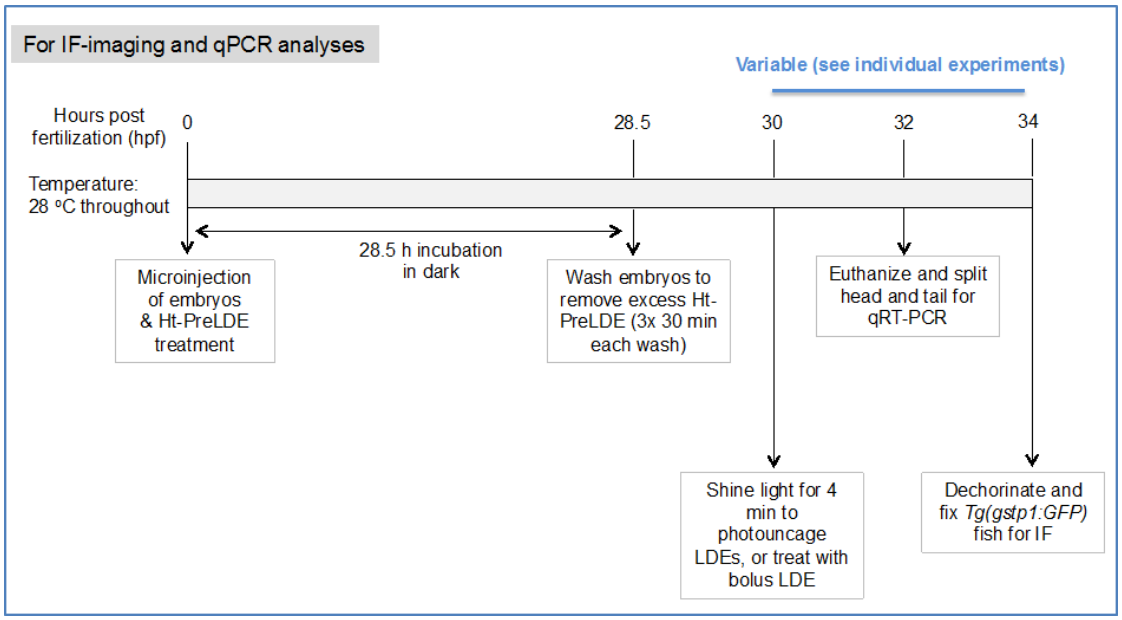

qRT-PCR: All qPCR experiments were performed in casper strain. 2 h post light illumination or bolus LDE treatment, 12–15 larvae per sample were euthanized by chilling, dechorionated, the head and tail separated using sharp forceps (11252-40 Dumont #5 Forceps - Biologie/Titanium), and transferred to separate Eppendorf tubes. The samples were washed twice with ice-cold PBS, and homogenized in 1 mL Trizol® (ThermoFisher Scientific, 15596018) together with vortexing with glass beads for 2 min. Total RNA was extracted per manufacturer's protocol. Glycoblue (ThermoFisher Scientific, AM9516) was used for visualization of the RNA pellet. Around 600 ng of total RNA was treated with AMP grade DnaseI (ThermoFisher Scientific, 18068015), reverse transcribed using Superscript III reverse transcriptase (ThermoFisher Scientific, 18080085) per manufacturer's instruction. qRT-PCR was performed for the indicated genes using primers specified in **Table 5.1**. All primers were validated as previously reported[23-25]. qRT-PCR analysis was performed with iQ™ SYBR® Green Supermix (Bio-Rad, 170-8880) on a Light Cycler 480 instrument (Roche). In a total volume of 10 µL the PCR reaction mix contained, in final concentrations, 1X iQ™ SYBR® Green Supermix, 0.30 µM each of the forward and reverse primers and 10–13 ng of template cDNA. The qPCR program was set for 3 min at 95 °C followed by 40-repeat cycles comprising heating at 95 °C for 10 s and at 55 °C for 10 s. The expected products were

of ~100–130 bp in size. The data was analyzed using $\Delta\Delta C_t$ method and presented relative to zebrafish actin, β2.

Table 5.1 Primers used for qRT-PCR

Gene-of-interest	**Fwd Primer sequence**	**Rev Primer sequence**
gstpi1	CTTCGCAGTCAAAGGCAGATG	CGCCCTTCATCCACTCTTCA
hmox1	ACAGAGACTGAGAGAGATTGGC	TCTATTGGCGCTCGTCACTC
gsta.2	AGAGCGAGCCATGATCGAC	ACTGTAGGTCTTTTCCTTGTTTTC
abcb6a	TACTGGGCAGTAGCTTTCGC	ACTCCATCTGTTGCTCGGAC
gstpi2	CGTGCTGGCCCTTTGAAGAT	GCTGTCCAAAGAGACATGTGG

Immunofluorescence: To assess AR upregulation in *Tg*(*gstp1*:*GFP)* fish, larvae 4 h post light illumination or bolus LDE treatment were dechorionated, washed twice in ice-cold PBS and fixed in 4% paraformaldehyde in 1X PBS for at least overnight with gentle rocking at 4 °C. Fixed larvae were permeabilized with chilled methanol at –20 °C for 4 h–overnight. Fish were then washed 2 times with PBS-0.1%Tween-1% DMSO for 30 min each with gentle rocking, then blocked in PBS-0.1%Tween containing 2% BSA and 10% FBS, then stained with anti-GFP FITC conjugated (Abcam, ab6662) primary antibody overnight at 4 °C in blocking buffer. Subsequently, the larvae were washed twice (30 min each wash), re-blocked for 1 h at room temperature, and incubated with the AlexaFluor 568-conjugated fluorescent secondary antibodies (Abcam, ab175707) in blocking buffer for 1.5 h at room temperature with gentle rocking, and then washed three times. Fish were imaged on 2% agarose plates on a Leica M205-FA equipped with a stereomicroscope. Quantitation of IF data was performed using ImageJ/FIJI (NIH).

Click chemistry and enrichment of modified proteins: Click chemistry and enrichment of modified proteins is explained in Chapter 2.

Data quantitation and analysis: Imaging data was quantitated using ImageJ (NIH). For assessing AR upregulation in *Tg*(*gstp1*:*GFP)* fish, the area around the head (excluding the eyes) or the tail (median fin fold) were selected using freeform selection tool. Corresponding illustrations are included in each sub-figure for clarity. The mean red fluorescence intensity of the selected region was measured and subtracted from the mean background fluorescence intensity (region with no fish). Any non-transgenic fish larvae were excluded from the quantitation.

References

(1) Driever, W.; Solnica-Krezel, L.; Schier, A. F.; Neuhauss, S. C.; Malicki, J.; Stemple, D. L.; Stainier, D. Y.; Zwartkruis, F.; Abdelilah, S.; Rangini, Z.et al. A genetic screen for mutations affecting embryogenesis in zebrafish. *Development* **1996,** *123* (1), 37.

(2) Howe, K.; Clark, M. D.; Torroja, C. F.; Torrance, J.; Berthelot, C.; Muffato, M.; Collins, J. E.; Humphray, S.; McLaren, K.; Matthews, L.et al. The zebrafish reference genome sequence and its relationship to the human genome. *Nature* **2013,** *496*, 498.

(3) Haffter, P.; Granato, M.; Brand, M.; Mullins, M. C.; Hammerschmidt, M.; Kane, D. A.; Odenthal, J.; van Eeden, F. J.; Jiang, Y. J.; Heisenberg, C. P.et al. The identification of genes with unique and essential functions in the development of the zebrafish, Danio rerio. *Development* **1996,** *123* (1), 1.

(4) Wang, D.; Jao, L.-E.; Zheng, N.; Dolan, K.; Ivey, J.; Zonies, S.; Wu, X.; Wu, K.; Yang, H.; Meng, Q.et al. Efficient genome-wide mutagenesis of zebrafish genes by retroviral insertions. *Proceedings of the National Academy of Sciences* **2007,** *104* (30), 12428.

(5) Talbot, W. S.; Hopkins, N. Zebrafish mutations and functional analysis of the vertebrate genome. *Genes & Development* **2000,** *14* (7), 755.

(6) MacRae, C. A.; Peterson, R. T. Zebrafish as tools for drug discovery. *Nature Reviews Drug Discovery* **2015,** *14*, 721.

(7) Postlethwait, J.; Amores, A.; Cresko, W.; Singer, A.; Yan, Y.-L. Subfunction partitioning, the teleost radiation and the annotation of the human genome. *Trends in Genetics 20* (10), 481.

(8) Li, L.; Kobayashi, M.; Kaneko, H.; Nakajima-Takagi, Y.; Nakayama, Y.; Yamamoto, M. Molecular Evolution of Keap1: two keap1 molecules with distinctive intervening region structures are conserved among fish. *Journal of Biological Chemistry* **2008,** *283* (6), 3248.

(9) Timme-Laragy, A. R.; Karchner, S. I.; Franks, D. G.; Jenny, M. J.; Harbeitner, R. C.; Goldstone, J. V.; McArthur, A. G.; Hahn, M. E. Nrf2b, Novel Zebrafish Paralog of Oxidant-responsive Transcription Factor NF-E2-related Factor 2 (NRF2). *The Journal of Biological Chemistry* **2012,** *287* (7), 4609.
(10) Suzuki, T.; Takagi, Y.; Osanai, H.; Li, L.; Takeuchi, M.; Katoh, Y.; Kobayashi, M.; Yamamoto, M. Pi class glutathione S-transferase genes are regulated by Nrf 2 through an evolutionarily conserved regulatory element in zebrafish. *Biochemical Journal* **2005,** *388* (Pt 1), 65.
(11) Kobayashi, M.; Li, L.; Iwamoto, N.; Nakajima-Takagi, Y.; Kaneko, H.; Nakayama, Y.; Eguchi, M.; Wada, Y.; Kumagai, Y.; Yamamoto, M. The Antioxidant Defense System Keap1-Nrf2 Comprises a Multiple Sensing Mechanism for Responding to a Wide Range of Chemical Compounds. *Molecular and Cellular Biology* **2009,** *29* (2), 493.
(12) Tsujita, T.; Li, L.; Nakajima, H.; Iwamoto, N.; Nakajima-Takagi, Y.; Ohashi, K.; Kawakami, K.; Kumagai, Y.; Freeman, B. A.; Yamamoto, M.et al. Nitro-fatty acids and cyclopentenone prostaglandins share strategies to activate the Keap1-Nrf2 system: a study using green fluorescent protein transgenic zebrafish. *Genes Cells* **2011,** *16* (1), 46.
(13) Kensler, T. W.; Wakabayashi, N. Nrf2: friend or foe for chemoprevention? *Carcinogenesis* **2010,** *31*.
(14) Hayes, J. D.; Dinkova-Kostova, A. T. The Nrf2 regulatory network provides an interface between redox and intermediary metabolism. *Trends in Biochemical Sciences 39* (4), 199.
(15) Hayes, J. D.; Dinkova-Kostova, A. T. The Nrf2 regulatory network provides an interface between redox and intermediary metabolism. *Trends in biochemical sciences* **2014,** *39* (4), 199.
(16) Parvez, S.; Fu, Y.; Li, J.; Long, M. J. C.; Lin, H.-Y.; Lee, D. K.; Hu, G. S.; Aye, Y. Substoichiometric Hydroxynonenylation of a Single Protein Recapitulates Whole-Cell-Stimulated Antioxidant Response. *J. Am. Chem. Soc.* **2015,** *137* (1), 10.
(17) Parvez, S.; Long, M. J.; Lin, H. Y.; Zhao, Y.; Haegele, J. A.; Pham, V. N.; Lee, D. K.; Aye, Y. T-REX on-demand redox targeting in live cells. *Nature protocols* **2016,** *11* (12), 2328.
(18) Florens, N.; Calzada, C.; Lyasko, E.; Juillard, L.; Soulage, C. O. Modified Lipids and Lipoproteins in Chronic Kidney Disease: A New Class of Uremic Toxins. *Toxins (Basel)* **2016,** *8* (12), 376.
(19) Seppanen, C. M.; Csallany, A. S. Incorporation of the toxic aldehyde 4-hydroxy-2-trans-nonenal into food fried in thermally oxidized soybean oil. *Journal of the American Oil Chemists' Society* **2004,** *81* (12), 1137.
(20) Haze, S.; Gozu, Y.; Nakamura, S.; Kohno, Y.; Sawano, K.; Ohta, H.; Yamazaki, K. 2-Nonenal newly found in human body odor tends to increase with aging. *J Invest Dermatol* **2001,** *116* (4), 520.
(21) Knowles, L. O.; Knowles, N. R. Toxicity and metabolism of exogenous alpha,beta-unsaturated carbonyls in potato (Solanum tuberosum L.) tubers. *J Agric Food Chem* **2012,** *60* (44), 11173.

(22) Lin, H.-Y.; Haegele, J. A.; Disare, M. T.; Lin, Q.; Aye, Y. A Generalizable Platform for Interrogating Target- and Signal-Specific Consequences of Electrophilic Modifications in Redox-Dependent Cell Signaling. *J. Am. Chem. Soc.* **2015,** *137* (19), 6232.
(23) Parvez, S.; Fu, Y.; Li, J.; Long, M. J.; Lin, H. Y.; Lee, D. K.; Hu, G. S.; Aye, Y. Substoichiometric hydroxynonenylation of a single protein recapitulates whole-cell-stimulated antioxidant response. *J Am Chem Soc* **2015,** *137* (1), 10.
(24) Long, M. J.; Lin, H. Y.; Parvez, S.; Zhao, Y.; Poganik, J. R.; Huang, P.; Aye, Y. beta-TrCP1 Is a Vacillatory Regulator of Wnt Signaling. *Cell Chem Biol* **2017,** *Epub ahead of print*.
(25) Long, M. J.; Parvez, S.; Zhao, Y.; Surya, S. S.; Wang, Y.; Zhang, S.; Aye, Y. Akt3 is a privileged first responder in isozyme-specific electrophile response. *Nature Chemical Biology* **2017,** *13*, 333.

CHAPTER 6

T-REX AS A DISCOVERY TOOL: IDENTIFYING NOVEL SIGNALING RESPONSES

Introduction

As discussed in earlier chapters, a key advantage of T-REX/Z-REX over bolus dosing method is that it significantly minimizes the off-target spectrum of any reactive electrophile/oxidant. During bolus dosing conditions, multiple redox-regulatory proteins in a given pathway are hit simultaneously. Thus, an observed downstream phenotype is most likely a result of activation/inactivation of multiple pathways at the same time. T-REX/Z-REX, on the other hand, enables selective modification of a target protein and thus is well-suited to evaluate the functional outcome of a single target modification. This ability of T-REX/Z-REX promises discovery of new signaling responses that would otherwise be hidden in the off-target spectrum of bolus dosing methods. We were curious to use this unique ability of T-REX/Z-REX to discover any novel signaling response mediated by Keap1-selective HNEylation. Having established T-REX as a versatile platform that is well-tolerated in zebrafish (Chapter 2) and that can be used to upregulate antioxidant response (AR) by selective modification of Keap1, we decided to investigate the possibility of identifying novel signaling responses in zebrafish.

---

* All fish experiments were performed in collaboration with Dr. Marcus Long. Fish injection with plasmids/mRNA, treatment with various compounds, and Z-REX were performed by Dr. Marcus Long. Unless otherwise specified, all downstream fish experiments were performed by Saba Parvez. Data collected by Dr. Marcus Long are specified throughout the text.

Results*

Z-REX identifies Keap1-HNEylation dependent downregulation of immune-responsive genes

To identify new signaling responses, we performed RNAseq subsequent to Z-REX-mediated HNEylation of Keap1. Total RNA from casper zebrafish was isolated 2 h after Z-REX. RNAseq was performed as specified in the methods section. Cuffdiff2 was used to perform pairwise comparison and analyze the differentially expressed (DE) transcripts in Z-REX samples compared to various controls. We also compared the DE genes in Z-REX to those treated with HNE using bolus dosing. A total of 32 genes were differentially upregulated in Z-REX samples compared to DMSO control samples (Appendix III). Additionally, a total of 14 genes were downregulated in Z-REX samples relative to DMSO. The small number of DE expressed genes precluded gene ontology analysis. However, a quick assessment of the differentially upregulated genes in Z-REX samples showed that they belonged to apoptosis signaling, lipid metabolism, and detoxification pathways (Appendix III). Surprisingly, we identified only a few canonical ARE-regulated genes that were differentially upregulated after Z-REX. As discussed in the earlier chapter, AR upregulation upon Z-REX is only observed in specific tissues especially in the tail (Chapter 5) of zebrafish embryos. These tissues contribute a very small portion towards the total RNA pool used for differential gene analysis. This may explain why few canonical ARE-regulated genes were differentially expressed in the Z-REX samples.

Interestingly, of the 14 differentially downregulated genes in Z-REX samples relative to DMSO, 3 genes (~20%) (Coronin1a (coro1a), lysozymeC (lyZ), and

macrophage expressed gene1.1 (mpeg1.1) were identified as important in innate immune response in zebrafish (**Figure 6.1**). Coro1a is an actin-binding protein that belongs to the CORONIN family and is highly enriched in leukocytes. Coro1a plays important roles in the migration, phagosome formation, and vesicle trafficking in zebrafish neutrophils and macrophages[1-4]. Lysozyme C in zebrafish plays a crucial role in defense against microbial pathogens[5,6]. Lysozyme C in fish is mainly expressed in myeloid-derived cells such as neutrophils and macrophages[6]. Mpeg1.1 is a macrophage expressed protein critical in regulating innate immune response[7-9]. Thus, RNAseq data analysis suggests that Keap1-specific HNEylation results in a downregulation in various markers of innate immune response in zebrafish. Interestingly, none of these genes were identified in the bolus dosing samples suggesting that bolus dosing does not trigger the same pathways as Z-REX.

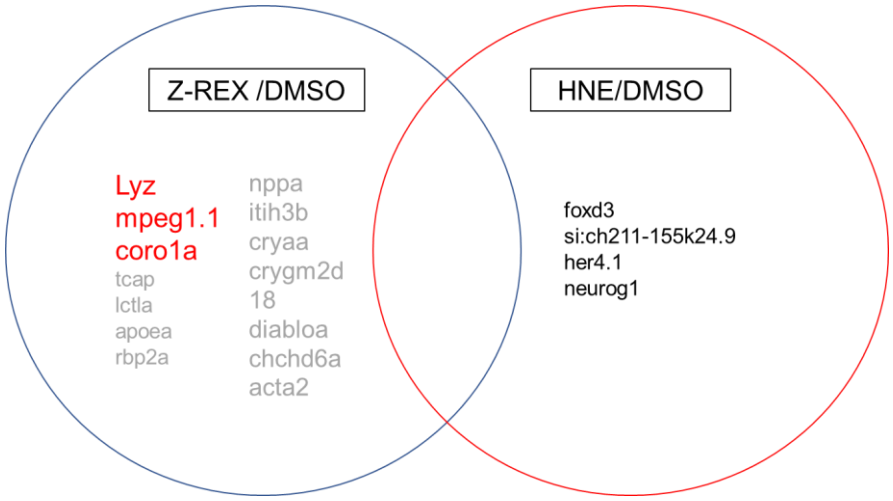

Figure 6.1 List of genes differentially downregulated in Z-REX sample relative to DMSO-treated sample. Interestingly, three of the top hits were identified as genes critical in innate immune response in zebrafish embryos. Bolus dosing of embryos downregulated a different set of genes in zebrafish.

Validation of immune-responsive gene downregulation

We next validated the data from RNAseq using qRT-PCR. All three genes were significantly downregulated after Z-REX in the validation experiments. No significant downregulation was observed for these genes after global HNE flooding (**Figure 6.2A**). Additionally, we also assessed the expression of two pro-inflammatory cytokines (interleukin6 and the chemokine interleukin8[10]), and the zebrafish granulocyte colony stimulating facor (gcsf) (an important regulator of immune cell development in fish[11]). All three immune-responsive genes were significantly downregulated compared to various Z-REX controls. Moreover, except *il6* none of the other genes showed suppression upon bolus dosing (**Figure 6.2B**). These data clearly demonstrate that Keap1-specific HNEylation suppresses innate immune response in developing zebrafish embryos.

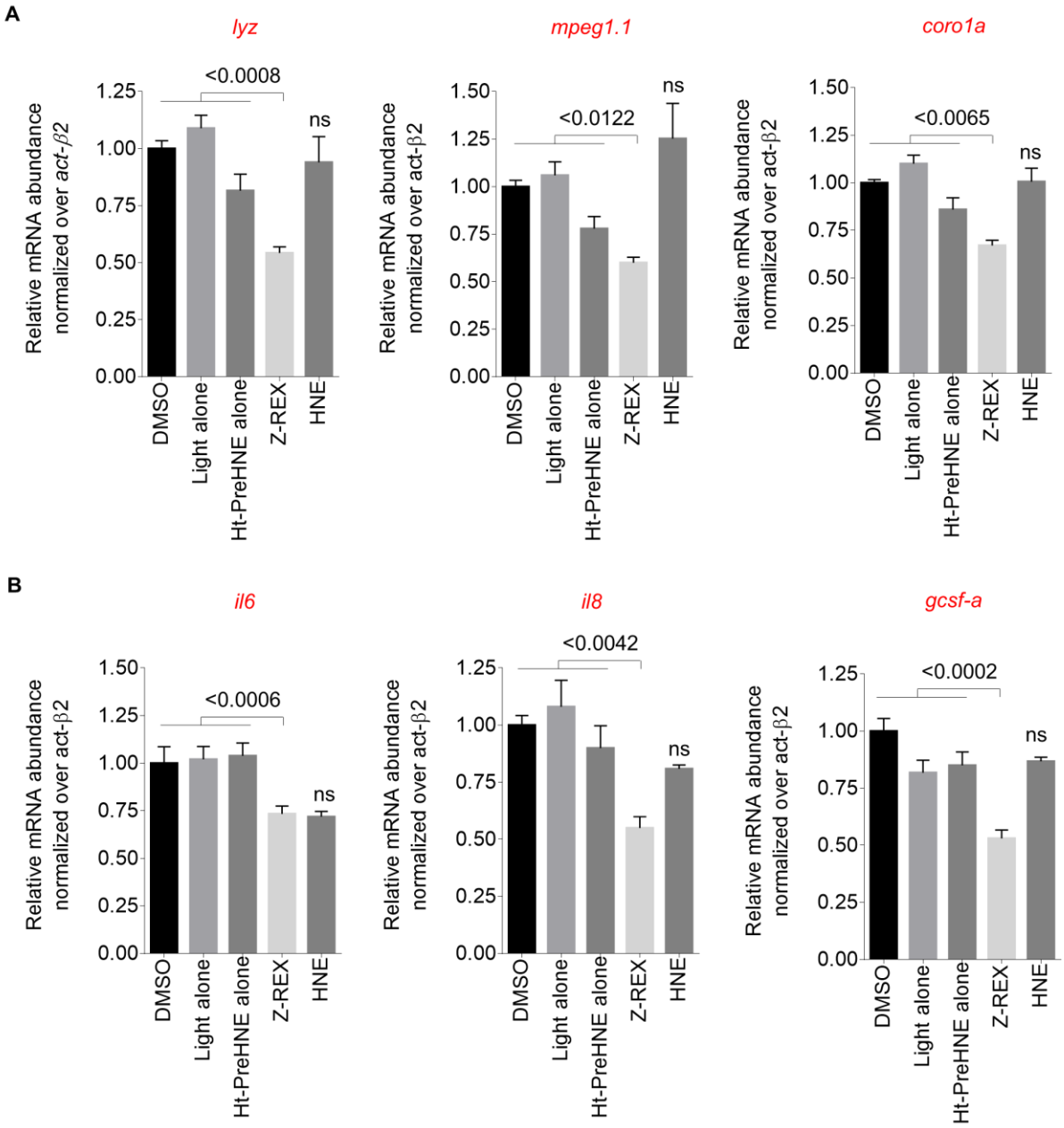

Figure 6.2 (**A**) Validation of the results obtained in RNAseq using qRT-PCR. (**B**) Select list three genes: two cytokines, produced by immune cells, and gcsf, an important regulator of macrophage and neutrophil development, were all downregulated after Z-REX. Bolus dosing with HNE showed no significant change in gene transcripts compared to control samples (except *il6*)

Tg neutrophil fish also show reduction in number of neutrophils

We used another independent approach to validate the findings from RNAseq and qRT-PCR. We used a *Tg(lyz:TagRFP)* transgenic fish that expresses red fluorescent protein under lyz promoter thereby selectively marking neutrophils[12-14]. Live whole fish imaging of *Tg(lyz:TagRFP)* 4 hours after Z-REX showed a strong reduction in the total number of neutrophils in zebrafish embryos (34–36 hour post fertilization (hpf)) (**Figure 6.3**).

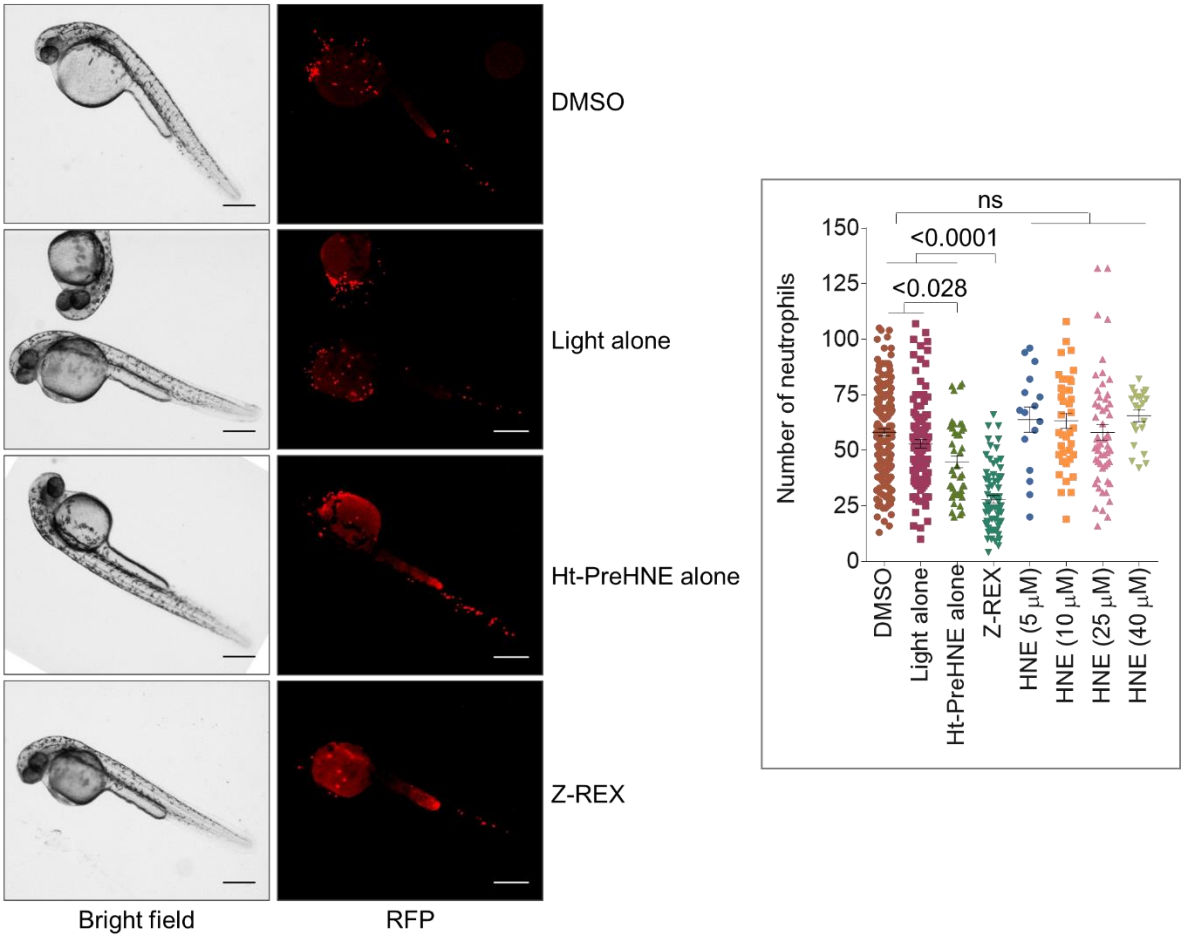

Figure 6.3 Z-REX-assisted Keap1 HNEylation shows a significant reduction in the total number of neutrophils in *Tg(lyz:TagRFP)* fish. Z-REX was performed as described in Chapters 2 and 5. 4 h post Z-REX (~34–36 hpf) fish were anaesthetized and imaged. Inset: Quantitation of total neutrophils in *Tg(lyz:TagRFP)* fish under various Z-REX

conditions. Bolus dosing with increasing HNE concentration did not show any downregulation in the total number of neutrophils

We were curious to investigate the mechanism of immune-responsive gene downregulation after Keap1-selective HNE modification. As shown in Chapter 5, Z-REX-mediated Keap1 HNEylation results in AR upregulation. AR upregulation mediated by the transcription factor Nrf2 has been shown to regulate immune response in mammals[15,16]. In a recent report, Nrf2 was shown to block the transcription of proinflammatory cytokine *il6 and il1b* independent of its redox-signaling activity[15]. The authors identified Nrf2 binding sites in proximity to the transcriptional start site (TSS) of the genes. It was proposed that Nrf2 binding to the region near the TSS interferes with binding of polymerase II resulting in suppression of transcription. This model contrasts with the more widely reported immune-modulatory role of Nrf2 by indirect regulation of the NF-κB pathway. Consistent with the latter model, pharmacologic activators of Nrf2 such as sulforaphane, phenyl isothiocyanates, tert-butylhydroquinone have been shown to downregulate NF-κB activation *in vitro*[16,17]. Additionally, $Nrf2^{-/-}$ mice show increased NF-κB pathway activation upon stimulation with lipopolysaccharides (LPS), and tumor- necrosis factor α (TNFα). Finally, $Nrf2^{-/-}$ mouse embryonic fibroblast cells show increased phosphorylation of IκB (phosphorylation targets IκB for degradation), a negative regulator of the NF-κB transcription factors[16,18]. These data collectively suggest that Nrf2-regulated pathways can control immune response in biological systems. We therefore investigated the role of Nrf2 and AR upregulation in controlling immune suppression after Z-REX.

Nrf2 positively regulates neutrophil numbers in zebrafish

We overexpressed human Nrf2 (hNrf2) in zebrafish embryos by mRNA injection. As expected, hNrf2 expression in *Tg(gstp1:GFP)* fish resulted in a strong upregulation of AR response (**Figure 6.4A**). Surprisingly, injection of hNrf2 mRNA in *Tg(lyz:TagRFP)* yielded an increase in total number of neutrophils demonstrating that Nrf2 positively regulates neutrophil numbers (**Figure 6.4B**). Consistent with this hypothesis, Nrf2a/b morphants showed strong suppression in the total number of neutrophils. Interestingly, co-expression of Halo-Keap1, a negative regulator of Nrf2, restored the number of neutrophils (**Figure 6.4C**) suggesting that Nrf2 and Keap1 act differently in regulating the number of neutrophils. This further implies that immune regulation by Keap1/Nrf2 is independent of their canonical AR regulatory roles.

Indeed, the regulation of myeloid cell (such as neutrophil) development by Nrf2 under non-stimulated conditions has been previously reported[19-21]. Nrf2 was shown to control the differentiation of hemopoietic stem cells (HSCs) (that results in the generation of myeloid cells such as neutrophils and macrophages) by multiple mechanisms. Nrf2 was found to induce differentiation of (HSCs) into granulocytic myeloid cells (such as neutrophils) at the expense of cells of lymphoid (lymphocytes) and erythroid (red blood cells) origin[19,20]. Additionally, Nrf2 regulated the survival of HSCs resulting in enhanced myeloid development[18,21]. Our data showing the basal regulation of neutrophil development by Nrf2 are consistent with these reports. However, the regulation of neutrophil development under these non-stimulated conditions (Keap1 is not modified) does not explain the suppression observed upon

Keap1-selective modification with HNE. Additionally, the data in **Figure 6.4C** suggests that Keap1 plays a role in neutrophil development independent of Nrf2. We further validated this hypothesis by showing that Z-REX-mediated Keap1 HNEylation results in downregulation in the number of neutrophils irrespective of Nrf2a levels in zebrafish embryos (**Figure 6.5A**). Thus, our data points to a *Nrf2a-independent* and *Keap1-HNEylation-dependent* signaling in neutrophil regulation.

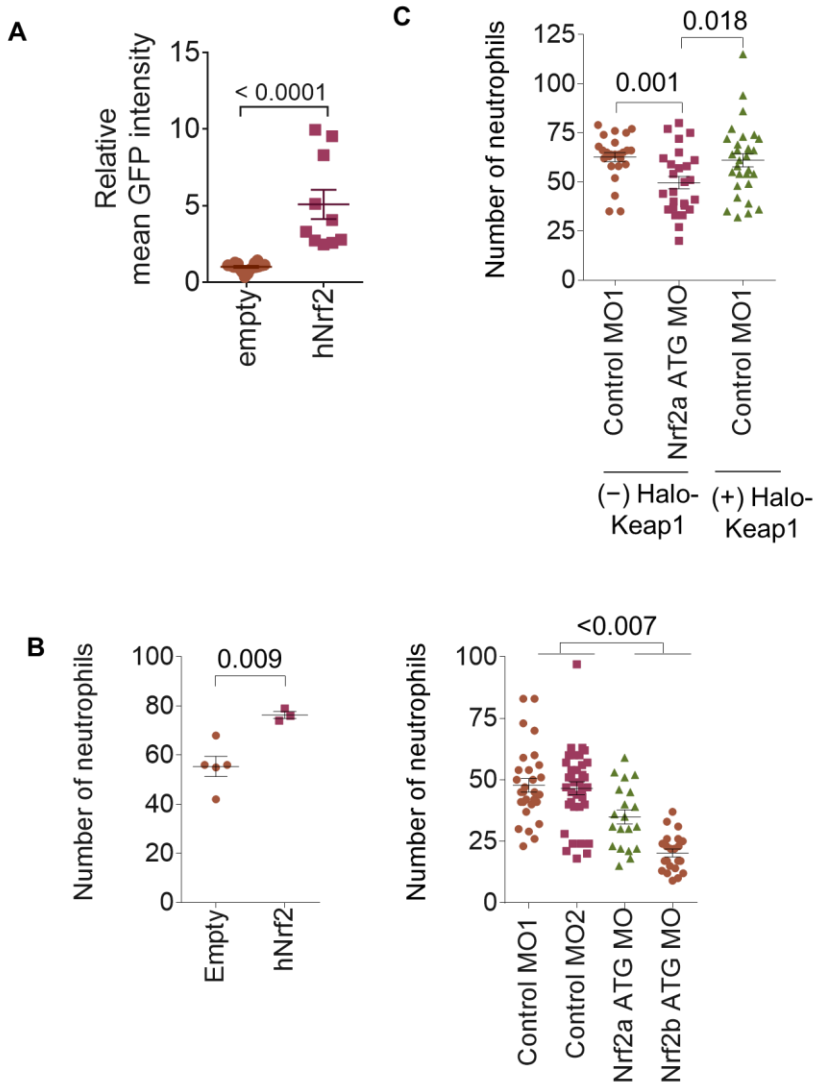

Figure 6.4 Nrf2 is a positive regulator of neutrophil development. (**A**) As expected, hNrf2 overexpression in *Tg(gstp1:GFP)* strongly upregulates AR. (**B**) Nrf2 overexpression in *Tg(lyz:TagRFP)* fish upregulates the total number of neutrophils whereas knock-down of either Nrf2a/b suppresses total neutrophil numbers. (**C**) Interestingly, co-expression of Halo-Keap1 in Nrf2a morphants restores neutrophil numbers in zebrafish.

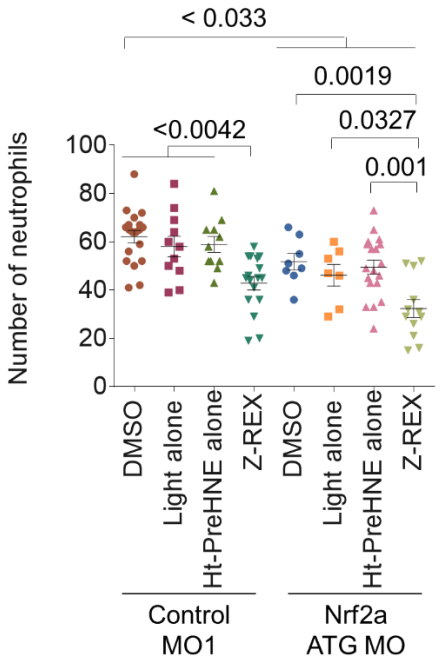

Figure 6.5 Nrf2a is dispensable in Keap1-HNEylation-mediated downregulation of the number of neutrophils in zebrafish. *Tg(lyz:TagRFP)* fish were co-injected with Halo-Keap1 mRNA and wither Control MO or Nrf2a-targeting MO. Z-REX was performed as specified earlier. Nrf2a knock-down resulted in decrease in total number of neutrophils. Keap1-specific HNEylation resulted in further decrease in total neutrophil numbers demonstrating that Nrf2a is dispensable for Keap1-HNEylation-dependent immune suppression.

Discussion

Our data thus far show that Z-REX downregulates the total number of neutrophils in zebrafish embryos through a Nrf2-independent but Keap-HNEylation-dependent pathway. The next significant step will be to identify the mechanism of

neutrophil downregulation. Two mechanisms are plausible: (1) HNEylated Keap1 suppresses neutrophil development (2) HNEylated Keap1 induces apoptosis of neutrophils. Our preliminary data (data not shown) as well qRT-PCR data supports the former hypothesis. Nevertheless, the most significant discovery will be to identify the molecular mechanisms of this regulation. A possible route to investigate would be to characterize the interactome of Keap1 and identify proteins that are critical in immune regulation. These investigations have the potential to identify novel regulators of the immune response that may prove to be valuable therapeutic targets. Additionally, the investigation promises to elucidate the underlying molecular mechanism of an electrophilic drug Tecfidera. The drug was clinically approved in 2013 for the treatment of relapsing remitting multiple sclerosis (MS). Despite its efficacy in treating the disease, its mechanism of action has remained unclear[22,23]. Unsurprisingly, treatment of patients with Tecfidera results in AR upregulation[24]. However, studies in mice have demonstrated efficacy in ameliorating experimental autoimmune encephalomyelitic (a model for MS) independent of Nrf2[22]. Alternative redox-sensitive proteins/pathways have been proposed to be the primary target of Tecfidera[25-27]. For example, a recent profiling experiment to characterize the targets of Tecfidera identified Protein Kinase C θ as an important target responsible for the immunomodulatory effect of the drug. Our results in zebrafish however suggests that electrophilic molecules can demonstrate immune suppression in a Keap1-HNEylation dependent pathway. Further experiments need to be done to fully characterize the mechanistic details of this regulatory pathway.

Experimental Setup

RNA isolation and RNAseq sample analysis: Casper zebrafish embryos were injected with Halo-Keap1 mRNA at 1–4 cell stage. Fish embryos were treated with Ht-PreHNE and allowed to develop for ~ 30 h at 28.5 °C. Z-REX was performed as described in previous chapters. 2 h post Z-REX, 5–7 embryos were dechorionated per sample, washed 2x with 1X chilled PBS, and homogenized in 1 mL Trizol in a 2 mL ceramic bead tubes (VWR, 10158-612) using a bead mill homogenizer (VWR, 10158-558). The samples were then transferred to a RNAse/DNAse free Eppendorf tube and total RNA was extracted as specified in Chapter 4. RNA quality was assessed using a Bioanalyzer (BRC Genomics Core facility). RNA samples were submitted to BRC Genomics Core Facility for sequencing and data analysis. Briefly, the total RNA was reverse transcribed using dA primers. Subsequently, the resulting cDNA was fragmented. Library preparation was performed using Illumina Library preparation kit (NEB) and the samples sequenced using an Illumina sequencing platform. Data analysis was performed using cuffdiff2 software.

Live fish Imaging: Tg(lyz:TagRFP) fish was a kind gift from Professor Anna Huttenlocher (University of Wisconsin). *Tg(lyz:TagRFP)* fish were crossed with wild type zebrafish. The embryos were injected with the Halo-Keap1 mRNA and/or the indicated morpholinos. Where applicable, Z-REX was performed as described previously. Live imaging was performed 4 h post Z-REX. Embryos were dechorionated and anaesthetized using 0.15−0.2 mg/mL Tricaine methanesulfonate solution in 10% Hank's buffer. Fish were images on an agarose plate.

References

(1) Li, L.; Yan, B.; Shi, Y.-Q.; Zhang, W.-Q.; Wen, Z.-L. Live Imaging Reveals Differing Roles of Macrophages and Neutrophils during Zebrafish Tail Fin Regeneration. *Journal of Biological Chemistry* **2012,** *287* (30), 25353.

(2) Yan, M.; Di Ciano-Oliveira, C.; Grinstein, S.; Trimble, W. S. Coronin Function Is Required for Chemotaxis and Phagocytosis in Human Neutrophils. *Journal of Immunology* **2007,** *178* (9), 5769.

(3) Yan, M.; Collins, R. F.; Grinstein, S.; Trimble, W. S. Coronin-1 Function Is Required for Phagosome Formation. *Molecular Biology of the Cell* **2005,** *16* (7), 3077.

(4) Ferrari, G.; Langen, H.; Naito, M.; Pieters, J. A Coat Protein on Phagosomes Involved in the Intracellular Survival of Mycobacteria. *Cell 97* (4), 435.

(5) Saurabh, S.; Sahoo, P. K. Lysozyme: an important defence molecule of fish innate immune system. *Aquaculture Research* **2008,** *39* (3), 223.

(6) Hall, C.; Flores, M. V.; Storm, T.; Crosier, K.; Crosier, P. The zebrafish lysozyme C promoter drives myeloid-specific expression in transgenic fish. *BMC Developmental Biology* **2007,** *7* (1), 42.

(7) Benard, E. L.; Racz, P. I.; Rougeot, J.; Nezhinsky, A. E.; Verbeek, F. J.; Spaink, H. P.; Meijer, A. H. Macrophage-Expressed Perforins Mpeg1 and Mpeg1.2 Have an Anti-Bacterial Function in Zebrafish. *Journal of Innate Immunity* **2015,** *7* (2), 136.

(8) Zakrzewska, A.; Cui, C.; Stockhammer, O. W.; Benard, E. L.; Spaink, H. P.; Meijer, A. H. Macrophage-specific gene functions in Spi1-directed innate immunity. *Blood* **2010,** *116* (3), e1.

(9) Spilsbury, K.; O'Mara, M.; Wu, W.; Rowe, P.; Symonds, G.; Takayama, Y. Isolation of a novel macrophage-specific gene by differential cDNA analysis. *Blood* **1995,** *85* (6), 1620.

(10) Arango Duque, G.; Descoteaux, A. Macrophage Cytokines: Involvement in Immunity and Infectious Diseases. *Frontiers in Immunology* **2014,** *5*, 491.

(11) Stachura, D. L.; Svoboda, O.; Campbell, C. A.; Espín-Palazón, R.; Lau, R. P.; Zon, L. I.; Bartůněk, P.; Traver, D. The zebrafish granulocyte colony-stimulating factors (Gcsfs): 2 paralogous cytokines and their roles in hematopoietic development and maintenance. *Blood* **2013,** *122* (24), 3918.

(12) Lam, P.-y.; Yoo, S. K.; Green, J. M.; Huttenlocher, A. The SH2-domain-containing inositol 5-phosphatase (SHIP) limits the motility of neutrophils and their recruitment to wounds in zebrafish. *Journal of Cell Science* **2012,** *125* (21), 4973.

(13) Kitaguchi, T.; Kawakami, K.; Kawahara, A. Transcriptional regulation of a myeloid-lineage specific gene lysozyme C during zebrafish myelopoiesis. *Mechanisms of Development* **2009,** *126* (5), 314.

(14) Li, L.; Yan, B.; Shi, Y.-Q.; Zhang, W.-Q.; Wen, Z.-L. Live Imaging Reveals Differing Roles of Macrophages and Neutrophils during Zebrafish Tail Fin Regeneration. *Journal of Biological Chemistry* **2012,** *287* (30), 25353.

(15) Kobayashi, E. H.; Suzuki, T.; Funayama, R.; Nagashima, T.; Hayashi, M.; Sekine, H.; Tanaka, N.; Moriguchi, T.; Motohashi, H.; Nakayama, K.et al. Nrf2 suppresses macrophage inflammatory response by blocking proinflammatory cytokine transcription. *Nature Comm.* **2016,** *7*, 11624.
(16) Wakabayashi, N.; Slocum, S. L.; Skoko, J. J.; Shin, S.; Kensler, T. W. When NRF2 Talks, Who's Listening? *Antioxidant. redox. signal.* **2010,** *13* (11), 1649.
(17) Gill, A. J.; Kolson, D. L. Dimethyl fumarate modulation of immune and antioxidant responses: application to HIV therapy. *Critical reviews in immunology* **2013,** *33* (4), 307.
(18) Thimmulappa, R. K.; Lee, H.; Rangasamy, T.; Reddy, S. P.; Yamamoto, M.; Kensler, T. W.; Biswal, S. Nrf2 is a critical regulator of the innate immune response and survival during experimental sepsis. *Journal of Clinical Investigation* **2006,** *116* (4), 984.
(19) Murakami, S.; Shimizu, R.; Romeo, P.-H.; Yamamoto, M.; Motohashi, H. Keap1-Nrf2 system regulates cell fate determination of hematopoietic stem cells. *Genes to Cells* **2014,** *19* (3), 239.
(20) Murakami, S.; Suzuki, T.; Harigae, H.; Romeo, P.-H.; Yamamoto, M.; Motohashi, H. NRF2 activation impairs quiescence and bone marrow reconstitution capacity of hematopoietic stem cells. *Molecular and Cellular Biology* **2017**, DOI:10.1128/mcb.00086-17 10.1128/mcb.00086-17.
(21) Merchant, A. A.; Singh, A.; Matsui, W.; Biswal, S. The redox-sensitive transcription factor Nrf2 regulates murine hematopoietic stem cell survival independently of ROS levels. *Blood* **2011,** *118* (25), 6572.
(22) Schulze-Topphoff, U.; Varrin-Doyer, M.; Pekarek, K.; Spencer, C. M.; Shetty, A.; Sagan, S. A.; Cree, B. A. C.; Sobel, R. A.; Wipke, B. T.; Steinman, L.et al. Dimethyl fumarate treatment induces adaptive and innate immune modulation independent of Nrf2. *Proceedings of the National Academy of Sciences* **2016,** *113* (17), 4777.
(23) Oral BG-12 in Multiple Sclerosis. *New England Journal of Medicine* **2013,** *368* (17), 1652.
(24) Bomprezzi, R. Dimethyl fumarate in the treatment of relapsing–remitting multiple sclerosis: an overview. *Therapeutic Advances in Neurological Disorders* **2015,** *8* (1), 20.
(25) Zhao, G.; Liu, Y.; Fang, J.; Chen, Y.; Li, H.; Gao, K. Dimethyl fumarate inhibits the expression and function of hypoxia-inducible factor-1α (HIF-1α). *Biochem. Biophys. Res. Commun.* **2014,** *448* (3), 303.
(26) Blewett, M. M.; Xie, J.; Zaro, B. W.; Backus, K. M.; Altman, A.; Teijaro, J. R.; Cravatt, B. F. Chemical proteomic map of dimethyl fumarate–sensitive cysteines in primary human T cells. *Science signaling* **2016,** *9* (445), rs10.
(27) Kastrati, I.; Siklos, M. I.; Calderon-Gierszal, E. L.; El-Shennawy, L.; Georgieva, G.; Thayer, E. N.; Thatcher, G. R. J.; Frasor, J. Dimethyl Fumarate Inhibits the Nuclear Factor κB Pathway in Breast Cancer Cells by Covalent Modification of p65 Protein. *Journal of Biological Chemistry* **2016,** *291* (7), 3639.

Appendix I

LC-MS/MS identification of HNE modifications on Keap1 from global HNE treatment.

Human Keap1 (100%), 70.0 kDa, Mascot Score 2610, 116 unique peptides with different modifications, 7 distinct tryptic peptides with added mass of 134 Da or 152 Da for possible modifications of dehydrated HNE-alkyne or HNE-alkyne.
All 7 modified peptides were found present in corresponding unmodified forms of the native peptides with Cys being alkylated by carbamidomethylation.
531/624 amino acids (85% coverage)
Matched peptide with HNE related modifications shown in **green**, other matched peptide shown in **red**

MQPDPRPSGAGACCRFLPLQSQCPEGAGDAVMYASTECKAEVTPSQHGNR
TFSYTLEDHT KQAFGIMNELRLSQQLCDVT LQVKYQDAPAAQFMAHKVVL
ASSSPVFKAM FTNGLREQGMEVVSIEGIHPKVMERLIEFAYTASISMGEK
CVLHVMNGAVMYQIDSVVRACSDFLVQQLDPSNAIGIANF AEQIGCVELH
QRAREYIYMH FGEVAKQEEF FNLSHCQLVTLISRDDLNVRCESEVFHACI
NWVKYDCEQR RFYVQALLRAVRCHSLTPNFLQMQLQKCEILQSDSRCKDY
LVKIFEELTLHKPTQVMPCRAPKVGRLIYTAGGYFRQSLSYLEAYNPSDG
TWLRLADLQVPRSGLAGCVVGGLLYAVGGRNNSPDGNTDSSALDCYNPMT
NQWSPCAPMSVPRNRIGVGVIDGHIYAVGG SHGCIHHNSVERYEPERDEW
HLVAPMLTRRIGVGVAVLNRLLYAVGGFDGTNRLNSAECYYPERNEWRMI
TAMNTIRSGAGVCVLHNCIYAAGGYDGQDQLNSVERYDVETETWTFVAPM
KHRRSALGITVHQGRIYVLG GYDGHTFLDSVECYDPDTDTWSEVTRMTSG
RSGVGVAVTM EPCRKQIDQQNCTC

Unique peptide with (dehydrated) HNE-alkyne modification (asterisk suggests modification site)	**MS spectra**
C77 **LSQQLC*DVT LQVK** p-value: 0.000001 Mascot Ion Score: 60 **Modification:** dehydrated HNE-alkyne	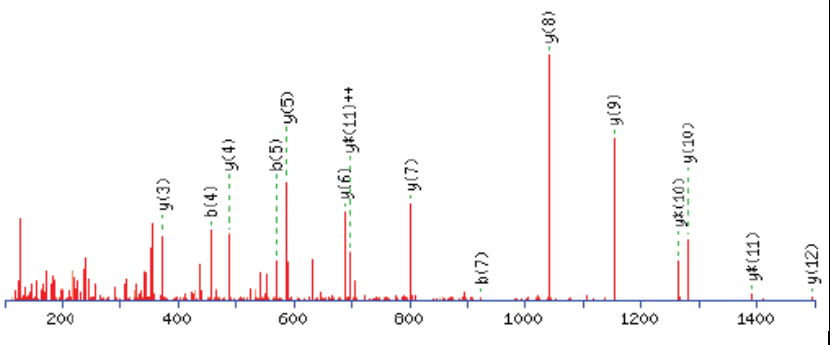

C151 **C*VLHVMNGAVMYQIDSVVR** p-value: 0.00000004 Mascot Ion Score: 74 **Modification:** dehydrated HNE-alkyne	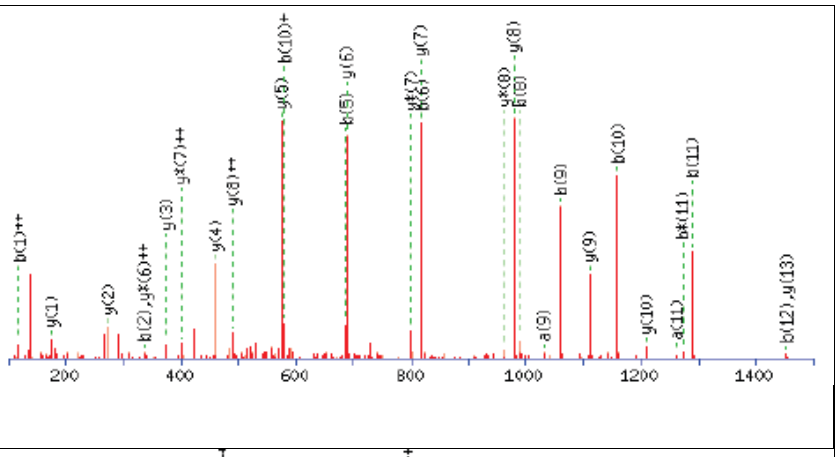
C226 **QEEFFNLSHC*QLVTLISR** p-value: 0.000004 Mascot Ion Score: 54 **Modification:** dehydrated HNE-alkyne	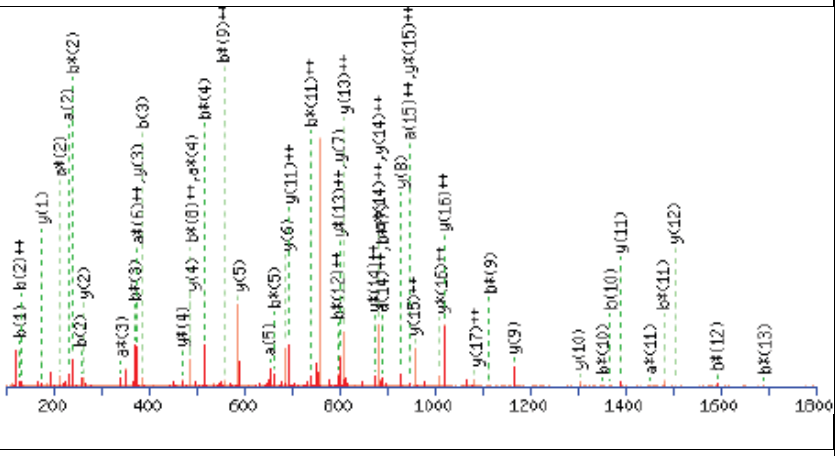
C273 **C*HSLTPNFLQMQLQK** p-value: 0.0000008 Mascot Ion Score: 61 **Modification:** dehydrated HNE-alkyne	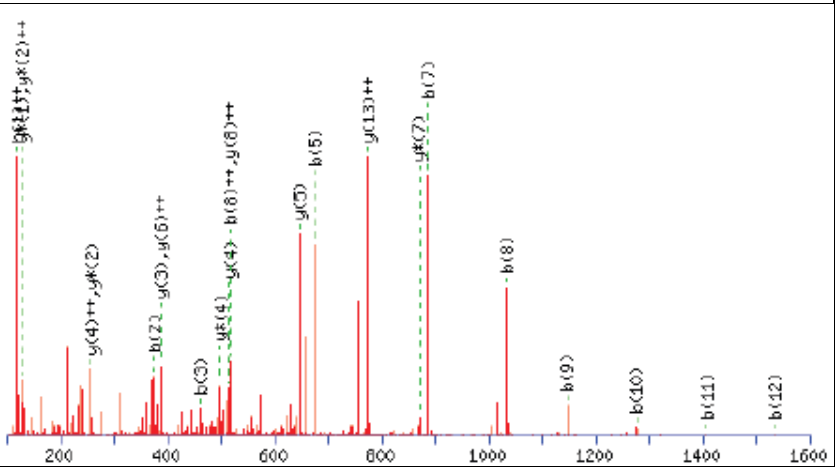

C273 **C*HSLTPNFLQ MQLQK** p-value: 0.00005 Mascot Ion Score: 43 **Modification:** HNE-alkyne	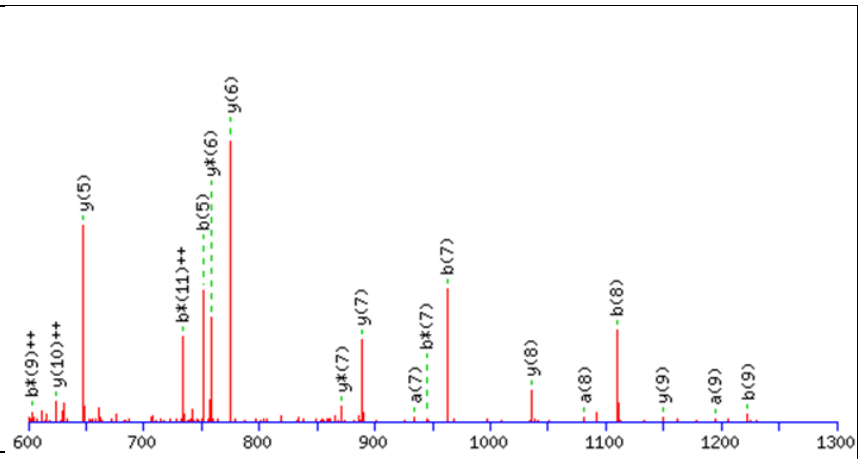
C319 **IFEELTLHKPT QVMPC*R** p-value: 0.0001 Mascot Ion Score: 40 **Modification:** dehydrated HNE-alkyne	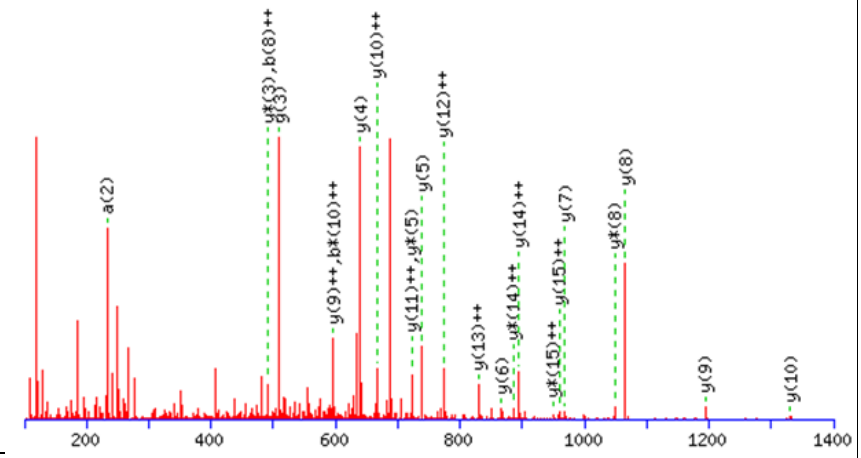
C368 **SGLAGC*VVG GLLYAVGGR** p-value: 0.0000000003 Mascot Ion Score: 95 **Modification:** dehydrated HNE-alkyne	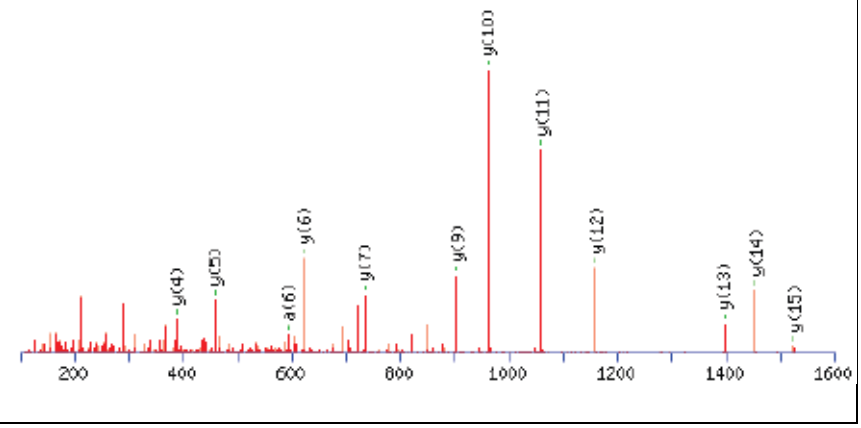

LC-MS/MS identification of HNE modifications on Keap1 from targeted HNEylation.

Human Keap1 (100%), 70.0 kDa, Mascot Score 1920, 105 unique peptides with different modifications, 2 distinct tryptic peptides with added mass of 134 Da for possible modifications of dehydrated HNE-alkyne.
Both of the two modified peptides were found present in corresponding unmodified forms of the native peptides with Cys being alkylated by carbamidomethylation.
530/624 amino acids (85% coverage)
Matched peptide with HNE related modifications shown in **green**, other matched peptide shown in **red**

MQPDPRPSGAGACCRFLPLQSQCPEGAGDAVMYASTECKAEVTPSQHGNR
TFSYTLEDHTKQAFGIMNELRLSQQLCDVTLQVKYQDAPAAQFMAHKVVL
ASSSPVFKAMFTNGLREQGMEVVSIEGIHPKVMERLIEFA YTASISMGEK
CVLHVMNGAVMYQIDSVVRACSDFLVQQLDPSNAIGIANFAEQIGCVELHQR
AREYIYMHFGEVAKQEEFFNLSHCQLVTLISRDDLNVRCESEVFHACINWVKY
DCEQRRFYVQALLRAVRCHSLTPNFLQMQLQKCEILQSDSRCKDYLVKIFEEL
TLHKPTQVMPCRAPKVGRLIYTAGGYFRQSLSYLEAYNPSDGTWLRLADLQV
PRSGLAGCVVGGLLYAVGGRNNSPDGNTDSSALDCYNPMTNQWSPCAMSVP
RNRIGVGVIDGHIYAVGGSHGCIHHNSVERYEPERDEWHLVAPMLTRRIGVGV
AVLNRLLYAVGGFDGTNRLNSAECYYPERNEWRMITAMNTIRSGAGVCVLHN
CIYAAGGYDGQDQLNSVERYDVETETWTFVAPMKHRRSALGITVHQGRIYVL
GGYDGHTFLDSVECYDPDTDTWSEVTRMTSGRSGVGVAVTMEPCRKQIDQQ
NCTC

Unique peptide with HNE-alkyne modification (asterisk suggests modification site)	**MS spectra**
<u>C226</u> **QEEFFNLSH C*QLVTLISR** p-value: 0.000008 Mascot Ion Score: 51 **Modification:** dehydrated HNE-alkyne	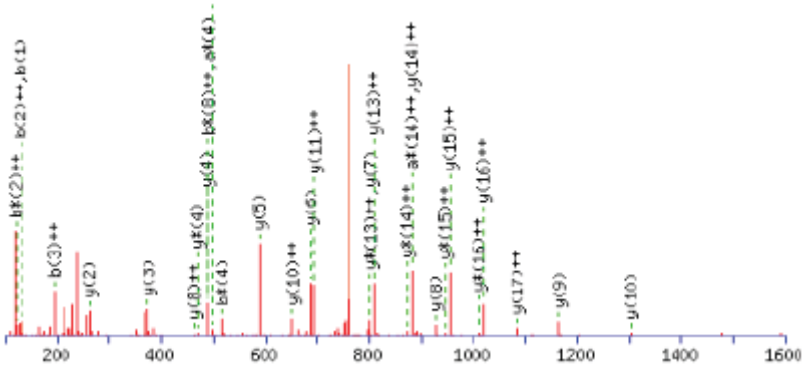

C368 **SGLAGC*VVGG LLYAVGGR** p-value: 0.0000008 Mascot Ion Score: 61 **Modification:** dehydrated HNE-alkyne	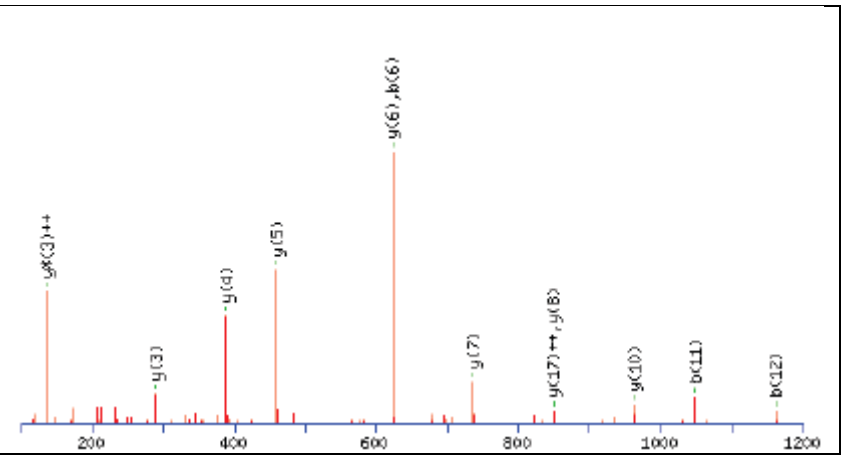

Chemical structures of HNE-adducts on cysteine residues on peptides

Entry		Chemical structures
A	Michael adduct	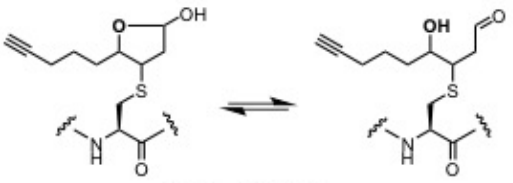 MW + 152.1 Da[a]
B	Reduced Michael adduct	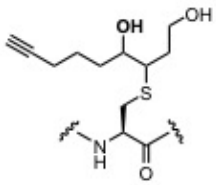 MW + 154.1 Da[a]
C	Dehydrated Michael adduct	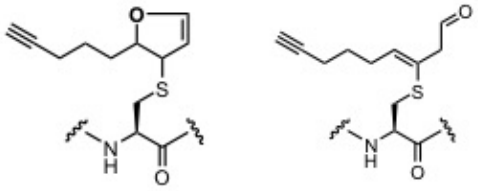 MW + 134.1 Da[a]

Appendix II

LC-MS/MS-based identification of the site of modification on Akt3 post targeted HNEylation in HEK 293T cells

<table>
<tr><td colspan="2">Human Akt3 isoform 2 (100%), 53.9 kDa, Mascot Score 5895.47, 52 unique peptides with different modifications, 1 distinct tryptic peptides with added mass of 154.1 Da for possible modifications of reduced HNE(alkyne) Michael adduct (See Supplementary Table 2). 391/464 amino acids (84.2% coverage). Matched peptide with HNE related modifications shown in green, other matched peptide shown in red.
MSDVTIVKEG WVQKRGEYIK NWRPRYFLLK TDGSFIGYKE
KPQDVDLPYP LNNFSVAKCQ LMKTERPKPN TFIIRCLQWT
TVIERTFHVD TPEEREEWTE AIQAVADRLQ RQEEERMNCS
PTSQIDNIGE EEMDASTTHH KRKTMNDFDY LKLLGKGTFG
KVILVREKAG KYYAMKILKK EVIIAKDEVA HTLTESRVLK
NTRHPFLTSL KYSFQTKDRL CFVMEYVNGG ELFFHLSRER
VFSEDRTRFY GAEIVSALDY LHSGKIVYRD LKLENLMLDK
DGHIKITDFG LCKEGITDAA TMKTFCGTPE YLAPEVLEDN
DYGRAVDWWG LGVVMYEMMC GRLPFYNQDH EKLFELILME
DIKFPRTLSS DAKSLLSGLL IKDPNKRLGG GPDDAKEIMR
HSFFSGVNWQ DVYDKKLVPP FKPQVTSETD TRYFDEEFTA
QTITITPPEK CQQSDCGMLG NWKK</td></tr>
<tr><td>Unique peptide with modification (asterisk suggests modification site)</td><td>MS/MS spectra</td></tr>
<tr><td><u>C119</u>
MNC*SPTSQID NIGEEEMDAS TTHHK
Ion score: 22.3
p-value:0.0059
Modification: M1 (oxidation), C3 (reduced HNE alkyne), N11 (deamidation)
Expectation value: 0.0059</td><td> 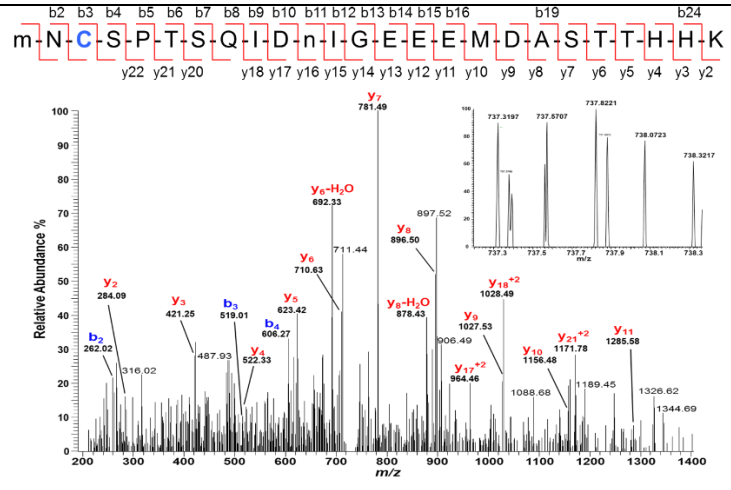 </td></tr>
</table>

C119 MNC*SPTSQID NIGEEEMDAS TTHHK Ion score: 15.6 p-value:0.0278 Modification: C3 (reduced HNE alkyne) Expectation value: 0.0278	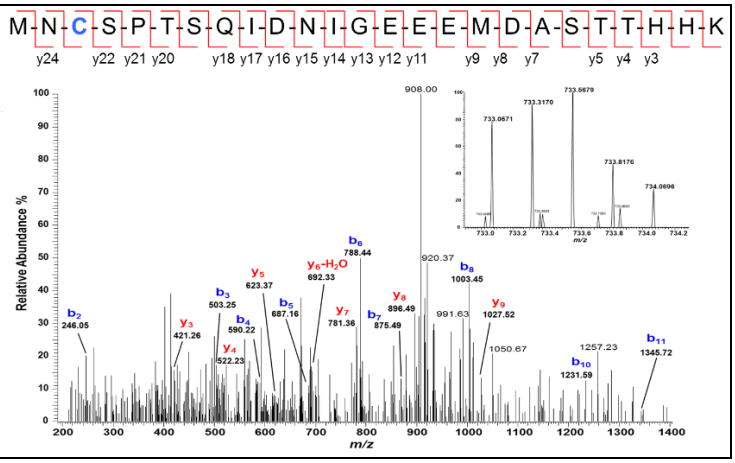

Appendix III

Venn diagram showing differentially upregulated/downregulated genes in Z-REX/Z-REX controls/HNE bolus dosing samples relative to DMSO.

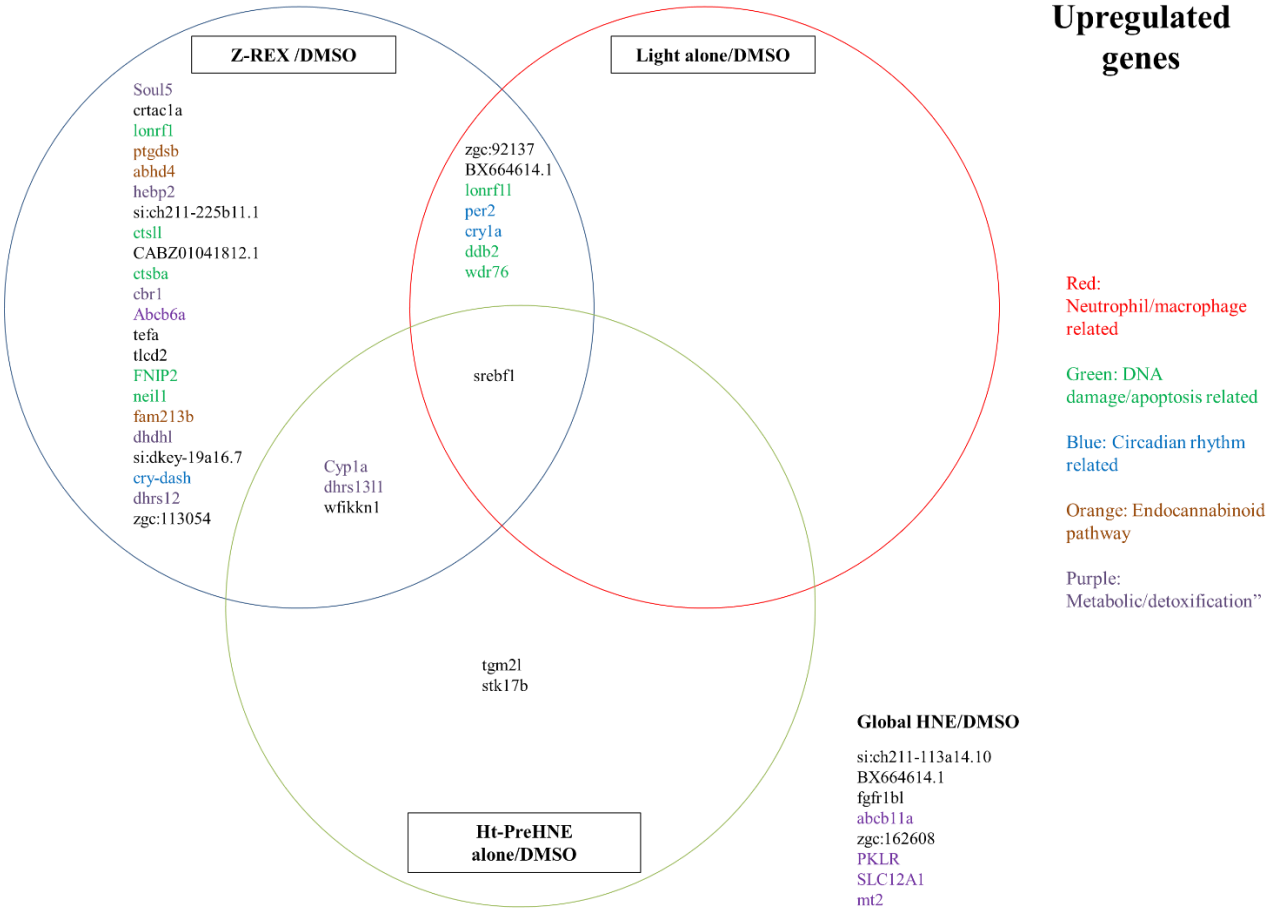

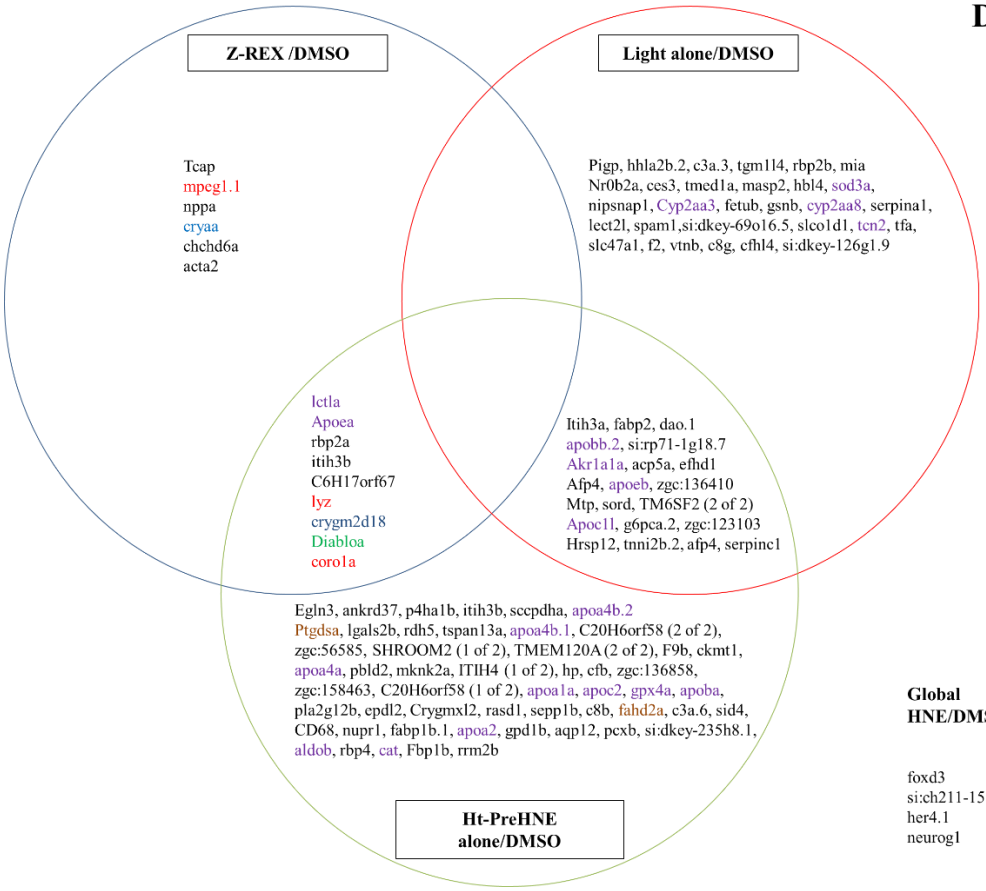

Downregulated genes

Red: Neutrophil/macrophage related

Green: DNA damage/apoptosis related

Blue: Circadian rhythm related

Orange: Endocannabinoid pathway

Purple: Metabolic/detoxification

Global HNE/DMSO

foxd3
si:ch211-155k24.9
her4.1
neurog1